UNIVERSITAT DE BARCELONA

Functional Role of Pentose Phosphate Pathway and Glutamine in Cancer Cell

Ibrahim Halil Polat

Functional Role of Pentose Phosphate Pathway and Glutamine in Cancer Cell Metabolism

Ibrahim Halil Polat

Doctoral Thesis

2016

The image used in the cover was obtained from the website http://www.mariasklodowska.com/.

Marie Sklodowska Curie (1867-1934) is the woman who opened the nuclear age and she is famous for her discoveries on radioactivity. She was not only the first woman who was awarded a Nobel Prize but also the only woman who had it in two different fields. Also, she was the first woman to become a professor at the University of Paris.

She was born in 1867 and named as Maria Salomea Skłodowska in Warsaw, Poland. She had her early education and practical scientific training in Warsaw and in 1891, she moved to Paris to get her higher degrees to conduct her subsequent scientific work. In 1895, she married Pierre Curie, a fellow scientist and together with Pierre, they did extensive research on the recently discovered phenomenon of radioactivity. Inspired by the discovery of radioactivity by Henri Becquerel in 1896, they conducted extensive researches and analyses which led to the isolation of two elements, Polonium and Radium.

For the work they carried out on radioactivity that led to the discovery of these two elements, Marie and Pierre Curie shared the 1903 Nobel Prize for Physics, jointly with Henri Becquerel and she was the first woman ever to win a Nobel. In 1906, when Pierre Curie died in an accident Marie Curie was offered to take over the professorship at Sorbonne and to lecture in Pierre's place, which made her the first woman to become a Professor at the Sorbonne. She accepted it hoping to create a world-class laboratory dedicated to Pierre.

Despite that Marie Curie had been devastated by Pierre's death, she continued her work on radioactivity stoutly. In 1910 she gained insights into the nature of the atom and finally she isolated Radium physically. Moreover, she defined an international standard for radioactive emissions that was eventually named after her and Pierre: the Curie. In that way, she obtained her second Nobel Prize in 1911, in Chemistry, for her work on Radium. Even today, she is the only woman in the list of multiple Nobel winners.

In 1914, she founded the Radium Institute in Paris (today's Curie Institute), which is a radioactivity laboratory created for her by the Pasteur Institute and the University of Paris. During World War I, Marie Curie developed mobile radiography units because of the need for field radiological centers in the battlefield to help surgeons. On the other hand, in 1915 Curie produced hollow needles containing 'radium emanation', in order to be used for sterilizing infected tissue.

After the War, Marie continued with her scientific work, and also with establishing the Radium Institute. She was honoured by many countries and participated various International scientific committees. Her health got deteriorated because of being exposed to radiation for long-term during her work and she died in 1934 due to Blood Cancer. Her daughter Irene Joliot-Curie followed her in scientific works and also won a Nobel Prize for Chemistry (1935). Marie Curie is regarded as one of the most influential scientists of all times.

Doctoral Program in Biotechnology

Department of Biochemistry and Molecular Biomedicine

Faculty of Biology

Functional Role of Pentose Phosphate Pathway and Glutamine in Cancer Cell Metabolism

Doctoral Thesis submitted by Ibrahim Halil Polat to obtain Ph.D degree from the Universitat de Barcelona and Université Grenoble Alpes in the frame of dual degree agreement

Dr. Marta Cascante Serratosa

Co-supervisor and tutor

Dr. Philippe Sabatier

Co-supervisor

Ibrahim Halil Polat

Doctoral Student

To Christian, my family and all the people who have shared my life experience during the last years.

My sincere thanks to Dr. Marta Cascante, Dr. Philippe Sabatier, Dr. Roldan Cortes and Dr. Silvia Marin for their support to make this Ph.D Thesis possible.

Also, special thanks to Dr. Miriam Tarrado, Dr. Anusha Jayaraman, Joseph Tarrago, Erika Zodda (que me sueña), and Dr. Esther Aguilar (canari@s) for always being there for me.

"Un científico es una persona a la que el sistema educativo no ha logrado destruir su curiosidad de niño y sigue preguntándose cosas como por qué el cielo es azul"

León Lederman (Premio Nobel de Física 1988)

TABLE OF CONTENTS

1. ABBREVIATIONS

1. ABBREVIATIONS

αKG: α-Ketoglutarate

2-DG: 2-Deoxy-D-glucose

3PG: 3-Phosphoglyceride

6PG: 6-Phosphogluconate

6PGD: 6-Phosphogluconolactone dehydrogenase

6PGL: 6-Phosphogluconolactonase

ACC: Acetyl-CoA Carboxylase

ACLY: ATP Citrate Lyase

Ac-CoA: Acetyl-CoA

ACO: Aconitase

BPTES: Bis-2-(5-phenylacetamido-1,3,4-thiadiazol-2-yl)ethyl sulfide

CS: Citrate synthase

DCA: Dichloroacetate

DHAP: Dihydroxyacetone phosphate

DHEA: Dehydroepiandrosterone

E4P: Erytrose-4-phosphate

EGF: Epidermal growth factor

ER: Estrogen receptor

ETC: Electron transport chain

F16BP: Fructose-1,6-biphosphate

F26BP: Fructose-2,6-biphosphate

F6P: Fructose-6-phosphate

FACS: Fluorescence-activated cell sorting

FAD^{2+}: Flavin adenine dinucleotide

FASN: Fatty acid synthase

FH: fumarate hydratase

G1P: Glucose-1-phosphate

G3P: Glyceraldehyde-3-phosphate

G6P: Glucose-6-phosphate

G6PD: Glucose-6-phosphate Dehydrogenase

GAP: Glyceraldehyde-3-phosphate

GAPDH: Glyceraldehyde-3-phosphate Dehydrogenase

GC-MS: Gas chromatography–mass spectrometry

GDH: Glutamate Dehydrogenase

GLS: Glutaminase

GLUT: Glucose transporter

GSH: Glutathione

GSMM: Genome scale metabolic model

HER2: Human epidermal growth factor receptor 2

HIF1: Hypoxia-Inducible Factor 1

HK: Hexokinase

IDH: Isocitrate Dehydrogenase

IDH1: Isocitrate Dehydrogenase isoform 1

IDH2: Isocitrate Dehydrogenase isoform 2

IGF1: Insulin-like growth factor 1

KEAP1: Kelch-like ECH-associated protein 1

LDH: Lactate Dehydrogenase

MAPK: Mitogen-activated protein kinases

MCT: Monocarboxylate transporter

MDH: Malate Dehydrogenase

ME: Malic Enzyme

ME1: Malic Enzyme isoform 1

ME2: Malic Enzyme isoform 2

MIDA: Mass isotopomer distribution analysis

mTOR: mechanistic target of rapamycin

MTT: 3-(4,5-Dimethylthiazol-2-yl)-2,5-diphenyltetrazolium bromide

NAD^+: Nikotinamid adenin dinükleotid

$NADP^+$: Nikotinamid adenin dinükleotid phosphate

NRF2: Nuclear factor erythroid 2-Related Factor 2

NMR: Nuclear magnetic resonance

OAA: Oxaloacetate

OT: Oxythiamine

OXPHOS: Oxidative phosphorylation

PC: Pyruvate carboxylase

PDH: Pyruvate dehydrogenase

PDK: Pyruvate dehydrogenase kinase

PEP: Phosphoenolpyruvate

PFK: Phosphofructokinase

PFKFB2: 6-phosphofructo-2-kinase/fructose-2,6-biphosphatase 2

PFKFB3: 6-phosphofructo-2-kinase/fructose-2,6-biphosphatase 3

PHD: prolyl hydroxylase domain

PHDGH: D-3-phosphoglycerate dehydrogenase

PI3K: Phosphatidylinositol 3- kinases

PK: Pyruvate kinase

PPP: Pentose phosphate pathway

PTEN: Phosphatase and tensin homolog

Pyr: Pyruvate

R5P: Ribose-5-phosphate

RB: Retinoblastoma

RPE: Ribulose-phosphate 3-epimerase

RPI: Ribose-5-phosphate isomerase

ROS: Reactive Oxygen Species

S7P: Sedoheptulose-7-phosphate

SDH: Succinate dehdyrogenase

SREBPs: Sterol regulatory binding proteins

TALDO: Transaldolase

TCA: Tricarboxylic acid cycle

TGF-β: Tumor growth factor β

TIGAR: TP53-inducible glycolysis and apoptosis regulator

TKT: Transketolase

TKTL1: Transketolase like 1

TNF: Tumor necrosis factor

VEGF-A: Vascular endothelial growth factor A

X5P: Xilulose-5-phosphate

2. INTRODUCTION

2. INTRODUCTION

2.1. CANCER

Cancer can be defined as a term that gathers up many heterogeneous sets of diseases in which some abnormal cells divide out of the control with a tendency to spread throughout the body and to found new colonies of cancer cells, which is termed as metastasis [1]. Metastasis is the major cause of the death from the cancer. Cancer is a prevalent multi-factorial disease which can be influenced by both environmental factors; such as, tobacco, infectious organisms, chemicals and radiation, or genetic susceptibility; such as, inherited mutations, hormones, immune conditions and some metabolic alterations [2]. Therefore, risk evaluation, diagnosis and treatment of cancer are quite challenging. It is often characterized by the loss of physiological control and malignant transformation of the cells and tumor development and progression requires that malignant cells gain certain functional and genetic abnormalities. Moreover, cancer is a heterogeneous disease as hundreds of types of cancer exist. World Health Organization (WHO) estimates that cancer causes more death than heart diseases or strokes [3]. In 2012, 14.1 million new cancer cases and 8.2 million cancer related deaths were reported worldwide, among which the most commonly diagnosed cancers were lung, breast and colorectal [4].

2.1.1. Breast Cancer

Breast cancer is the most common type of cancer in women and the second leading cause of cancer related deaths, next to lung cancer [4-7]; therefore, developing new therapeutic and preventive means in order to control this disease is a matter of vital

importance. Breast is an epithelial organ that develops from galactic band which remains quiescent until puberty until when the sexual hormonal balance is not active. Breast cancer is the result of subtle imbalance in the complex regulatory agents to which the breast tissue is exposed; such as sex hormones, epidermal growth factor and other agents that influence the normal growth and function. Breast cancer is a quite complex and heterogeneous disease. Various studies of cellular and molecular mechanisms that are involved in the onset and development of this disease have contributed significantly to our understanding of its heterogeneity at a molecular level based on basic measures, such as histological type, tumor grade, lymph node status and the presence of predictive markers like estrogen receptor (ER) and human epidermal growth factor receptor 2 (HER2) [8, 9]. There are various symptoms of breast cancer among which lumps, pulled in nipples, dimpling, dripping, redness/rash and skin changes are the most common ones [7].

2.1.2. Colorectal Cancer

Colorectal cancer, on the other hand, is the third most prevalent cancer in men and second in women especially in western world but it has a considerably lower mortality rate compared to lung or breast cancer [4]. However, further development of therapeutic and preventive tools of controlling colorectal cancer is also clearly needed. Colon cancer is the cancer of large intestine, also called colon, which takes place at the lower part of the digestive system. The cancer in the last centimeters of the colon is referred as rectal cancer. Combined, they are usually named as colorectal cancer (CRC). The intestinal colon walls consist of four layers. The inner most layer called mucosa is where colonic epithelium renews itself. Any mutation which disturbs this self renewal process can interrupt normal intestinal development triggering apoptotic or DNA repair mechanisms, which end up in malignancy. Most cases of the colorectal cancer start as benign polyps, clumps of cells, which are formed in the inner lining of the colon or rectum and grow toward the center. Certain types of those polyps called adenomas can further become cancer and form adenocarcinomas, which are the cancers that start in gland cells [10].

2.2. HALLMARKS OF CANCER

Cancer is a disease which involves dynamic changes in the genome. Discovery of mutations leading to activation of growth promoting genes called “oncogenes” or deactivation of growth inhibiting genes called “tumor suppressor genes” specific for different types of cancer was the corner stone of cancer research [11-13]. The transformation of healthy cells into malignancy (tumorigenesis) is a multistep process which involves genetic alterations resulting in progressive transformation of healthy cells into malignant cells [14]. Nonetheless, the research conducted within the last two decades have demonstrated that there are essential capabilities shared by most cancer cells to regulate tumorigenesis, which are outlined by Hanahan and Weinberg (2011) as “hallmarks of cancer” [15]. These essential alterations that together lead malignant growth of the cells are described below in brief and schematically depicted in figure 2.1.

Cancer cells sustain proliferative stimuli and evade growth suppressors: Noncancerous cells carry a highly regulated balance between cell proliferation and cell death in order to maintain the cell biomass homeostasis by carefully controlling the production and release of growth-promoting signals transuded via signal transduction pathways. These signals are mostly growth factors binding cell surface receptors with intracellular tyrosine kinase domains. Cancer cells, however, have altered signaling pathways and alterations in mitogenic signaling which promotes cell division lead them to proliferate continuously and autonomously. Cancer cells can either produce growth factor stimuli themselves or they can send stimulating signals to neighboring healthy cells; so that, they can supply cancer cells with various growth factors [16].

Cancer cells enable replicative immortality and resist to cell death: Activation of oncogenes or deactivation of tumor suppressor genes help cancer cells to overcome the checkpoints of cell division cycle and apoptotic (programmed cell death) mechanisms, which give them immortality [17-20]. Key oncogenes like myc, AKT and tyrosine kinase receptors (epidermal growth factor, EGF; insulin like growth factor 1, IGF-1 etc.) can activate RAS or RAF-mitogen activated protein kinase (MAP kinase), phosphatidylinositol 3- kinases (PI3Ks), mechanistic target of rapamycin (mTOR) pathways or hypoxia induced factor (HIF). Once activated, those can cause an extreme upregulation of transcription of

several genes which encode key enzymes taking place in glycolysis and glutaminolysis pathways, which are two major pathways in cancer cell energetic metabolism [21]. On the other hand, tumor suppressors like p53, retinoblastoma (RB), Bax or phosphatase and tensin homolog (PTEN), which control cell cycle, apoptosis, signal transduction to inhibit cell proliferation and DNA repair, are usually bypassed in cancer cells [22].

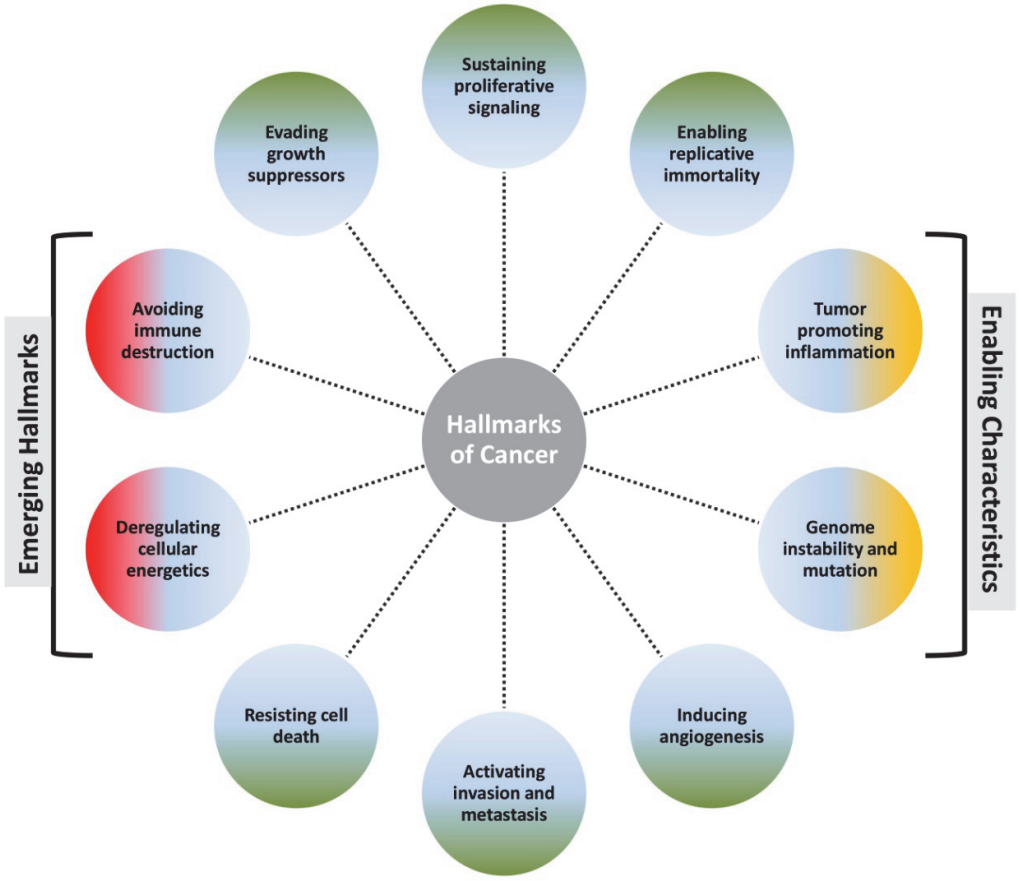

Figure 2.1. Hallmarks of cancer

This illustration depicts hallmarks of cancer that are main capabilities required for multistep tumor development and malignancy. In the light of intense research conducted in the last decade, two more capabilities that cancer cells acquire were defined as emerging hallmarks. Deregulating cellular energetic; that is metabolic reprogramming, is an emerging hallmark and it is a promising target for the treatment of cancer since malignant cells exhibits abnormal use of metabolic pathways in order to sustain their energetic needs. Besides that, also two enabling characteristics are depicted, which facilitate cancer cells to acquire both core and emerging hallmarks. The figure is adapted from Hanahan, D. and Weinberg R.A., Hallmarks of cancer: the next generation. Cell, 2011. 144(5): p. 646-74, Copyright© 2011, with permission from Elsevier.

Alterations in oncogenes and tumor suppressor genes have been observed in the majority of cancers; however, cancer cells also require infinite proliferation potential for the tumor formation. After a certain number of cell divisions, normal human somatic cells enter to a quiescent state named cellular senescence where the cells are non-proliferative as no active DNA replication takes place. Those cells, eventually, enter to another state called crisis where the cell death is observed [23]. Nevertheless, enabling replicative immortality is one of the key hallmarks of cancer cells where the cells acquire continuous proliferation potential thanks to the telomerase enzyme which plays an important role in the resistance to the induction of both senescence and crisis [24]. Telomerase is the enzyme which is responsible for the extending the end of the chromosomes in cell replication and in healthy adults it is active only in germ cells, and some type of stem cells, such as embryonic stem cells and certain white blood cells [25]. However, malignant cells are reported to show an upregulation of telomerase expression [26].

Angiogenesis is Induced to Support Tumor Progression: Normal tissues require an intake of nutrients and oxygen together with continuous evacuation of the metabolic wastes and carbon dioxide in order to sustain their nature. Neoplastic cells, due to their ability to proliferate uncontrollably and infinitely, have the same requirements but in higher rates. During tumor progression, angiogenesis, the development of a new and more extensive local vasculature, is imperative to be created for the sustenance of the cells. In adults, the mechanisms of vasculogenesis (the formation of new tubes) and angiogenesis (sprouting) of new vessels from preexisting ones are quiescent except that they are switched on as part of some physiologic processes such as wound healing. In tumors, however, the angiogenic switch is almost always on to sustain massive neoplastic growth [27]. It has been reported that angiogenic process is the result of a balance between pro- and anti-angiogenic signals. These signals activate angiogenesis inducers, such as vascular endothelial grosth factor-A (VEGF-A), which is the gene that encodes the main ligand involved in the formation of new blood vessel [28].

Cancer cells have active invasion and metastasis mechanisms: The cancer cells are not content only with above described hallmarks and as part of their immortality, they are capable of spreading to the parts of the body other than their origin in a process of

invasion and metastasis. This is a multistep process that starts with the biological change of the cells. Then, local invasion begins and the intravasation by cancer cells into nearby blood and lymphatic vessels takes place. These cancer cells are transited through the lymphatic and hematogenous system to escape into the parenchyma of distant tissues (extravasation). At the new destination, they form small nodules of cancer cells (micrometastasis), which finally ends up in growth of macroscopic tumors (colonization) [29]. Through this process, cancer cells undergo several alterations including their shapes and attachment abilities to the other cells or extracellular matrix (ECM). Of note, E-cadherin and β-catenin, important cell-to-cell adhesion molecules and metastasis markers as well, have been reported by several researchers to be downregulated or inactivated by mutation in human carcinomas [30-32].

When Hanahan and Weinberg first put the common characteristics shared among various cancer types together in 2000, they pointed out six hallmarks which are enumerated above [14]. These are acquired functional characteristics that allow tumor cells to survive, proliferate and disseminate and they are gained in various cancer types with different mechanisms and at different times during tumor formation. Nevertheless, when they reviewed their study in 2011 in the light of the intensive research in cancer over the last years, they suggested two common enabling characteristics which are considered to be necessary to make the acquisition of these characteristics possible and two new emerging hallmarks of cancer (see figure 2.1) [15].

The most prominent enabling characteristic is the development of genomic instability in cancer cells due to some defects affecting DNA maintenance machinery. This instability generates random mutations involving chromosomal rearrangements which lead to rare genetic changes, such as over-expression of telomerase, that can take place in the acquisition of hallmark capabilities [15]. On the other hand, heritable phenotypes such as inactivation of tumor suppressor genes or activation of oncogenes, may also occur via epigenetic mechanisms such as DNA methylation or histone modification and cells with these acquired phenotypes exhibit selective advantages on neighboring cells, enabling infinite proliferation and other tumor characteristics [33, 34]. The other enabling characteristic is the inflammatory state of precancerous and cancerous tissues which is induced by immune system and this may contribute to cancer formation in different

ways [15, 35]. In fact, inflammation can lead to acquisition of several hallmarks since it provides tumor microenvironment with bioactive molecules, such as growth factors, survival factors, proangiogenic factors and inductive signals in order to sustain proliferative signaling, to facilitate angiogenesis, invasion and metastasis and to activate the epithelial-mesenchimal transition [36].

Besides enabling characteristics, evading immune destruction has been pointed out as an emerging hallmark of cancer. The cancer cells are capable of evading both the innate and adaptive arms of immune system, which are responsible for detection and elimination of the vast majority of incipient cancer cells and nascent tumors. Even though this mechanism is still not very clear, there are several factors that aid cancer cells to evade immune system. Cancer cells secrete abundant tumor growth factor-β (TGF-β) which converts the regulatory immune cells to suppressive forms. Also, defective antigen presentation, immune suppressive mediators, tolerance and immune deviation and apoptosis of cytotoxic T cells are among the main scenarios helping cancer cells to overcome immune system [37].

The second emerging hallmark is the reprogramming in cancer cell metabolism. Cancer cells have a different metabolism than normal cells and several types of cancer are characterized by specific metabolic alterations [19]. That is, they must reorganize their energy metabolism in order to maintain uncontrolled cell proliferation, which is the main characteristic of cancer cells [18, 38]. Moreover, the microenvironment of cancer cells is different than that of healthy cells; thus, cancer cells must show quick adaptive responses to some stress conditions, such as hypoxia and nutrient restriction by changing their cellular bioenergetics [39]. The study of the tumor metabolic reprogramming taking place in cancer is the main topic of this dissertation; therefore, the essential characteristics of this hallmark are discussed in detail throughout the next section.

2.3. UNDERSTANDING CANCER METABOLISM

Metabolism is the sum of all the chemical transformations taking place within a living cell or organism, which occurs through a series of enzyme-catalyzed reactions that constitute metabolic pathways. These pathways allow organisms to grow and reproduce, maintain their structures, and respond to their environments. In order to carry out these cellular functions, all the cells require certain amount of nutrients and oxygen. Nutrients can either undergo the degradative phase of the metabolism in which organic nutrient molecules (carbohydrates, fats, and proteins) are converted into smaller, simpler end products (such as lactic acid, CO_2, NH_3) and energy with a process called catabolism or they are used to built up larger and more complex molecules (such as lipids, polysaccharides, proteins and nucleic acids) with means of anabolism or biosynthesis.

To understand cancer, metabolism knowledge has always played a crucial role. At present, there are more than 16,000 metabolites and over 8,500 reactions defined in the Kyoto Encyclopedia of Genes and Genomes (http://www.genome.jp/kegg/pathway.html). Most of these metabolic reactions were discovered in the first half of 20^{th} century, including that several decades ago, German physiologist Otto Warburg has described so-called term “aerobic glycolysis” in which, cancer cells rather metabolizing glucose with an oxygen independent way even in the presence of excess oxygen [40-44]. This phenomenon is widely called as the “Warburg effect” in scientific world. Why tumor cells undergo this dramatic shift has become the key question of the cancer research, yet this was just the starting. Since cancer is a very complex and multifactorial disease [45], over many years, the altered cancer metabolism has lost the interest of researchers and the solution to cancer has been sought in large and complex projects, mostly focusing on the activation of primary proliferative and survival signals. Thanks to this approach, the roles of the majority of oncogenes and tumor suppressor genes, and their proteins, involved in signal transduction pathways, proliferation, survival and anti-apoptotic processes in carcinogenesis have been widely elucidated. Also, high throughput technology has revealed new metabolites and the connections between pathways that were not possible to predict by conventional

biochemistry [46] and in that way, relevance of metabolism to all other cellular processes has become a current awareness. Now, it is time to revisit the Warburg's original and simple metabolic hypothesis for cancer as it can really be the Achilles' heel of the cancer [44, 47].

2.3.1. An Emerging Hallmark: Tumor Metabolic Reprogramming

Proliferating cells have higher needs of nutrients to both maintain their metabolic balance and generate a daughter cell. Due to their highly proliferative nature, cancer cells often rewire the role of metabolism for growth and proliferation [18]. Tumor cells also, rely on metabolic reprogramming to proliferate and achieve a fully malignant phenotype. Energy and macromolecule demand must be satisfied by cell metabolism in order to provide cancer cells with ATP and building blocks [15, 48]. The prominent characteristics in metabolic reprogramming of cancer include enhanced glycolysis and pentose phosphate pathway (PPP), upregulation of the lipid and aminoacid metabolism, augmented mitochondrial biogenesis, elevated glutamine metabolism and macromolecule synthesis [48]. Figure 2.2 outlines the key reactions that often take place in metabolic reprogramming.

With the inspiration taken from Hanahan and Weinberg, Pavlova and Thompson have outlined the emerging hallmarks of cancer metabolic reprogramming, which are the main metabolic changes observed in many cancer types, if not all [38]. These metabolic characteristics are shown in figure 2.3.

During malignant transformation most of the components of the signaling pathways that control proliferation, survival and metabolic network remain intact. However, an extracellular stimulation is required by non-tumor cells for the initiation of signaling while cancer cells often contain mutations that trigger a sustained activation of the signaling process [49]. These signaling pathways lead cancer cells to reorganize their metabolism in order to fulfill energetic and bioenergetic requirements. Healthy cells do not import metabolites constantly even when they are in nutrient rich environments.

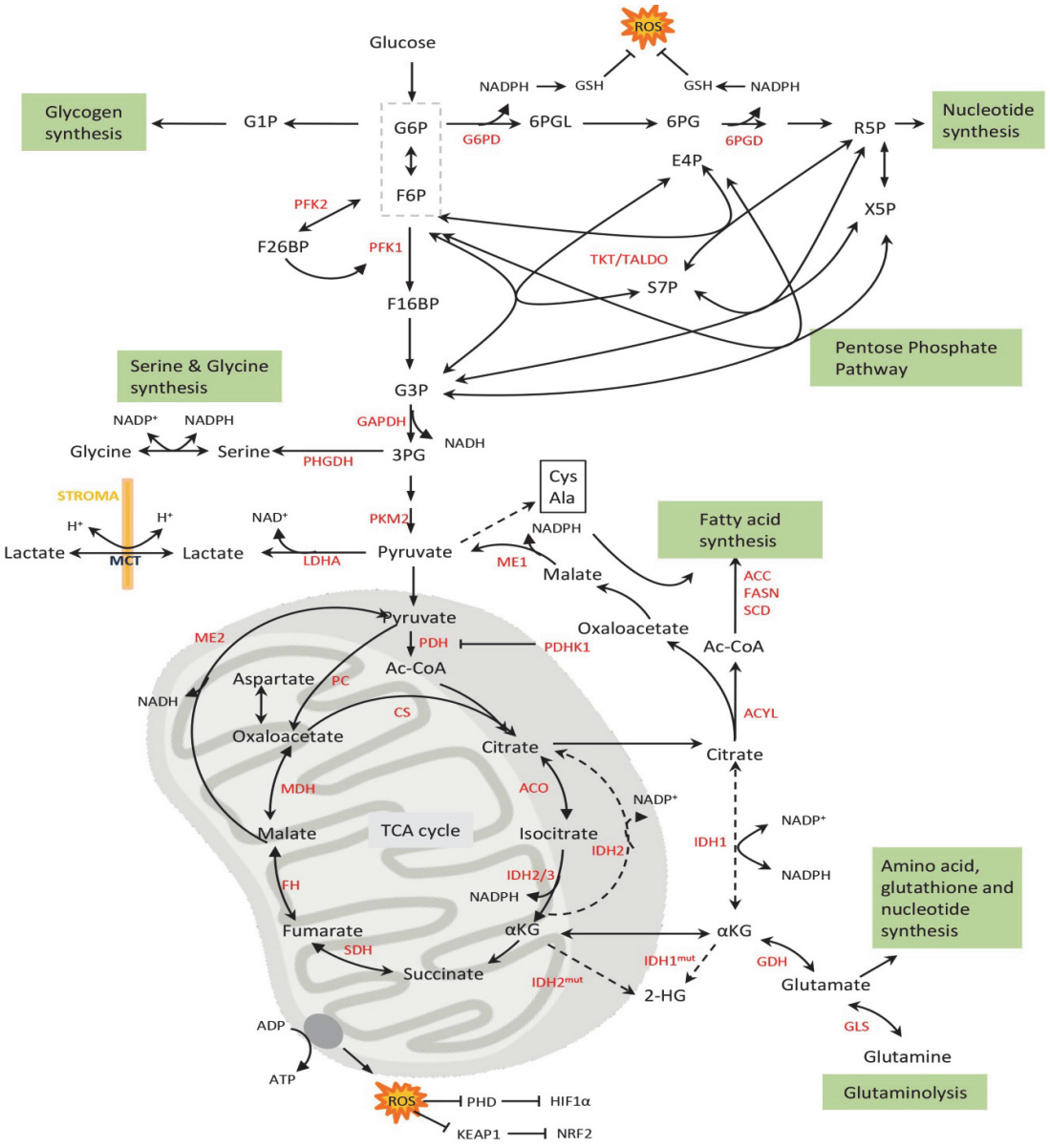

Figure 2.2 Main metabolic pathways involved in tumor metabolic reprogramming

The image outlines the major metabolic pathways involved in the synthesis of macromolecules: The enzymes involved in these pathways are shown in red. Reductive carboxylation of α-KG by IDH1 and IDH2 produces citrate for lipid synthesis. ACC, acetyl-CoA carboxylase; ACYL, ATP citrate lyase; ACO, aconitase; Ac-CoA, acetyl coenzyme A; CS, citrate synthase; E4P, erytrose-4-phosphate; FASN, fatty acid synthase; F1,6BP, fructose-1,6-bisphosphate; F2,6BP, fructose-2,6-bisphosphate; F6P, fructose-6-phosphate; FH, fumarate hydratase; GAPDH, glyceraldehyde-3-phosphate dehydrogenase; GLS, glutaminase; GDH, glutamate dehydrogenase; GSH, glutathione; G1P, glucose-1-phosphate; G3P, glyceraldehyde-3-phosphate; G6P, glucose-6-phosphate; G6PD, glucose-6-phosphate dehydrogenase; IDH, isocitrate dehydrogenase; HIF, hypoxia inducible factor; KEAP1, kelch-like ECH-associated protein 1; LDHA, lactate dehydrogenase A; MCT, monocarboxylate transporters; MDH, malate dehydrogenase; ME,

Malignant cells, on the contrary, have a constant influx of certain metabolites, especially glucose and glutamine, due to the genetic alterations in key oncogenes, such as PI3K/Akt, mTOR1, and c-myc or in the negative regulators such as RB and PTEN [50, 51]. Defective growth factor signaling in cancer cells ends up in elevated expression of plasma membrane glucose transporter, GLUT1, and hexokinase (HK) which is the first enzyme of the glycolytic pathway [52]. In the same way, glutamine uptake is facilitated via transporters coupled to increased glutaminase (GLS) activity, as after conversion to glutamate by GLS, it cannot exit the cell [53]. Besides this, cancer cells, under scarce nutrient conditions, may use of opportunistic nutrient acquisitions. When free amino acids are not available in cells' environment, cancer cells may recover amino acids via macropinocytosis of extracellular proteins, entosis of living cells or phagocytosis of apoptotic bodies [54, 55].

Another emerging hallmark of tumor metabolism is the higher demand of cancer cells for nitrogen which is mostly generated from amino acids [56]. The high demand of nitrogen is to fulfill the requirement of producing several macromolecules; such as nucleotides, non essential amino acids and polyamines so as to keep cancer cells proliferating.

Growth signals play a pivotal role in cancer cell metabolism; however, metabolic networks of cancer cells also transmit the information about the cellular metabolic state to various regulatory enzymes, so that they change epigenetic marks from chromatin. For example, activation of oncogens in tumor cells alters also metabolite driven gene regulation and it has been reported that activated Akt signaling leads to increased total histone acetylation [57]. Methylations, butyrylation or gain of function mutations can head neoplasma to similar epigenetic variations [58].

malic enzyme; NRF2, nuclear factor (erythroid-derived 2)-like 2; PC, pyruvate carboxylase; PDH, pyruvate dehydrogenase; PDHK1, pyruvate dehydrogenase kinase; PFK, phosphofructokinase; PHD, prolyl hydroxylases; PHGDH, phosphoglycerate dehydrogenase; PKM2, pyruvate kinase M2; R5P, ribose-5-phosphate; ROS, reactive oxygen species; S7P, sedoheptulose-7-phosphate; SCD, stearoyl-CoA desaturase; SDH, succinate dehydrogenase; TKT, transketolase; TALDO, transaldolase; X5P, xylulose-5-phosphate; 3PG, 3 phosphoglyceride; 6PGL, 6-phosphoglucanolactone; 6PG, 6-phosphogluconate; 6PGD, 6-phosphogluconate dehydrogenase.

In order to comprehend better the cancer cell metabolism and be able to compare it from the metabolism of noncancerous cells in order to get a better understanding of tumor metabolic rewiring, the major elements of the central carbon metabolism are elaborated in next sections.

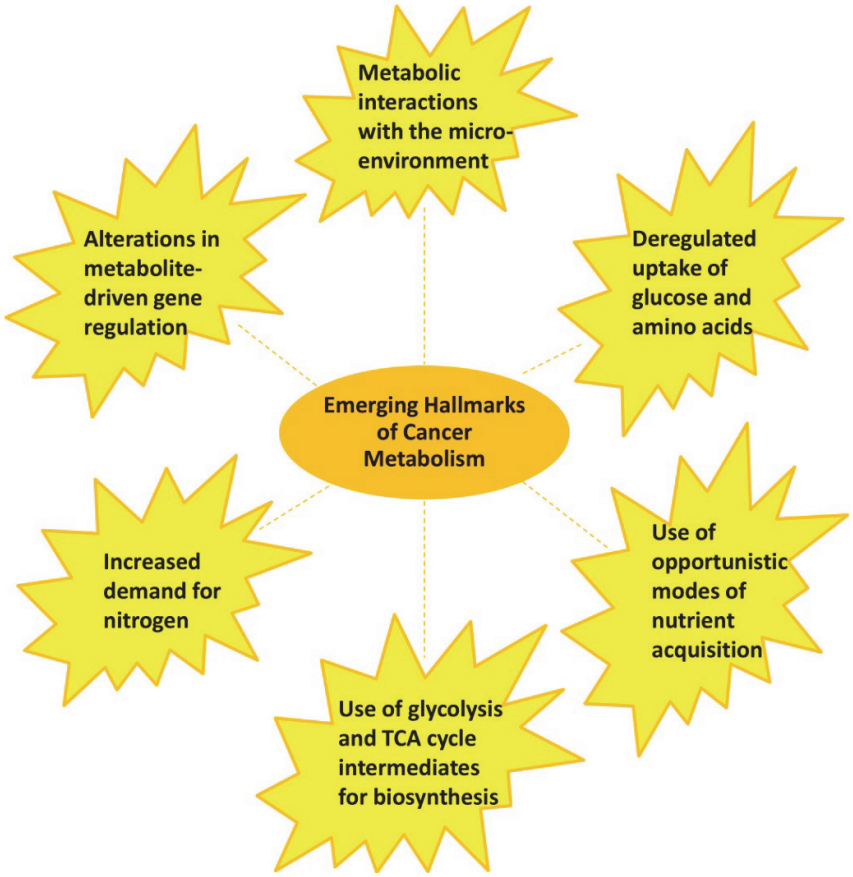

Figure 2.3. The Emerging Hallmarks of Cancer Metabolism

An emerging hallmark of cancer, metabolic reprogramming, has been identified as a strong and promising target in cancer therapy. Cancer cells utilize excess amount of nutrients to maintain its viability and proliferate. Cancer associated metabolic reprogramming accompanied to alterations in intracellular and extracellular metabolites has deep effects on various cellular process including gene expression, cellular differentiation, and tumor microenvironment. This illustration depicts the known cancer associated metabolic changes. Many of them are common in various tumors.

2.3.2. Glycolysis and Learnings from Warburg

The biochemical pathways explained in textbooks often contradicts with the metabolism of proliferating cells, including cancer cells [59]. As mentioned above, contrary to

healthy cells, neoplastic cells predominantly produce energy via enhanced glucose fermentation even in the presence of sufficient oxygen to support mitochondrial oxidative phosphorylation (OXPHOS) [60]. Of note, the amount of ATP produced per molecule of glucose catabolised through glycolysis is far less efficient compared to OXPHOS (2 versus 36, respectively) [61]. Even though the reasons of enhanced glycolysis observed in cancer cells are not fully elucidated, there are several recent works proposing noteworthy explanations [62, 63]. Four decades ago, it was reported that not ATP production but ATP consumption is actually limiting glycolysis in proliferating cells, since glycolytic enzymes, such as phophofructokinase, may be inhibited with elevated ATP levels [64]. Contrary to what was believed by Warburg [65] and many subsequent investigators, aerobic glycolysis does not take place because of inefficient or damaged mitochondria in cancer cells. In fact, it has been recently demonstrated that cancer cells with depleted mitochondrial DNA show reduced tumorigenic potential both in vivo and in vitro [66]. Also, in cancer cells, further activation of pyruvate dehydrogenase (PDH) by inhibiting PDH kinase (PDK) with a specific inhibitor leads to elevated OXPHOS [67], which proves that cancer cells do not have defective mitochondria. However, in malignant cells mitochondria are used less actively than in healthy cells. The reason behind that cancer cells use a less efficient metabolic pathway despite their intense need of growing and proliferating is now in the major focus: Use of glycolytic and TCA cycle intermediates for biosynthesis and production of NADPH which is a reducing equivalent for lipid synthesis and reactive oxygen species (ROS) detoxification. In order to understand why cancer cells prefer aerobic glycolysis, it is imperative to consider the specific requirements of a cancer cell and the purpose of cell metabolism as a whole. In order to proliferate continuously, the vast amounts of various macromolecules are needed and these molecules are derived from the intermediates of central carbon metabolism. To avoid excess ATP production, which allostericly regulates carbon metabolism, cancer cells go through aerobic glycolysis; so that they can maximize the flux of carbon into macromolecular synthetic pathways and NADPH production [59, 68-71].

On the other hand, cancer cells need reprogramming their microenvironment to assist tumor growth and dissemination. The excess lactate generation with the subsequent

acidification of extracellular matrix favors tumors invasion due to the pH dependent activation of some proteins that degrade extracellular matrixes and membranes [47, 72]. Furthermore, Warburg effect may lead cancer cells to avoid apoptosis, which is one of the cancer hallmarks, since it is reported that enhanced mitochondrial metabolism induces apoptosis [67]; therefore, less actively used mitochondria will produce fewer sources of apoptotic stimuli.

Nowadays, Warburg effect has been demonstrated in various cancer types and has successfully formed the basis of tumor diagnosis and staging via positron emission tomography (PET)-based imaging of the uptake of radioactive fluorine-labeled glucose analog, ^{18}F-fluorodeoxyglucose (^{18}F-FDG) [73]. In this method, malignant tissues are detected via imaging as they consume much more glucose than healthy tissue.

2.3.3. Pentose Phosphate Pathway

Glycolysis forms the backbone of central carbon metabolism; however, proliferating cells also rely highly on pentose phosphate pathway (PPP) in order to synthesize nucleotides for DNA replication and RNA production. PPP provides an alternative pathway to glycolysis for the metabolism of glucose, and the percentage of glucose metabolized through PPP is known to vary from 5 to 30 % depending on the tissue type [74]. Both DNA and RNA are polymers of nucleotides, which consist of a five-carbon sugar (ribose or deoxyribose), a nitrogen containing base and a phosphate group. Of these, five carbon sugars, which are also called pentoses, are mainly synthesized through the PPP; therefore this pathway is essentially important for nucleotide synthesis. Furthermore, PPP also produces the reducing equivalents, NADPH, which not only is involved in the regulation of reactive oxygen species through the maintenance of reduced glutathione (GSH) pool, but also serves as a cofactor in biosynthesis of several essential macromolecules; such as lipids and amino acids. Therefore, in tissues with higher lipid synthesis; such as liver and white adipose tissue, PPP rate might be even more elevated. [18, 75, 76]. Besides serving as a crucial pathway for the biosynthesis and the maintenance of redox status, PPP also plays important roles in various aspects

related to cancer cells viability, including proliferation, apoptosis, invasiveness, drug resistance, and metastasis [74, 77]. Because of all these important aspects, cancer cells are known to be significantly dependent on PPP to maintain their highly proliferative state [76, 78, 79]. The relation between elevated PPP and tumor proliferation has been studied widely, since PPP mediates cancer cells to meet their anabolic needs together with overcoming oxidative stress [80].

PPP consists of two different branches that converge in the production of ribose-5-phosphate, which is essential for the synthesis of nucleotides (figure 2.4). The oxidative phase of PPP (ox-PPP) is a non-reversible metabolic pathway and it starts with the transformation of glucose-6-phosphate (G6P) into 6-phosphoglucono-δ-lactone, which is a cyclic and unstable lactone ester of phosphogluconic acid. This reaction is catalyzed by glucose-6-phosphate dehydrogenase (G6PD) enzyme. G6PD catalyzes the rate-limiting step in the ox-PPP that generates the first molecule of NADPH; so its expression and activity are tightly regulated. $NADP^+$/NADPH ratio plays a key role in the regulation of the activity of this enzyme and when this ratio is low, G6PD stability is negatively affected [74, 81, 82]. In healthy cells, G6PD usually works at 1-2 % of its maximal potential as NADPH concentration in quiescent condition is high. However, similar to the tissues with active metabolism; such as, liver, adipose or mammary glands, tumor cells, including breast cancer cells, are reported to have high levels of G6PD since cancer cells have a higher consumption of NADPH compared to quiescent cells [83-85]. On the other hand, NADPH produced via G6PD is also used in lipid synthesis and it has been reported that palmitoyl-CoA, a lipogenesis intermediate, also takes place in down-regulation of this enzyme as a directly binding cofactor [86, 87]. Of note, G6PD deficiency is a very common enzymopathy which affects more than 400 million people in the world [82]. In these cases, decrease in NADPH production leads to decrease in cholesterol and fatty acid synthesis [88], together with less ROS detoxification activity [82].

Due to its fundamental activity in the cells for pentose and NADPH production, there is no doubt that PPP is also regulated by other oncogenes and tumor suppresser genes. K-Ras (which is a subfamily of Ras) and PI3K, one of the most frequently activated oncogenes, increase the activity of G6PD [89]; whereas, tumor suppressor gene p53 downregulates G6PD activity by decreasing its stability upon directly binding to it [90].

Moreover, transcription factors taking place in response to cellular stress, such as Nuclear factor (erythroid-derived 2)-like 2 (NRF2), have also reported to regulate G6PD activity [91]. NRF2 plays a key role in tumorigenesis and it is usually upregulated in several cancer types which in turn overactivates its target genes; such as G6PD, malic enzyme 1 (ME1) and isocitrate dehydrogense 1 (IDH1) [87, 91, 92].

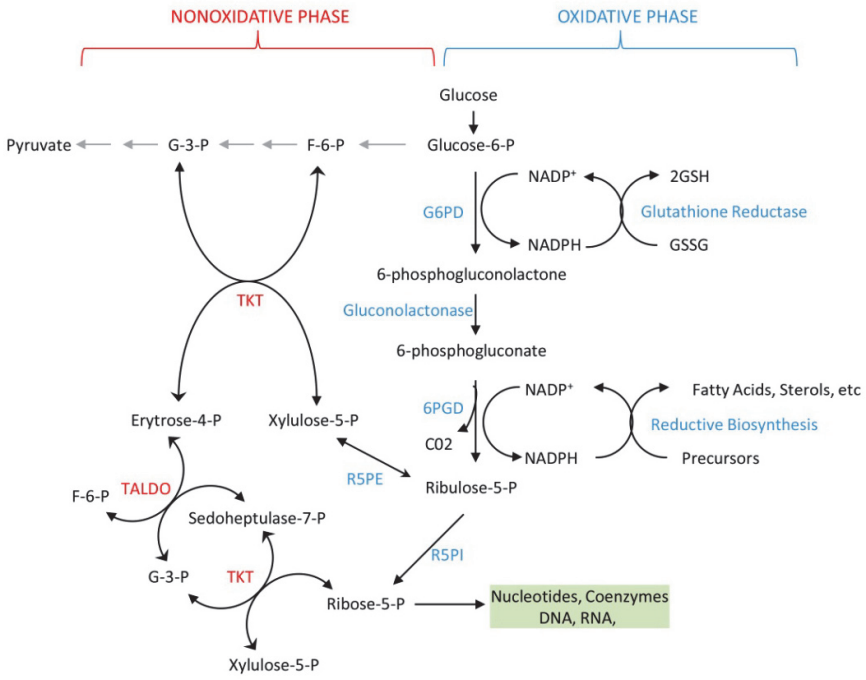

Figure 2.4. Outline of Pentose Phosphate Pathway

The irreversible ox-PPP phase is catalyzed by G6PD, 6PGL (not shown) and 6PGD (6-phosphogluconate dehydrogenase). This phase produces NADPH, used for ROS detoxification and synthesize fatty acids. The reversible nonoxidative pathway takes role a carbon exchange between PPP and glycolysis, either recycling the excess of pentoses or synthesizing ribose from glycolytic intermediates. The main enzymes involved in this branch are TKT and TALDO. CO_2, carbondioxide; E-4-P, erytrose-4-phosphate; F-6-P, fructose-6-phosphate; GSH, glutathione; GSSG, glutathione disulfide, G-3-P, glyceraldehyde-3-phosphate; G-6-P, glucose-6-phosphate; G6PD, glucose-6-phosphate dehydrogenase; NADPH, Nicotinamide adenine dinucleotide phosphate; R-5-P, ribose-5-phosphate; R5PI, ribulose-5-phosphate isomerase; R5PE, ribulose-5-phosphate epimerase; S-7-P, sedoheptulose-7-phosphate; TKT, transketolase; TALDO, transaldolase; X-5-P, xylulose-5-phosphate; 6PGD, 6-phosphogluconate dehydrogenase.

In the next step of ox-PPP, 6-phosphoglucono-δ-lactone is converted to 6-phosphogluconate by 6-phosphogluconolactonase (6PGL), the second enzyme of ox-PPP. Ultimately, 6-phosphogluconate is transformed to ribulose-5-phosphate by 6-phosphogluconate dehydrogenase (6PGD) with concomitant production of NADPH and CO_2. [87]. 6PGD is also an excellent target since it plays an important role in both the synthesis of nucleotides and the generation of NADPH required for ROS detoxification [93]. The importance of 6PGD had till now been overshadowed by G6PD and TKT (nonox-PPP enzyme) [84, 94], but recent evidences suggest that G6PD alone has minimal effect on tumor growth of HepG2 and Non-Small cell lung cancer cell lines cells in-vitro [95, 96]. Moreover, Chan *et al.* reported that 6PGD has role in cancer cell migration and c-Met (a tyrosine kinase receptor) signaling, since they observed that reducing the activity of 6PGD in cancer cells downregulated c-Met receptor activation and cell migration, in turn [97]. That is, new promising evidences which highlight the potential of 6PGD as a promising therapeutic target in certain forms of cancer have emerged [96, 98].

Ribulose-5-phosphate resulted in ox-PPP is then converted to ribose-5-phosphate by ribulose-5-phosphate isomerase (RPI) or to xylulose-5-phosphate by ribulose-5-phosphate epimerase (RPE), which are the enzymes of non-oxidative phase of PPP (nonox-PPP). Ribose-5-phosphate can further be used for nucleotide synthesis. Nonox-PPP consists of a set of reversible reactions in which ribose-5-phosphate and xylulose-5-phosphate are converted to glyceraldehyde-3-phosphate (G3P) and fructose-6-phosphate (F6P) producing several different carbon length sugar phosphates as intermediates by the main nonon-PPP enzymes, transketolase (TKT) and transaldolase (TALDO). G3P and F6P are then cycled into glycolysis [74, 79, 87] (Figure 2.4). Of note, two isoforms of transketolase has been identified, namely, transketolase (TKT) and transketolase-like-1 (TKTL1) [99] and it is worth noting that a recent study has demonstrated that HIF-1 activation induces TKTL1, the rate-limiting enzymes of non-oxidative phase of PPP, in human colorectal cancer [100].

Among two phases of PPP, ox-PPP is especially interesting because it is able to produce NADPH, and therefore it also plays a key role in the scavenging of ROS levels. The balance between ROS production and removal has been demonstrated to be altered in

some tumors, and has also been proposed to be an attractive therapeutic target on its own [101]. On the other hand, the pivotal role of G6PD in proliferation and survival has been the interest of various scientists in the field and in many studies it has been pointed as a promising target [77, 80, 102].

2.3.4. Mitochondrial Metabolism

Mitochondria are cellular organelles involved in several cellular processes, among which are the oxidation of nutrients into carbon dioxide through the tricarboxylic acid cycle (TCA cycle or Krebs Cycle) regulation of metabolic flux, modulation of redox status of the cells, contribution to biosynthesis of lipids and initiation of apoptosis [103-106]. Increased mitochondrial biogenesis is advantageous for cancer cells [48] and alterations in mitochondrial function may lead to several anomalies including cardiovascular dysfunction, neurodegenerative disorders and cancer [104, 107].

Oxidative phosphorylation (OXPHOS) is a metabolic pathway in which the respiratory enzymes of mitochondria are used to oxidize nutrients in order to produce energy in the form of ATP. In healthy cells, when oxygen is present, OXPHOS is the most efficient mechanism to synthesize ATP [108]. OXPHOS takes place with oxidation of reduced nicotinamide adenine dinucleotide (NADH) and flavin adenine dinucleotide ($FADH_2$), which are produced in TCA cycle, through the electron transport chain (ETC). The ETC is located in the inner membrane of the mitochondria and is composed of four complexes (I to IV) which are responsible for the oxidation of the reducing equivalents in the form of NADH and $FADH_2$ together with reduction of O_2 (the final electron acceptor) to H_2O. During this process, the protons are pumped into the inner membrane space of mitochondria and this result in a proton gradient that is used by ATPase (complex V) to synthesize ATP [109].

Especially when the cells prefer aerobic glycolysis, the cells must activate an influx of carbons for anaplerotic reactions in order to sustain TCA cycle function since it is used as a hub of macromolecule precursors [110]. For example, the export of citrate for lipid synthesis is a crucial function of mitochondria or TCA cycle as Ac-CoA derived from

citrate is the main source of lipid formation. Several mechanisms exist to support anaplerotic activity of the cells among them pyruvate carboxylase (PC) which converts pyruvate to oxaloacetate (OAA), a TCA cycle intermediate.

Genetic studies have revealed that various mutations in the genes that encode the TCA cycle enzymes; such as, citrate synthase (CS), aconitase, isocitrate dehydrogenase (IDH), succinate dehydrogenase (SDH) and fumarate hydratase (FH) leads to a nonfunctional TCA cycle, which is associated to some tumor types [111-113]. Besides, SDH and FH have been reported to be important tumor suppressor genes [114].

Mitochondria have two major nutrient inputs: pyruvate, which enters to TCA cycle after its conversion to Ac-CoA, derived mostly from glucose via glycolysis and glutamine which is integrated into TCA cycle by conversion to alpha-ketoglutarate (αKG) [115]. Despite that dysfunctional mitochondria was believed to be a characteristic of tumor cells and that was leading them to aerobic glycolysis, recent studies revealed that cancer cells have fully functional mitochondria and that mitochondria are important parts of cancer cell metabolism [104]. Cancer cells often switch their bioenergetic requirements from OXPHOS to glycolysis for several reasons [116] and since glucose is mostly used in aerobic glycolysis, glutamine becomes the major substrate required for sustaining TCA cycle in order to produce precursor for biosynthesis of macromolecules. Thus, it will be useful also to elaborate the glutamine metabolism.

2.3.4.1. Glutamine Metabolism

Glutamine is a non-essential amino acid which has several cellular functions including donation of nitrogen for nucleotide and protein synthesis, energy production and lipid synthesis, and production of some other non-essential amino acids [117-119]. It is the most abundant amino acid and it is consumed at much higher rates than other amino acids by cancer cells [117, 120]. Even though glutamine is not an essential amino acids, it has vital importance for proliferation and viability of several tumor cells which have addiction to glutamine [121]. In 1955, it was first discovered that proliferating cells could not maintain their viability in the absence of glutamine [122]. Then, glutamine was

observed to be consumed more than other amino acids by certain cancer cells and that the carbon dioxide that is released by cells may carry carbon atoms from glutamine [123]. Ultimately, recent studies revealed that many cancer cells, including some breast cancer cells, exhibit glutamine addiction habits, which is reliance on glutamine as the source of energy rather than glucose [124]. That is, glutamine is switched from a nonessential to essential amino acid and this is particularly interesting since glutamine is a nonessential amino acid that can be synthesized from glucose. The role of glutamine in cell metabolism has been widely explored in recent decade [125, 126].

Proliferating cells require nitrogen to synthesize nucleotides and nonessential amino acids; therefore, it is clear that the most important function of glutamine is to provide cells with nitrogen for protein and nucleotide synthesis. Glutamine is first converted to glutamate by deamination reaction catalyzed by glutaminase (GLS) which is a key enzyme in regulation of glutamine metabolism and it is pointed to be a promising target in cancer therapy [127]. Glutamate can either be used as a precursor of GSH and non-essential amino acids, such as, aspartate, proline, alanine and arginine or is converted to αKG by glutamate dehdrogenase (GDH) or transaminases to foster the TCA cycle (Figure 2.2). αKG is further oxidized to malate and might leave the TCA cycle through conversion to pyruvate by malic enzyme (ME) which also produces NADPH [125]. When glutamine is oxidized to pyruvate, the derived NADPH allows tumor cells to reduce the ROS associated with mitochondrial respiration and rapid cell proliferation. In addition, glutamine oxidation, as an alternative to glycolysis, provides tumor cells with the precursors for major anaplerotic processes, such as TCA cycle intermediates, to fulfill their bioenergetic and metabolic needs.

As an alternative to oxidative metabolism, glutamine can also go through the reductive carboxylation, in which αKG derived from glutamine is directly converted to citrate by IDH reversible reaction, especially to sustain cell growth under hypoxic conditions or when the mitochondrial respiration is impaired [115, 128-132]. The cytosolic $NADP^+$ dependent isoform of isocitrate dehdyrogenase (IDH1) is the main enzyme catalyzing this reaction; however, IDH2 (mitochondrial isoform) can also carry out reductive carboxylation also in $NADP^+$ dependent manner [128]. In fact, the reductive carboxylation of glutamine allows cells to produce Ac-CoA for biosynthesis of lipids in a

glucose-independent pattern, so that, the glucose can be conserved for the biosynthesis of precursors which are specifically generated from glucose [128].

2.3.5. Amino Acid Metabolism

Amino acids are organic molecules which consist of a specific side chain and both amino and carboxyl groups which allow them to form proteins by polymerization reactions. They can also be used as a source of carbon and nitrogen for biosynthesis. 20 different amino acids are defined and among them 11 are non-essential amino acids which means that they can be synthesized by our cells while the rest are essential and they must be supplied by dietary intake. The essential roles of glutamine in cancer cell metabolism has already been discussed in the previous section but it is worth noting that there are other amino acids that also have vital role in proliferative metabolism and are required for cell survival [133, 134]. Non-essential amino acids can be produced from glycolytic intermediates, such as serine synthesis from 3-phosphoglycerate or alanine synthesis from pyruvate. Serine can further generate cystein and glycine [133]. Similarly, TCA cycle intermediates are also used to synthesize non-essential amino acids. For example, aspartate, aspargine and glutamate are synthesized from OAA and αKG. Also, glutamate takes role in arginine synthesis via urea cycle [135].

Tumor cells, due to their highly proliferative nature, consume amino acids from external sources because their capacity of endogenous synthesis is not sufficient to comply their elevated needs to amino acids [136]. Of note, four amino acid transporters (SLC1A5. SLC7A5, SLC7A11 and SLC6A14) have been reported to be over expressed in tumor cells and in that way, they increase the amino acid uptake to fulfill their elevated needs [136]. On the other hand, in cancer cells, some amino acids are consumed far beyond the need for protein synthesis, thus, it can be assumed that they are used as the metabolic intermediates to form other amino acids or to take role in other biosynthetic pathways. To illustrate, glutamine and aspartate are needed for nucleotide biosynthesis and glutamate also takes role in urea cycle [133].

Recently, it has been reported that non-essential amino acids serine and glycine support tumor growth since serine and glycine are required for one-carbon metabolism, generation of precursors for lipid biosynthesis, proteins and nucleotide, reduction of the ROS and methylation of proteins and nucleic acids [137, 138]. Serine is reversibly converted to glycine by cytosolic or mitochondrial serine hydroxymthyltransferase (SHMT1 and SHMT2, respectively) and this reaction produces one-carbon units which enters to the tetrahydrofolate (THF) cycle [139]. A specific study revealed that inhibition of mitochondrial isoform SHMT2 decreased the proliferation rate of several rapidly proliferating cancer cell lines [134].

The importance of the amino acids in cellular metabolism can be further emphasized by understanding the amino acid sensing system that the cells develop through the mammalian target of rapamycin (mTOR) signaling in order to determine if sufficient amino acids are available for protein synthesis [140]. Rapamycin is an mTOR inhibitor which affects the protein synthesis, ribosome biogenesis, cell cycle arrest and autophagy in the same way as the amino acid starvation. Specifically, amino acids which are important nitrogen sources such as glutamine, leucine and arginine are key signaling molecules that activate mTOR pathway and in the situations of amino acid deficiency, mTOR is rapidly inhibited. mTOR inhibition due to deprivation of nitrogen leads cells to suppress protein biosynthesis and induce autophagy as a way to maintain a free amino acid pool for any further amino acid starvation [140-142].

2.3.6. Lipid Metabolism

Lipids are hydrophobic small molecules and contrary to many other large macromolecules (such as proteins, nucleic acids), they are not formed of several small homologous molecules linked by chemical bonds [143]. For all living organism, lipids are essential for maintaining the structure of the cells, providing energy and cellular signaling [144]. The signaling networks connected by lipid metabolism regulates not only the growth, survival, proliferation and differentiation of cells, but apoptosis, cell motility and membrane homeostasis as well [145]. Moreover, alterations in lipid metabolism can

lead to defects in membrane composition and permeability which could contribute to the development and progression of several diseases including some types of cancers [146].

Proliferating cells, including tumors, have high demands of fatty acids to maintain a constant supply of lipids. Fatty acids can be obtained from dietary sources or they can be biosynthesized in the cells. Tumor metabolic reprogramming involves an enhanced lipid biosynthesis since cancer cells need vast amount of lipids as building blocks for membrane formation due to their high proliferative nature. To this end, they upregulate many of the enzymes; such as fatty acid synthase (FASN), ATP citrate lyase (ACLY) and Ac-CoA carboxylase (ACC), involved in *de novo* fatty acid synthesis [147, 148]. Lipogenesis requires also NADPH; therefore, NADPH generated by conversion of oxaloacetate to pyruvate (by cytosolic isoform of malic enzyme) or oxidative phase of pentose phosphate pathway is used for synthesis of lipids. Lipid biosynthesis starts with the export of mitochondrial citrate to the cytosol, where it is converted to lipogenic precursor Ac-CoA and oxaloacetate by ACLY [149]. Then, Ac-CoA is converted to malonyl-CoA by ACC and both acetyl and malonyl groups are charged to the corresponding thiol groups of FASN. Fatty acid chain is formed by donation of two-carbon units of activated malonate (coupled to FASN), and at each step a molecule of CO_2 is released. In that way, after a cyclical series of reactions, long chain fatty acids are produced. The final product is a 16 carbon fatty acid, palmitate. Newly synthesized palmitate can be further elongated and desaturated through the action of elongases and desaturases [48, 146]. Of note, fatty acids can be degraded in mitochondria via a set of reactions called β-oxidation which produces large amount of ATP and ROS by oxidative phosphorylation [150].

2.3.7. Cell Metabolism Plays a Key Role in the Regulation of Redox Status, Cell Cycle and Apoptosis

Reactive oxygen species (ROS) are heterogeneous molecules with increased reactivity such as superoxide (O_2-), hydrogen peroxide (H_2O_2), hydroxyl radical (·OH) and singlet

oxygen ($^1O_2$) and are produced in all cells as normal metabolic by-products. The effect of ROS on cells depends on its concentration and low ROS concentrations are reported not only to contribute to cell survival and proliferation as it takes role in post translational modification of phosphatases and kinases [151, 152] but also to be required for homeostatic signaling events, cell differentiation and cell mediated immunity. While moderate ROS levels lead to the expression of some stress responsive genes involving HIF-1, which in turn triggers the expression of pro-survival proteins [153], high ROS levels may induce severe damages to several cellular macromolecules involving proteins, lipids, nuclear and mitochondrial DNA and cause induction of cell senescence or crisis [154]. High ROS levels may also lead permeabilisation of mitochondria which causes the release of cytochrome c and in turn, apoptosis [155]. Therefore, in order to prevent any irreversible cellular damage and restore redox homeostasis the ROS levels must be carefully controlled and this control is succeeded by modulation of the ROS generation and elimination of ROS by scavenging systems, such as, superoxide dismutases (SODs), nuclear factor (erythroid-derived 2)-like 2 (NRF2), catalases, glutathione peroxidases (GPXs) or peroxiredoxins (PRXs) (see figure 2.5) [156]. Each scavenger has a distinct mechanism, to illustrate, superoxide dismutase catalyze the dismutation of O2− into molecular oxygen (O2) and H2O2, and GPXs catalyze the reduction of H2O2 to water, by oxidizing reduced glutathione (GSH). Oxidized glutathione is reduced back by glutathione reductase using electrons from NADPH, which indicates the importance of NADPH for redox balance [157]. To remember, NADPH can be produced via several ways the most important of which are ox-PPP and ME ractions [41, 138]. This further emphasizes the importance of PPP for cancer cell survival and proliferation.

Due to their enhanced proliferation rates, malignant cells need to produce high levels of ATP which leads to the accumulation of ROS, thus, they have up-regulated antioxidant systems so as to ensure their survival [158]. The effects of ROS in cancer cell survival and proliferation has been studied widely and at low to moderate levels, ROS has been reported to induce tumorigenesis by promoting mutations in DNA or stimulating signaling molecules, such as mitogen-activated protein kinase (MAPK), extracellular signal-regulated kinase (ERK) or expression of cyclin D1, which promote tumor growth and survival [101, 159-161]. ROS, moreover, can reversibly inactivate some tumor

suppressor genes such as PTEN as it has redox-sensitive cysteine residues in their catalytic centre [162] On the other hand, since high ROS levels cause cell damage and death, malignant cells, particularly in the early stages of tumorigenesis need to fight against elevated ROS levels by mostly developing a stronger antioxidant mechanism to regulate ROS levels compatible with their metabolism. However, their ROS level remains higher than healthy cells [158, 163], thus targeting their increased antioxidant defense mechanisms may be used to selectively kill tumor and tumor initiating cells.

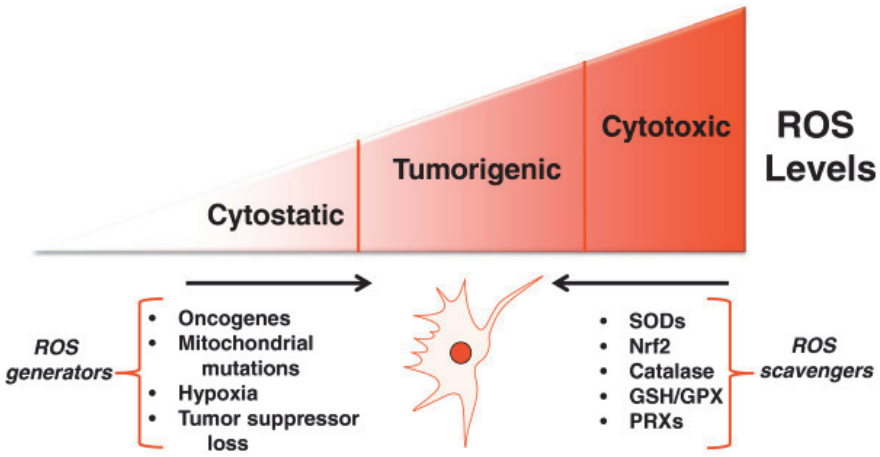

Figure 2.5. Levels of ROS and Cancer

Mitochondrial ROS generation can be activated by oncogenes, unfunctional tumor suppressors, mutations in mitochondria or hypoxic conditions and this may facilitate tumor formation. Further increase in ROS level may have cytotoxic effect on cells, so, cancer cells must keep a balanced ROS level. This is achieved by ROS detoxification systems. Reprinted from BioMed Central, The Open Access Publisher. Sullivan, L.B. and N.S. Chandel, *Mitochondrial reactive oxygen species and cancer*. Cancer Metab, 2014. 2: p. 17. Copyright © 2014

Cell cycle is the period between two mitotic divisions and it consists of a set of processes resulting in cell growth and division. Cell cycle is formed of two gap phases (G1 and G2), and a synthesis (S) phase taking place between two gap phases, in which DNA replication takes place, followed by mitosis (M). Cell growth and division are the fundamental processes of the biological systems; therefore, elucidation of the checkpoints and balance that ensure proper cell division has vital importance. Cells grow, replicate its DNA and divide by cell cycle which is controlled by a set of signaling

networks. This process also includes a proofreading mechanism in which the committed errors are corrected and in case of that not being possible, the cells go through apoptosis [164]. In cancer cells, on the other hand, this mechanism does not work properly due to genetic mutations, which leads those cells to uncontrolled proliferation. Therefore, cancer is a proliferation disorder and it is considered to be a disease related to cell cycle, that is, each tumor lacks one or more aspects of the cell cycle control; however, cell cycle defects alone are not the cause of cancer [165]. To this end, several studies are designed targeting cell cycle machinery in cancer therapy research [166].

From metabolic point of view, cell cycle is an energy demanding process which requires a highly active metabolism in order to fuel the rapid increase of cell mass [167]. Several proteins including cyclin D1 which has a key role in G1 phase of cell cycle progression and metabolic enzymes such as 6-phosphofructo-2-kinase/fructose-2,6-bisphosphatase, isoform 3 (PFK/FB3) and glutaminase 1 (GLS1) are reported targets in metabolism-cell cycle crosstalk [164]. Also, it is worth noting that cell cycle is directly related to PPP as R5P and NADPH produced via PPP are important elements in nucleotide synthesis and ROS detoxification. Therefore, stimuli to initiate cell growth also activate PPP genes [80]. Despite that glucose availability being a metabolic check point in cell cycle was observed few decades ago [168], and that cell cycle elements and regulatory elements have been elaborated in past years, the connection between cell cycle process, availability of nutrients, biological intermediates and energetic balance is still to be fully elucidated [169].

Organisms have evolved in a way that unnecessary or unhealthy cells are eliminated from the body with a programmed cell death program called apoptosis. Unlike normal cells, tumors are under constant stress because of activated oncogenes, instable genome, hypoxia or similar reasons which induce tumorigenesis. Under normal circumstances, this stress cause apoptotic stimuli; nevertheless, cancer cells, as a hallmark, have ability to avoid this cellular response [170], supporting that inhibition of apoptosis has a key role in survival of cancer cells and development of tumors. Apoptosis can be initiated by extrinsic signaling pathway in which tumor necrosis factor (TNF) receptor is included, where the death signal is introduced via these receptors. On the other hand, an intrinsic signaling pathway initiated by mitochondria which is

independent of receptors may also initiate apoptosis [171]. Enhanced aerobic glycolysis and decreased mitochondrial respiration, therefore, helps cancer cells also to evade from apoptosis. In healthy cells for induction of intrinsic mitochondrial pathway inactivation of anti-apoptotic proteins such as BCL2 which is located in mitochondria is required. Tumor suppressor p53 gene has role in activating several pro-apoptotic BCL2 signaling proteins such as NOXA and PUMA. However, many cancer cells have defected intrinsic apoptotic pathway due to the loss of p53 and BCL2 has been reported as an oncogene in several cancers [172, 173]. This suggests that mitochondrial metabolism is highly related with cancer cell survival and tumor growth, and modulation of mitochondrial respiration may have anticancer effects [173].

2.3.8. Crosstalk between Signaling Events and Cancer Metabolism

Cell metabolism is regulated by several means among which are the availability of the nutrients, levels of certain metabolites and activity of the certain key enzymes of metabolism. Also, as one of the cancer hallmarks, cancer cells sustain proliferative stimuli by uncontrolled growth promoting signals transuded by signal transduction pathway [15]. Studying altered cellular metabolism provides deep information for a better understanding of the complex networks of oncogenic signaling pathways, which is the reason laying beneath tumorigenesis. Many oncogenic signaling pathways converge to adapt cancer cell metabolism to sustain the existence of tumor cells [41]. Also, in the last years several metabolism based anticancer therapy strategies targeting the relation between altered cellular metabolism and signaling networks regulating the proliferation and survival have been suggested [174]. Various oncogenes, tumor suppressor genes and cell cycle regulators which control cell proliferation and survival are involved in modulation of key cellular metabolic pathways including glycolysis, PPP, OXPHOS, lipogenesis, glutaminolysis and several others (Figure 2.6). Mutations causing oncogenesis or loss of tumor suppressors lead cancer cells to change their energetic and biosynthetic requirements via interactions between enzymes, metabolites, transporters and regulators [50]. Thanks to high throughput sequencing data, today it is known that genetic alterations causing tumor development are much more complex than estimated

and even tumors with same histopathological features may have different mutational range [175]. Despite that several metabolic adaptations controlled by oncogenes often have common characteristics in different cancer cells, metabolic profile can also be tissue or cell specific [120]. In figure 2.6, some of the most studied oncogenes and tumor suppressors together with their influence of alteration of metabolism have been highlighted.

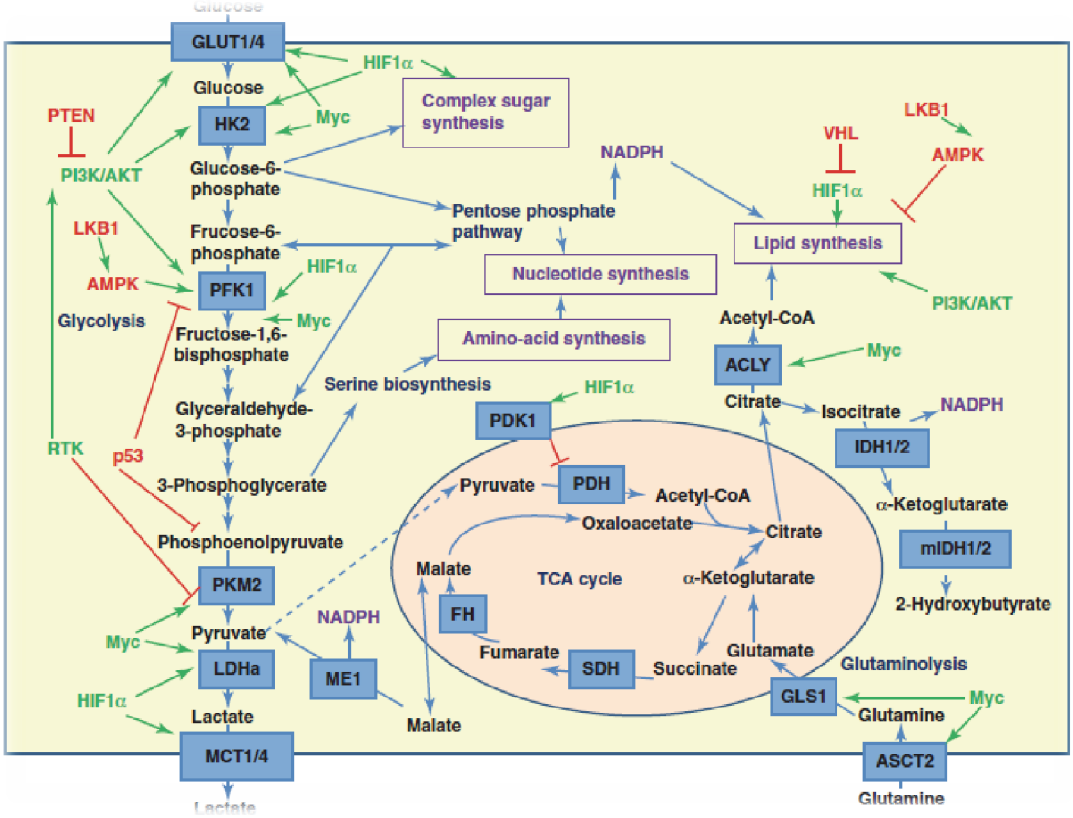

Figure 2.6. The Effects of Oncogenes and Tumor Suppressors on Metabolic Reprogramming

Tumor metabolic reprogramming is regulated by several oncogenes and tumor suppressor genes by signaling pathways. This figure outlines the complex regulatory mechanism and key pathway interactions required for growth and proliferation. Oncogenic pathways are depicted in green and tumor suppressor pathways are shown in red. Reprinted from Elsevier. Jones, N.P. and A. Schulze, Targeting cancer metabolism--aiming at a tumour's sweet-spot. Drug Discov Today, 2012. 17(5-6): p. 232-41.Copyright ©2011.

To begin, HIF-1 (hypoxia inducible factor) promotes a metabolic shift from OXPHOS to glycolysis through the activation of transcription of several genes including glycolytic

enzymes and glucose transporters; so that, lactate production via glycolysis enhances considerably, which is the key component of Warburg effect [176]. Besides this, HIF-1 also plays role in downregulation of OXPHOS by activating PDK1 to inhibit pyruvate entry into mitochondria. Additionally, HIF-1 also takes place in inhibition of β-oxidation, ROS generation, alteration of the expression of tumor suppressor genes and epithelial mesanchimal transformation of cancer cells [50, 176, 177]. Similarly, Myc oncogene also activates a transcriptional program that augments the glycolysis by directly targeting glucose transporters and glycolytic enzyme genes. Even though Myc provides cancer cells with the metabolic advantages on oxygen dependent mechanisms similar to HIF-1, the activation of Myc has more important consequences due to the fact that it regulates also many other biosynthetic pathways, such as glutaminolysis, besides glycolysis [42]. Myc activation provides cancer cells with enhanced glutamine uptake and glutaminolysis by overexpressing of the glutamine transporter genes and GLS [178]. Moreover, Myc oncogene regulates both cell cycle and apoptosis. Myc is involved in the activation and repression of several cyclins including cyclin D1 and cyclin dependent kinases which are key elements in cell cycle progression. However, the mechanism behind that Myc induces apoptosis is not fully elucidated yet [179].

Another signaling pathway which is one of the most common oncogene signaling cascades is PI3K/Akt/mTOR pathway and it is a motivating target in anticancer research [180]. PI3K/Akt/mTOR pathway is crucial for tumor cell survival and proliferation as it helps cancer cells to get their high energetical and biosynthesis demands by promoting metabolic transformation through multiple pathways including an increase in glucose and amino acid uptake, enhanced glycolysis and lipogenesis and high rates of protein synthesis via Akt-dependent mTOR activation [141, 181]. Lipid metabolism is modulated by activation of sterol regulatory element binding proteins (SREBPs) and these proteins regulate Akt/mTOR signaling pathway [146, 182]. In fact, several genes included in lipid biosynthesis; such as ACLY, ACC and FASN are targets of SREBPs [183]. Moreover, it has been reported that PI3K, one of the most frequently activated oncogenes, increases the activity of PPP by activating G6PD enzyme [89].

Since it has very important roles in tumorogenesis, cell survival, cell cycle and apoptosis and it is altered in several cancers, p53 (or also called TP53) is probably the most studied

tumor suppressor gene of the recent years. Its loss of function induces Warburg effect by activating glycolysis, more specifically, increasing the expression of glucose transporters and glycolytic enzymes, such as hexokinase (HK). This, in turn, represses mitochondrial respiration. Moreover, p53 deficiency alters also the TP53-induced glycolysis and apoptosis regulator (TIGAR) which leads cells to go through tumorogenesis [184-186]. In addition, p53 regulates the GLS2, mitochondrial glutaminase gene in a way that any activation of p53 will, therefore, cause an enhanced mitochondrial metabolism [187] and FASN, the key enzyme of fatty acid synthesis is also indirectly regulated by p53 [188]. On the other hand, p53, when functional, directly binds to dimeric structure of G6PD and decreases the activity of PPP [90].

There are several other genes which play role as oncogenes or tumor suppressors in tumor development. For example, mutated tumor suppressor PTEN is the main activator of the PI3K/Akt/mTOR signaling and this pathway is quite active in bladder cancer [189]. Furthermore, there are recent studies pointing FH, SDH and IDH genes, which are the main enzymes of TCA cycle, as tumor suppressors [132, 190-193].

2.3.9. Current Approaches in Cancer Therapy Targeting Metabolic Reprogramming

Since the discovery of aerobic glycolysis by Warburg, cancer metabolism has been the focus of cancer research and high throughput techniques increased our understanding of tumor metabolism profoundly. Many cancer related pathways and the roles of several certain enzymes taking place in cancer metabolism have been elucidated and the idea of targeting tumor metabolic reprogramming in order to identify new therapeutics has been one of the main focuses in cancer research [194, 195]. In 1950s, the nucleic acid synthesis [196] and some glycolytic enzymes such as HK, GAPDH and PDK [197] were already suggested as putative targets in anti cancer therapy and since then, several metabolic pathways and enzymes have been pointed out and used in cancer therapy [62]. Among the many anti-glycolytic agents, 2-deoxy-D-glucose (2-DG) is the most studied one. It is a glucose analog which inhibits glucose uptake leading the glycolysis to stop after first step [198]. Also, dicloroacetate (DCA) is a strong anti-Warburg effect

drug. It inhibits PDK so that pyruvate is directed to entry into mitochondria via PDH. Preclinical studies demonstrated that DCA has additive or synergistic effects when it is combined with other agents targeting tumor oxidative stress [199]. Another promising anti-glycolytic chemical is 3-bromopyruvate (3-BrPA) with its ability to deactivate GAPDH [200]. On the other hand, tumor metabolic reprogramming is also linked to drug resistance in cancer treatment [201]; therefore, 3-BrPA is a good anti cancer agent due to its ability to enhance the effects of cytotoxic drugs and overcome drug resistance in cancer [202].

Under normal circumstances, the enzyme 6-phosphofructokinase/fructose-2,6-bisphosphatase 2 (PFKFB2) is a bifunctional enzyme with both phosphatase and kinase activities and it activates 6-phosphofructokinase (PFK1) by generating the allosteric glycolysis regulator, fructose-2,6-bisphosphate (F26BP) [203]. Most cancer cells, however, express PFKFB3 isoform, which has very little phosphatase activity and therefore, they trigger aerobic glycolysis by increased F26BP production [204]. Clem *et al.* have reported that some small molecule inhibitors of PFKFB3 decrease the F26BP formation, so that, they inhibit the growth of cancer cells and xenograft tumors [205]. Similarly, cancer cells express majorly the pyruvate kinase 2 (PKM2) isoform despite that its activity is lower than PKM1 isoform. In that way, they prevent the production of excess ATP which is an allosteric regulator of glycolysis. Thus, inhibition of PKM2 isoform in cancer therapy has been hypothesized to have promising anti-tumor effects [206]. On the other hand, lactate dehydrogenase (LDH) has long been targeted in anticancer therapy, yet because of its position being at the end of the glycolytic pathway, LDH-inhibition based approaches have several challenges and still under wide investigation [207].

Although glycolysis has been a very prominent pathway to target in cancer therapy, other metabolic pathways having significant roles in tumor metabolic rewiring have also been elaborated to encounter new therapeutic targets [194, 208]. With its pivotal roles at nucleotide biosynthesis and NADPH production for ROS detoxification and lipid biosynthesis, PPP has been widely studied and the main enzymes of PPP, such as G6PD, 6PGD and TKT have been proposed as potential targets in cancer therapy [94-96]. G6PD deficiency has been observed in around 400 million people worldwide and its deficiency

does not have any severe consequences except for mild anemia [209], so, inhibition of this enzyme in cancer treatment is highly promising. In cancer cells, reduced levels of G6PD enzyme ends up in decreased proliferation [80]; nonetheless, embryonic stem cells with knockout G6PD do not perform a decreased proliferation but they show a stronger sensibility to antioxidants [210]. Moreover, in human foreskin fibroblast cells decreased G6PD activity leads to reduced growth and induction of cellular senescence [211].

Also, 6PGD, another important enzyme of ox-PPP has recently taken the interest of the scientists and reported to be a potential anticancer target. Recent reports have demonstrated that inhibition of 6PGD decreases the growth of lung cancer cells by senescence induction [96]. Furthermore, 6PGD has been proven to take role in cell migration and lung cancer cells with decreased activity of this enzyme showed less migration activity in vitro [97]. Another recent report have elucidated that decreased 6PGD level in various cancer cell lines lead to reduced lipid and RNA biosynthesis together with enhanced ROS levels, which in turn attenuated cancer cell proliferation and tumor growth [212]. There still remains a lot to be explored about this promising target for cancer therapy.

Targeting ox-PPP in cancer therapy is an interesting approach as it also plays a crucial role in ROS detoxification in cancer cells. Since cancer cells often have active ROS detoxification mechanisms in order to deal with enhanced ROS levels, ROS mediated mechanisms has been proposed to be targeted in therapeutic studies. The balance between ROS production and removal in cancer cells is very subtle; thus, disruption of this balance is an interesting approach [101]. Knowing the role of G6PD and 6PGD in ROS detoxification, inhibition of these enzymes is likely to disrupt this balance and lead to cell death.

In addition, TKT enzyme has also been studied for its anticancer efficiency and the studies showed that inhibition of nonox-PPP lead to stronger decrease in tumor proliferation than the inhibition of ox-PPP [213]. Moreover, chemical inhibition of both TKT via oxythiamine (OT) and G6PD via dehydroepiandrosterone (DHEA) resulted in a cell cycle arrest in G1 phase in Ehrlich's ascites tumor *in vivo* and the combined

administration of both chemicals showed a synergic effect [214]. On the other hand, other nonox-PPP enzymes such as ribose-5-phosphate isomerase (RPIA) and ribulose-phosphate 3-epimerase (RPE) have also particular role in tumor growth and decrease in their activity has been reported to decrease tumor growth in xenograft model of KRAS-induced pancreatic ductal adenocarcinoma [68]. All in all, PPP has strong roles in cancer cell proliferation and survival and inhibition of the PPP can be a potential strategy in anticancer therapy.

Inhibiting glutamine metabolism of the cancer cells has also attracted the scientists in the field and GLS1 has been pointed out to be a promising target in anti-cancer therapy, especially for the cancer cells with overexpression of Myc, that is, glutamine addicted cells [121]. Various specific GLS1 inhibitors have recently been discovered among which compound 968, CB-839 and bis-2-(5-phenylacetamido-1,2,4-thiadiazol-2-yl)ethyl sulfide (BPTES) are some prominent anti-tumor agents and they have passed several preclinical tests successfully in various tumor types [215-217]. Furthermore, lipid biosynthesis pathway has also been studied for encountering any possible target to use in fight against cancer. To illustrate, three inhibitors, cerulenin, triclosan and orlistat, have been reported for their activity to inhibit FASN [218] and inhibition of ACLY by RNAi or by chemical SB-204990 has limited tumor proliferation and survival [110, 219]. Also, inhibition of fatty acid synthesis by activation of AMPK, a metabolic regulator, by acadesine or rosiglitazone has been shown to have antitumor effects [220, 221].

On the other hand, targeting oncogenic signaling is also a strong approach in fighting against cancer. For example, idelalisib which is an inhibitor of PI3K is reported to inhibit the pro-survival pathways of B-cell lymphoma and decrease the chemotaxis of cancer cells into protective tissue microenvironment which helps with better chemotherapy results [222, 223]. Targeting Ras proteins is also studied widely since they control the signaling pathways which are key regulators of normal cell growth and tumorigenesis. Some small molecules which suppress the oncogenic Ras signaling in laboratory models have been discovered; however, complementary studies will be needed to see effectiveness of these molecules as anticancer drugs [224]. Moreover, Myc is an important anticancer target since it controls several metabolic pathways including cell

cycle and apoptosis. Of note, quarfloxin a Myc inhibiting small molecule has been in phase II of clinical trials for neuro-endocrinal carcinomas [179].

2.4. TOOLS USED TO STUDY CANCER METABOLISM

Genomics, transcriptomics and proteomics approaches focus on gene, mRNA, and protein profiles respectively and have provided with broad sets of information for identification of new biomarkers of certain cancer types, targetable mutations and new tumor subtypes [225-227]. Similarly, metabolomics which is concentration based metabolite profiling and fluxomics which refer to quantification of metabolic fluxes provide investigators with a dynamic portrait of the metabolic status of the living systems are among the newest “omics” sciences and they have introduced new insights to understand the environment of the cells and metabolic fluxes as a whole [228]. Particularly fluxomics strategies have been used to quantify and analyze the dynamic changes in metabolites and metabolic pathways which provided investigators with a better comprehension of the metabolic rewiring lying beneath tumor development. The study of tumor metabolism requires consideration of the entire metabolic network and it has pivotal importance to introduce this data in Systems Biology studies where different kinds of omics data are integrated to obtain a holistic perspective of the complex behavior of biological systems [229, 230].

2.4.1. Metabolomics

Metabolomics can be defined as a large study of analysis of complete set of small molecules, which are known as metabolites, within cells, biofluids, tissues or entire organisms and it is simply based on profiles arising from their concentrations. [231]. Metabolomics has an edge on other omics strategies due to several advantages it offers. First of all, metabolomics allows revealing the changes in the cell metabolome (an entire set of endogenous metabolites and their interaction within a biological system) which is the final downstream product of the central dogma and is more amplified than

transcriptome and proteome data [232]. Also, metabolome is directly linked to the current status of the cells, that is, it reflects better the phenotype of the investigated biological system and it is cheaper to identify metabolic biomarkers than identifying mRNAs or proteins. Furthermore, in metabolomics research, comparison of the data over several biological conditions is easier than other omics, because a certain metabolite is identical in every cells or organisms contrary to transcript or proteins [233, 234]. Therefore, metabolomics has been started to be used widely to determine the biomarkers involved in certain diseases or certain stages of a very disease development.

Metabolomics studies can be targeted or untargeted. In the former one, the certain metabolites which are suspected to be altered in the studied conditions are investigated. In the latter one; however, a global metabolite profiling which permits to quantify a vast number of metabolites under related conditions is achieved. A complete metabolomics study consists of several steps; such as, metabolite extraction, quantification of the metabolite and analysis and integration of the data by bioinformatics tools [235, 236]. There are several analytical techniques used for metabolome analysis depending of the metabolite of interest and nature of the samples and among which nuclear magnetic resonance (NMR) spectroscopy, gas or liquid chromatography coupled to mass spectrometry (GC-MS, LC-MS), direct-infusion mass spectrometry (DIMS), Fourier transform infrared spectroscopy (FTIR) and capillary electrophoresis (CE) are widely used ones [230, 237, 238]. Among all, mass spectrometry and NMR are the most powerful and commonly used techniques and table 2.1 gives an overview of some commonly employed analytical techniques for metabolomics studies [238].

Despite the fact that metabolomics has several advantages over genomics, transcriptomics and proteomics the availability of metabolomics data is still scarce and limited. There are only few repositories of metabolomics data including Human Metabolome Database which provides structural information of many metabolites of human cell [239, 240]. On the other hand, the data provided by metabolomics is a static metabolic map and in order to complete the metabolic view, determination of the dynamics of the metabolite pools from the many reactions they take role by using metabolic pathway based approaches are crucial. To this end, a new omic science,

fluxomics, has arisen in order to analyze the metabolic flux distributions within the cells [230, 241, 242]. That is, fluxomics has emerged as a complementary tool to metabolomics and together, they provide with a better comprehension of the metabolism and tumor metabolic reprogramming lying behind cancer and tumor progression.

Analytical method	GC-MS	LC-MS	NMR	FTIR
Advantages	• Sensitive • Robust • Large linear range • Large commercial and public libraries	• No derivatization required (usually) • Many modes of separation available • Large sample capacity	• Rapid analysis • High resolution • No derivatization method • Non-destructive	• Rapid analysis • Complete fingerprint of sample chemical composition • No derivatization needed
Disadvantages	• Slow • Often requires derivaization • Many analytes thermally-unstable or too large for analysis	• Slow • Limited commercial libraries	• Low sensitivity • Convoluted spectra • More than one peak per component • Libraries of limited use due to complex matrix	• Extremely convoluted spectra • More than one peak per component • Metabolite identification nearly impossible • Requires samples drying
Comments	• **Chemical consideration:** on its own will not generally lead to metabolite identification. However, coupled with MS and NMR is very powerful for analyte identification • **Chemical bias:** solvent extraction bias: non-polar vs. polar analytes. Need for chemical derivatization • **Speed:** very useful for separation, but typically take 10–30 min	• **Chemical consideration:** on its own will not generally lead to metabolite identification. However, coupled with MS and NMR is very powerful for analyte identification • **Chemical bias:** solvent bias means it is usually more applicable to polar compounds • **Speed:** very useful for separation, but typically take 10–30 min	• **Chemical consideration:** gives detailed strucutural information, particularly using 2-D-NMR of isolated metabolites • **Chemical bias:** these methods have little chemical bias and can be used directly on the sample • **Speed:** few minutes to hours. Depends on the strength of the magnet, sensitivity can be improved by magic angle spinning	• **Chemical consideration:** provide limited structural information, but useful for identification of functional groups • **Chemical bias:** these methods have little chemical bias and can be used directly on the sample • **Speed:** 10–60 s

Table 2.1. Comparison of common analytical tools employed in metabolomics studies

Adapted from Frontiers, an Open Access Publisher. Vernocchi, P., et al., *Integration of datasets from different analytical techniques to assess the impact of nutrition on human metabolome.* Front Cell Infect Microbiol, 2012. **2**: p. 156. Copyright © 2012

2.4.2. Fluxomics

Fluxomics is a recent strategy used to estimate the metabolic production and consumption rates in biological systems. Metabolic fluxes are the final consequences of the interaction of gene expression, protein concentration, enzyme kinetics and regulations, and metabolite concentrations. By comparison to other omics analyses, the analysis of metabolic fluxes is named as "fluxomics" and it integrates *in vivo* or *in vitro* measurement results of metabolic fluxes with mathematical models in order to determine the absolute flux through the metabolic network of a given biological entity. It offers a better overview of the metabolic phenotypes than other omics and it can be quite useful to study the aberrant metabolic adaptations in diseases with robust metabolic components such as cancer [230]. In fluxomics, experimental measurements are mainly based on the overall rates of the consumption or production of nutrients such as glucose, glutamine and lactate which define the exchange reactions whose metabolic fluxes can easily be measured. Moreover, intracellular metabolic fluxes can be estimated by using metabolomic data obtained from isotope labeling experiments which are based on the introduction of isotopic tracers, mostly ^{13}C labeled substrates (a non-radioactive and stable isotope of ^{12}C), at specific locations and tracking them by using MS or NMR based analytical techniques. These experimental measurements of ^{13}C-enrichment of metabolites allow the mathematical tools to fit intracellular fluxes [243]. Identification of the distribution of metabolic fluxes employing ^{13}C substrates is called ^{13}C based metabolic flux analysis (^{13}C-MFA) [243].

In fact, tracer based data obtained by culturing the cells with tracer substrates; such as glucose or glutamine, can provide with a descriptive map of the changes in the metabolic network. In that way, the altered pathways and the contribution of nutrients to the production of other metabolites can be monitored [244]. The consumption and production rates of extracellular metabolites can be estimated by measuring concentration change of the certain metabolites in the extracellular medium in a certain time. However, the consumption and production of intracellular metabolites keep a dynamic balance and the reaction balance can easily be estimated by using tracers like ^{13}C [245, 246]. The data obtained from ^{13}C mediated experiments can be used to

estimate metabolic fluxes by direct interpretation of the labeling patterns; however, the data can also serve as substrate for computational model based approaches [247].

In order to derive information about the activity of different metabolic pathways within a cell, stable isotope containing susbtrates (also called tracers), such as ^{13}C, has long been used. ^{13}C assisted metabolomics experiments are conducted by incubating the cells with tracers in a time dependent manner and at the end of the required time; the newly formed metabolites contain ^{13}C atoms coming from the initial substrates. The metabolic pathway followed by a specific tracer can be tracked as ^{13}C atoms are incorporated in unique numbers and positions in the newly synthesized molecules. That is, the different mass isotopomers (also called isotopologues) and positional isotopomers derived from the distribution of ^{13}C of a specifically labeled precursor provide information about the metabolic pathways via which they have been formed [230, 248]. Different mass isotopomers (isomers with a specific number of ^{13}C substitutions) refer to molecules that vary only in the isotopic composition. For example, 2 or 3 ^{13}C containing lactate molecules are lactate mass isotopomers independent of their position. Nevertheless, for the positional isotopomers (isomers with ^{13}C substitutions in a specific carbon position) the position of the ^{13}C incorporated is also important. Therefore, lactate molecules containing one ^{13}C atom in position 1 and one ^{13}C atom in position 2 are lactate position isotopomers [248]. For a specific metabolite with *n* carbons, the theoretical number of possible ^{13}C mass isotopomers is *n+1* and the number of possible ^{13}C positional isotopomers is 2^n. To illustrate, three carbon metabolites (n=3); such as lactate or serine, can potentially give 3+1=4 mass isotopomers (m0, m1, m2 and m3 depending on the ^{13}C number) and 2^3=8 positional isotopomers (for m0: $^{12}C_1$-$^{12}C_2$-$^{12}C_3$; for m1: $\mathbf{^{13}C_1}$-$^{12}C_2$-$^{12}C_3$, $^{12}C_1$-$\mathbf{^{13}C_2}$-$^{12}C_3$, $^{12}C_1$-$^{12}C_2$-$\mathbf{^{13}C_3}$; for m2: $\mathbf{^{13}C_1}$-$\mathbf{^{13}C_2}$-$^{12}C_3$, $^{12}C_1$-$\mathbf{^{13}C_2}$-$\mathbf{^{13}C_3}$, $\mathbf{^{13}C_1}$-$^{12}C_2$-$\mathbf{^{13}C_3}$; and for m3: $\mathbf{^{13}C_1}$-$\mathbf{^{13}C_2}$-$\mathbf{^{13}C_3}$). Of note, tracer based experiments carried out via GC/MS give information only about mass isotopomers whereas NMR can resolve the positional isotopomer distributions [249, 250].

The selection of the optimum tracers is a major challenge to determine the quality of metabolic flux analysis results. Therefore, some algorithms have been developed in order to select the proper tracer for determining the fluxes of interest [251, 252]. The selected tracer determines the isotopomers to be formed and the sensitivity of their

measurements related to flux changes [253]. The selection of the optimum tracer depends on whether the fluxes to be estimated are an overall picture of the metabolism of the studied biological system or only certain fluxes of interest are sought. It is important to note that choosing a proper tracer is more complicated in complex systems; such as mammalian, especially tumor cell systems, because these cells have requirements of multiple carbon sources and complex media containing multiple nutrients (e.g. amino acids, nucleotides, lipids) which can compete with tracers [251-254].

Most mammalian cells can easily metabolize glucose and glutamine; therefore, these two are widely used substrates in ^{13}C based metabolic flux analyses. Several ^{13}C-glucose and ^{13}C-glutamine tracers have been evaluated and the following outputs were noted. [1,2-$^{13}C_2$]-glucose is one of the most informative and widely used tracers since it provides with a reliable metabolic assessment of glycolysis, PPP, pyruvate oxidation/carboxylation and lipogenesis (Figure 2.7). On the other hand, [U-$^{13}C_5$]-glutamine is the most informative for TCA cycle studies, some amino acids' metabolism and also lipogenesis (Figure 2.8) [77, 252, 255-257]. In addition, if the fluxes that are being studied are very specific, some other glucose tracers such as [3,4,5,6-$^{13}C_4$]-glucose (for PPP fluxes), [2,3,4,5,6-$^{13}C_5$]-glucose (for ox-PPP fluxes) or [3,4-$^{13}C_2$]-glucose (for PC fluxes) could be used [258].

2.4.2.1. Parallel Labeling Approach in ^{13}C Assisted Metabolomics Experiments

^{13}C assisted metabolomics experiments can be divided in two major categories; either single labeling or parallel labeling. In single labeling experiments, a single experiment with either a single tracer, such as [1,2-$^{13}C_2$]-glucose, or with the mixture various tracers, such as [1,2-$^{13}C_2$]-glucose and [U-$^{13}C_6$]-glucose or [1,2-$^{13}C_2$]-glucose and [U-$^{13}C_5$]-glutamine are employed. For parallel labeling experiments, however, two or more tracer based experiments are carried out in parallel. That is, each experiment is conducted by one different tracer. The most common one is using [1,2-$^{13}C_2$]-glucose for one set of samples and [U-$^{13}C_5$]-glutamine for the other set.

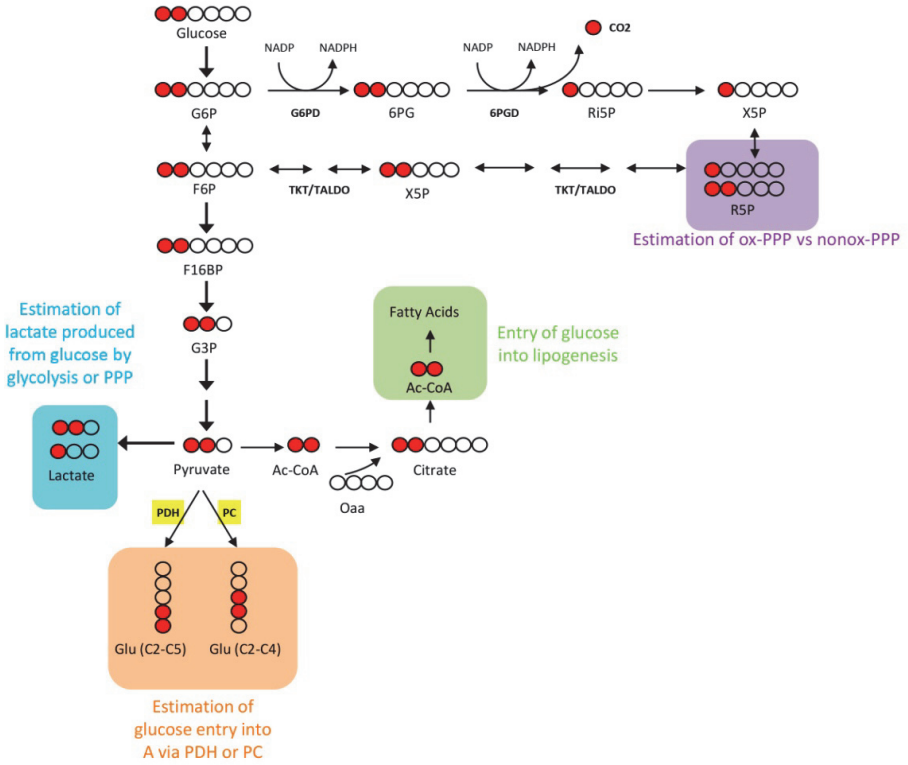

Figure 2.7. ^{13}C-assisted metabolomics experiments using [1,2-$^{13}C_2$]-glucose.

Using [1,2-$^{13}C_2$]-glucose permits tracking of several major metabolic pathways such as glycolysis, PPP, TCA cycle or lipogenesis. i) The mass isotopomer distribution of lactate (Lac) is used to estimate the relative contribution of glycolysis and PPP to lactate production. [2,3-$^{13}C_2$]-Lac (m2 lactate) is produced directly by glycolysis while [3-$^{13}C_1$]-Lac (m1 lactate) is produced by a combination of glycolysis and PPP pathways, where [1-$^{13}C_1$]- ribose-5-phosphate (R5P) is reintroduced into glycolysis through the nonox-PPP to produce m1 labeled glycolytic intermediates (to keep the figure simple, glycolytic intermediates corresponding to this process are not indicated in the figure). ii) The mass isotopomer distribution of RNA ribose through the measurement of the percentage of R5P molecules containing one ^{13}C atom (m1 ribose, [1-$^{13}C_1$]-R5P) or two ^{13}C atoms (m2 ribose, [1,2-$^{13}C_2$]-R5P) is used to estimate the contribution of both ox-PPP and nonox-PPP to the production of R5P, which is needed for nucleotide synthesis. iii) Analyzing mass isotopomer distribution of glutamate (Glu) reveal the manner of the entry of pyruvate obtained from labeled glucose into mitochondria. In fact, the positional isotopomer distribution of glutamate varies depending on the pathway used to include pyruvate into TCA cycle. If pyruvate enters via PDH, [4,5-$^{13}C_2$]-Glu is formed while entry via PC leads to [2,3-$^{13}C_2$]-Glu formation. iv) Similarly, if pyruvate entry is via PDH, Ac-CoA yielded for lipid synthesis will always include two labeled carbons; however, the Ac-CoA produced via PC will have no tracer carbon (not shown in the figure). In section 4.17, all these procedures are explained in detail. To make the image clear, only the main isotopomers are represented. G6P, glucose-6-phosphate; G6PD, glucose-6-phosphate dehydrogenase; 6PG, 6- phosphogluconate; 6PGD, 6-phosphogluconate dehydrogenase; Ri5P, ribulose-5-phosphate; X5P, xylulose-5- phosphate; TKT, transketolase; TALDO, transaldolase; F6P, fructose-6-phosphate; F16BP, fructose-1,6-bisphosphate; G3P, glyceraldehyde-3-phosphate; Pyr, pyruvate; Cit, citrate; OAA, oxalacetate; αKG, alpha-ketoglutarate.

Then, the data obtained from parallel experiments can be integrated for MFA by fitting all the data into a single flux model. Of note, the initial culture for the parallel experiments must be set together in order to minimize the biological variability. On the other hand, parallel labeling experiments offer many advantages compared to single labeling ones. First of all, it reduces the length of the labeling experiments toachieve the isotopic steady-state as it presents multiple entry points for tracers and it is easier to observe a global network. Also, it improves the precision of specific fluxes and allows validation of the biochemical network models by placing more stringent constraints on the network model assumptions, in turn improving the performances of ^{13}C-MFA [259-262].

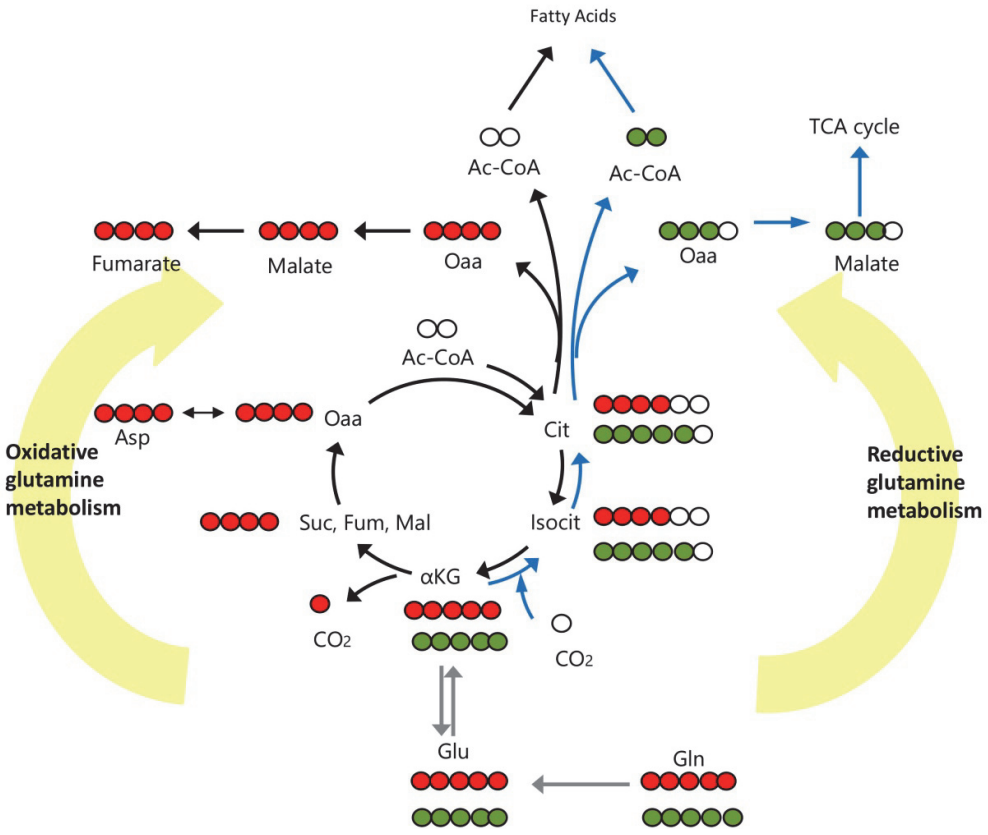

Figure 2.8. ^{13}C-assisted metabolomics experiments using [U-$^{13}C_5$]-glutamine.

Using [U-$^{13}C_5$]-glutamine, TCA cycle can be tracked. The incorporation of glutamine carbons into fatty acids can also be followed. Oxidative (red molecules) and reductive (green molecules) glutamine metabolisms are depicted here. Of note, the m3 labeled malate which is produced through reductive glutamine metabolism can be reintegrated into TCA cycle by producing m3 labeled OAA, citrate, isocitrate and m2 labeled αKG, succinate and fumarate.

2.4.2.2. Mass Isotopomer Distribution Analysis

As explained at above sections, intracellular fluxes in central carbon metabolism can be estimated by employing ^{13}C labeled tracer nutrients as cellular substrates. The metabolization of these substrates leads to a unique rearrangement pattern of the ^{13}C tracers through the corresponding metabolic pathway and this can give us an idea about the flux distribution of central carbon metabolism [263, 264]. The mass isotopomer distribution of newly synthesized ^{13}C labeled metabolites together with the extracellular metabolic flux measurements can help to deduce certain intracellular fluxes and the ratios between them. This is achieved by using simple analytical formulas based on previous knowledge of the reactions within the metabolic network. In fact, label propagation has been used widely to elucidate the reactions related to metabolic pathways so that the flux distribution of two or more experimental conditions can be compared and the relevant metabolic pathways can be targeted. This comparative analysis of tracer based metabolomics data is known as mass isotopomer distribution analysis (MIDA) and it permits metabolic flux distribution analysis without any bioinformatics tools [230]. For instance, approximate contribution of the oxidative and nonoxidative phases of PPP can be determined by analyzing the ^{13}C tracer propagation from [1,2-$^{13}C_2$]-glucose to ribose (figure 2.7). Metabolization of [1,2-$^{13}C_2$]-glucose-6-phosphate through the oxidative phase results in the loss of one labeled carbon atom, that is, m1 ribose ([1-$^{13}C_1$]-ribose). Nonetheless, if the ribose is synthesized through non-oxidative phase of PPP where [1,2-$^{13}C_2$]-glucose-6-phosphate is converted to [1,2-$^{13}C_2$]-glucose-6-phosphate and ends up in m2 ribose ([1,2-$^{13}C_2$]-ribose) [102, 265]. Similarly, mass isotopomer distribution analysis together with its extracellular concentration measurements can be used to estimate the flux of glucose to lactate either via direct glycolysis or via PPP. Also, the flux of lactate synthesized from other sources can be deduced. Moreover, the percentage of glucose metabolism that is used for fatty acid synthesis can also be deduced by checking the even-numbered isotopologues, such as m2, m4, m6… of the fatty acids. In addition, whether the pyruvate entry into mitochondria is catalyzed by PC or PDH enzymes can be estimated by analysis of ^{13}C propagation from [1,2-$^{13}C_2$]-glucose to glutamate [255, 266] (for details see section 4.17). Hence, MIDA provides a simple and quick way to obtain some metabolic fluxes

and the relative use of certain metabolic pathways. Of note, the analytically estimated flux ratios obtained by MIDA can also be used as inputs to obtain a more complete metabolic flux analysis using the computational modeling based flux estimation approaches which are explained in the following section.

2.4.2.3. Computational Modeling Based Flux Estimation

The biological systems are highly complex, so relying only on empirical observations to predict the behavior of these systems are inadequate and new approaches are clearly needed [267]. The omics revolution has provided new tools enabling the study of many biological processes at the same time working with large numbers of molecular components (genes, transcripts, proteins or metabolites), and allows the emergence of a new discipline: the Systems Biology. Each of these disciplines (from the study of gene expression to proteomics and metabolomics) provides an overview of biological phenomena from their point of view [268]. It is known that the overall metabolome of a cell dynamic is continuously transformed in the cell. In order to characterize the metabolic networks and their functional states, it is required to know the quantitative intracellular metabolic fluxes, which can be quantified by analyzing the incorporation of introduced labeled substrates in metabolic products using the correct bioinformatic tools [269].

A powerful tool to analyze the intracellular metabolic fluxes complementary to MIDA is the software “Isodyn” that allows the simulation of the dynamics of the ^{13}C redistribution in metabolites from central carbon metabolism pathways of living cells. In order to make these simulations possible, Isodyn uses a classical kinetic model of metabolic pathways linked to a module that computes the distribution of ^{13}C isotopologues in metabolites [269-271]. Isodyn, on the other hand, can be supplemented with algorithms to demonstrate the compartmentation of intracellular metabolic reactions from ^{13}C isotopologue data [272]. In one part of this study, the metabolic flux estimation of breast cancer cells with glutamine deprivation or impaired mitochondria has been realized using this powerful program.

3. OBJECTIVES

3. OBJECTIVES

Over the last decade, comprehensive understanding of metabolic pathways in cancer has considerably increased. Despite that continuous research activities in the field of cancer accomplished quite a lot, there are still much to explore in the metabolic profile of tumors in order to open new venues in cancer treatment. The main aim of this dissertation is to explore certain metabolic pathways of cancer cells so as to propose new targets for cancer treatment. To achieve this main aim, four specific objectives are to be considered:

1. Investigation of the role of pentose phosphate pathway (PPP) within tumor metabolism and validation of PPP enzymes as potential therapeutic targets using breast and colon cancer models.
2. Exploration of glutamine metabolism and unveiling the link between PPP and glutamine metabolism and how they regulate each other using breast and colon cancer models.
3. Providing various omics data in order to establish a genome scale metabolic model of different regulatory levels of breast cancer cells in the frame of a multinational European project (METAFLUX EC-FP7)
4. Characterization of the metabolic reprogramming and potential metabolic vulnerabilities in the cells with eitger glutamine deprivation or defective mitochondria using breast cancer model.

4. MATERIALS AND METHODS

4. MATERIAL AND METHODS

4.1. Cell Culture

Cancer cell lines; MCF7, HT29 and HCT116 were purchased from ATCC and T47D was a generous gift from Dr. Timothy Thompson's laboratory (Molecular Biology Institute of Barcelona, IBMB, CSIC, Spain). Both cell lines were cultured in MEM without phenol red (Gibco, Thermo Fisher Scientific Inc., Waltham, MA, USA) containing 10% Fetal Bovine Serum (Gibco), 10mM d-Glucose (Sigma-Aldrich), 1mM Sodium Pyruvate (Biological Industries), 2mM Glutamine (Gibco), 0.1% antibiotic (Penicillin 10 Units/ml-Streptomycin 10 Units/ml, Gibco), 0.01 mg/ml Insulin (Sigma), and 1% Non-essential amino acids (Biological Industries). HT29 cells were cultured in DMEM (Gibco) containing 10% Fetal Bovine Serum (Gibco), 10mM d-Glucose (Sigma-Aldrich), 2mM Glutamine (Gibco) and 0.1% antibiotic (Penicillin 10 Units/ml-Streptomycin 10 Units/ml, Gibco). HCT116 cell lines were cultured in the mixture of DMEM (Gibco) and HAM-F12 (Biowest) (1:1 v/v) containing 10% Fetal Bovine Serum (Gibco), 10mM d-Glucose (Sigma-Aldrich), 2mM Glutamine (Gibco) and 0.1% antibiotic (Penicillin 10 Units/ml-Streptomycin 10 Units/ml, Gibco). The cells were maintained at 37 °C with 5% CO2 and saturated humidity. Growth medium was replaced every 2-3 days.

4.2. siRNA Transfection

For the transfection of MCF7 and T47D, cells were seeded at a density of $1x10^5$ cells per well in a 6-well plate with antibiotic-free growth medium. After 24 hrs they were transfected in triplicates with 50 nM of either siNEG or siRNAs against 6PGD using Metafectene® Pro (Biontex, Ref: T040-1.0) according to manufacturer's protocol. The

medium was replaced after 6hr with complete medium containing antibiotic. The siRNA sequences targeted against 6PGD were purchased from Dharmacon and are listed as follows: si6PGD, ON-TARGET Plus J-008371-06, GAUCAUCUCUUACGCUCAA (si6PGD-1); si6PGD, ON-TARGET Plus J-008371-08, GAGCAGGCCACUUCGUGAA (si6PGD-2). Control siRNA (siNEG) was also purchased from Dharmacon: siNEG ON-TARGET Plus Non-Targeting siRNA D-001810-03-20 (Sequence not provided by the manufacturer).

For the transfection of HT29 and HCT116, cells were seeded at a density of $5x10^4$ cells per well in a 6-well plate with antibiotic-free growth medium. After 24 hrs they were transfected in triplicates with 50 nM of either siNEG pool or siRNA pool against G6PD using RNAi/Max (Invitrogen) according to manufacturer's protocol. The medium was replaced after 6hr with complete medium containing antibiotic as well. The siRNA pool targeted against G6PD was purchased from Dharmacon and is listed as follows: siG6PD, ON-TARGETPlus SMARTpool L-008181-02-0010 with the sequences: ACAGAUACAAGAACGUGAA; CCGUGUACACCAACAUGAU; CAGAUAGGCUGGAACCGCA; AUUCACGAGUCCUGCAUGA. Control siRNA pool (siNEG) was also purchased from Dharmacon: siNEG ON-TARGET Plus Non-Targeting siRNA D-001810-10-20 (Sequence not provided by the manufacturer).

4.3. RNA isolation and gene expression analysis

RNA isolation from the transfected cells in order to check the knockdown efficiency was done from fresh or frozen plates using Trizol reagent (Sigma) according to manufacturer's protocol. Briefly, Trizol cell homogenates were mixed with chloroform and centrifuged so that an aqueous phase and an organic phase were obtained. Cold isopropanol was added to the aqueous phase in order to precipitate RNA and the samples were incubated overnight at 4 ^{o}C. Then, the samples were centrifuged at 12,000 g for 15 min at 4 ^{o}C. RNA was purified by washing several times by 75 % cold ethanol and finally resuspended in RNAse free water. After that, purified RNA was quantified using a Nanodrop spectrophotometer (ND 1000 V3.1.0, Thermo Fisher Scientific Inc.). Conversion of RNA into cDNA (Reverse transcription) was carried out at 37 ^{o}C using 1µg

of RNA added to mixture containing 5x Buffer (Invitrogen), 0.1 M dithiothreitol (DTT) (Invitrogen), Random Hexamers (Roche), 40 U µL-1 RNAase inhibitor (Promega, Fitchburg, WI, USA), 40 mM dNTPs (Bioline, London, UK), 200 U µL-1 M-MLV-RT (Invitrogen). Gene expression analysis was performed by RT-PCR system (Applied Biosystems® 7500 Real Time PCR) in standard protocol provided by the manufacturer employing Taqman® (Applied Biosystems) gene specific probes for 6PGD (Hs.464071) or 6PGD (Hs00166169_m1). Reactions were performed in a volume of 20 µL containing 9 µL of cDNA mixture and 11 µL of corresponding Taqman in Master Mix (Applied Biosystems). RT-PCR was programmed with the following parameters: i) initial incubation at 50 ^{o}C for 2 minutes, ii) denaturalization at 95 ^{o}C for 10 minutes, iii) amplification of 40 cycles alternating between 95 ^{o}C for 15 seconds and 60 ^{o}C for one minute. The expression levels were quantified using ΔΔCt method using PPIA (Hs99999904_m1, Applied Biosystems) as a reference gene.

4.4. Cell proliferation and Viability Assays

Proliferation kinetics and viability of the cells were measured using Flow cytometry combining direct cell counting and Propidium Iodide (PI) staining. 96 hrs after transfection (if not mentioned differently), cells were trypsinized and resuspended in 500 µL of a solution containing 450 µL of complete media, 45 µL of Flow-Count Fluorospheres (Beckman Coulter, Brea, CA, USA) and 5 µL of 1 mg per mL PI (Bender Medsystem). The analysis was performed using Beckman Coulter® Epics® XLTM Flow Cytometer adjusted to 1x10^{4} Fluorospheres cut-off and total cell number was registered allowing discrimination between dead and alive cells.

Cell viability assay when testing any drug that interact with DNA was conducted described by Mosmann [273] with slight modifications. An increasing concentration of the drug of interest was added in sextuplicate in 96-well-flatbottomed microtitre plates where 7.5×10^{3} cells/well had been seeded 24 h before. 72 hrs later, 1 mg/mL 3-(4,5-dimethylthiazol-2-yl)-2,5-diphenyltetrazolium bromide (MTT) in PBS was added at a final concentration of 0.5 mg/mL and the plate was incubated at 37 ^{o}C for one hr. Then, the

supernatant was aspirated and the formazan product was dissolved in 100 µL of dimethyl sulfoxide (DMSO). The absorbance was measured on an ELISA plate reader (Tecan Sunrise MR20-301, TECAN, Salzburg, Austria) at 550 nm. Values were normalized to the absorbance of the cells cultured in media without any drug but with the proportional amount of the drug vehicle within the same plate.

4.5. Cell Cycle distribution analysis.

For cell cycle analysis, 96 hrs after transfection or inhibition (if not mentioned differently), cells were harvested by trypsinization and resuspended in 0.2 mL 1X TBS buffer and fixed. Then the samples were stained with 200 µl of Vindelov-PI solution containing 10X TBS, RNase (from stock of 10 mg/mL), PI (from stock of 1 mg/mL) and Igepal CA-630 (Sigma) and incubated at room temperature for 30 mins in the dark. Fluorescence-activated cell sorter (FACS) analysis was performed at 488 nm employing Beckman Coulter® Epics® XLTM Flow Cytometer(Coulter Corporation, Hialeah, FL, USA) with a cutoff at $1x10^4$ cells. Cell cycle distribution analysis was done using FlowJo® software, through which the percentage of cells in G1, S and G2 phases was obtained. All experiments were performed three times with three replicates per experiment.

4.6. Apoptosis measurement.

The apoptosis measurement was conducted as previously described [274]. In short, 96 hrs after transfection or inhibition (if not mentioned differently), the cells were washed twice with PBS and trypsinized. The cells were then collected and incubated in 195µL of 1X binding buffer (10mM Hepes/NaOH, pH 7.4, 140 mM NaCl, 2.5 mM CaCl2) and 5µL of Annexin V coupled with fluorescein isothiocyanate (FITC) (Benders System, MedSystem, Viena, Austria) for 30 mins in dark, which is recommended at Annexin V-FITC kit's instructions. 10µL of 20µg/mL Propidium Iodide was added to the samples before analysis and the percentage of apoptotic cells was measured using Beckman Coulter® Epics® XLTM flow cytometer with a cut-off range of 1x104 cells. Data analysis was

carried using FlowJo® Software. Experiments were performed in triplicate and repeated three independent times.

4.7. Enzyme Activity Assays

Fresh cell culture plates were rinsed with PBS and lysed with lysis buffer (20 mM Tris-HCl, pH 7.5, 1 mM dithiothreitol, 1 mM EDTA, 0.02% (v/v) Triton X-100, 0.02% (v/v)sodium eoxycholate) supplemented with protease and phosphatase inhibitor cocktails (Sigma and Thermo Scientific, respectively) for 30 minutes at 4 ^{o}C. The cells were scrapped and collected in eppendorf tubes and the cell lysate was disrupted by sonication using titanium probe (Vibracell, Sonics & Materials Inc., Tune 50, Output 20, 3 cycles of 5 seconds each). Then, the tubes were centrifuged at 12000 g at 4 °C for 20 minutes. The supernatant was separated and immediately used for the determination of specific enzyme activities using COBAS Mira Plus chemistry analyzer (ABX Diagnostics). All enzymatic activities were determined by monitoring NAD(P)H increment or decrement at 340 nm wavelength. The enzyme activity for each sample was then normalized to the total protein content of the samples quantified by BCA Assay at 550nm (Pierce, Thermo Scientific)

4.7.1. 6-Phosphogluconate Dehydrogenase (6PGD), Glucose-6-Phosphate Dehydrogenase (G6PD) Malic Enzyme (ME) and Isocitrate Dehydrogenase (IDH)

6PGD specific activity was measured by adding samples to a cuvette containing 0.5 mM NADP+ in 50 mM Tris-HCl (containing 0.2 mM MgCl2 for ME and IDH activities), pH 7.6, at 37 °C. Reaction was initiated by the addition of 6-phosphogluconate (6PG), glucose-6-phosphate (G6P), malate or isocitrate, respectively, up to a final concentration of 2 mM.

4.7.2. Lactate dehydrogenase

LDH specific activity was measured by adding samples to a cuvette containing 0.2 mM NADH in 100 mM KH2PO4/K2HPO4, pH 7.4, at 37 °C. Reaction was initiated by the addition of 10 mM pyruvate up to a final concentration of 0.2 mM.

4.8. Mammosphere formation assay (3D cell culture)

The capability of breast cancer cell lines to grow as single cell colonies in low-attachment conditions was analyzed by mammosphere formation assay. siRNA transfection was performed as mentioned at section 4.2 and the transfected cells were trypsinized 24 hrs after transfection. The cells were reseeded at a density of 7500 cells/well into 24-well Ultra low attachment plates (Corning Costar, NY, USA) along with 1.5ml of complete media supplemented with 20 ng mL-1 EGF, 20 ng mL-1 bFGF, 10 µg mL-1 heparin, B27 (1:50) and 0.5 µg mL-1 hydrocortisone. The cells were allowed to grow undisturbed for 10 days and then checked under microscope for the mammosphere formation. The quantification of mammosphere formation capability was done using MTT assay [273] by addition of MTT reagent (5mg/ml) to a final concentration of 0.5mg/ml into each well followed by incubation at 37 °C for 2h. The plates were then scanned using HP ScanJet G-4010 scanner at a pixel density of 2400 ppp and analyzed using ImageJ® Software (public domain National Institutes of Health, USA, http://rsbweb.nih.gov/ij/). Quantification of the mammosphere formation capability was done by calculating the total area occupied by mammospheres with a size greater than 0.000785 cm2.

4.9. Total Protein Extraction from Cell Culture

The cells were seeded and treated according to the experiment carried out. At the end of the treatment the plates were used either freshly or frozen ion liquid nitrogen for later use. In both cases, cells were washed twice with ice-cold PBS and incubated for 30 min on ice with RIPA buffer containing 50 mM Tris (pH 8.0), 150 mM sodium chloride,

1% Triton X-100, 0.5% sodium deoxycholate, 0.1% sodium dodecyl sulphate (SDS), 1% protease inhibitor cocktail (Thermo Fisher Scientific Inc.) and 1% phosphatase inhibitor cocktail (Thermo Fisher Scientific Inc.). Cells were scraped, sonicated and centrifuged at 15,000 g for 20 minutes at 4 ^{o}C. Supernatants were recovered and the protein content was quantified by the BCA kit (Pierce Biotechnology).

4.10. Western Blot

Cell extracts were obtained from either fresh plates or frozen plates using the protocol mentioned at the above section. Western blot analysis was carried out size-separating an equal amount of protein by electrophoresis on SDS polyacrylamide gels, and then the proteins were electroblotted onto polyvinylidene fluoride transfer membranes (PVDF) (Bio-Rad Laboratories, Hercules, CA, USA). The membranes were blocked with 5 % of non-fat dry milk in PBS with 0.1% Tween, and then incubated with specific primary antibodies overnight at 4 ^{o}C. Next, membranes were treated with the appropriate secondary antibody for 1 hr at room temperature. All blots were visualized on Fujifilm X-ray (VWR International, Radnor, PA, USA) with chemiluminescence detection using Immobilon ECL Western Blotting Detection Kit Reagent (EMD Millipore, Billerica, MA, USA). The antibodies used were p53 polyclonal (Merck, Millipore), G6PD (Abcam) and β-actin (MP Biomedicals). Also, anti-mouse (Dako), Anti-rabbit (Amersham Biosciences) and anti-goat (Santa Cruz Biotechnology) secondary antibodies were used.

4.11. ROS level Measurement

Fresh cells with around 70 % of confluence were washed once with warm PBS and incubated with 5μM 2'-7'-dichlorodihydrofluorescein diacetate (H_2DCFA) (Sigma) in PBS supplemented with glucose and glutamine for 30 minutes at 37 oC. Afterwards, PBS was replaced with complete growth medium and cells were incubated for another 30 minutes at 37°C and 5% CO2. Next, cells were trypsinized and resuspended thoroughly in a solution containing 50 μM H2DCFA and 20μg/mL propidium iodide. Internalized

probes reacted with ROS and emitted fluorescence when excited at 492nm. Emitted fluorescence was recorded employing Epics XL flow cytometer (Coulter Corporation, Hialeah, FL, USA) at 520 nm. For ROS analysis, data of DCF fluorescence intensity from $1X10^4$ PI-negative cells were considered and analyzed using Multicycle program (Phoenix Flow Systems, San Diego, CA, USA).

4.12. Biochemical Assays

In order to measure the concentration of each metabolite, media samples were collected at the beginning and at the end of the experiments, and frozen until being analyzed. Glucose, lactate, glutamine and glutamate concentrations were determined by using spectrophotometer (COBAS Mira Plus, Horiba ABX) from frozen cell culture medium as previously described [275-277]. Extracellular glucose concentration for each time point was measured by calculating the NAD(P)H concentration decrease after the conversion of total glucose by hexokinase and conversion of resulting glucose-6-phosphate into D-gluconate-6-phosphate by G6PDH using coupled enzymatic reactions (ABX Pentra Glucose HK CP, HORIBA ABX, Montpellier, France). Lactate concentration was determined by lactate dehydrogenase (LDH) reaction which was carried out at 37°C by adding media to a cuvette containing 1.55mg/ml NAD+ and 87.7 U/ml LDH in 0.2M hydrazine 12mM EDTA buffer (pH 9). Measuring the change in NADH concentration helps to estimate the concentration of extracellular lactate in medium. Similarly, the glutamate concentration was analyzed by measuring the change in NADH concentration which is produced by glutamate dehydrogenase (GDH) reaction converting glutamate to α-ketoglutarate in the presence of ADP. This reaction was also carried out at 37 ^{o}C and took place by adding media samples to 2.41 mM ADP, 3.9 mM NAD+ and 39 U mL-1 of GDH (Roche) in 0.5 M glycine/0.5 M hydrazine buffer (pH 9). To measure glutamine concentration, glutamine was first converted to glutamate by glutaminase (GLS) reaction and then glutamate concentration was quantified as described above. GLS reaction was performed by agitating the media samples with 125 mU mL-1 GLS in 125 mM acetate buffer (pH 5) for 30 min at 37 ^{o}C. All the absorbances were measured at 340 nm. Metabolite consumption/production rates in the cells were analyzed by measuring the

decrease or increase in concentration of the extracellular concentration in the media at the time of interest, compared to the initial concentration of the metabolite, with respect to the total cell number at each time point. The results are expressed in micromoles of metabolite consumed or produced per hour and per million cells.

Essential and non-essential amino acids (alanine, aspartate, asparagine, proline, glycine, serine, arginine, cysteine, threonine, isoleucine, leucine, lysine, methionine, valine, tryptophan, histidine, phenylalanine, tyrosine, glutamate and glutamine) concentrations in cell media were measured by ion-exchange chromatography with a Biochrom 30 amino acid analyser (Pharmacia Biochrom Ltd, Cambridge, UK). 70 µL of 150 µM norleucine were added to 500 µL of medium as an internal standard. Later, the samples were dried by SpeedVac (Thermo Fisher Scientific Inc.), resuspended in 500 µL of lithium citrate buffer (pH 2.2) and filtrated with 0.22 µm filter. 30 µL of each sample was injected into the Biochrom 30 lithium system according to the manufacturer's protocol. As mobile phase, a set of lithium citrate buffers were used for separation during 115 minutes and post column derivatisation relized with ninhydrin allowed amino acid detection at 570 and 440 nm. Amino acids were identified by the retention time of the peak on the chart and were quantified using the area under the peak of corresponding amino acid. Amino acid consumption/production rates in the cells were analyzed by measuring the decrease or increase in concentration of the extracellular concentration in the media at the time of interest, compared to the initial concentration of the metabolite, with respect to the total cell number at each time point. The results are expressed in nanomols of metabolite consumed or produced per hour and per million cells.

4.13. Transcriptomic analysis

Frozen plates with cells were used to isolate total RNA by Trizol reagent (Sigma) and the RNeasy Mini Kit (Qiagen, Hilden, Germany) as recommended by the manufacturer. Lab-on-a-chip technology on the BioAnalyzer 2100 (Agilent, Palo Alto, CA, USA) was used to test the integrity of isolated RNA. RNA was used to produce biotinylated cRNA that was

hybridised to Affymetrix GeneChipR human genome U133 Plus 2.0 arrays (Affymetrix Inc., Santa Clara, CA, USA) following the manufacturer's instructions. This array chip contains over 55,000 probe sets representing over 47,000 transcripts derived from approximately 39,500 human genes. Comparative transcriptomic analyses between control cells, oligomycin treated and glutamine deprived cells were performed on independent triplicate samples and raw data were exported to multiple .CEL files. Those files were uploaded to the R-Project Bioconductor statistical tools package and standardized using the Robust Multi-array Average (RMA) method [278]. In that way, the background was corrected, normalization to remove systematic errors and biases was managed and combination of multiple probe intensities from a probe set was summarized. Then, simpleaffy package [279] was used to compute the RMA expression values (signal intensities (SI) on the base 2 logarithm scale (log2SI) representing gene expression levels) and the differential gene expression was assessed using the limma package [280] from Bioconductor. Multiple testing adjustment of p-value was performed [281]. A fold change (FC) value is provided based on this normalization criterion. Fold changes quantification of differential expression for a probe set were defined as the ratio of normalized intensity values in oligomycin treated cells or glutamine deprived cells relative to normalized intensity values in control cells. The following formula was used to calculate the FC: 2^(mean (experimental condition replicates in log2SI))/(2^mean (Control replicates in log2SI) if the expression was upregulated; -1×2^(mean (Control replicates in log2SI))/(2^mean (experimental condition replicates in log2SI) if the expression was downregulated.

4.14. ^{13}C Mediated Metabolomics

For the experimental part, 1x10^6 MCF7 cells were seeded in each p100 plate. 48 h later, the medium was changed with an adaptation medium, DMEM medium without phenol red (Ref: A14430, Gibco) containing 10% Dialyzed Fetal Bovine Serum (Ref. F0392, Sigma) and other above mentioned supplements. After 24 h of incubation with adaptation medium, the plates were introduced the same medium containing [1,2-$^{13}C_2$]-glucose (Sigma) or [U-$^{13}C_5$]-glutamine (Sigma) together with either oligomycin (1 µM) or

deprivation of glutamine. Oligomycin is dissolved in pure ethanol so the other conditions were introduced the same concentration of ethanol as vehicle. The cells were counted at 0 h, 8 h and 24 h after tracer introduction the plates, or cell pellet and media were immediately frozen to use in later analysis. Glucose, lactate, glutamine and glutamate concentrations were measured as mentioned above from media. Also, mass isotopomer distribution of glucose, lactate and glutamate were determined from media. The pellets were used for analysis of ribose and fatty acids' mass isotopomer distribution. Cultured plates were used to determine the mass isotopomer distribution of TCA cycle elements.

Mass isotopomer distribution analyses of all intracellular and extracellular metabolites were done by gas chromatograph coupled to mass spectrometry (GC-MS). All GC-MS analysis was carried out using an Agilent 7890A GC equipped with HP5 capillary column connected to an Agilent 5975C MS. Only GC-MS analysis of fatty acids was carried out using a GCMS-QP 2012 Shimadzu coupled with bpx70 (SGE) column. For all measurements, 1 µL of sample was injected at 250 ^{o}C, helium being the carrier gas, at a flow rate of 1 mL per minute. Each metabolite or metabolite set has different isolation, derivatization and detection procedures as explained below.

4.14.1. Glucose

Glucose was isolated by using a tandem set of Dowex-1X8 / Dowex 50WX8 ion-exchange columns from frozen cell culture media and eluted with water. Then, water was completely evaporated to dryness under continuous airflow and isolated glucose was derivatized by adding 2 % (v/v) hydroxylamine hydrochloride in pyridine and incubating at 100 ^{o}C for 30 min. After that, acetic anhydrade was added and 1 hr incubation was done at the same conditions. The excess solvents were evaporated under continuous N_2 flow and derivatized glucose was dissolved in ethyl acetate to analyze with GC-MS under chemical ionization mode [266]. Sample injection was performed at 250 ^{o}C. Oven temperature was kept at 230 ^{o}C until 2 minutes after injection and then increased to 260 ^{o}C at a rate of 10 ^{o}C per min. The detector was run at SIM mode and ion abundance of

C1 to C6 in the range of 327-336 m/z was recorded. The retention time at which the peak was observed was 3.8 minutes.

4.14.2. Lactate

Lactate was isolated by first acidification of the sample media by addition of HCl and straight after, ethyl acetate was added to extract lactate. The solvent part was completely evaporated under continous N_2 and dried lactate was incubated at 75 ^{o}C for one hour after adding dimethoxypropane and methanic chloride. Later, n-propilamine was added to the reaction mixture and the samples were incubated at 100 ^{o}C for one hour. The samples were evaporated completely to dryness under continuous N_2 flow and the precipitates were dissolved in dichloromethane and heptafluorobutyric anhydrade. After 10 minutes of incubation at room temperature, samples were evaporated completely to dryness under continuous N_2 flow and resuspended in dichloromethane to analyze at GC-MS [266]. The analysis was performed under chemical ionization mode. Sample injection was performed at 200 ^{o}C. Oven temperature was kept at 100 ^{o}C until 3 minutes after injection and then increased to 160 ^{o}C at a rate of 20 ^{o}C per min. The detector was run at SIM mode and ion abundance of C1 to C3 in the range of 327-332 m/z was recorded. The retention time at which the peak was observed was 5.4 minutes.

4.14.3. Glutamate

Glutamate was isolated by using Dowex 50WX8 (H+) columns from cell culture media and eluted from the column with 2N NH_4OH. Then, the solution was completely evaporated to dryness under continuous airflow. In order to separate the glutamate from glutamine, the amino acid mixture was passed through a Dowex-1X8 ($C_2H_3O_2^-$) column, where the glutamine was washed with water and glutamate was collected with 0.5N acetic acid. The acid fraction which contains glutamate was evaporated to dryness under the airflow and the dried glutamate was dissolved in butanolic-HCl and kept at

100 ^{o}C for one hour. Then, the mixture was evaporated under continuous N_2 flow to dryness and the precipitate was first dissolved in methylene chloride and then trifluoroacetic anhydride was added. After that, the samples were evaporated under continuous N_2 flow and derivatized glutamate was dissolved in methylene chloride to be analyzed with GC-MS under electron impact mode. Sample injection was performed at 250 ^{o}C. Oven temperature was kept at 215 ^{o}C until 2 minutes after injection and then increased first to 225 ^{o}C at a rate of 9 ^{o}C per min and then to 233 ^{o}C at a rate of 3 ^{o}C per min. The detector was run at SIM mode and ion abundance of two different glutamate fragments; C2 to C4 in the range of 151-157 m/z and C2 to C5 C4 in the range of 197-203 m/z, was recorded. The retention time at which the peak was observed was 3.9 minutes.

4.14.4. Alanine, Glycine, Aspartate/Aspargine, Glutamate/Glutamine, Serine, Proline, Methionine

Amino acids were isolated by using Dowex 50WX8 (H+) columns from cell culture media and eluted from the column with 2N NH_4OH. Following, the solution was completely evaporated to dryness under continuous airflow. The samples were dissolved in butanolic-HCl and kept at 100 ^{o}C for one hour. Then, the mixture was evaporated under continuous N_2 flow to dryness and the precipitate was first dissolved in dichloromethane and then trifluoroacetic anhydride was added. After that, the samples were evaporated under continuous N_2 flow and derivatized amino acids were dissolved in dichloromethane to be analyzed with GC-MS under chemical ionisation mode. Sample injection was performed at 250 ^{o}C. Oven temperature was kept at 110 ^{o}C until 1 minute after injection and then increased first to 125 ^{o}C at a rate of 10 ^{o}C per min, then to 153 ^{o}C at a rate of 5 ^{o}C per min, next to 216 ^{o}C at a rate of 50 ^{o}C per min (held at 216 ^{o}C for 1 min) and finally to 250 ^{o}C at a rate of 50 ^{o}C per min. The detector was run at SIM mode and ion abundance of various amino acids (listed below) was measured.

Metabolite	RT (min)	m/z range
Alanine	5.3	241-246
Aspartate/Aspargine	11.5	341-348
Glutamate/Glutamine	12.8	383-390
Glycine	5.7	227-231
Methionine	10.8	329-336
Proline	9.6	295-302
Serine	6.6	353-358

4.14.5. Ribose

The ribose from RNA was isolated from frozen cell pellets using the aqueous phase after addition of Trizol® (Invitrogen) as described in the section 4.3. Purified RNA was dissolved in 2N HCl for hydrolization and incubated at 100 ^{o}C for 2 hrs. The solvent was evaporated to complete dryness under continuous airflow and the precipitate was derivatized in the same way as glucose (Section 4.14.1) and analyzed with GC-MS under chemical ionization mode [282]. Sample injection was performed at 250 ^{o}C. Oven temperature was kept at 150 ^{o}C until 1 minute after injection and then increased first to 275 ^{o}C at a rate of 15 ^{o}C per min and then to 300 ^{o}C at a rate of 40 ^{o}C per min. The detector was run at SIM mode and ion abundance of C1 to C5 in the range of 256-261 m/z was recorded. The retention time at which the peak was observed was 5.3 minutes.

4.14.6. Palmitate and Stereate

The inter- and lower phases of the trizol extract that was described at section 4.3 was used to isolate fatty acids from the pellets that were used to extract ribose. Those phases were added 100 % EtOH and 30 % KOH and were incubated overnight at 100 ^{o}C. Free fatty acids were isolated with petroleum ether and the samples were evaporated completely under continuous N_2 flow. To derivatize, 0.5N methanolic-HCl was added to samples and incubated at 70 ^{o}C for one hour [283]. Then, the samples were analyzed with GC-MS under chemical ionization mode. Sample injection was performed at 250 ^{o}C. Oven temperature was kept at 120 ^{o}C until 1 minute after injection and then increased

to 220 ^{o}C at a rate of 5 ^{o}C per min. The detector was run at SIM mode and ion abundance of palmitate (C16) within the range of 269-279 m/z and stearate (C18) within the range of 297-307 were recorded. The retention time at which the peak was observed was 9.2 and 11.9 minutes respectively.

4.14.7. TCA Cycle Intermediates

The liquid nitrogen frozen cultured plates were used to isolate TCA cycle intermediates by scrapping on ice after addition of 100 % MeOH:H2O (1:1) mixture. Next, the cell extracts were sonicated using a titanium probe (VibraCell, Sonics & Materials Inc., Tune: 50, Output: 30) and agitated at 4 ^{o}C for 30 minutes. Later, the samples were centrifuged and the upper aqueous phase was separated and evaporated to complete dryness under continuous airflow at RT. For derivatization, 2 % (v/v) methoxyamine in pyridine was added to samples and the samples were incubated at 37 ^{o}C for 90 minutes. After that, the samples were incubated at 55 ^{o}C for one hour after N-methyl-N-(tert-butyldimethylsilyl)trifluoroacetamide (MBTSTFA) + 1% tert-butyldimetheylchlorosilane (TBDMCS) addition and analyzed with GC-MS under electron impact mode. Sample injection was performed at 270 ^{o}C. Oven temperature was kept at 100 ^{o}C until 3 minutes after injection and then increased first to 165 ^{o}C at a rate of 10 ^{o}C per min, then to 225 ^{o}C at a rate of 2.5 ^{o}C per min, later, to 265 ^{o}C at a rate of 25 ^{o}C per min and finally to 300 ^{o}C at a rate of 7.5 ^{o}C per min. The detector was run at SIM mode and ion abundance of different TCA cycle intermediates (listed below) was measured.

Metabolite	Empirical Formula	RT (min)	m/z range
Pyruvate	$C_6H_{12}O_3NSi$	8.2	173-177
Citrate	$C_{20}H_{39}O_6Si_3$	37.6	458-466
α-ketoglutarate	$C_{14}H_{28}O_5NSi_2$	24.6	345-352
Fumarate	$C_{12}H_{23}O_4Si_2$	18.2	286-292
Malate	$C_{18}H_{39}O_5Si_3$	27.6	418-424
Aspartate	$C_{18}H_{40}O_4NSi_3$	28.9	417-423

4.15. GC-MS Data Reduction

Spectral data derived from mass spectrometry represents simply the distribution of the ions of a compound or its fragments with varying molecular weights. The value from each observed m/z value is the sum of the experimental isotope incorporation, the presence of isotopes in heteroatoms, the presence of ^{13}C in the background, and when corresponds, the ^{12}C isotope impurity in the ^{13}C labeled precursors (i.e. glucose and glutamine). Moreover, the reagents used for derivatizing may also contain isotopes contributing to the mass isotopomer distribution of the derivitized compound such as silicon. In order to determine the amount of isotope incorporation and its distribution in the compound of interest, it is important todo a correction by subtracting these impurities. This correction is managed by using a in-house developed software which uses regression analysis [284]. The algorithm used corrects all the previously mentioned contributions over the observed spectral intensities of each ion cluster, providing us with the distribution of mass isotopomers in the metabolite of the study owing to the incorporation of ^{13}C atoms from the tracer precursor. Results of the mass isotopomers in any of the ion clusters were reported as fractional enrichments of molecule isotopomers, which are defined as the fraction of molecules having a certain number of isotope substitutions. They are designated as m0, m1, m2 etc. where the number shows the labeled carbon (^{13}C) number in the corrected molecule as explained above. The sum of all mass isotopomers of the ion clusters is equal to 1 or 100 %.

4.16. Data Analysis and modeling by using Isodyn

Our in-house developed software, Isodyn, was used to simulate the transfer of the tracers from [1,2-$^{13}C_2$]-glucose or [U-$^{13}C_5$]-glutamine medium into intracellular metabolites. Isodyn is a program written in C++ and designed to analyze the data from stable isotopic tracers [269-272, 285]. This is a program that automatically constructs and solves a large system of ordinary differential equations which describe the evolution of isotopomer concentrations of metabolites produced in glycolysis, TCA cycle and PPP. All the reactions of non-oxidative branch of PPP catalyzed by transketolases or

transaldolases are counted, considering pentose-5-phosphates as a single pool. Similarly, the reactions of oxidative branch of PPP are assumed as one reaction converting G6P to pentose-phosphates. Initially, all the metabolites except for introduced labeled substrates with known isotopomer composition in the medium are considered to be non-labeled and initial total concentrations of intracellular metabolites are calculated as a function of model parameters assuming a steady state at the initial moment. There is a function designed specifically for each type of reaction (i.e. carboxylation, decarboxylation) and these functions simulate transformation of carbon skeleton (specific transition of labeled carbon) and consumption and production rates of each isotopomer in the considered system. These transformations redistribute ^{13}C isotopes in all metabolites, so that, individual rates which determine the values of the derivatives for the isotopomers are calculated for each isotopomer. To solve this system, a method of numerical integration is chosen arbitrarily (Runge-Kutta, BDF, Dassl). Isodyn simulates a real-time course of label propagation starting from the initial values of experimental conditions of incubation. As it compares the experimental and computed data for corresponding time points, reaching an isotopic steady state is not necessary.

4.17. Mass isotopomer distribution analysis (MIDA)

Mass isotopomer distribution analysis (MIDA) allows us to estimate the contribution of specific metabolic pathways to the synthesis of certain metabolites based on the mass isotopomer results. Contribution of specific metabolic pathways to the synthesis of a certain compound can be estimated using some ratios and calculations with mass isotopomer results (m0, m1, m2, etc.). Some of these calculations are explained along with the results part yet some are detailed here owing to the numerous equations that must be taken into account.

4.17.1. Calculation of pathway specific production of lactate

The amount of lactate produced from glucose via glycolysis, PPP or other pathways can be calculated by combining lactate concentrations and the mass isotopomer distribution of lactate in cell culture media, using [1,2-$^{13}C_2$]-glucose as a tracer. Calculating pathway specific lactate, it is assumed that MCF7 cells only produce (do not consume) lactate under the experimental conditions conducted (with glucose and glutamine availability). Therefore, any lactate present in the medium in the beginning of the experiment contributes to only m0 lactate as no ^{13}C labeled lactate is present in the medium. In our case, there was no lactate in the initial medium and dialyzed FBS also does not include any lactate, so m0 lactate pool is also completely produced by any of the lactate producing pathways. Therefore, the absolute mass isotopomer distribution of accumulated lactate in mM at the end of the incubation ($[Lac_{Total}(m0,m1,m2,m3)]_{t=f}$ (mM)) was obtained from the product of the produced lactate concentration ($[Lac]_{t=f}$ (mM), and its mass isotopomer distribution ($Lac_{Total}(m0,m1,m2,m3)_{t=f}$ (%)) (Equation i).

$$[Lac_{Total}(m0,m1,m2,m3)]_{t=f}\ (mM) = [Lac]_{t=f}\ (mM) \times Lac_{Total}(m0,m1,m2,m3)_{t=f}\ (\%) \quad \text{(i)}$$

Under normal circumstances, in order to obtain the produced lactate in mM which does not contain tracer ($[Lac_{Prod}(m0)]$ (mM), the initial lactate concentration ($[Lac]_{t=0}$) is to be subtracted from the concentration of total lactate m0 $[Lac_{Total}(m0)]_{t=f}$ (mM) (Equation ii). However, as our initial medium does not contain any lactate, this substraction will not change the result of the equation ii.

$$[Lac_{Prod}(m0)]\ (mM) = [Lac_{Total}(m0)]_{t=f}\ (mM) - [Lac]_{t=i}\ (mM) \quad \text{(ii)}$$

Next, relative mass isotopomer distribution of produced lactate ($Lac_{Prod}(m0,m1,m2,m3)_{t=f}$ (%)) was recalculated by dividing the absolute mass isotopomer distribution of produced lactate ($[Lac_{Prod}(m0,m1,m2,m3)\ ]_{t=f}$ (mM)) by total produced lactate ($[Lac_{Prod}]$ (mM)) (Equation iii), which in turn was obtained by subtracting initial lactate concentration ($[Lac]_{t=i}$ (mM)) from final lactate concentration ($[Lac]_{t=f}$ (mM)) (Equation iv). It is worth noting down these equations yet in our case, having no initial lactate will eliminate the need of the first four steps of the calculations.

$$Lac_{Prod}(m0,m1,m2,m3)_{t=f}\ (\%) = [Lac_{Prod}(m0,m1,m2,m3)\ ]_{t=f}\ (mM) / [Lac_{Prod}]\ (mM) \quad \text{(iii)}$$

$$[Lac_{Prod}]\ (mM) = [Lac]_{t=f}\ (mM) - [Lac]_{t=i}\ (mM) \quad \text{(iv)}$$

The percentage of lactate coming from glucose through direct glycolysis (glycolytic tax, GT) was derived from the recalculated mass isotopomer distribution of produced lactate (Equation v).

$$GT = Lact_{Prod}(m2)_{t=f}\ (\%) \times 2 / Glc(m2)_{t=i}\ (\%) \quad \text{(v)}$$

Here, $Glc(m2)_{t=i}$ (%) is the percentage of [1,2-$^{13}C_2$]-glucose in culture medium at the beginning of the experiment. Then, maximum feasible amount of lactate coming from glycolysis ($[Lac_{ProdGlyc}]$ (mM)) was obtained from the product of glycolytic tax and produced lactate ($[Lac_{Prod}]$ (mM)) (Equation vi).

$$[Lac_{ProdGlyc}]\ (mM) = GT \times [Lac_{Prod}]\ (mM) \quad \text{(vi)}$$

The Pentose Cycle (PC) parameter is defined as the relative amount of glucose metabolised through glycolysis related to the glucose metabolised through PPP [283]. To estimate the amount of lactate from glucose coming through PPP, PC parameter using values of mass isotopomer distribution of total lactate was calculated first (Equation vii).

$$PC = (Lac_{Total}(m1)_{t=f} / Lac_{Total}(m2)_{t=f}) / (3 + Lac_{Total}(m1)_{t=f} / Lac_{Total}(m2)_{t=f}) \quad \text{(vii)}$$

Then, lactate from glucose coming through PPP ($[Lac_{ProdPPP}]$ (mM)) was obtained from the product of PC and the maximum feasible amount of lactate coming from glycolysis ($[Lac_{ProdGlyc}]$ (mM)) (Equation viii).

$$[Lac_{ProdPPP}]\ (mM) = PC \times [Lac_{ProdGlyc}](mM) \quad \text{(viii)}$$

Finally, to calculate the amount of lactate produced from other sources than glucose ($[Lac_{ProdOS}]$ (mM)), the maximum lactate produced from glycolysis ($[Lac_{ProdGlyc}]$ (mM)) and lactate coming from glucose through PPP ($[Lac_{ProdPPP}]$ (mM)) were subtracted from produced lactate ($[Lac_{Prod}]$ (mM)) (Equation ix).

$$[Lac_{ProdOS}]\ (mM) = [Lac_{Prod}]\ (mM) - [Lac_{ProdGlyc}]\ (mM) - [Lac_{ProdPPP}]\ (mM) \quad \text{(ix)}$$

4.17.2. Calculation of glucose contribution to Mitochondria (via PC or PDH)

Glucose can enter to TCA cycle in two ways; either via pyruvate dehaydrogenase (PDH) which converts pyruvate to acetyl-CoA, or via pyruvate carboxylase (PC) which transforms pyruvate to oxaloacetate by addition of a carbon. With PDH, acetyl-CoA is combined with oxaloacetate via citrate synthase (CS) to produce citrate and citrate will be oxidized to α-ketoglutarate which is in equilibrium with glutamate. When a molecule of [1,2-$^{13}C_2$]-glucose enters to TCA cycle with PDH, [1,2-$^{13}C_2$]-acetyl-CoA will be obtained and this molecule will end up in glutamate as [4,5 -$^{13}C_2$]-glutamate. However, when PC mediates pyruvate entrance to TCA cycle, oxaloacetate derived from a molecule of [1,2-$^{13}C_2$]-glucose will yield [2,3 -$^{13}C_2$]-glutamate. Therefore, the pathway used to make glucose enter to TCA cycle can be estimated by analyzing the mass isotopomer distribution of glutamate molecule fragments C2-C4 and C2-C5 as described in the below table.

Then, the relative contribution of both PDH and PC pathways (%) to glucose entrance into TCA cycle was calculated as previously reported [286] (Equation x and xi).

$$\%\ PDH = (Glu_{C2\text{-}C4}(m2) - Glu_{C2\text{-}C5}(m2)) / Glu_{C2\text{-}C5}(m2) \quad \text{(x)}$$

$$\%\ PC = Glu_{C2\text{-}C4}(m2) / Glu_{C2\text{-}C5}(m2) \quad \text{(xi)}$$

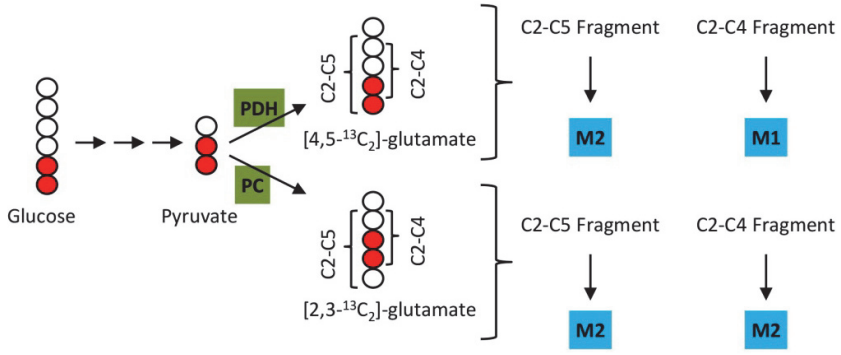

Figure 4.1: Glucose contribution to mitochondria either by PDH or PC

4.17.3. Calculation of glucose and glutamine contribution to fatty acid synthesis

In order to calculate the relative contribution of glucose or glutamine to fatty acid synthesis, first, the fraction of ^{13}C-Ac-CoA (which is denoted as *q*) in total Ac-CoA pool of the cells cultured with either [1,2-$^{13}C_2$]-glucose or [U-$^{13}C_5$]-glutamine was calculated [287, 288]. Determination of ^{13}C-Ac-CoA fraction of fatty acids was done as follows (Equation xii):

$$Fa(m4)_{t=f} / Fa(m2)_{t=f} = (n-1)/2*(p/q) \quad \text{(xii)}$$

In this equation, n stands for the number of acetyl units in the fatty acid chain which is being analysed (n=8 for palmitate and n=9 for stearate). *q is* the labeled fraction and *p* is un labeled fraction, where p*+q=1*.

To estimate the contribution of glucose or glutamate to synthesis of fatty acids, the theoretical fraction of ^{13}C-Ac-CoA of cells cultured with labeled inputs should first be calculated. For [1,2-$^{13}C_2$]-glucose input, it is the percentage of [1,2-$^{13}C_2$]-glucose at the beginning of the tracer based metabolomics experiment (Equation xiii).

$$\text{Theoretical Fraction of } ^{13}\text{C-Ac-CoA} = Glc(m2)_{t=I}\ (\%) \quad \text{(xiii)}$$

For glutamine, it is more complicated to calculate the theoretical fraction of ^{13}C-Ac-CoA. As demonstrated at figure 4.1, Ac-CoA can be produced from glutamine in two ways; either via oxidative glutamine metabolism (OGM) where m0 Ac-CoA is produced, or via reductive glutamine metabolism (RGM) where m2 Ac-CoAis produced. Theoretically, also malate dehdyrogenase (MDH) and malic enzyme (ME) can produce m2 Ac-CoA, nevertheless, in our experiments the glutamine incorporation to pyruvate was less than 0.1 %, which can be ignored. Figure 4.1 also shows that OGM produces m4 citrate while RGM produces m5 citrate. Hence, the following equation is used to calculate the theoretical fraction of ^{13}C-Ac-CoA from glutamine (Equation xiv):

$$\text{Theoretical Fraction of } ^{13}\text{C-Ac-CoA} = RGM/(RGM+OGM) = Cit(m5)_{t=f}/(Cit(m5)_{t=f} + Cit(m4)_{t=f}) \quad \text{(xiv)}$$

Now that the theoretical fractions were calculated, the rate of glucose or glutamine contribution to fatty acid synthesis was calculates as shown in equation xv.

% of Contribution = q / Theoretical Fraction of ^{13}*C-Ac-CoA* (xv)

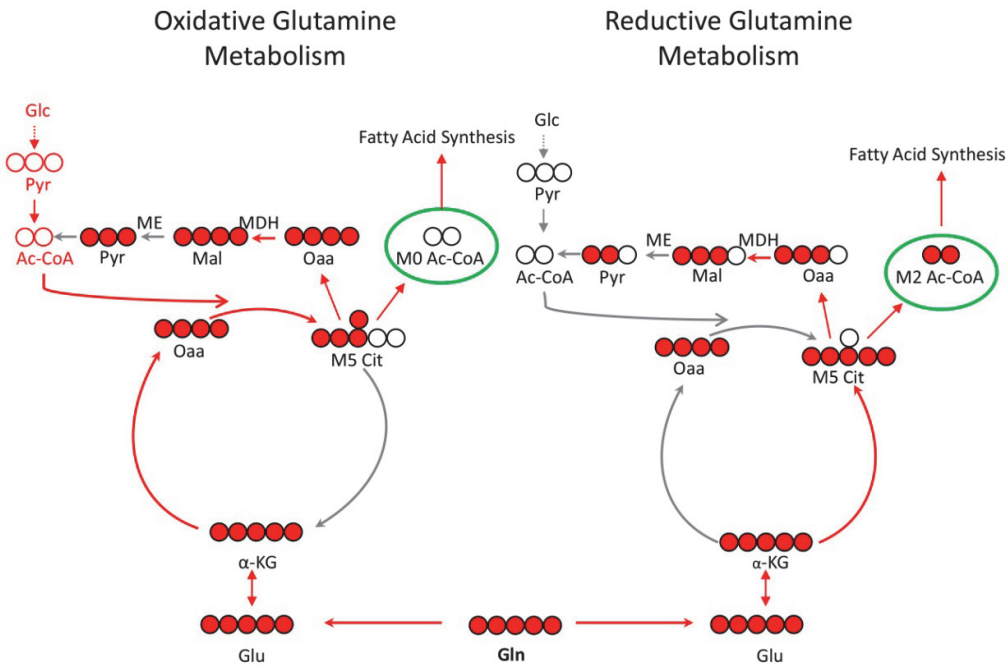

Figure 4.2: Contribution of glutamine to Ac-CoA synthesis (Red arrows show the active pathway)

4.17.4. Calculation of Approximate Flux ratio of Glutamate Dehydrogenase (GDH) to Isocitrate Dehdrogenase (IDH)

As explained above, glutamine can be metabolized in TCA cycle either with oxidative way in which glutamate (derived from glutamine) is converted to αKG and subsequently to succinate and so on, or with reductive metabolization where αKG is converted to isocitrate [289]. The influx of [U-^{13}C] glutamine into the TCA cycle via glutamate dehdyrogenase (GDH) produces m5 mass isotopomer of αKG, while the flux of citrate to αKG via isocitrate dehdyrogenase (IDH) produces m1 - m4 labeled αKG. Therefore,, the

ratio between m5 and m1 - m4 mass isotopomers for αKG corresponds roughly to the flux ratio of GDH to IDH (eqution xvi).

$$GDH/IDH = \alpha KG(m5) / \alpha KG(m1 - m4) \quad \text{(xvi)}$$

4.18. Statistical analysis

For statistical analysis, parametric unpaired two-tailed independent samples Student's t-test was used. In all figures, bars represent mean ± SD, and number of samples (n) is indicated in each case. One asterisk (*) denotes p-value<0.05, two asterisks (**) denote p-value<0.01 and three asterisks (***) denote p-value<0.001.

In the case of metabolic flux estimation using Isodyn, an annealing algorithm was used to minimize the difference between calculated and experimental data (χ^2). The goodness of best fit which corresponds to the minimal deviation of calculated isotopomer fractions of experimental ones was checked based on the χ^2 value and number of degree of freedom. According to that checking, in the case that the fit was deemed acceptable, the metabolic fluxes which correspond to the best fit were accepted as consistent with the measured isotopomer distributions [272].

5. RESULTS AND DISCUSSION

Chapter 5.1

5.1. The Role of 6-Phosphogluconate Dehydrogenase (6PGD) in Breast Cancer Cells: A Novel Therapeutic Target Against Breast Cancer

5.1.1. Introduction

Cancer cells are known to show a wide variety of metabolic alterations [15]. Many observations made during the early period of cancer biology research revealed metabolic changes like the Warburg effect to be a common feature of cancer cells [40, 290]. Nowadays, multiple molecular mechanisms both intrinsic and extrinsic are known to play a vital role in reprogramming cellular metabolism in order to fulfill the three basic needs for cancer cell survival: i) maintenance of energy status, ii) increased biosynthesis of macromolecules, and iii) maintenance of appropriate redox status [291]. Nevertheless, many mechanisms regulating metabolic reprogramming are still unknown, and the search for new tumor-specific metabolic dependencies exploitable in the impairment of neoplastic proliferation is a growing field in cancer research.

In the introduction part of this dissertation, it has been shown that tumor metabolism highly depend on PPP to maintain their highly proliferative state [76, 78, 79], since PPP plays important roles in not only nucleotide biosynthesis and redox detoxification, but also many other aspects related to cancer cells' viability, including proliferation, apoptosis, invasiveness, drug resistance, and metastasis [74, 77]. Therefore, the therapeutic potential of targeting PPP has attracted the interest of researchers in the

field and both oxidative and non-oxidative phases of this metabolic pathway have been of keen interest to be used as therapeutic drug targets [77, 98, 102].

The oxidative branch of PPP is especially interesting because it is able to produce NADPH; therefore, it plays a key role in the regulation of reactive oxygen species (ROS) levels. The balance between ROS production and removal has been demonstrated to be altered in some tumors, and has also been proposed to be an attractive therapeutic target on its own [101]. Unpublished data obtained within our group have revealed that inhibition of glucose-6-phosphate dehydrogenase (G6PD) has important effects; such as decreased cell proliferation, increased cell death and ROS together with cell cycle arrest on MCF7 breast cancer cells' metabolism. As a complement to previous studies carried out in our group, we further inhibited another important enzyme in this pathway in MCF7 breast cancer cells: 6-Phosphogluconate dehydrogenase (6PGD), the third enzyme of the ox-PPP which catalyzes the conversion of 6-phosphogluconate (6-PG) to ribulose-5-phosphate whose results are shown in this section.

We suggest 6PGD as a better target than G6PD for various reasons. First, despite that the entire PPP is regulated by several factors, being the rate limiting enzyme of PPP as it catalyzes the irreversible conversion of glucose-6-phosphate to 6-phosphogluconolactone, G6PD is much more tightly regulated by means of several levels involving transcriptional, translational, post-translational, and metabolic regulations [292]. Besides, NADPH/$NADP^+$ ratio is an important regulator of G6PD and since up to 75 % NADPH required for *de-novo* lipid synthesis in cellular organisms is produced by G6PD, this enzyme is also considered as a part of lipogenic enzyme family and it is further regulated by hormone and nutritional factors [293]. Therefore, altering the function of G6PD is more challenging than other PPP enzymes. On the other hand, inhibition of 6PGD leads to the accumulation of 6-PG which is an important glycolysis regulator [294]. 6-PG takes role directly in the activation of glycolytic enzyme phosphofructokinase (PFK) [295], pyruvate kinase (PK) [296] and phosphoglucomutase (PGM) which takes role in glycogen breakdown [297]. Moreover, glycolytic enzyme phosphoglycerate mutase 1 (PGAM1) is reciprocally regulated by 6-PG in a way that 3-phosphoglycerade (3-PG), the substrate of this enzyme, is also a competitive inhibitor of 6PGD [294]; therefore, accumulation of 6-PG affects the activity of PGAM1.

In short, in this study we have characterized the metabolic reprogramming induced by the knockdown of 6PGD by RNAi mediated silencing, in order to further explore this enzyme's potential as a therapeutic drug target in two breast cancer cell lines. In addition, knowing that p53 has several vital functions in cellular metabolism among which are cell cycle regulation, apoptosis induction and regulation of glycolysis and PPP [90], we speculated that any effect induced by 6PGD knockdown might be related to p53 activation; therefore, we also aimed to investigate the relation between p53 activation and PPP. Because of the high reliance of breast cancer cells on PPP and their dependence on ROS detoxification to manage their oxidative stress and maintain their survival [76, 298], we chose breast cancer cell lines as models in which to target 6PGD enzyme. On the other hand, for a better and more critical understanding of the effects of 6PGD inhibition on breast cancer cells, we employed another breast cancer cell line, T47D, which has similar characteristics to MCF7 cells [9].

5.1.2. Results

5.1.2.1. 6PGD Knockdown in MCF7 and T47D Cells

In order to test the dependence of breast cancer cells on oxidative phase of PPP, we tested two different siRNA sequences targeting different exonic regions of 6PGD gene for their RNAi machinery expression at mRNA level. Also, a non-targeting siRNA sequence (siNEG) was used as negative control in all experiments in order to obtain a coherent comparison. The knockdown of 6PGD was measured at mRNA level 72 hrs after transfection and both siRNA sequences showed moderate level of inhibition on both cell lines, with a decrease in fold change of around 60 % when compared to the cells transfected with siNEG (see figure 5.1.1A). On the other hand, the knockdown of 6PGD activity was also assesed 96 hrs after transfection by measuring specific enzyme activity. At protein level, both siRNA sequences induced an inhibition of around 25 % of enzyme

activity in T47D cells, while for MCF7 cells the inhibition of enzyme activity was closer to 50 % (figure 5.1.1B).

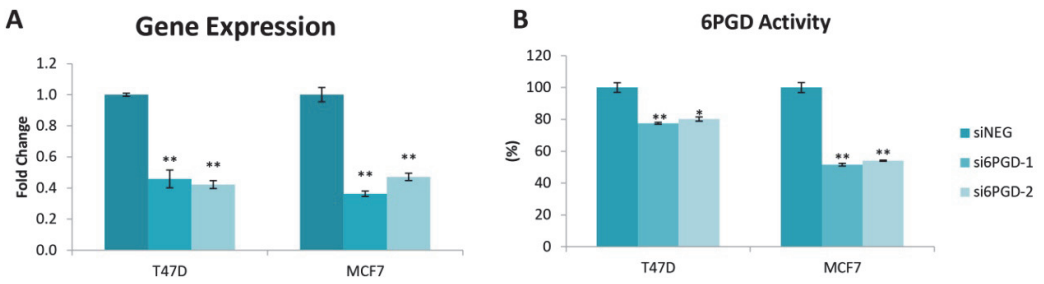

Figure 5.1.1. Knockdown of 6PGD enzyme with two different siRNA sequences targeting 6PGD

A) 6PGD mRNA expression 72 hrs after transfection with non-targeting siRNA (siNEG) or siRNA's against 6PGD. Fold change was calculated with respect to siNEG. **B)** 6PGD enzyme activity levels 96h post transfection using either non-targeting siRNA or siRNAs against 6PGD. Fold change was quantified relative to siNEG. The bars correspond to mean ± SD of n = 3. Statistically significant differences between 6PGD inhibited and control cells were indicated at $p < 0.05$ (*), $p < 0.01$ (**) and $p < 0.001$ (***).

5.1.2.2. Inhibition of 6PGD Reduces *in vitro* Proliferation of Breast Cancer Cells

PPP is an anabolic pathway that has critical role in cell proliferation. Therefore, we tested the functional role of 6PGD in breast cancer cells' proliferation using MCF7 and T47D cells as models. The effect of 6PGD knockdown on the proliferation rates of both cell lines was measured via flow cytometry, combining direct cell counting and propidium iodide (PI) staining. Notably, 96 hrs after transfection, 6PGD knockdown had a clear effect over MCF7 cells proliferation rates: cell number was around 25 % lower compared to siNEG transfected cells. The effect was less dramatic in the case of T47D cells, since final cell number for si6PGD-transfected cells was only 10% lower compared to cells transfected with non-targeting siRNA (figure 5.1.2A). In any case, our results prove that the altered cellular metabolism that results from 6PGD knockdown entails a reduction in cell proliferation rates. It is worth noting that the reduction in both cell lines' proliferation rates results from a limited decrease of 6PGD enzyme's activity (close to 50 % in the case of MCF7 cells, and only around 25 % in the case of T47D cells), which

highlights the importance of 6PGD activity in breast cancer cells' proliferation. This could be explained because 6PGD inhibition entails a decrease in pentose biosynthesis capability, which is essential to synthesize DNA; and therefore, is indispensable and of great importance for proliferating cells. Besides, the knockdown of 6PGD is also expected to provoke an accumulation of 6-phosphogluconate (6PG), which has been reported to cause a slower proliferation of cells by a mechanism which has not yet been elucidated [96]. We suppose that a stronger inhibition of this gene is expected to lead to decrease the proliferation of breast cancer cells at more significant levels.

5.1.2.3. 6PGD Knockdown Leads to Cell Cycle Arrest and Apoptosis Induction

Taking into account that one of the essential roles of ox-PPP is to provide cells with nucleotides and NADPH to maintain cell proliferation, and that G6PD was reported to be upregulated during the G1 and S phases of the cell cycle [77], we hypothesized that 6PGD knockdown might also induce a cell cycle arrest in G1 or S phase. Decreased cell proliferation rate in MCF7 and T47D cells upon 6PGD knockdown may be due to a cell cycle arrest in either S or G1 phase of cell cycle. To study the effect of 6PGD knockdown over the cell cycle distribution, the cells were stained with vindelov-PI solution after fixation and were analyzed by FACS to quantify their DNA content. Analysis of cell cycle distribution after 96 hrs of 6PGD knockdown demonstrated a significant arrest in S phase and a subsequent decrease in G1 phase in MCF7 cells. T47D cells, on the other hand, showed only slight decrease in G1 phase with no significant variation in the distribution of the cells across various cell cycle phases (figure 5.1.2B).

Cell cycle is a process through which cells grow and proliferate and any alteration in cell cycle may induce apoptosis [299]. To check whether together with the arrest in cell cycle, any apoptosis has been induced in either MCF7 or T47D cells we carried out apoptosis assays 96 hrs after inhibiting 6PGD gene expression with the two different siRNA sequences. FACS analysis using annexin-V and PI has been used to assess the presence of non-apoptotic cells (no interaction with neither annexin-V nor PI), early apoptotic cells (interaction with only annexin-V), and late apoptotic or necrotic cells

(interaction with both annexin-V and PI) [274, 300]. Our results demonstrated that the knockdown of 6PGD in MCF7 caused a significant increase in the number of late apoptotic and necrotic cells, whereas, 6PGD knockdown in T47D cells slightly increased the number of early apoptotic cells (Figure 5.1.2C). Although the 6PGD-knockdown achieved with si6GPD is similar in both cell lines at RNA level, final effect over 6PGD enzyme activity is higher in MCF7 cells, which might explain why the induction of cell cycle arrest and apoptosis induction is higher in MCF7 than in T47D cells.

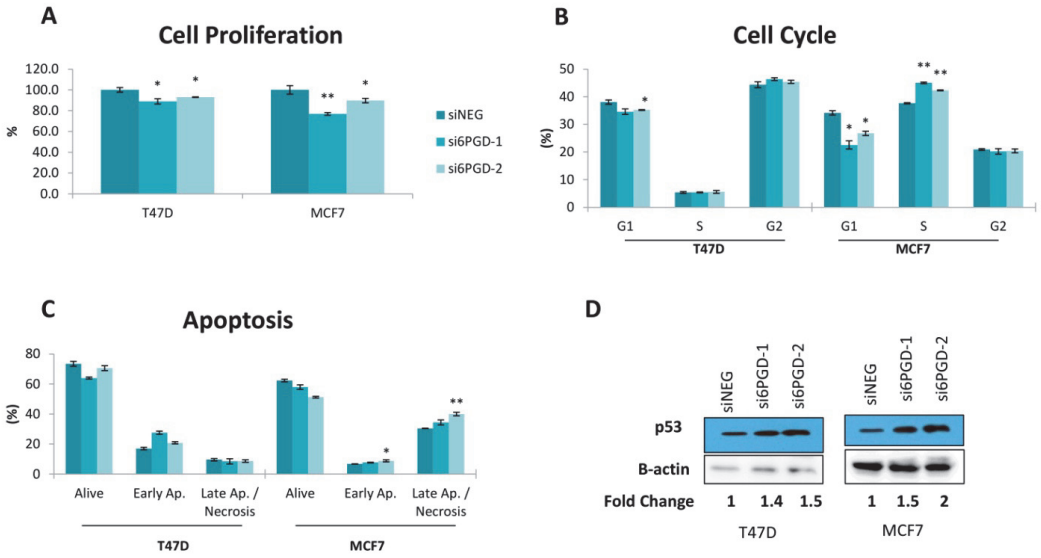

Figure 5.1.2. The role of PPP enzyme 6PGD in cell survival, cell cycle, apoptosis and p53 activation.

A) Flow cytometric measurements of cell proliferation, 96 hrs after transfection, for 6PGD-knockdown cells and cells transfected with siNEG. **B)** Cell cycle distribution analysis of MCF-7 and T47D cells after 96h of siRNA transfection. The percentage of cells in the different cell cycle phases was calculated using FlowJo® software. **C)** Percentage of apoptotic cells out of a $1x10^4$ cells, measured by flow cytometry using Annexin V FITC kit, 96 hrs after transfection. **D)** Western blot analysis of p53 expression in cells transfected with si6PGD vs. cells transfected with siNEG, 120 hrs after transfection. The bars correspond to mean ± SD of n = 3. Statistically significant differences between 6PGD inhibited and control cells were indicated at $p < 0.05$ (*), $p < 0.01$ (**) and $p < 0.001$ (***).

5.1.2.4. 6PGD Knockdown Upregulates p53

Tumor suppressor gene p53 has been proven to have effects on the regulation of cell cycle arrest and apoptosis [19]. Moreover, it is reported to suppress PPP which takes an

important role in tumor cell growth and proliferation [90]. Taking this into account, we decided to assess if the inhibition of 6PGD activity could have an effect on p53 expression. As demonstrated in figure 5.1.2D, western blot analysis has demonstrated that there is an increase in p53 protein expression after the inhibition of 6PGD gene in both MCF7 and T47D cells. MCF7 cells are known to have wild type p53 gene [301, 302], and therefore we can conclude that p53 over expression resulting from 6PGD inhibition eventually leads to cell cycle arrest and apoptosis induction, which in turn slows down proliferation rates in MCF7 cells. On the contrary, p53 gene is mutated on T47D cells, which further explains why p53 over expression resulting from 6PGD inhibition does not entail a significant cell cycle arrest or a high level of apoptosis induction in this cell line. This is also consistent with a lower effect of 6PGD inhibition over T47D cells proliferation, when compared to MCF7 cells. Taken together, these results highlight an interesting connection between 6PGD activity and p53 expression, although further studies will be needed to elucidate the relation between these proteins in a more detailed manner.

5.1.2.5. NADPH Produced by 6PGD does not Take Role in ROS Detoxification

As it has been mentioned earlier, the NADPH produced in PPP provides reducing equivalents for protecting the cells against the toxicity of ROS by regenerating reduced glutathione (GSH) [74]. Since redox homeostasis plays a very important role in tumor survival, particularly in breast cancer cells, we speculated that inhibiting 6PGD, which is involved in NADPH production, might provoke changes in breast cancer cells' ROS level. However, the measurement of ROS using H_2DCFA probes in MCF7 and T47D cells transfected with si6PGD did not show any significant changes in their ROS production compared to cells transfected with siNEG (Figure 5.1.3), thus indicating that 6PGD might not be involved in maintenance of redox status of these cell lines or that the cells are able to resort to alternative pathways to maintain their required NADPH levels. In any case, our results indicate that the antiproliferative activity resulting from G6PD inhibition is probably not related to the existence of an enhanced oxidative stress.

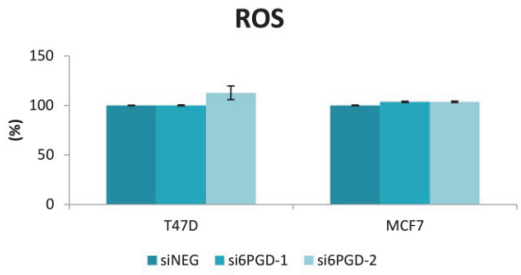

Figure 5.1.3. The effect of 6PGD inhibition over ROS generation.

Relative ROS level measured by flow cytometry using H_2DCFA probes. ROS levels are expressed as fold change with respect to siNEG ROS levels. The bars correspond to mean ± SD of n = 3.

5.1.2.6. Central Carbon Metabolism is Reprogrammed in Response to 6PGD Inhibition.

Cancer is not only a disorder of proliferation but also a metabolic disease. Therefore, metabolic changes that occur in cancer cells are considered to have a vital role in explaining tumor formation. In order to obtain deeper information about the implications of PPP in cancer cell metabolism, we performed some basic metabolic flux measurements. To this end, we measured the extracellular fluxes of certain metabolites such as glucose, lactate and glutamine. The analysis of consumption and production rates of extracellular glucose and lactate showed a slight decrease in glucose consumption 96 hrs after knockdown of 6PGD gene in both cell lines. Similarly, the lactate production was found to be reduced, but in a slightly higher rate (figure 5.1.4A). Figure 5.1.4B shows the decrease in glycolytic efficiency in both cell lines with 6PGD knockdown, calculated as lactate produced (in moles) divided into the glucose consumed (in moles) [261, 303]. A decreased rate of glucose to lactate could be due to a shift from glycolysis towards TCA cycle for the production of energy and other TCA cycle intermediates needed for bioenergetics reactions and cells' survival. This result is concordant with the reduced lactate dehdyrogenase (LDH) enzyme activity when 6PGD gene is inhibited, as shown in figure 5.1.5A. LDH is the enzyme catalyzing the conversion of the pyruvate into lactate, and reduced LDH activity means that glucose might be directed to TCA cycle; therefore, an increase the key activities of this pathway is expected.

While glucose is the main nutrient for many biological systems, glutamine has also pivotal role in metabolism of various cells, particularly for tumor cells. Glutamine is an abundant and very important amino acid which plays role in energy formation, redox homeostasis, synthesis of various macromolecules and several signaling pathways relevant in cancer cells [121, 304]. Among them, redox homeostasis has close connection with PPP pathways as one of the main functions of the latter is also the same; therefore, impaired PPP is expected to alter glutamine consumption flux in the cancer cells. To this end, we measured the effect of 6PGD knockdown over glutamine flux of breast cancer cells. We observed an altered glutamine metabolism when the cells were subjected to 6PGD knockdown, especially in MCF7 cells, since glutamine

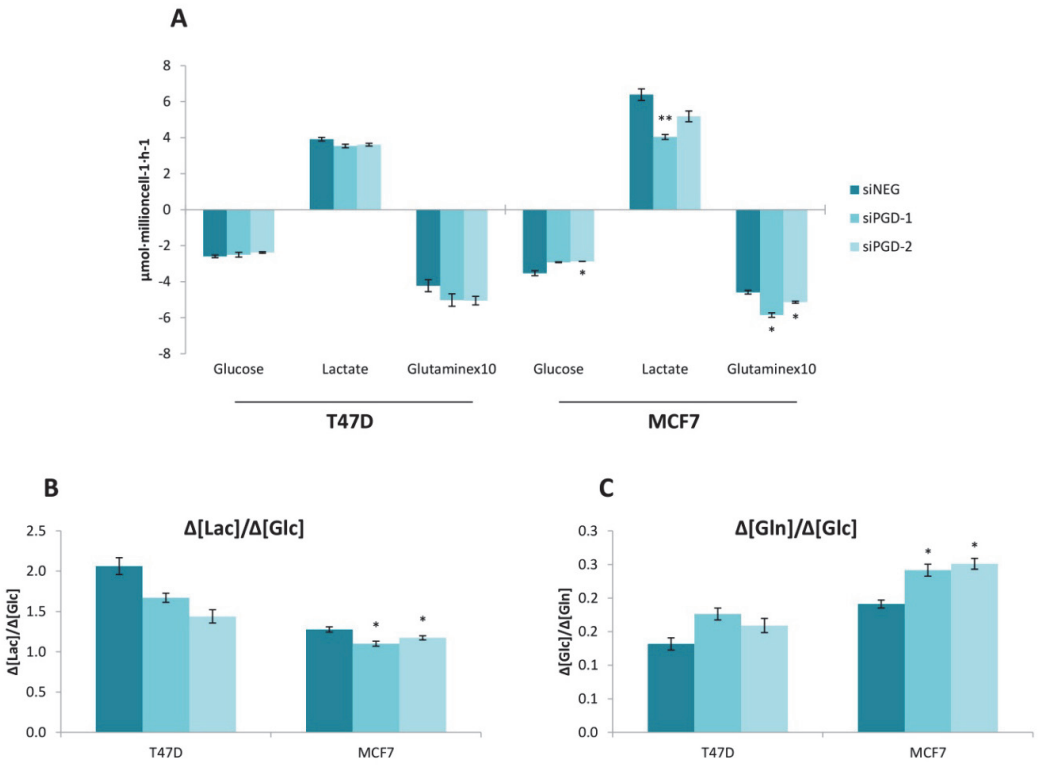

Figure 5.1.4. The effect of 6PGD inhibition on glucose, lactate and glutamine metabolism

A) Consumtion of glucose and glutamine, and production of lactate were measured 96 hrs after transfection either by si6PGD or siNEG. **B)** Glycolytic activity which shows the conversion rate of glucose to lactate **C)** Consumption rate of glutamine over glucose. The bars correspond to mean ± SD of n = 3. Statistically significant differences between 6PGD inhibited and control cells were indicated at $p < 0.05$ (*), $p < 0.01$ (**) and $p < 0.001$ (***).

consumption rate augmented and the ratio between glutamine and glucose consumptions was higher after 6PGD inhibition in these cells (see figure 5.1.4A and C).

Above, we indicated that knockdown of 6PGD gene did not cause any noticeable accumulation of ROS in neither of the breast cancer cell lines (figure 5.1.3). Therefore, we hypothesized that the increased consumption of glutamine could be used in order to produce NADPH via malic enzyme (ME) and isocitrate dehydrogenase (IDH), and in that way, the cells maintained the reductive capacity of the cells to compromise after 6PGD inhibition. We observed that 6PGD knockdown increased ME and IDH activities in MCF7 cells (Figure 5.1.5B and C), which is consistent with our hypothesis. Nonetheless, we did not observe any strong alteration of ME or IDH activity in T47D cells. It has also been reported that MCF7 cells are more dependent on glutamine than glucose compared to T47D cells [305], which explains why T47D cells show less alteration in glutamine flux.

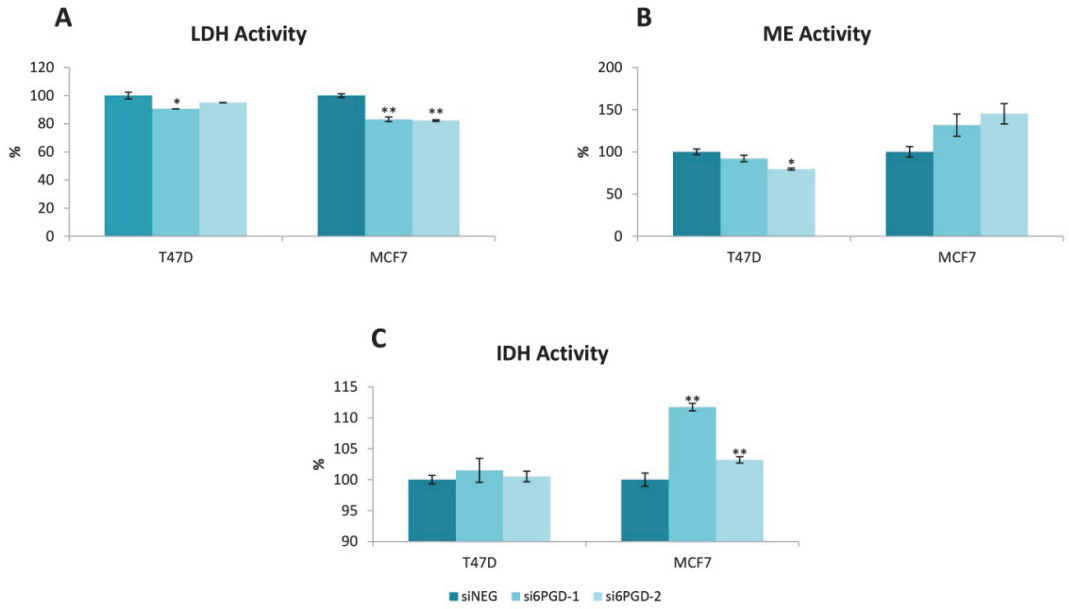

Figure 5.1.5. 6PGD inhibition alters the activity of glycolyisis and glutaminolysis enzymes

A) Lactate Dehydrogenase, **B)** Malic enzyme and **C)** Isocitrate Dehydrogenase activity levels measured at 96 hrs post transfection using either siRNAs against 6PGD or non-targeting siRNA. Fold change was quantified as a percentage relative to enzyme activity levels in siNEG-transfected cells. The bars correspond to mean ± SD of n = 3. Statistically significant differences between 6PGD inhibited and control cells were indicated at $p < 0.05$ (*), $p < 0.01$ (**) and $p < 0.001$ (***).

5.1.2.7. 6PGD Knockdown Alters 3D *in vitro* Culture of Breast Cancer Cells

One of the biggest challenges in the clinical treatment of tumors is cancer resurrection, a phenomenon occurring due to stem cell like properties of cancer cells [306]. Despite that PPP is involved in several essential processes in healthy and cancer cells, there is not many proven links between PPP and stem cell like characteristics of tumors. Therefore, we decided to check whether targeting 6PGD could be an effective approach to disrupt the acquisition of stem cell like properties in breast cancer cells. The ability to form single cell colonies is one of the characteristic features of cancer stem cells (CSC) [30], so the effect of 6PGD inhibition over the stem cell characteristics of MCF7 and T47D cells was assessed by measuring their mammosphere formation capability after seeding the transfected cells to low attachment plates and using a supplemented medium that triggers the formation of mammospheres. Our results showed that

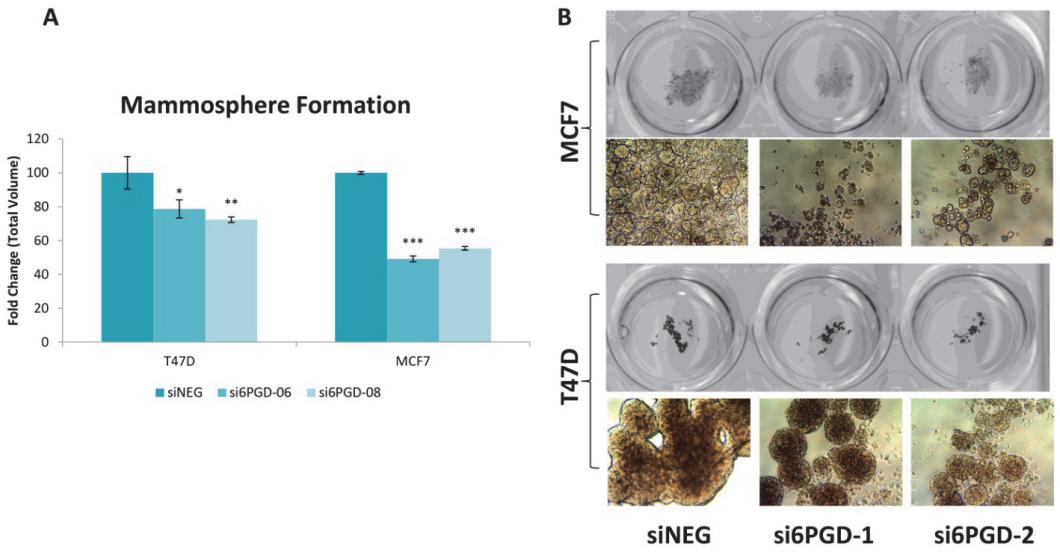

Figure 5.1.6. 6PGD knockdown reduces mammosphere formation capacity of breast cancer cells

A) Mammosphere formation capability of MCF7 and T47D cells after treatment with siNEG or siG6PD siRNA. The total mammophere area for each condition was represented as a percentage relative to the total mammosphere area of siNEG-transfected cells. **B)** Representative photographs showing the different shape, size of mammospheres in each experimental condition. The bars correspond to mean ± SD of n = 3. Statistically significant differences between 6PGD inhibited and control cells were indicated at $p < 0.05$ (*), $p < 0.01$ (**) and $p < 0.001$ (***).

mammosphere formation capability of MCF7 cells decreased around 50 % when the cells were transfected with si6PGD, while T47D cells' mammosphere formation capability decreased around 25 % in the same conditions (Figure 5.1.6A). Besides, the size of the mammospheres was found to be smaller in cells with reduced 6PGD expression, compared potential of 6PGD as a promising drug target. to those with no knockdown in 6PGD (Figure 5.1.6B). This indicates that 6PGD has an important role in maintaining the stem cell characteristics of these luminal breast cancer cell lines. The fact that inhibition of 6PGD decreases mammosphere formation capability highlights the potential of 6PGD as a promising drug target.

5.1.3. Discussion

This study reveals 6PGD as a key ox-PPP enzyme, with an important role in the metabolism of breast cancer cell lines MCF7 and T47D and that it is modulated by p53. Several previous studies have highlighted the importance of PPP in breast cancer tumors, especially those in advanced states, such as MCF7 [85, 307, 308]. Also, former studies carried out in our group have supported the idea that investigating the PPP is noteworthy. Previously, we have inhibited the G6PD (the first enzyme of the oxidative phase of PPP) and TKT (an enzyme of nonoxidative phase of PPP) in MCF7 cells and we observed that especially G6PD had marginal effects on the cell proliferation and cell cycle arrest but strong effects on ROS detoxification. Moreover, inhibition of either G6PD or TKT led breast cancer cells to reprogram their metabolism (data not published). Therefore, we focused our attention to investigate the role of the 6PGD, another dehdyrogenase enzyme on oxidative phase of PPP. We included another breast cancer cell line, T47D, which has similar characteristics to MCF7 (ER positive, hormone dependent breast cancer cells) except that T47D carries mutated p53. In that way, we were able to compare not only the effects of 6PGD inhibition on different cell lines but the functional role of p53 tumor suppressor in the regulation of PPP as well.

Here, we have first demonstrated that 6PGD has a pivotal role in the proliferation of MCF7 cells, while it has only marginal effects on the proliferation of T47D cells. The high dependency of these cells to 6PGD is clear considering the fact that partial inhibition of the activity of this enzyme (around 50 % for MCF7 cells and around 25 % for T47D cells) led to around 25 % and 10 % decrease in cell proliferation for MCF7 and T47D cells respectively. There are several scenarios which might have taken role in the attenuation of breast cancer cells when 6PGD is impaired. First, decreased nucleotide and NADPH synthesis with inhibition of PPP leads to decrease in proliferation since nucleotides are needed for the biosynthesis of genetic material and NADPH is needed for lipid biosynthesis and redox balance. Moreover, we suggest that the accumulation of glycolytic pathway metabolites due to the inhibition of 6PGD might have taken role in lower proliferation rate of breast cancer cells. Besides accumulation of glycolysis metabolites, 6PGD inhibitions also results in accumulation of 6-phosphogluconate and 6-phosphogluconolacton, which in turn alters the proliferation of MCF7 and T47D cells. Even though the exact mechanism of act of 6PGD is not totally elucidated, its importance in cell proliferation has been reported in several studies [96, 212] and a permanent and stronger knockdown of this gene using small-hairpin RNA (shRNA) is expected to result in even more significant reductions of the proliferation kinetics of the breast cancer cells.

Furthermore, cell cycle was also altered in 6PGD inhibited breast cancer cells. For MCF7 cells, an arrest at G1 phase was observed as expected, since nucleotide synthesis was partly impaired. T47D cells did not show any strong arrest in any phase, however, the inhibition of 6PGD managed in T47D cells was less than MCF7 cells, which may explain why a successful cell cycle arrest did not occur. Also, T47D cells have much higher activity of cyclin dependent kinase 1 (CDK1) [309], which takes role in transition from various phases in cell cycle and this may also be the reason for not seeing a strong arrest in this cell line. Similarly, 6PGD knockdown has also induced apoptosis in breast cancer cell lines. In MCF7 cells this induction was visible on late apoptosis/necrosis level, while for T47D, the population of the cells in early apoptosis phase was bigger. That inhibition of 6PGD could not be managed at the same level in both cell lines is an important reason to observe different results. On the other hand, it has been reported that these two cell

lines have kinetically different apoptotic mechanisms as MCF7 does not possess caspase-3 which plays a central role in apoptotic events, while T47D cells are caspase-3 positive and that in MCF7 cells, the programmed cell death events occur quicker than T47D cells [309, 310]. Thus, we can assume that 6PGD inhibition leads to apoptosis in pathway independent manner. On the other hand, we showed that p53 is augmented in both cell lines with 6PGD inhibition, which confirms our hypothesis that 6PGD knockdown decrease proliferation of breast cancer cells in a way which is mediated by p53.

Knowing that p53 has important roles in modulation of cell cycle and apoptosis [19] and also knowing that MCF7 cells have wild type p53 contrary to T47D cells [302], we can expect different effects of 6PGD knockdown on these cell lines regarding cell cycle progression and apoptosis induction. Since MCF7 cells have wild type of this tumor suppressor, the increase in p53 levels resulted through 6PGD inhibition led MCF7 cells to alter cell cycle progression with an arrest in G1 phase. However, T47D cells have mutant copies of this gene; therefore, the increase of p53 levels due to 6PGD knockdown didn't result in any strong arrest in cell cycle in this cell line. Moreover, different apoptotic mechanisms when 6PGD is inhibited in these two cell lines may also be explained depending on having mutant or wild type copy of p53 gene. Thus, we can conclude that PPP enzymes including 6PGD are regulated by p53 since PPP inhibition affects in a greater degree the cells with wild type p53 than those with mutated p53.

Next, we observed that 6PGD knockdown did not change the ROS level of either of the cell lines. Filosa *et al.* previously demonstrated that G6PD-knockdown mouse embryonic fibroblasts encountered another source of NADPH production to rescue ROS [311]. We assume that 6PGD inhibition in our cell lines also recover the missing NADPH for redox detoxification from other sources; such as glutaminolysis and that the decreased proliferation rate with inhibited 6PGD has a NADPH independent mechanism. Other reports, including not published studies within our group demonstrated that G6PD enzyme does not have strong effect on cellular proliferation, but it is crucial for defense against oxidative stress [312]; nonetheless, our findings prove the importance of functional 6PGD activity for cell survival contrary to G6PD activity. On the other hand, Sukhatme *et al.* showed that 6PGD inhibition increased G6PD activity considerably in lung cancer cells [96]. Even though in our cell lines 6PGD ablation didn't cause a strong

G6PD activity augmentation (data not shown), knowing that breast cancer cells have a very active PPP and that especially MCF7 cells have very high G6PD levels, we assume that NADPH produced by G6PD together with increased glutaminolysis is enough to compensate the decrease of NADPH redulting from 6PGD inhibition and in that way, cells with reduced 6PGD activity do not present elevated ROS levels.

In order to have a more complete idea about the effect of 6PGD ablation in breast cancer, we assessed some flux measurements related to glucose and glutamine metabolism. Similar to previously reported studies [96], in our cells also glucose consumption and lactate production decreased leading to a lower glycolytic efficiency in both cell lines with reduced 6PGD activity. Also, LDH activity decreased in both cell lines, thus, we estimate that 6PGD inhibition caused a shift from glycolysis to TCA cycle. Tumor suppressor p53 has functional roles in the regulation of glycolysis [185]. Taking into account that T47D cells have mutant p53 gene while MCF7 cells have wild type p53, it is reasonable that the effects of 6PGD knockdown in decreased glucose consumption and lactate production in MCF7 cells are greater than in T47D cells. On the other hand, 6-PG accumulation has been reported to activate glycolytic enzymes PFK and PK in hepatic cells to carry the excess glucose away from PPP in order to produce pyruvate for lipid biosynthesis [295, 296]. Nevertheless, we observed reduced glucose consumption in MCF7 and T47D cells with 6PGD inhibition which might be due to the fact that glucose metabolism in malignant cells are distinct from that of non-transformed cells.

On the other hand, this study uncovers a link between PPP and glutaminolysis due to the fact that cells with reduced 6PGD activity consumed more glutamine compared to control cells. Also, the ratio of glutamine consumption rate over glucose consumption rate was significantly increased. As we discussed before, increased glutamine metabolism must be taking place in order to compensate both the missing NADPH and nucleotides caused by 6PGD inhibition. Our results also reveal that inhibiting 6PGD entails the upregulation of ME and IDH, which probably constitutes an adaptive mechanism that breast cancer cells undergo in order to produce NADPH even after the oxidative phase of PPP has been blocked. Interestingly, this could propose an alternative metabolic vulnerability that could be targeted in order to hamper breast cancer cells' adaptation to 6PGD inhibition. The simultaneous inhibition of 6PGD together with ME or

IDH therefore represents a promising strategy to deprive tumor cells of their ability to compensate oxidative stress through NADPH production. In fact, a recent publication showed that even though 6PGD enzymatic activity is not indispensable, the inhibition of 6PGD together with any enzyme of nonoxidative PPP (transketolase, transaldolase, ribulose epimerase or ribulose isomerase) is not endured [313]. That is, targeting other metabolic targets along with 6PGD could result in the development of better therapies against breast cancer cells [208, 314] and 6PGD forms a good pair in synthetic lethality.

One of the most striking findings in this study is the uncovered link between PPP and cancer stem cell characteristics. The results provided in this chapter clearly show that 6PGD inhibition decreased considerably not only the mammosphere formation capability, but also the size and number of formed mammospheres in both cell lines. That is, to best of our knowledge, this is the first study conducted to reveal that an enzyme of oxidative phase of PPP has significant effect on diminishing the stem cell like characteristics of breast cancer cells. This could be not only efficient in preventing breast cancer growth, but also helpful in addressing the very serious problem of cancer reappearance which is one of the most challenging problems faced by many of the currently targeted therapies. The fact that inhibition of 6PGD decreases mammosphere formation capability highlights the potential of 6PGD as a promising drug target and targeting 6PGD could also sensitize cells to current chemotherapeutics, thus improving the efficacy of the most used clinical approaches [315].

All in all, the experimental evidences presented in this work highlight the potential of 6PGD as a putative therapeutic drug target in breast cancer treatment. Targeting 6PGD not only decreases cell proliferation through cell cycle arrest and apoptosis induction, but also activates p53 (one of the most important tumor suppressor genes) and decreases the stem cell like characteristics of breast cancer cells. Moreover, the cells with reduced 6PGD activity show increased fluxes of glutamine metabolism. Besides our results, a recent study indicated that 6PGD played an important role in the migration of tumor cells in vitro [97]. Therefore, validation of this proof of concept in vivo through xenograft experiments will have to be conducted in order to further assess the potential of G6PD inhibition as a therapeutic strategy in breast cancer treatment, and our results; nevertheless, highlight the interesting potential of this new approach.

Chapter 5.2

5.2. A study to Unveil the Adaptation Mechanisms Used by MCF7 Cells Related to Their Glutamine Dependency

5.2.1. Introduction

Metabolism knowledge has always played a crucial role in the study of the molecular mechanisms underlying cancer, ever since the discovery of one of its main metabolic shifts, the aerobic glycolysis [40-44]. Tumor cells rely on metabolic reprogramming to proliferate and achieve a fully malignant phenotype: the increased energy and macromolecules demand of proliferating cells must be satisfied by cell metabolism, which has to adapt to be able to provide cancer cells with the ATP and molecular building blocks that they need [15, 48]. Additionally, complex tumor microenvironment where hypoxic and low-nutrient zones arise forces cells to rewire metabolism in order to grow and survive in those atypical and harsh conditions. Therefore, in oncogenic-driven tumorigenesis, metabolic networks are reorganized so as to fulfill tumor cells' needs. In this way, the metabolic network associated to cancer progression becomes a valuable study field and opens new avenues in the research of potential therapeutic targets [316-318].

The omics revolution has given us new tools which allow the study of many biological processes at the same time, by analyzing large numbers of molecular components including genes, transcripts, proteins or metabolites. Each of these disciplines (from transcriptomics to proteomics and metabolomics) provides an overview of biological phenomena from their point of view. However, without combining different approaches it is not possible to obtain a more integrated view of the more complex biological

problems. Under this premise, the discipline of Systems Biology arises, providing a new way of understanding biological mechanisms. This new approach to biology includes the parallel study of genes, proteins and metabolites, and the use of bioinformatics as an integrative agent responsible for the joint interpretation of these layers of highly heterogeneous information [268].

In the previous chapter we explored the functions of one of the most important ox-PPP enzymes, 6PGD, in the survival and metabolic reprogramming of breast cancer cells. One of the noteworthy metabolic alterations observed in response to 6PGD inhibition was the decrease of glucose consumption and increase of glutamine consumption, suggesting a modulation of the Warburg phenomenon. Many cancer cells, including MCF7 cells, exhibit glutamine addiction habits; that is, they rely on glutamine as the main source of energy rather than on glucose [124]. The switch from glucose to glutamine as the main energy substrate in many tumors is considered an adaptive mechanism that confers cancer cells with survival and proliferating advantages in the tumor microenvironment [41]. Nevertheless, this glutamine dependence can at the same time be considered a cancer-specific vulnerability with the potential to be exploited therapeutically.

The study performed in this chapter intents to provide a comprehensive, genome-scale computational model of different regulatory levels of breast cancer cells in the frame of a multinational European project (METAFLUX EC-FP7), in order to elucidate the way that these regulatory levels affect or determine each other. In this multinational project, a genome-scale metabolic model (GSMM) of MCF7 cell line will be built using transcripomics, proteomics, phosphoproteomics, metabolomics and fluxomics data. Transcriptomics, metabolomics and fluxomics data to be used in the GSMM creation are provided by our group, and they form the subject of this chapter. Another of the groups involved in this project is responsible for producing proteomics and phospho-proteomics data, while the third group is expert in modeling strategies and they will take part in building the GSMM to deeply study the regulation of breast cancer metabolism.

A good GSMM should predict the system's response to any perturbations applied; therefore, different incubation conditions should be tested in order to generate

different metabolic profiles that will help to validate if the generated model of breast cancer metabolism is working well [319]. Therefore, the aim of this section was to generate transcriptomics, metabolomics and fluxomics data to be used in the construction of a GSMM of MCF7 cells in the presence of two different perturbations. Considering glutamine addiction habits in this cell line, in order to further explore the mechanisms regulating glutamine dependence and adaptation to glutamine deprivation in MCF7 cells, we decided to study glutamine deprivation as the first perturbation applied. Moreover, taking into account that that breast cancer cells, including MCF7, have elevated mitochondrial activity [320, 321], and considering hypoxia is a common condition in the tumor environment which also affects mitochondrial function, the study of mitochondrial metabolism in the presence of strong stress conditions such as hypoxia is also particularly interesting. In this regard, we applied oligomycin A (an ATP synthase inhibitor which therefore suppresses OXPHOS and mimics hypoxia) [116] to MCF7 cells as the second perturbation applied. While the raw data obtained from this study is on itself an essential part of the construction of the GSMM, we also used the same data to explore the metabolic adaptations that MCF7 cells undergo when glutamine is scarce in the microenvironment or when they need to grow and survive in hypoxic conditions.

When studying metabolic reprogramming under different conditions, it is necessary to consider that the overall metabolome of a cell is dynamic and the metabolites are continuously transformed over time. In order to characterize the metabolic networks and their dynamic functional states, it is required to know the state of the intracellular metabolic fluxes, which can be quantified by analyzing the incorporation of introduced labeled substrates in metabolic products using the right bioinformatic tools [269]. Considering this, we performed a parallel labeling approach using [1,2-$^{13}C_2$]-glucose or [U-$^{13}C_5$]-glutamine as tracers [261], analyzed isotopomer distribution by GC-MS, and quantified metabolic fluxes in the different conditions using our *in-house* developed software, Isodyn [269-272, 285] in order to generate fluxomics data to be used in the GSMM of MCF7 cells either with the deprivation of glutamine or in the presence of oligomycin. To better adjust our generated model of metabolic flux network we also included measurements of concentrations of main carbon source metabolites present in the culture media, such as glucose, lactate, glutamine, and glutamate, together with

several amino acid concentrations measured by HPLC. Besides providing data for the construction of a GSMM which intents to study the multi-layer regulation of breast cancer metabolism, this chapter also provides with new data on its own for a better understanding of the role of glutamine metabolism in breast cancer adenocarcinoma, and of the metabolic network adaptations that MCF7 cells undergo to circumvent glutamine deprivation and general mitochondrial impairment/hypoxia. This study also highlights the importance of Systems Biology approaches to comprehend the molecular mechanisms underlying complex multifactorial diseases in order to point out new potential therapeutic targets.

5.2.2. Results

5.2.2.1. Gene Expression Profile of MCF7 Cells

To study the effects of glutamine deprivation and oligomycin supplementation in MCF7 cells, we performed transcriptomics analysis as described in the section 4.13. When MCF7 cells were subjected to glutamine deprivation, high-throughput transcriptomics analysis using *Affymetrix GeneChip* arrays identified 319 upregulated and 396 downregulated genes whose expression differed >1.5 fold compared to control cells. When the cells were treated with oligomycin, on the other hand, microarray analysis provided with 971 upregulated and 947 downregulated genes with fold change >1.5 compared to non-treated cells. This transcriptomics data that we generated was used as the first layer for the construction of a GSMM in the frame of a multinational European project, in order to study the multi-layer regulation of breast cancer metabolism (Significantly upregulated and downregulated genes with glutamine deprivation or oligomycin supplementation are listed in appendix I).

5.2.2.2. Glucose, Lactate, Glutamine and Glutamate Production/Consumption Rates

To observe the effect of glutamine deprivation on MCF7 cells and the metabolic changes that take place when the cells don't have fully functional mitochondria, we first cultured the cells for 8 or 24 hrs with a medium either deprived of glutamine or supplemented with oligomycin. We then measured the extracellular concentrations of glucose, glutamine, lactate and glutamate, and calculated the consumption and production rates of each metabolite after each incubation time (only 24 hrs measurements are exhibited

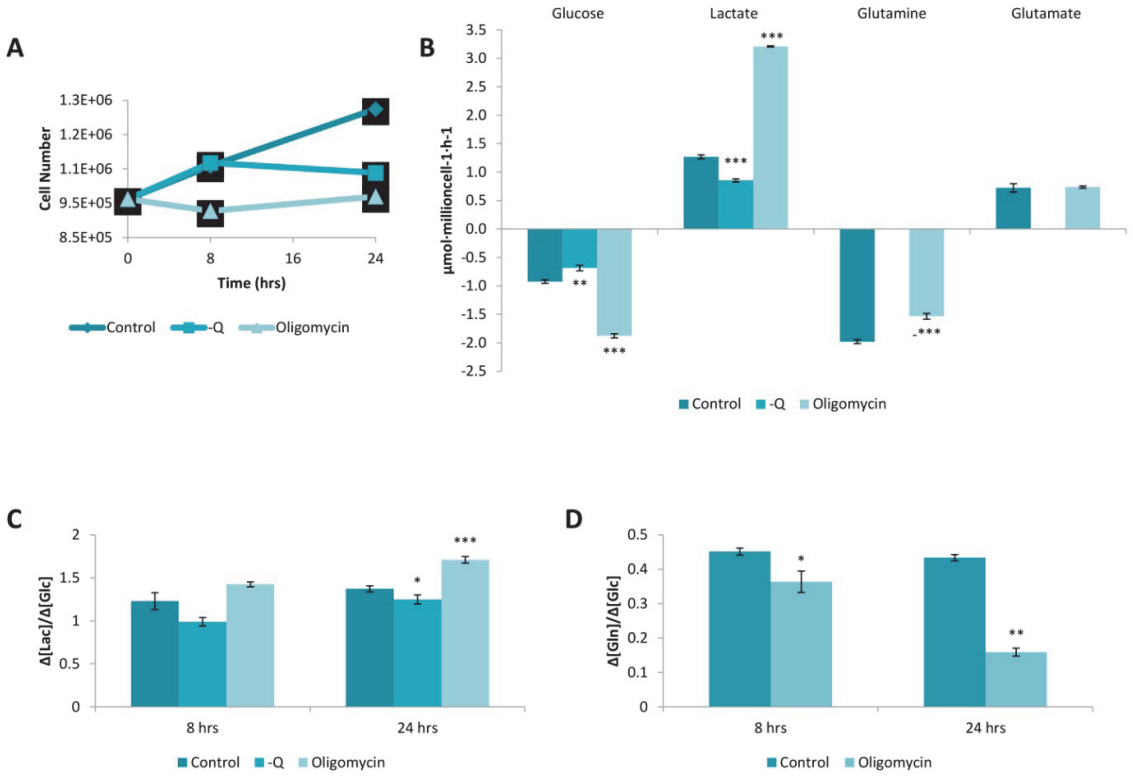

Figure 5.2.1. Metabolite consumption and production rates.

A) Proliferation rate of MCF7 cells under glutamine deprivation or oligomycin supplementation conditions. **B)** Glucose and glutamine consumption rates and lactate and glutamate production rates are calculated as µmoles consumed by 1 million cells per hour. **C)** Glycolytic activity which shows the conversion rate of glucose to lactate. **D)** Ratio between cumulative consumptions of glutamine over glucose. The bars correspond to mean ± SD of n = 3. Statistically significant differences between glutamine deprived / oligomycin supplemented and control cells were indicated at $p < 0.05$ (*), $p < 0.01$ (**) and $p < 0.001$ (***).

in this section, 8 hrs measurements results can be found at appendix II). As shown in figure 5.2.1A, the proliferation of cells cultured in the absence of glutamine or in the presence of oligomycin is halted, indicating that both glutamine and fully functional mitochondria are requisites for MCF7 cells' proliferation. Surprisingly, glutamine deprivation also causes a considerable decrease in glucose consumption and lactate production rates (figure 5.2.1B), while also causing a decrease in the percentage of the consumed glucose which is converted to lactate (figure 5.2.1C). For the cells treated with oligomycin, on the other hand, a significant increase in glucose consumption and lactate production was observed, and glucose was found to be redirected from entering the TCA cycle into lactate production (figure 5.2.1B and C). Furthermore, after 24 hrs of incubation with oligomycin the cells consumed less glutamine than control cells, although the produced glutamate amount did not show any significant differences (figure 5.2.1B), thus indicating that glutamine carbons were used for biosynthesis. Finally, oligomycin treatment directed MCF7 cells to significantly decrease the ratio between glutamine and glucose consumption rates (figure 5.2.1D) indicating that cells depended more on glucose than glutamine for their survival.

5.2.2.3. Isotopologue distribution of extracellular and intracellular metabolites after incubation with [1,2-$^{13}C_2$]-glucose or [U-$^{13}C_5$]-glutamine

Glucose and glutamine are the two major sources of both energy and building blocks for the biosynthesis of macromolecules in living organisms. We observed clear changes in the metabolism of these two molecules under either glutamine deprivation or oligomycin administration, and consequently we sought to explore the differences in the utilization of carbons from both substrates through the main metabolic pathways involved in the central carbon metabolism of MCF7 cells. To this end, we conducted ^{13}C-based metabolic flux analysis in order to characterize the alterations in the metabolic fluxes that MCF7 cells undergo in each experimental condition. To do this, we first incubated the cells with the tracer substrates for 8 hrs and 24 hrs, under either glutamine withdrawal or oligomycin supplementation. Then we measured the label (^{13}C) enrichments in several metabolites by GC-MS, and performed mass isotopomer

distribution analysis (MIDA) in order to estimate the differences in the fluxes through a selection of central carbon metabolism pathways under the different conditions. The label enrichments of several metabolites were also used in order to calculate a complete set of fluxes of central carbon metabolism by using Isodyn software (see appendix III for the detailed ^{13}C measurement results).

5.2.2.4. Lactate, ribose and glutamate production

GC-MS analysis allows the determination of the ^{13}C enrichment of different metabolites, as well as their isotopologue distributions. The percentages of the different ^{13}C isotopologues in lactate, ribose and glutamate after incubations with [1,2-$^{13}C_2$]-glucose are presented in figures 5.2.2A, C, and E. We did not observe any significant changes in the enrichment of lactate (m2) when the cells were deprived of glutamine. However, ^{13}C enrichment in lactate (m2) was higher after oligomycin treatment. By using mass isotopomer distribution analysis, we calculated the pathway specific lactate production percentages as explained in section 4.17.1 (figure 5.2.2B), and observed that only oligomycin treatment increased the production of lactate from glucose, which is in concordance with the results of section 5.2.2.1. Furthermore, we observed that both glutamine deprivation and oligomycin supplementation decreased the activity of PPP, and much less lactate was produced from PPP-cycled glucose. On the other hand, when using ^{13}C-enriched glutamine as our labeled substrate, label incorporation was observed neither in lactate nor in ribose (data not shown).

Figure 5.2.2C and D show ribose isotopologue distribution and total label enrichment after the addition of ^{13}C-enriched glucose. We observed that ribose enrichment decreased considerably after both glutamine deprivation and oligomycin treatment. This result is concordant with the decreased PPP activity suggested in figure 5.2.2B for both conditions. On the other hand, we calculated the relative contribution of both pyruvate dehydrogenase (PDH) and pyruvate carboxylase (PC) enzymes to glucose entrance into TCA cycle as previously reported [286], considering the m2 label pattern in glutamate molecule fragments C2-C5 and C2-C4 as explained in section 4.17.2. We observed that,

when MCF7 cells are deprived of glutamine or don't have fully functional mitochondria, they favor PC over PDH when introducing glucose-derived pyruvate into the TCA cycle (figure 5.2.2E, F).

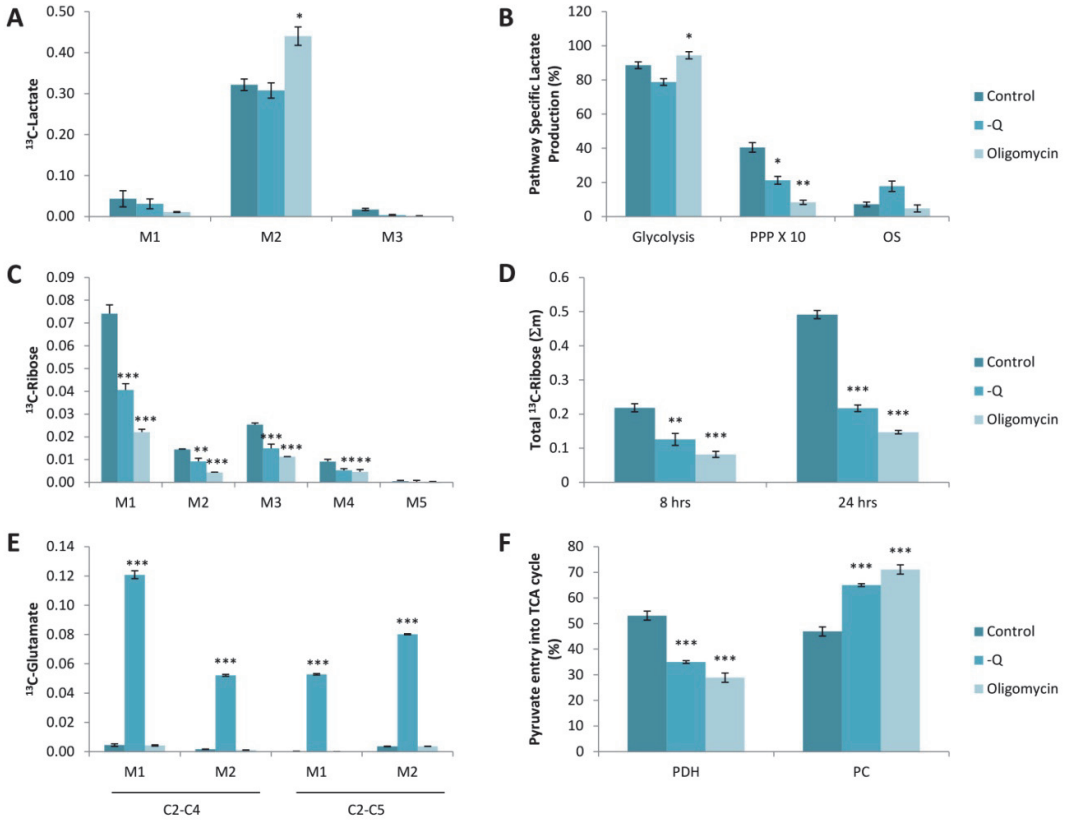

Figure 5.2.2. Mass isotopomer distribution analysis (MIDA) of lactate, ribose and glutamate derived from ^{13}C glucose

A,C,E) Enrichments of the different isotopologues of lactate, ribose, and glutamate, respectively. **B)** Pathway specific lactate production percentages. **D**) Total ribose ^{13}C enrichment rates. **F)** Rate of pyruvate entry into the TCA cycle via PDH or PC enzymes. The bars correspond to mean ± SD of n = 3. Statistically significant differences between glutamine deprived / oligomycin supplemented and control cells were indicated at $p < 0.05$ (*), $p < 0.01$ (**) and $p < 0.001$ (***).

5.2.2.5. TCA cycle intermediates

After characterizing the metabolic reprogramming triggered by glutamine deprivation or oligomycin treatment in the upper part of the carbon metabolism, we decided to also explore the metabolic alterations caused by these conditions downstream of pyruvate.

In order to address this, we applied a parallel labeling approach [262] to obtain deep information about the metabolic changes occurring in the mitochondria of MCF7 cells with these induced mitochondria impairments. We incubated the cells in parallel with medium containing 100 % [1,2-$^{13}C_2$]-glucose (applying either glutamine deprivation or oligomycin treatment), or with medium containing 100 % [U-$^{13}C_5$]-glutamine together with oligomycin treatment, for either 8 hrs or 24 hrs. The results of 8 hrs of incubation and 24 hrs of incubation were quite similar, and in the sake of simplification only the results obtained after 24 hrs of incubation are shown in this section (see appendix II for the measurement results obtained after 8 hrs of incubation).

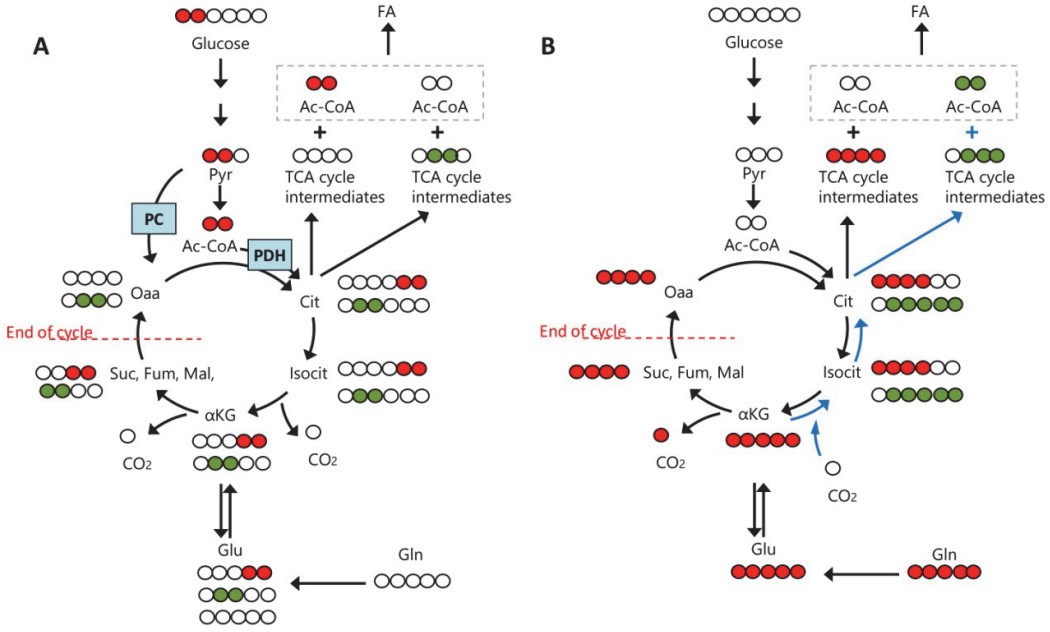

Figure 5.2.3. Label incorporation in TCA cycle

A) Carbon atom transition map in TCA cycle intermediates when using [1,2-$^{13}C_2$]-glucose as a tracer. Pyruvate entry into mitochondria can take place in two ways: via PDH (red molecules) or via PC (green molecules). **B)** Carbon atom transition map in TCA cycle intermediates when using [U-$^{13}C_5$]-glutamine as a tracer. For each metabolite, red molecules demonstrate the ^{13}C labeling pattern corresponding to the first cycle of oxidation. On the other hand, green molecules indicate the reductive carboxylation pathway followed by glutamine ^{13}C atoms (indicated by blue arrows). Reductive glutamine metabolism may produce m5 labeled TCA cycle intermediates, such as isocitrate and citrate, and m3 labeled TCA cycle intermediates, such as malate, fumarate and aspartate. For clarity reasons, only the first turn of TCA cycle is depicted here for both schemes.

First, we explored the glucose utilization in mitochondria by analyzing the isotopologue distributions of various TCA cycle elements. Figure 5.2.3A depicts the fundamental possibilities of label incorporation in TCA cycle intermediates derived from labeled glucose depending on whether the entrance of pyruvate into the TCA cycle is done via PC or PDH enzymes. Because the cells were incubated in the presence of [1,2-$^{13}C_2$]-glucose, metabolites of TCA cycle were expected to have m2 labeling in higher proportions. However, because pentose cycle can produce m1 pyruvate and we incubated the cells with 100 % labeled glucose, we also expected to see certain levels of m1, m3 and m4 labeling. We analyzed the isotopologue distributions of citrate, α-ketoglutarate, malate, fumarate, and aspartate, and in general we observed that while

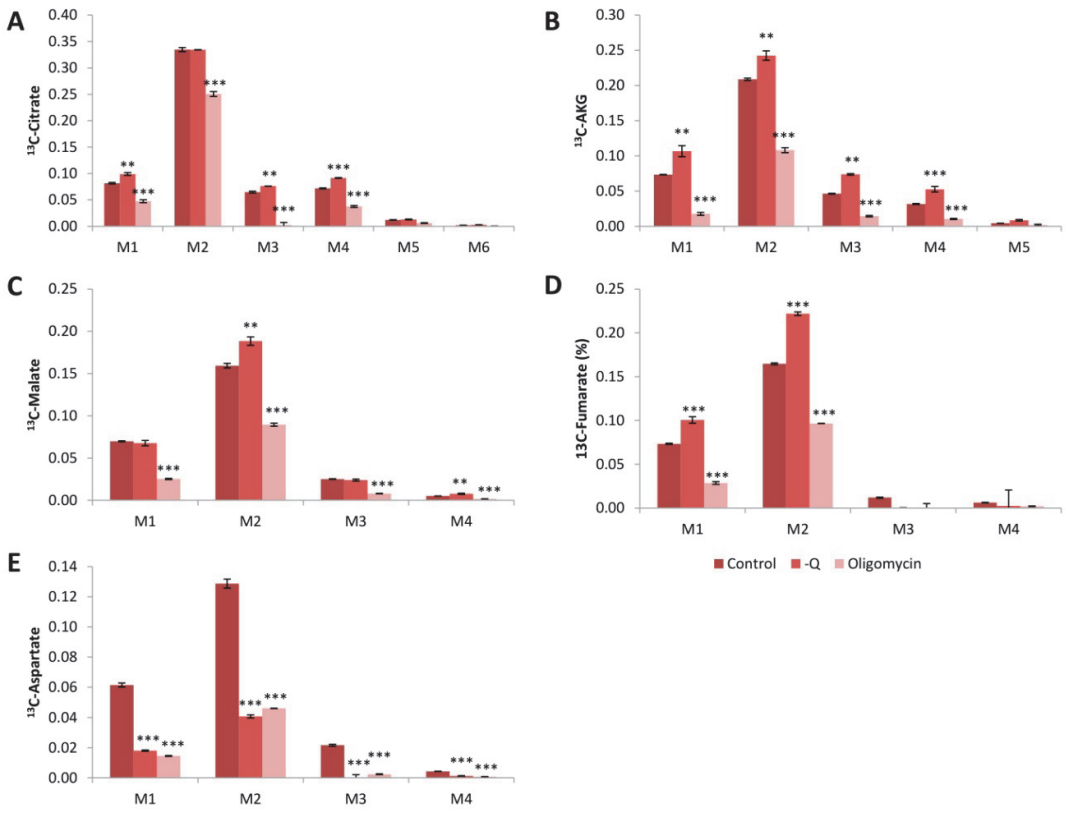

Figure 5.2.4. Label incorporation in TCA cycle intermediates derived from ^{13}C –labelled glucose

Isotopologue distribution of TCA cycle molecules 24 hrs after culturing the cells with the medium containing 100 % [1,2-$^{13}C_2$]-glucose. **A)** Citrate, **B)** α-ketoglutarate, **C)** Malate, **D)** Fumarate, **E)** Aspartate label enrichments are presented here. The bars correspond to mean ± SD of n = 3. Statistically significant differences between glutamine deprived / oligomycin supplemented and control cells were indicated at $p < 0.05$ (*), $p < 0.01$ (**) and $p < 0.001$ (***).

glutamine deprivation led to more glucose incorporation into the TCA cycle, oligomycin treatment decreased glucose incorporation into TCA cycle considerably (figure 5.2.4). The exception to this trend was the aspartate molecule, since the label incorporation from glucose decreased significantly in both conditions.

Results indicate that when cells are deprived of glutamine, more glucose is used to fuel the TCA cycle. More label incorporation was observed in citrate than in α-ketoglutarate, indicating that a portion of the glucose-derived carbons that enter the TCA cycle are dispensed through other metabolic pathways such as lipid biosynthesis. Moreover, malate, fumarate and aspartate (synthesized from oxaloacetate) possessed less label incorporation than α-ketoglutarate, which hints to the fact that glucose may also be used to synthesize glutamate (figure 5.2.4). This is concordant with the higher label incorporation from glucose in glutamate when the cells are deprived of glutamine (figure 5.2.2E). On the other hand, when the cell mitochondria are impaired with oligomycin, we see a dramatic decrease in the incorporation of labels coming from glucose in TCA cycle intermediates, which is concordant with glucose being redirected into lactate production. This decrease is much stronger in α-ketoglutarate than citrate, indicating that oligomycin treatment also leads MCF7 cells to redirect citrate out of the TCA cycle for the biosynthesis of other metabolites (such as lipids). Nevertheless, and unlike the condition of glutamine deprivation, the following elements of TCA cycle show similar label incorporation than α-ketoglutarate, which points out that when the cells are cultured in the presence of oligomycin, glucose-derived carbons are not directed to the synthesis of glutamate. The fact that labeled aspartate levels decreased considerably in both conditions indicates that oxaloacetate may be used in other metabolic events such as pyruvate cycling [322].

Our results show that glucose significantly supplements mitochondria, although glutamine usually remains the main substrate of the mitochondrial metabolism. In order to better understand the alterations that the glutamine metabolism of MCF7 cells undergoes after mitochondrial impairment, we cultured the cells in medium containing 100 % [U-$^{13}C_5$]-glutamine. Figure 5.2.3B demonstrates the integration of glutamine carbons into mitochondrial metabolism. Glutamine is first transformed into glutamate by GLS, and then converted into α-ketoglutarate which is subsequently decarboxilated

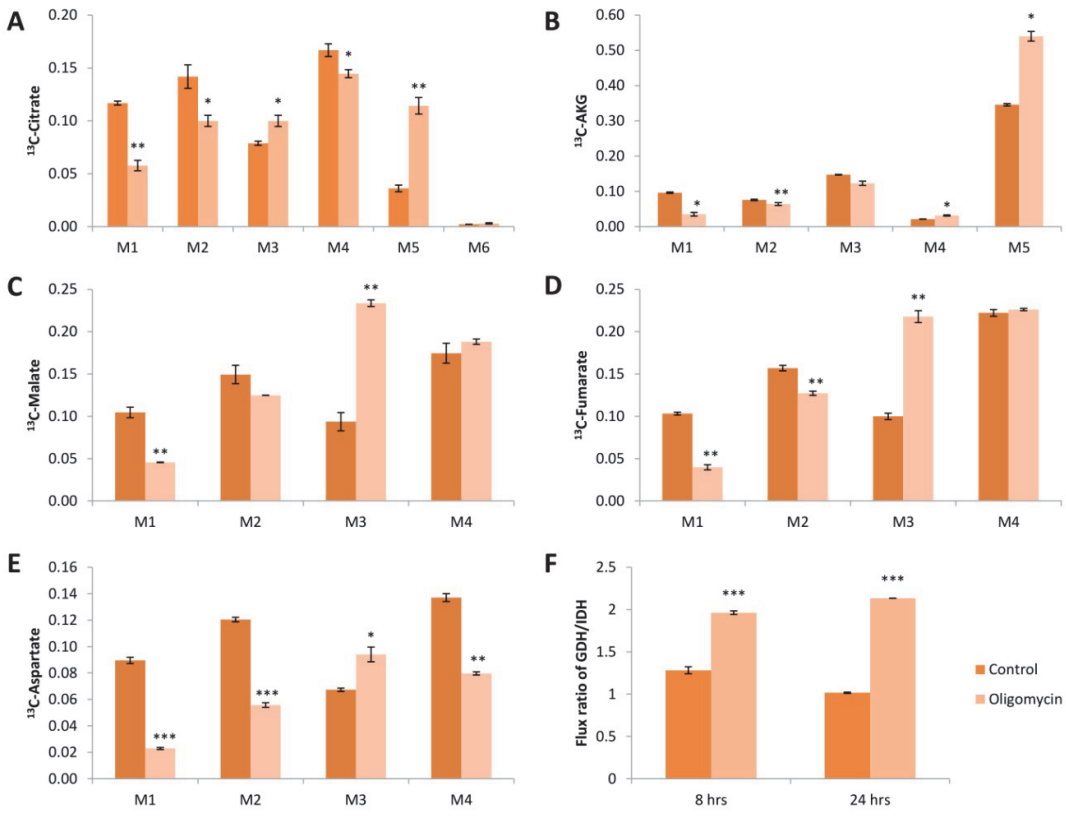

Figure 5.2.5. Label incorporation in TCA cycle intermediates derived from glutamine

Isotopologue distribution of TCA cycle molecules 24 hrs after culturing the cells with 100 % [U-$^{13}C_5$]-glutamine. **A)** Citrate, **B)** α-ketoglutarate, **C)** Malate, **D)** Fumarate, **E)** Aspartate label enrichments are presented here .**F)** The flux ratio of reductive vs oxidative glutamine metabolism was roughly calculated as the ratio between m5 labeled αKG which is estimated to be produced by GDH and m1 – m4 labeled αKG which is estimated to be produced by IDH. The bars correspond to mean ± SD of n = 3. Statistically significant differences between oligomycin supplemented and control cells were indicated at $p < 0.05$ (*), $p < 0.01$ (**) and $p < 0.001$ (***).

into succinate [323]. Thus, the TCA cycle intermediates directly obtained from uniformly labeled glutamine will contain 4 atoms of ^{13}C (m4). On the other hand, the addition of a carbon atom can transform α-ketoglutarate into isocitrate, which can be later converted into citrate by the mechanism known as reductive carboxylation [128] (figure 5.2.3B, green molecules). Reductive carboxylation of glutamine will therefore produce m5 labeled citrate and m3 labeled TCA cycle elements derived from oxaloacetate, such as malate, fumarate and aspartate. When using [U-$^{13}C_5$]-glutamine as our tracer substrate, we studied only the effects of oligomycin treatment on MCF7 cells since the glutamine

deprivation condition was not applicable. In the oligomycin supplementation condition, we measured a significant increase in the proportions of m5 isotopologues of citrate and α-ketoglutarate and m3 isotopologues of other TCA cycle intermediates, indicating that oligomycin strongly favors reductive carboxilation of glutamine (figure 5.2.5A-E). Moreover, we calculated the approximate flux ratio of GDH to IDH as explained in section 4.17.4 [261] and we observed an increase in the GDH metabolism when the cells are treated with oligomycin (figure 5.2.5F). This further evidences that oligomycin causes MCF7 cells to alter their glutamine metabolism in order to favor the reductive carboxylation of glutamine.

5.2.2.6. Lipid synthesis

Besides producing energy, mitochondrial metabolism also provides intermediates for the synthesis of various macromolecules such as lipids, which are fundamental for cell proliferation. Therefore, changes in lipid metabolism can be an interesting aspect of the metabolic reprogramming associated to glutamine deprivation and mitochondrial impairment in MCF7 cells. Citrate can be exported to the cytoplasm and cleaved to Ac-CoA and oxaloacetate by means of ATP citrate lyase (ACLY), with the generated Ac-CoA being further used to fuel lipogenesis [128]. In order to explore the metabolic changes occurring in the lipogenesis of MCF7 cells after glutamine deprivation or oligomycin treatment, we performed isotopologue distribution analysis of palmitate (the first synthesized fatty acid in lipid biosynthesis), using either glucose or glutamine as a ^{13}C-enriched tracer. Both for glutamine deprivation and oligomycin treatment conditions, a notable decrease in label incorporation derived from [1,2-$^{13}C_2$]-glucose was observed (figure 5.2.6A). Similarly, a parallel decrease was observed when the cells were incubated with [U-$^{13}C_5$]-glutamine in the presence of oligomycin (figure 5.2.6B). Furthermore, the increase in the levels of m6 and m8 isotopologues evidences that lipogenesis is supported by reductive carboxylation of glutamine when the mitochondria of the MCF7 cells are impaired with oligomycin.

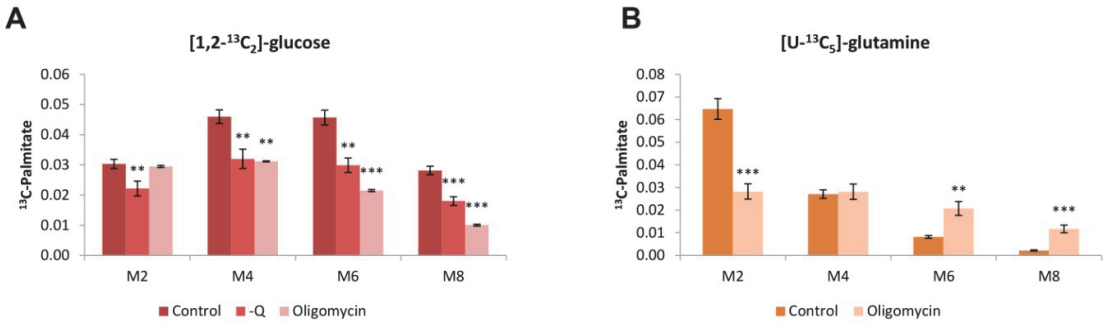

Figure 5.2.6. Label incorporation into the fatty acids derived from glucose or glutamine

Isotopologue distribution of palmitate 24 hrs after culturing the cells with the medium containing **A)** 100 % [1,2-$^{13}C_2$]-glucose or **B)** 100 % [U-$^{13}C_5$]-glutamine. The bars correspond to mean ± SD of n = 3. Statistically significant differences between glutamine deprived / oligomycin supplemented and control cells were indicated at $p < 0.05$ (*), $p < 0.01$ (**) and $p < 0.001$ (***).

5.2.2.7. Estimation of metabolic fluxes using Isodyn

The data obtained from spectrophotometric measurements and ^{13}C assisted metabolomics experiments has given us information about many metabolic alterations of MCF7 cells when subjected to glutamine deprivation or oligomycin treatment. However, in order to get a complete picture of the dynamic state of the metabolic fluxes, a Systems Biology approach is needed. In this way, we can simulate the dynamics of isotopologue distribution in central metabolic pathways using tools and algorithms which facilitate the transition between various analyzed metabolic schemes, in order to obtain a complete map of the flux alterations that occurr in MCF7 cells under different disturbances. We introduced all the data obtained from the different measurements that we carried out into our in-house developed software, Isodyn, in order to determine the metabolic flux profiles of MCF7 breast cancer cells in the different conditions. Figure 5.2.7 summarizes the qualitative changes in the metabolites and their inferred by Isodyn (data analysis using Isodyn has been explained in detail at section 4.16). Concordant with spectrophotometric measurements and isotopologue distribution analysis, Isodyn demonstrated a decrease in the fluxes of glycolysis, lactate production, PPP activity, TCA cycle utilization and fatty acid synthesis when the cells are deprived of glutamine. Moreover, increased pyruvate cycle, which is the conversion of pyruvate to oxaloacetate via PC followed by its conversion to malate and consequently back to pyruvate via malic

enzyme, was emphasized as a metabolic alteration occurring in MCF7 cells when cultured without glutamine. On the other hand, when the cells are grown in the presence of oligomycin, increased glycolysis, lactic acid fermentation and pyruvate cycle were estimated, together with decreased TCA cycle activity, PPP and lipogenesis. All of the measured fluxes and their values are listed in appendix IV.

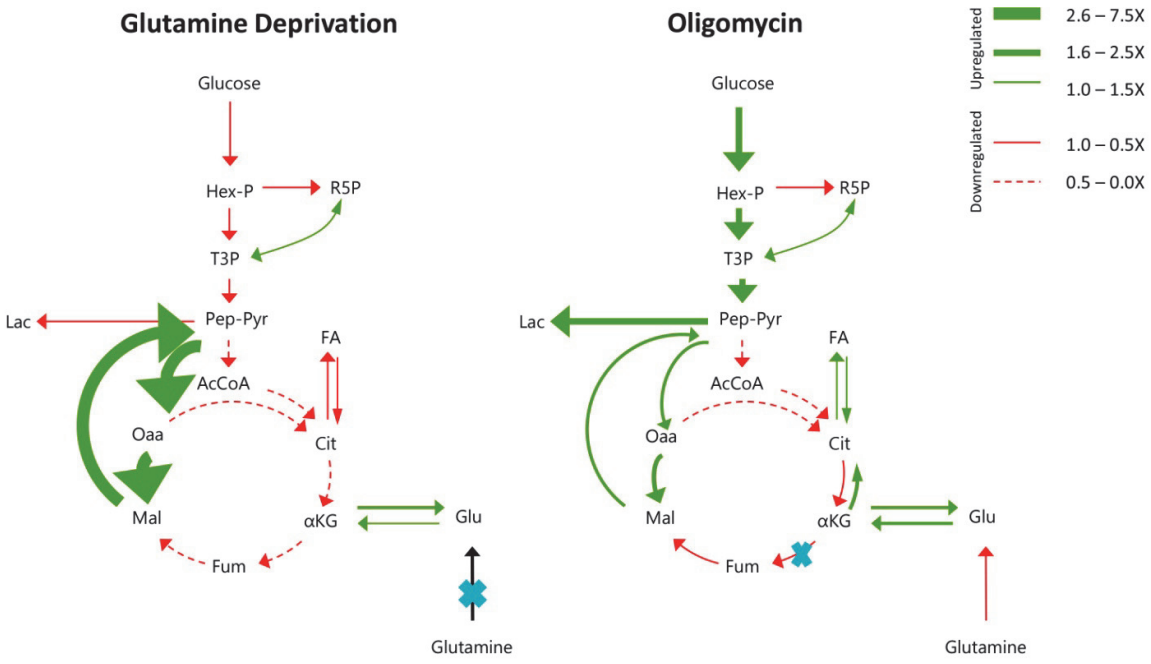

Figure 5.3.7. Metabolic flux changes in MCF7 cells with not fully functional mitochondria
Metabolic flux map of MCF7 cells under glutamine deprivation or oligomycin treatment. The flux values were estimated by Isodyn software. In each condition, the calculated flux was normalized against the control condition flux, in order to calculate its net change.

5.2.3. Discussion

The importance of bioenergetics and cellular metabolism reprogramming in cancer is receiving renewed interest of the scientist in the field [44, 324]. Thanks to abundant advances in high-throughput technologies, “omics” sciences can now quantify a great abundance of various biological molecules and determine the difference between

various biological states on the levels of transcription (transcriptomics), protein (proteomics), metabolite (metabolomics), dynamic state of molecules level (fluxomics) and so on [325]. Nevertheless, the deep complexity and inter-connectivity of biological systems makes individual “omics” approaches unable to explain the gap between genotype and phenotype. Therefore, to obtain a complete picture of living organisms, multi-omics approaches which are able to integrate multiple layers of information derived from different omics sciences are needed [326]. Several multi-omics studies have been performed in order to understand multi-level regulations of bacterial systems [327-329]; however, no such models are commonly available to understand human cancer cell metabolism from a holistic point of view. Accordingly, we decided to construct a genome scale metabolic model (GSMM) which is able to combine various layers of different omics data, in order to reveal the mechanisms regulating the metabolic adaptations of breast cancer cells.

To generate different conditions able to validate the accuracy of the predictions of our model, we applied different conditions and studied the metabolic adaptations undergone in response by breast cancer cells. Glutamine is, along glucose, the main carbon source of the mitochondria [125], but there is still a lack of information available regarding the functional importance of glutamine in cancer cells. The amount of consumed glutamine is known to be increased during aerobic glycolysis or under hypoxic conditions, but the regulation and use of glutamine by cells whose mitochondria is not fully functional is not fully elucidated [128]. Therefore, to understand the role of glutamine metabolism in breast cancer cells and their adaptation to its deprivation, we chose glutamine deprivation as the first challenging condition in our model. On the other hand, functional mitochondria are essential for cancer cells, since proliferating cells require to build macromolecules from certain precursors which are provided by mitochondrial metabolism [59]. Nevertheless, hypoxia is a common feature of tumor microenvironment, and elucidating the mechanisms adopted by cancer cells to survive after hypoxia-like mitochondrial impairment could be another challenging condition to test our model. Construction of GSMMs is costly and usually the collaboration among various research groups is needed. Therefore, as one part of this multinational European project, we generated the needed transcriptomics, metabolomics and fluxomics data

from MCF7 breast cancer cells in normal conditions and after they were deprived of glutamine or supplemented with oligomycin (to mimic hypoxia).

In any case, our results are able on their own to explain an important part of the metabolic adaptations that MCF7 cells undergo when glutamine is scarce in the culture medium or when their mitochondria are impaired. In this chapter, we explored the metabolism of MCF7 breast cancer cells employing ^{13}C-assisted metabolic flux analysis with parallel labeling experiments, and applied a Systems Biology approach that allowed us to estimate the state of the metabolic fluxes under both glutamine deprivation and mitochondrial impairment (achieved through oligomycin supplementation) conditions. To do this, we grew MCF7 cells in parallel, in the presence of either [1,2-$^{13}C_2$]-glucose or [U-$^{13}C_5$]-glutamine as the ^{13}C-labeled tracers, since they are reported to be optimal for measuring glycolytic and TCA cycle fluxes [251, 254, 262]. Next, we measured the production and consumption rates of certain metabolites such as glucose, glutamine, lactate and amino acids, and we performed a comprehensive analysis of the isotopologue distributions of many intracellular and extracellular metabolites by GC-MS. In order to demonstrate the metabolic alterations that MCF7 cells undergo under deprivation or glutamine or in the presence of oligomycin, we conducted flux analysis using a detailed metabolic network model which consists of all major central carbon metabolic pathways.

Our results show that glucose metabolism of MCF7 cells is altered in the absence of glutamine. Both consumed glucose and produced lactate fluxes were decreased with regards to the cells cultured in control conditions. When the cells were deprived of glutamine, lactic acid fermentation was hindered and pyruvate was fostered to enter into the TCA cycle, so conversion rate of glucose to lactate was decreased. Glutamine is a vital metabolite for MCF7 cells as they show addiction to it and redirection of glucose into TCA cycle may be to supply cells with biomolecules that are scarce due to glutamine deprivation. When the cells were treated with oligomycin in order to mimic hypoxia, on the other hand, spectrophotometric flux measurements demonstrated an increased level of glucose consumption and lactate production. Previous reports have indicated that under hypoxic conditions, glutamine consumption of the cells might be elevated [128], but even though oligomycin mimics the major characteristics of hypoxic condition,

here we showed that oligomycin impairment of mitochondria function entails a decrease in glutamine consumption rates. On the other hand, with oligomycin supplementation, the amount of produced glutamate did not show any diffirence which indicate that use of glutamine was mostly for providing carbon backbone and due to decreased cell proliferation, less amount of bioprecursors produced from glutamine were needed.

The analysis of isotopologue distributions of different metabolites yielded concordant results. Pathway specific lactate production calculations and ribose enrichment data showed that MCF7 cells have a less active PPP when they are deprived of glutamine or have mitochondrial impairment, which concurs with similar results in other cancer cells under hypoxia [330]. PPP has vital importance not only for nucleotide synthesis, but also for NADPH production, and therefore it could be hypothesized that MCF7 cells subjected to glutamine deprivation/oligomycin supplementation may be either more sensitive to oxidative stress or able to activate alternate sources for NADPH production. On the other hand, both glutamine deprivation and oligomycin treatment lead cells to have lower fluxes of TCA cycle reactions. Considering that OXPHOS is an important source of ROS [331], it is deducible that under these conditions cells need less NADPH than complete growth conditions. Moreover, both glutamine deprivation and oligomycin treatment halted MCF7 cells proliferation (figure 5.2.1A); therefore, both ribose required for DNA synthesis and NADPH required for lipid synthesis decreased, in further correlation with PPP flux reduction. Finally, isotopologue distribution analysis revealed that both glutamine-deprived and oligomycin-treated cells show a higher pyruvate cycle activity (figure 5.2.7A), which in turn may provide the cells with an alternate NADPH-producing mechanism through malic enzyme[332]. This increase in the fluxes of the pyruvate cycle may be a mechanism cells use to compensate the decrease in NAPDH levels produced by a reduced flux through the oxidative branch of PPP. Mass isotopomer distribution analysis also showed that both glutamine deprivation and oligomycin treatment increased the pyruvate carboxylase (PC) activity in detriment of pyruvate dehdyrogenase (PDH) activity.

Next, we performed ^{13}C-assisted metabolic flux analysis through parallel labeling experiments using either [1,2-$^{13}C_2$]-glucose or [U-$^{13}C_5$]-glutamine as the ^{13}C-labeled

substrates. We observed an increased proportion of m2 isotopologues derived from labeled glucose in TCA cycle intermediates when the cells were deprived of glutamine. This indicates that, in the absence of glutamine, MCF7 cells rearrange their metabolism so that TCA cycle is fostered with carbon atoms derived from glucose. Isotopologue distribution analysis of glutamate showed that when glutamine is withdrawn from the culture medium, MCF7 cells tend to greatly increase the glutamate produced from glucose-derived carbons. This glutamate could be used by the cells as a precursor for the synthesis of other macromolecules, which would be built using glucose carbons as a response to the lack of glutamine available. On the other hand, when the mitochondria of MCF7 cells were impaired by oligomycin treatment, the m2 label incorporation in TCA cycle intermediates decreased significantly, which concurs with an expected decrease in TCA cycle activity.

Glutamine, when introduced to TCA cycle, is converted to glutamate, then to αKG, and subsequently oxidatively decarboxylated to succinate. Nonetheless, several works maintain that some cells may reductively carboxylate αKG molecule to produce citrate through enzyme IDH2 [132, 257, 289]. When glutamine was used as tracer, we observed an increase in the proportion of m5 citrate isotopologue, together with an increase in the proportion of m3 isotopologues of other TCA cycle intermediates such as malate and fumarate. Our results strongly suggest that MCF7 cells have reductive carboxylation activity, which is further increased in the presence of oligomycin. In this reductive carboxylation pathway, NADPH dependent IDH2 (mitochondrial isoform) and IDH1 (cytosolic isoform) enzymes are used to produce citrate, and which is a substrate to produce both Ac-CoA for lipid synthesis and other four carbon intermediates related to macromolecular precursors [333]. This increase in reductive carboxylation in the presence of oligomycin can be interpreted as a mechanism MCF7 undergo to overcome the impairment of normal mitocohondrial oxidative function, thus maintaining synthesis of the TCA cycle intermediates needed to support cell growth in a mechanism that seems to be dominant in several malignant cells with defective mitochondria [128]. It is interesting to point out that this increase in reductive carboxylation needs a contribution of NADPH, which would further explain the observed increase in the fluxes of pyruvate cycle after oligomycin treatment, in order to generate NADPH through malic

enzyme. According to this results, targeting IDH isoenzymes and/or malic enzyme together with ordinary mitochondrial activity could potentially halter MCF7 cells' adaptive mechanisms to mithocondrial impairment, therefore affecting growth and proliferation in a more efficient way.

Mitochondrial metabolism is the main source of precursors required for the biosynthesis of lipids. When using glutamine as the ^{13}C-labelled substrate, we observed increased label incorporation in palmitate (especially in the proportion of M6 and M8 isotopologues) after oligomycin treatment, which furthers strengthens the hypothesis that MCF7 cells activate reductive carboxylation to mediate lipogenesis when the mitochondrial oxidative function is impaired. Lipids are essential for creating new cell membranes, but since the cells attenuated their proliferation rate when they were treated with oligomycin (figure 5.3.1A), the exact fate of the fatty acids newly synthesized from glutamine after oligomycin treatment is not clear. However, lipids are also essential for maintaining cell structure, providing energy and cellular signaling [144]. Another possible explanation for this result may be the activation of the recycling of lipids via β-oxidation, which would generate a futile cycle with lipogenesis. Besides, newly synthezised fatty acids might have been secreted into the culture medium, since extracellular fatty acid concentration was not measured.

Consumption and production rates of different metabolites measured extracellularly together with isotopologue distribution meaurements have been combined using a computationally-assisted Systems Biology approach in order to obtain a dynamic view of the metabolic flux maps and their rearrangement under glutamine deprivation or oligomycin supplementation. This has provided us with the fluxomics data to be introduced into the GSMM to be built in order to explore the regulation of breast cancer metabolism. We used our *in-house* developed software Isodyn to quantitatively analyze the metabolic flux distributions in MCF7 cells, in order to further explore the mechanisms these cells can use to compensate for their glutamine dependency when adapting to glutamine deprivation or mitochondrial impairment. Analyses was conducted assuming a metabolic steady state (not an isotopic steady state), and rapid mixing of isotopic isomers of the same metabolite throughout different intracellular compartments. The high initial glucose or glutamine concentration ensured the excess

availability of these metabolites for cells to uptake the required amount. The other incubation conditions didn't change; therefore it is reasonable to assume a metabolic steady state. Rapid mixing of isotopic isomers of the same species throughout the cell is accepted for analyses of stable isotopes' data [334]. The fitting of the experimental data (spectrophotometric measurements of extracellular molecules and mass isotopomer distributions) in a model of central carbon metabolism revealed the state of a set of metabolic fluxes for each condition, which has allowed us to better understand the way MCF7 cells adapt to glutamine deprivation or mithocondrial impairment and confirm some of the the metabolic observations directly inferred from the spectrophotometric measurements or isotopologue distribution analysis (figure 5.3.7). When glutamine was withdrawn from the incubation medium, glycolytic and PPP fluxes decreased significantly, while TCA cycle fluxes also showed a decrease. When cells were supplemented with oligomycin, on the other hand, glycolytic fluxes for lactic acid fermentation increased while PPP and TCA cycle fluxes showed a decrease. Pyruvate cycle, however, showed a dramatic increase in both cases. As it has been already discussed, one possible reason for this rearrangement is the generation of NADPH, which might be needed to compensate a decreased NADPH production through PPP and also to sustain an increase in reductive glutamine carboxylation.

In the previous chapter we underlined the role and importance of glutamine molecule in breast cancer models, and in this chapter we confirmed its importance in breast cancer cells by applying metabolic flux analysis. Besides their glutamine addiction habits [124], breast cancer cells are also reported to contain intratumoral hypoxial regions where O_2 availability is strongly reduced [335]. Under these circumstances, their mitochondria are not fully functional and they might also be subjected to nutrient availability restrictions. Therefore, it is important to thoroughly characterize the metabolic adaptations induced in these cells under glutamine deprivation and hypoxia-mimicking conditions. The mechanisms related to these metabolic adaptations might be exploited therapeutically as part of novel combined therapies, in order to hinder the survival of the cells in the tumoral microenvironment.

Chapter 5.3

5.3. Glucose 6-Phosphate Dehydrogenase (G6PD) Expression and Function are regulated via Glutamine in Colon Cancer Cells

5.3.1. Introduction

In many tumors, energy metabolism is strictly reprogrammed in order to generate sufficient energy required for uncontrolled growth which defines cancer [15, 336].There are different strategies to counteract metabolic changes associated to cancer cell proliferation. On account of its roles in fundamental cellular needs such as nucleotide biosynthesis and anti-oxidative defense, PPP has been a promising target to further investigate in cancer cell metabolism [76, 78]. In the previous studies performed within our team using breast cancer cell lines, we demonstrated that inhibition of glucose 6-phosphate dehydrogenase (G6PD), the first enzyme of ox-PPP, leads to a decrease in cell proliferation and alterations in the central carbon metabolism. Similarly, in the first chapter of this thesis, we found out that 6-phosphogluconate dehydrogenase (6PGD), the third enzyme of ox-PPP, had also significant importance in the proliferation of breast cancer cells. In particular, we discovered that besides leading to cell cycle arrest and induction of apoptosis, 6PGD inhibition also affected the metastatic potential of the cells which is characterized as the capacity to grow in suspension. Moreover, we observed a significant link between PPP and glutamine metabolism in breast cancer cells, since the inhibition of 6PGD enzyme led to enhanced glutaminolysis and increased activities of some enzymes involved in glutamine metabolism such as malic enzyme (ME) and isocitrate dehydrogenase (IDH).

Similar to PPP, glutamine metabolism is also involved both in redox detoxification and nucleotide synthesis [118], implying a possible crosstalk between both pathways. In the second chapter of this dissertation, as part of a multinational European project aiming to build a genome scale metabolic model (GSMM) to explore deeply the regulations of breast cancer metabolism, we investigated the effects of glutamine deprivation on breast cancer cells using high-throughput omics technologies and we demonstrated a link between PPP and glutamine metabolism. We expect that once completed, the GSMM will uncover among all, the exact mechanism through which PPP and glutamine metabolism regulate each other in breast cancer cells.

However, while construction of GSMM goes on, we wanted to further validate this link in other cell models. Being one of the most prevalent causes of cancer related deaths along with breast cancer in Western world [4] and having also high reliance on PPP [76], we also decided to study the effect of reduced PPP activity and the link between glutamine metabolism and PPP in colon cancer cells. Therefore, in this chapter we investigated whether the inhibition of oxidative phase of PPP had any effects on the proliferation and the other vital activities of colon cancer cells. Moreover, we also wanted to validate whether the cross regulation between PPP and glutamine metabolism in breast cancer cells can be generalized to colon cancer cells as well.

In short, in this chapter we have analyzed the metabolic alterations induced by the knockdown of G6PD enzyme by RNAi-mediated silencing and the deprivation of glutamine, in order to elucidate the potential of this enzyme to be used as a therapeutic target in cancer therapy and the relationship between glutamine metabolism and ox-PPP in colon cancer cells. We used HT29 cell line as a study model and we confirmed our key results by employing another colon cancer cell line, HCT116.

5.3.2. Results

5.3.2.1. G6PD Inhibition Alters the Proliferation of HT29 Cells

In order to test the reliance of HT29 cells on oxidative phase of PPP for proliferation and other cellular functions, we inhibited G6PD using a pool of small interference RNA (siRNA) containing four different sequences targeting different exonic regions of G6PD gene. In order to obtain a relative comparison, we used as a negative control (siNEG) which also contains a pool of four different siRNA sequences that did not target any specific region of the genome. The analysis of G6PD gene expression 72 hrs after transfection confirmed a successful inhibition at the mRNA level in HT29 cells, with a decrease in fold change of more than 90 % when compared to cells transfected with non-targeting siRNA pool (control cells) (see figure 5.3.1A). Moreover, the protein level of G6PD was assessed 96 hrs after transfection by measuring the specific enzyme activity and further confirmed through western blot (see figure 5.3.1B and C). We found that in HT29 cell line siG6PD pool decreased G6PD enzyme activity around 80 % and western blot analysis further demonstrated a visible decrease in the protein levels of this enzyme.

Several studies including the results that we presented in the first chapter of this thesis have shown that PPP has an important role in cell growth and proliferation [102, 212, 313, 337]. Taking this into account, we examined the role of G6PD enzyme in the proliferation of HT29 colon cancer cell model. The effect of G6PD knockdown on the proliferation rate of HT29 cells was measured via flow cytometry combining direct cell counting and propidium iodide (PI) staining 120 hrs after transfection against G6PD or control siRNA pools. Significantly, G6PD knockdown caused a reduction of approximately 25 % in the proliferation of HT29 cells compared to control cells (figure 5.3.3D). This result indicates that HT29 colon cancer cells with altered metabolism through reduced G6PD activity have a decreased proliferation rate compared to those with fully functional PPP.

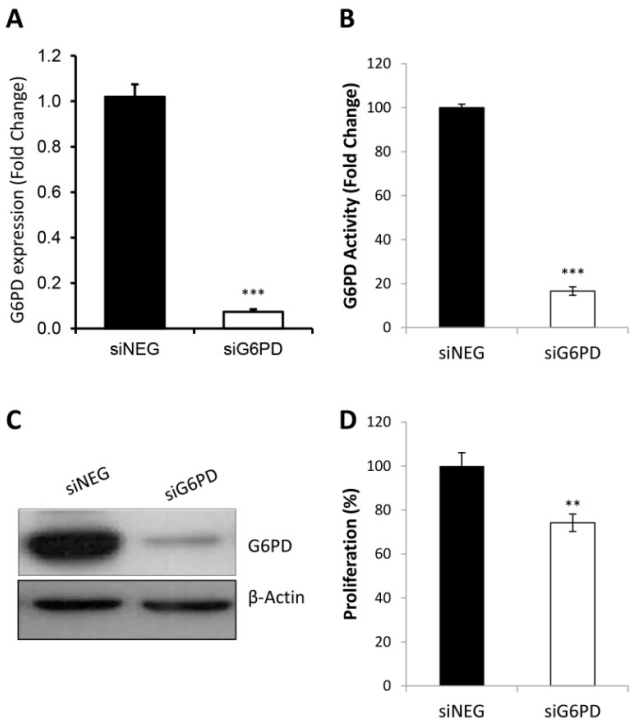

Figure 5.3.1. G6PD knockdown caused the inhibition of G6PD activity and reduced the proliferation of HT29 cells

A) G6PD mRNA expression 72 hrs after transfection with non-targeting siRNA pool (siNEG) or siRNA pool against G6PD. Fold change was calculated with respect to cells transfected with siNEG pool. **B**) Total G6PD enzyme activity normalized to intracellular protein content measured 96 hrs after transfection using either non-targeting siRNA pool or siRNA pool against G6PD. Fold change was quantified relative to cells transfected with siNEG pool. **C**) G6PD protein levels 96 hrs post transfection using either non-targeting siRNA pool or siRNA pool against G6PD. **D**) Effect of G6PD knockdown on cell proliferation measured by flow cytometry 120 hrs after transfection, for G6PD inhibited cells and cells transfected with siNEG pool. Fold change was quantified relative to cells transfected with siNEG pool. The bars correspond to mean ± SD of n = 3. Statistically significant differences between G6PD inhibited and control cells were indicated at $p < 0.05$ (*), $p < 0.01$ (**) and $p < 0.001$ (***).

On the other hand, it has been reported that G6PD is more actively involved in the maintenance of the reduced pool of glutathione used for ROS detoxification than in the production of pentose phosphates used for nucleotide synthesis [338]. Therefore, we speculated that investigating the effects of G6PD inhibition on cell proliferation under a strong stress-causing condition, such as hypoxia [339], which may further enhance the activity of G6PD [340], would further highlight the importance of this enzyme in colon cancer cells. To test our hypothesis, we transfected HT29 cells either with siRNA pool targeting G6PD or non-targeting siRNA pool and cultured them under normal conditions

for 72 hrs. Then, we induced hypoxia for another 72 hrs by shifting the cells to a culture condition harboring only 1 % of O_2. Nevertheless, we did not observe any significant difference in the effects of G6PD knockdown on proliferation between the cells subjected to high stress by hypoxia and the ones cultured under normoxic conditions (figure 5.3.2).

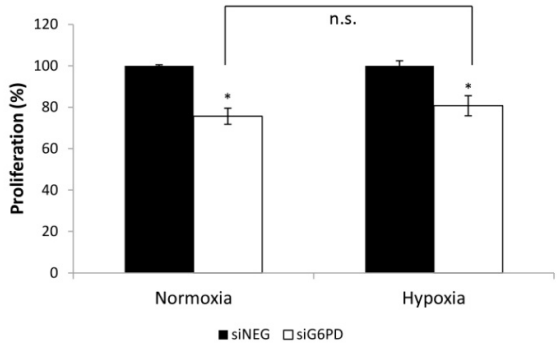

Figure 5.3.2. G6PD knockdown decreased HT29 cells proliferation both in normoxia and hypoxia

72 hrs after transfection with either siG6PD or siNEG pool, HT29 cells were incubated in normoxia or hypoxia (1% O_2) for another 72 hrs. Then, cell proliferation was determined by flow cytometry. Fold change was quantified relative to cells transfected with siNEG pool. The bars correspond to mean ± SD of n = 3. Statistically significant differences between G6PD inhibited and control cells were indicated at $p < 0.05$ (*), $p < 0.01$ (**) and $p < 0.001$ (***).

5.3.2.2. Glutamine Deprivation Increases G6PD Activity and Reduces Cell Proliferation

Even though oxidative phase of PPP is the major source of NADPH required for redox detoxification and several other key biosynthetic processes, the cytosolic isoform of the malic enzyme (ME1) and NADP-dependent isocitrate dehydrogenase (IDH) are additional sources of NADPH in the cells, playing also a major role in glutamine metabolism [71]. Associated with this, Jiang *et al*. have recently demonstrated that inhibition of both oxidative phase of PPP and IDH enhances ROS levels in lung cancer cells [289]. Moreover, in the previous chapters, we observed a crosstalk between glutamine metabolism and ox-PPP in breast cancer cells. Thus, we hypothesized that there might

be a relation between G6PD and glutamine-dependent reactions for NADPH production. Since colon cancer cells have highly active glutamine metabolism, inhibition of glutaminase (GLS) has been reported to lead some colon cancer cells, including HT29 cells, to suppress cell proliferation and induce apoptosis [341]. GLS is the enzyme that generates glutamate from glutamine; therefore, when it is inhibited, glutamine cannot be metabolized in the cells. Besides inhibition of glutamine metabolism enzymes, there are several other strategies to study glutamine metabolism such as deprivation of the cells of glutamine [342], which we used in our study.

Taking this into account, we first wanted to uncover whether there is a direct link between glutamine deprivation and G6PD expression level. To this end, we incubated HT29 cells with glutamine-free medium for several time points and measured the expression levels of G6PD gene at each time point. Interestingly, we observed a significant increase in G6PD expression with glutamine deprivation in HT29 cells starting after 72 hrs of deprivation (figure 5.3.3A). Similarly, we measured the effect of glutamine deprivation on G6PD enzyme activity and, as showed in figure 5.3.3B, we also observed an increased activity of G6PD enzyme with the absence of glutamine in the culture medium of HT29 cell line at various time points. These results show evidence of a metabolic relation between G6PD and glutamine metabolism in HT29 colon cancer cell model. Knowing that glucose is vital for cancer cell survival due to their high dependence on aerobic glycolysis, we also decided to see the effect of glucose deprivation on G6PD levels in HT29 cells at 72 hrs in order to compare it with the effect of glutamine withdrawal. Even though glucose deprivation also led to overexpression of both G6PD expression and enzyme activity, the increase observed at mRNA and protein levels was at a lesser extent than glutamine deprivation (figure 5.3.3C).

Next, we wanted to observe the effect of glutamine and glucose deprivations on the proliferation of HT29. To this end, 24 hrs after seeding the cells, we deprived the cells of glutamine or glucose during several time intervals. As shown at figure 5.3.3D, HT29 cells deprived of either glutamine or glucose decreased their proliferation rate compared to those cultured with complete medium. On the other hand, cells deprived of glutamine did not show an increased death rate while cells cultured without glucose showed a significantly higher death rate (figure 5.3.3E). Interestingly, unlike glucose withdrawal,

glutamine deprivation led HT29 cell line to decrease its proliferation without increasing cell death.

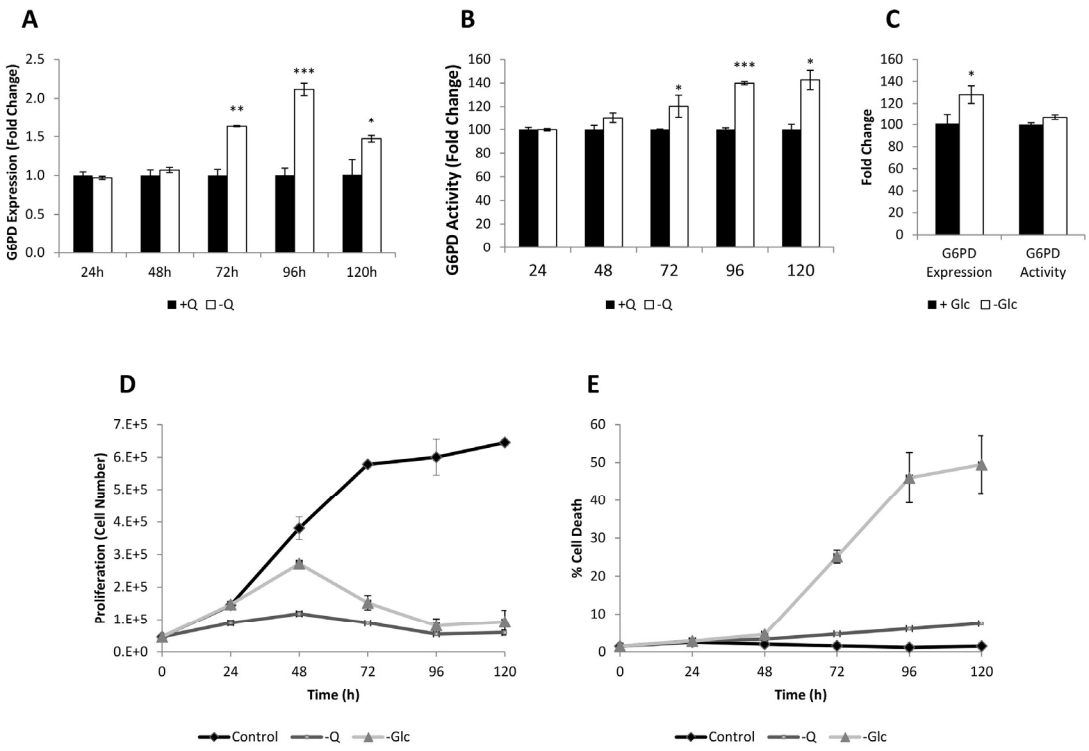

Figure 5.3.3. Both glutamine and glucose deprivations lead to overexpression of G6PD enzyme and alter the proliferation of HT29 cells

A) 6PGD mRNA expression after different time points of glutamine deprivation in HT29 cells (-Q). Fold change was calculated with respect to cells cultured in the medium containing glutamine (+Q). **B)** Total G6PD enzyme activity normalized to intracellular protein content measured after different time points of depriving HT29 cells of glutamine. Fold change was quantified relative to cells cultured in the medium containing glutamine. **C)** G6PD mRNA expression and total G6PD enzyme activity after 72 hrs of incubation of HT29 cells in glucose-free medium (-Glc) compared to the cells cultured in complete medium (+Glc) **D)** Cell proliferation rate of HT29 cells at 24,48,72,96 and 120 hrs after withdrawal of glutamine or glucose from culture medium. **E)** Cell death rate of HT29 cells at 24,48,72,96 and 120 hrs after withdrawal of glutamine or glucose from culture medium. The Bars correspond to mean ± SD of n = 3. Statistically significant differences between glutamine or glucose deprived cells and control cells were indicated at $p < 0.05$ (*), $p < 0.01$ (**) and $p < 0.001$ (***).

5.3.2.3. HCT116 Colon Cells Responds to G6PD Knockdown and Glutamine Deprivation in a Similar Pattern as HT29 Cells

Above, we showed not only that both G6PD inhibition and glutamine deprivation have significant effects on cell proliferation but also a strong relation between the PPP enzyme G6PD and glutamine availability in HT29 colon cancer cells. To see if the effects of both G6PD inhibition and nutrient deprivation observed in this cell line can be also generalized to other cell lines, we decided to employ HCT116 cells as another colon cancer cell model with similar characteristics to HT29 cells. In order to test the dependence of HCT116 cells on ox-PPP for their proliferation, we transfected the cells using either siG6PD or siNEG pool. The analysis of G6PD expression after transfection confirmed a successful inhibition at the mRNA level (with a decrease in fold change of gene expression greater than 90 %) and at protein level (with a decrease in fold change of enzyme activity greater than 80 %) when compared to HCT116 cells transfected with non-targeting siRNA pool. Western blot analysis further confirmed the successful G6PD inhibition in these cells (see figure 5.3.4A-C).

Next, we observed that similar to HT29 cells, G6PD inhibition significantly decreased the proliferation of HCT116 cells (figure 5.3.4D). Also, both glucose and glutamine deprivations lead to an alteration in the proliferation of HCT116 cells in a similar pattern as HT29 cells. While both the decrease in proliferation and the increase in cell death were solely marginal in the absence of glutamine, glucose deprivation led to a strong decrease in proliferation and an increase in the death of HCT116 cells (figure 5.3.4E, F). On the other hand, the link between glutamine deprivation and the enhancement of G6PD expression was also present in HCT116 cells since glutamine deprivation augmented both gene expression and enzyme activity of G6PD (figure 5.3.4G). In fact, HCT116 cells showed similar characteristics to HT29 but the effects were weaker than the latter cells; therefore, we continued performing the rest of the study using only HT29 cell line.

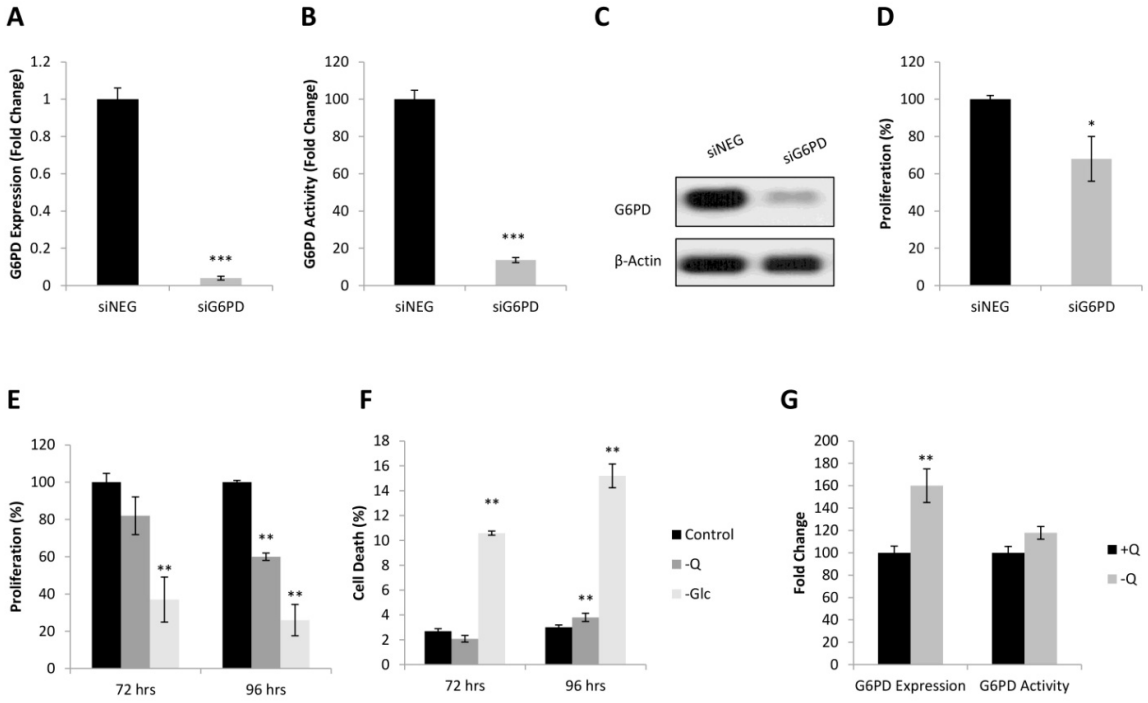

Figure 5.3.4. G6PD inhibition and glutamine deprivation affects HCT116 colon cancer cells in the same way as HT29 cells.

A) G6PD mRNA expression in HCT116 cells 72 hrs after transfection with non-targeting siRNA pool (siNEG) or siRNA pool against G6PD. Fold change was calculated with respect to cells transfected with siNEG pool. **B**) Total G6PD enzyme activity in HCT116 cells normalized to intracellular protein content measured 96 hrs after transfection using either siNEG or siG6PD pool. Fold change was quantified relative to cells transfected with siNEG. **C**) G6PD protein levels in HCT116 cells 96 hrs post-transfection using either siG6PD or siNEG pool. **D**) Effect of G6PD knockdown on proliferation of HCT116 cells measured by flow cytometry 120 hrs after transfection, for G6PD inhibited cells and cells transfected with siNEG pool. **E)**. Cell proliferation rate of HCT116 cells 72 and 96 hrs after withdrawal of glutamine or glucose from the culture medium. **F)** Cell death rate of HCT116 cells 72 and 96 hrs after withdrawal of glutamine or glucose from the culture medium. **G)** G6PD mRNA expression and total G6PD enzyme activity after 72 hrs of incubation of HCT116 cells in glutamine-free medium. The bars correspond to mean ± SD of n = 3. Statistically significant differences between G6PD inhibited and control cells or glutamine- / glucose- deprived cells and control cells were indicated at $p < 0.05$ (*), $p < 0.01$ (**) and $p < 0.001$ (***).

5.3.2.4. Both G6PD Inhibition and Glutamine Deprivation Leads to Cell Cycle Arrest and Induction Apoptosis in HT29 cells

PPP is essential for the biosynthesis of the nucleic acids required for cell proliferation and is associated with cell cycle progression through G6PD, which has been described to be regulated through the development of cell cycle, showing the highest activity at G1

and S phases [77, 343]. Similarly, glutamine metabolism has also been linked to cell cycle machinery by means of redox detoxification, nucleotide biosynthesis and other metabolic activities [344]. Therefore, we speculated that G6PD enzyme and glutamine availability might play an important role on the progression of cell cycle. To this end, we analyzed the population of HT29 cells in each cell cycle phase upon G6PD knockdown or glutamine deprivation. To do this, 96 hrs after transfecting the cells with siG6PD/siNEG pools or depriving them of glutamine, we stained the cells with vindelov-PI solution after fixation and analyzed them using FACS in order to quantify the DNA content. The analysis of cell cycle distribution 96 hrs after G6PD inhibition indicated a significant arrest in S and G2 phases and a subsequent decrease in G1 phase. On the other hand, glutamine withdrawal led HT29 cells to an arrest in G1 phase with a decrease in the population of the cells in S phase (figure 5.3.5A).

As we mentioned before, alterations in cell cycle may induce apoptosis since cell cycle allows cell growth and proliferation [299]. In order to check whether, besides an arrest in cell cycle, apoptosis has been induced in HT29 cells with either G6PD inhibition or glutamine deprivation, we conducted apoptosis assays 96 hrs after each treatment. FACS analysis using annexin-V and PI can assess the presence of non-apoptotic cells (no interaction with neither annexin-V nor PI), early apoptotic cells (interaction with only annexin-V), and late apoptotic or necrotic cells (interaction with both annexin-V and PI) [274, 300]. Our results showed that both G6PD inhibition and glutamine withdrawal led to an increase in the population of apoptotic cells; however, the mode of apoptosis was distinct in both conditions. While G6PD inhibition induced late apoptosis/necrosis, glutamine deprivation led to an increase in the population of the HT29 cells in early apoptosis (figure 5.3.5B). Different apoptotic cell populations may be obtained depending on the different pathways of apoptosis induced by each of two stress-causing conditions that we applied in HT29 cells.

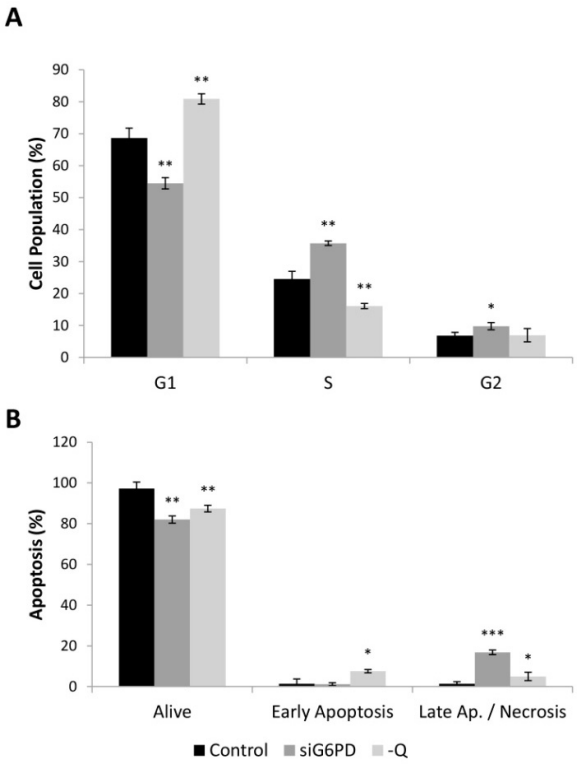

Figure 5.3.5. G6PD Knockdown and Glutamine Deprivation Result in Cell Cycle Arrest and Induce Apoptosis

A) Cell cycle distribution analysis of HT29 cells 96 hrs after transfection against G6PD or glutamine deprivation. The percentage of cells in the different cell cycle phases was calculated using FlowJo® software. **B)** Percentage of HT29 cells at different apoptosis modes 96 hrs after transfection against G6PD or glutamine deprivation. $1x10^4$ cells were measured by flow cytometry using Annexin V FITC kit. The bars correspond to mean ± SD of n = 3. Statistically significant differences between G6PD inhibited / glutamine deprived and control cells were indicated at $p < 0.05$ (*), $p < 0.01$ (**) and $p < 0.001$ (***).

5.3.2.5. Glutamine Availability Regulates G6PD by Means of NRF2 activation

The above explained results evidenced that there is an interaction between glutamine availability and G6PD enzyme. Thus, we wanted to explore the mechanism underlying the increase of G6PD activity after glutamine deprivation in HT29 cell line. Nuclear factor (erythroid-derived 2)-like 2 (NRF2) protein has been described as a transcription factor regulating the expression of antioxidant proteins in order to protect the cells against oxidative damage [345]. In addition, it has been reported that cells with activated RAS pathway, such as HT29 cells, have elevated levels of NRF2 expression [92, 346]. Moreover, it is known that G6PD is regulated by NRF2 transcription factor [91]. In fact,

NRF2 is further regulated by Kelch-like ECH-associated protein 1 (KEAP1) in a way that under normal circumstances, NRF2 is constantly ubiquitinated by KEAP1 for its degradation; however, under oxidative stress conditions KEAP1 is inactivated, so that NRF2 is released and migrates to the nucleus to activate an antioxidant response program involving several PPP genes [347]. Besides, we showed that glutamine deprivation enhances G6PD expression in HT29 cells. Considering all this, we hypothesized that glutamine deprivation might trigger a genetic program that is initiated by elevated intracellular ROS levels and modulated by NRF2.

To test this, we first wanted to confirm that glutamine deprivation has a correlation with ROS levels in HT29 cells. So, we measured the cellular ROS production using H_2DCFA probes in cells deprived of glutamine for various time points (figure 5.3.6A). We observed that starting from 24 hrs of glutamine deprivation, there is a significant increase in ROS levels of HT29 cells cultured without glutamine, indicating that glutamine is involved in the maintenance of the redox status of this cell line. In redox detoxification, as it has been mentioned earlier, glutamine is not only involved in the production of NADPH but in the production of glutathione (GSH) as well [323]. Therefore, the elevated ROS levels observed in HT29 cells with glutamine deprivation are expected and strengthen our hypothesis.

Next, to explore the NRF2 activation with glutamine deprivation, we measured the expression level of NRF2 gene (codified as NFE2L2) and some other validated NRF2 target genes; such as NQO1 [91] and HMOX1 [92] in HT29 cells cultured with or without glutamine by using quantitative real time PCR. We found out that, in cells cultured without glutamine, not only G6PD (see figure 5.3.3A), but also both of the NRF2 target genes (HMOX1 and NQO1) were upregulated. On the other hand, the expression levels of NRF2 did not change (see figure 5.3.6B). Taking into account that NRF2 is constantly ubiquitinated by KEAP1 for its degradation, we speculated that we might observe the activation of NRF2 at protein level by performing western blot analysis. As seen in figure 5.3.6C, 24 hrs after glutamine withdrawal from the culture medium of HT29 cells, an enhanced expression of NRF2 protein was observed. This clearly demonstrates the activation of a genetic response mediated by NRF2 in the absence of glutamine. To sum up, we found that glutamine deprivation in HT29 cells elevates ROS levels, which in turn

increase the oxidative stress. Increased oxidative stress inactivates KEAP1 leading to the release and accumulation of NRF2 transcription factor which, in turn, triggers the increase of G6PD expression to balance the increased oxidative stress.

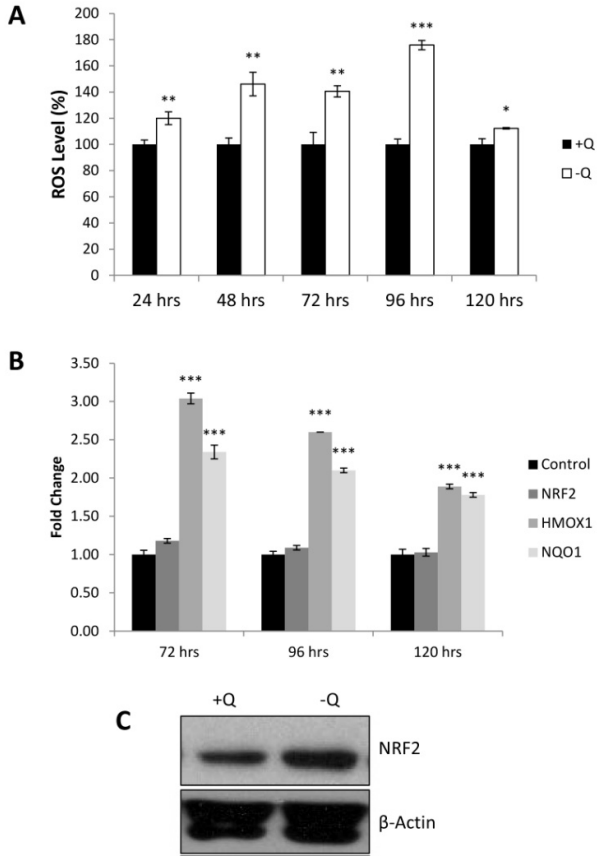

Figure 5.3.6. G6PD is Regulated by Glutamine Availability

A) Relative ROS levels measured by flow cytometry using H_2DCFA probes. ROS levels of HT29 cells cultured without glutamine (-Q) are compared as fold change with respect to cells cultured with glutamine (+Q). **B)** NRF2, HMOX1 and NQO1 mRNA expression levels 72, 96 or 120 hrs after depriving HT29 cells of glutamine. Fold change was calculated with respect to cells cultured with medium containing glutamine. **C)** NRF2 protein level 24 hrs after withdrawal of glutamine from the culture medium. The bars correspond to mean ± SD of n = 3. Statistically significant differences between glutamine deprived and control cells were indicated at $p < 0.05$ (*), $p < 0.01$ (**) and $p < 0.001$ (***).

5.3.3. Discussion

Several tumors have higher dependence on PPP, particularly on oxidative phase of PPP, compared to non-transformed cells [77, 78, 265]. G6PD is a rate-limiting metabolic enzyme that catalyzes the first step of ox-PPP and is highly expressed in various cancers, including colon cancer [348]. The function of G6PD is highly impacted and to illustrate, G6PD deficient erythrocytes have a life span much shorter than healthy ones [349]. In fact, G6PD has been proposed as an attractive therapeutic target in the fight against cancer in several studies [95, 348] as it plays an important role in the biosynthesis of ribose and the production of NADPH, which is vital for regulation of ROS levels [350]. However, the entire mechanism by which G6PD inhibition impacts on cancer progression is not fully elucidated [351]. One popular approach is that taking into account that the redox detoxification system is altered in several types of tumors [101], it has been reported that G6PD knockdown renders HepG2 liver cancer cells susceptible to apoptosis in ROS dependent manner [95]. On the other hand, a recent study has revealed that G6PD knockdown decreases migration of HeLa cells by changing the biophysical cell properties, thus indicating that G6PD also takes role in metastasis [351].

Glutamine, on the other hand, is a versatile nutrient having vital importance for most cancer cells [118]. In fact, there are both *in vivo* and *in vitro* studies conducted previously that demonstrate the importance of glutamine for cancer cells [352]. In addition, the cytoplasmic isoform of glutaminase (GLS1), which catalyzes the first step of glutamine metabolism, is highly expressed in colon cancer [341]. Despite the fact that many studies have been conducted to unveil the metabolism of glutamine in tumors, there is much to be explored yet. Unpublished data within our group have demonstrated the importance of G6PD together with glutamine availability in breast cancer cells which are highly dependent on PPP and have glutamine dependence. To see whether these results are reproducible in other cell models, we decided to explore the functional importance of G6PD and its regulation by the presence of glutamine in colon cancer cell models.

Here, we first showed that G6PD has an important role in the proliferation of HT29 colon cancer cells. G6PD gene expression was reduced more than 90 % by employing RNA

interference technology, which in turn reduced the activity of this enzyme about 80 %. This reduction led HT29 cell line to a decrease in proliferation about 25 %, which highlights the importance of this enzyme in the proliferation of colon cancer cells. Considering that in non-transformed cells G6PD usually works only around 2 % of its maximum potential [353] while in cancer cells this percentage is significantly higher, it is vital to highlight the key role of G6PD in the proliferation of tumor cells. Several other studies in various tissues also demonstrated the importance of G6PD in cell viability [354-356]; thus, our results showing the effect of G6PD activity on the proliferation of HT29 is not to be underrated. It has been reported that inhibition of G6PD activity by dehydroepiandrosterone (DHEA) in colon cancer cells augmented the flux of nonoxidative phase of PPP by increasing the transketolase (TKT) activity for ribose synthesis [102], which evidences the metabolic flexibility of PPP. Moreover, G6PD has been reported to be more involved in redox detoxification than in the biosynthesis of nucleic acid precursors [338], which agrees with our findings that G6PD inhibition alters the proliferation of HT29 cells with a mechanism involving increased ROS levels. Taking this into account, we considered that increasing the cellular stress would augment the decrease in proliferation of colon cancer cells with reduced G6PD activity. However, the combination of hypoxic culture conditions and G6PD knockdown did not decrease the proliferation of HT29 cells in comparison to normoxic culture conditions (figure 5.3.2). Despite the fact that G6PD activity was reduced up to 80 %, apparently the cells still exhibit enough G6PD activity to cope with increased cellular stress. Therefore, we can assume that the observed decrease in proliferation is not only caused by the increased ROS levels resulting from the reduction on NADPH generation, but also by other factors that might include reduced lipid biosynthesis in which also NADPH takes important role.

NADPH used to cope with the cellular stress is produced through several pathways, among them PPP [74] and glutamine metabolism [323] are the most important ones. In previous studies within our group, we observed an increased glutamine consumption rate in breast cancer cells with reduced G6PD activity. Similarly, in the first chapter of this thesis, we found out that inhibition of 6PGD (the third enzyme of oxidative phase of PPP) also resulted in an increase in the glutamine consumption. So, we speculated that there might be a crosstalk between oxidative PPP and glutamine metabolism. Moreover,

in chapter two, we observed a clear modulation of PPP by glutamine availability in breast cancer cells. On the other hand, G6PD activity was also reported to be regulated by glucose availability in some cell lines [357]. Therefore, we also wanted to explore the effects of glucose deprivation on G6PD activity and viability of HT29 cells to compare them with the effects caused by glutamine deprivation. To this end, we deprived cells of glutamine or glucose and observed that glutamine withdrawal led to an increase in both the expression and the enzyme activity of G6PD at different time points, while glucose withdrawal caused much milder effects (data not shown). Hence, we evidenced a strong link between G6PD and glutamine or glucose availability. Interestingly, when testing whether glutamine and glucose had effects on the viability of HT29 cells, we observed that both glutamine and glucose withdrawal significantly reduced the proliferation of colon cancer cells at various time points. The cells proliferate for 48 hrs after glucose deprivation and then significantly reduced their proliferation. A recent report has demonstrated that colon cancer cells, including HT29, increase their glutamine metabolism when glucose is scarce in the microenvironment in order to support survival [358]. Therefore, we can assume that cells cultured without glucose consume glutamine and other nutrients present in the culture medium to proliferate; however, when nutrients are scarce, the cells start to die. In contrast, cells cultured without glutamine do not use other nutrient sources of the culture medium to maintain the proliferation rate, since they just enter a quiescent state without exhibiting cell death.

To broaden our study, we performed the same analysis using HCT116 cells, a colon cancer cell line with similar characteristics to HT29 cells, and we observed that the effects of G6PD inhibition and glutamine/glucose deprivation on cell proliferation were in the same direction as on HT29 cells but to a lesser extent. Moreover, both glutamine and glucose deprivation in HCT116 cells enhanced the expression levels of G6PD as in HT29 cells. Nevertheless, since the effects of glucose deprivation were similar but weaker than those from glutamine deprivation and the responses of HCT116 cells to G6PD inhibition or nutrient deprivation were less prominent than in HT29 cells, we centered our study on HT29 cells and glutamine deprivation.

Cell cycle is the period between two mitotic divisions that covers a set of processes through which cell growth and division takes place. Cell cycle progression consists of

three phases; S phase where DNA is replicated and two gap phases before and after S phase, called G1 and G2, respectively. The nucleotides produced by PPP are used in S phase for DNA replication. We measured the population of the cells in each phase of the cell cycle and we observed that HT29 cells with reduced G6PD activity were arrested in the S and G2 phases of the cell cycle. In fact, since cells must have enough nucleotides to overcome the checkpoint at G1 phase [77], the decreased rate of precursors for nucleotides synthesized in the PPP must have been compensated by the activation of the non-oxidative pathway of PPP. Besides that, Saqcena *et al.* reported that DNA damaging agents induce apoptosis selectively in cancer cells arrested in S and G2 phases of cell cycle, implying that phase specific cytotoxic drugs in combination with G6PD inhibitors may create synthetic lethality that can be a novel therapeutic approach in the combat against cancer [359]. On the other hand, we observed that glutamine withdrawal arrested HT29 colon cancer cells in G1 phase, which is in concordance with the described key roles of glutamine in the transition from G1 to S phase in cell cycle and the nucleotide synthesis [63].

Among others, alterations in cell cycle and increased oxidative stress are strong apoptosis inducers [156]. Since both of the experimental conditions we have studied altered cell cycle progression and are oxidative stress stimulants, we expected to see an apoptosis induction in HT29 cells with experimental conditions of the study. In order to confirm the decreased proliferation of HT29 cells with G6PD inhibition or glutamine deprivation, we assessed apoptosis assay. In both conditions, we observed a decrease in non apoptotic cells; nonetheless, G6PD inhibition resulted in an increase in late apoptotic and necrotic cell population, while upon glutamine deprivation, the population of early apoptotic cells was bigger. This might be caused by an earlier response to apoptotic signals in the cells with G6PD knockdown compared to those cultured without glutamine. Moreover, each stress causing factor may induce a different apoptotic pathway [360]; thus explaining the different apoptotic populations in G6PD-inhibited and glutamine-deprived HT29 cells.

NRF2 is a pivotal transcription factor taking role in protection against oxidative stress. It is negatively regulated by KEAP1 protein, which constantly ubiquitinates NRF2 for its degradation through proteosomes. In the presence of enhanced oxidative stress, KEAP1

is inactivated which in turn releases NRF2 and then, NRF2 orchestrates a ROS detoxification program [91]. Moreover, G6PD expression and activity is controlled by many factors, among them is also NRF2 [361]. In fact, NRF2 regulates G6PD promoter via its antioxidant response elements (ARE) [347]. Apart from that, Son *et al.* has previously reported that besides feeding mitochondrial reactions, glutamine is also a substrate for malic enzyme which converts malate to pyruvate in return of NADPH production, and withdrawal of glutamine from the cell environment, therefore, increases the ROS level [362]. In our case, both expression and enzyme activity of G6PD and the level of ROS in HT29 cells increased upon deprivation of glutamine in the culture medium. Reasonably, we hypothesized that the augmentation of G6PD might be mediated by NRF2. To test this, we checked the gene expression level of NRF2 and some of its target genes, HMOX1 and NQO1. Despite that NRF2 expression level was constant; its target genes had a great increase in fold change. Checking at the protein level by western blot, we observed an overexpression in the NRF2 protein. Thus, we confirm a direct relation between glutamine availability and G6PD activity mediated by NRF2 transcription factor. The expression level of NRF2 gene was constant even upon glutamine withdrawal as its transcription and translation is constantly active and its synthesized proteins are dominated by KEAP1. However, KEAP1 is inactivated by increased oxidative stress and the amount of free NRF2 protein increases (figure 5.3.6C) which in turn, leads to activation of G6PD. To best of our knowledge, this is the first study unveiling a direct relation between glutamine metabolism and PPP enzymes.

In this chapter we manifestly showed the importance of the PPP enzyme G6PD, as well as glutamine for the proliferation of colon cancer cells. We demonstrated that both G6PD inhibition and glutamine deprivation led HT29 cells in cell cycle arrest and a subsequent induction of apoptosis. Also, we unveiled the relation and regulation between glutamine availability and the enzymes of the oxidative phase of the PPP. We showed that G6PD is overexpressed in HT29 cells upon glutamine withdrawal as a consequence of the increase of ROS and the induction of NRF2. Together with the results of the previous chapters, we exhibited the potential of oxidative PPP enzymes as therapeutic targets in the combat against cancer.

6. GENERAL DISCUSSION

6. GENERAL DISCUSSION

Cancer is a broad term that defines several diseases characterized by the uncontrolled proliferation of cells, which eventually form tumors. Acquirement of different functional and genetic abnormalities may lead non-transformed cells to escape proliferation control mechanisms, leading to tumorigenesis and tumor progression. These abnormal cells can aquire the capability to spread throughout the body and start a new tumor in a distant tissue in a process called metastasis [1], which is the main reason of cancer related deaths. The latest global cancer statistics report indicated that in 2012, 14.1 million new cancer cases and 8.2 million cancer caused deaths were detected worldwide. Among those, the most commonly diagnosed cancers were lung (1.82 million), breast (1.67 million) and colorectal (1.36 million) [4]. These statistics show that cancer is one of the most important causes of death worldwide, and therefore it is vital to better understand cancer cell biology in order to design new therapeutic strategies against the disease.

Research conducted within the last two decades has demonstrated that cancer cells share common essential capabilities required for malignant transformation which are sequentially acquired during tumor formation. These characteristics, defined by Hanahan and Weinberg as hallmarks of cancer [14, 15], include a process of metabolic reprogramming. This implies that, in order to meet the increased requirements of energy and molecular building blocks related to accelerated cell growth, cancer cells need to adapt their metabolism by augmenting key metabolic pathways such as glycolysis, pentose phosphate pathway (PPP), glutaminolysis, and amino acid, lipid and nucleic acid synthesis pathways [18, 48]. Activation of oncogenes or deactivation of tumor suppressor genes lead tumor cells to overcome the check points of cell cycle and induction of apoptosis, and these give them immortality [17-20]. Key oncogenes and tumor suppressor genes which control cell cycle, apoptosis, cell proliferation and DNA

repair have been reported to be involved in the modulation of cancer cell metabolic reprogramming, including Myc, hypoxia inducible factor 1 (HIF1), phosphoinositide-3-kinase (PI3K), protein kinase B (Akt), the mechanistic target of rapamycin (mTOR), p53, retinoblastoma (RB), Bax or phosphatase and tensin homolog (PTEN)[21, 22, 41, 363]. Considering this, the study of the metabolic adaptations of cancer cells and their connection with different oncogenic signaling pathways is a key strategy to identify new targets for cancer therapy.

The oxidative branch of PPP is a metabolic pathway directly related with nucleotide biosynthesis and redox detoxification, but it also has important roles in many other aspects related to the viability of cancer cells, including proliferation, apoptosis, invasiveness, drug resistance, and metastasis [74, 77]. Thus, the the targeting of this pathway as a potential therapeutic approach against cancer has been considered an interesting possibility [77, 98, 102]. Previous studies performed within our team have demonstrated that the inhibition of one of the most important enzymes of this pathway, glucose-6-phosphate dehydrogenase (G6PD), has important effects over MCF7 breast cancer cells cancer cells, including decreased cell proliferation, increased cell death, increased ROS concentrations, cell cycle arrest and altered central carbon metabolism (data not published). In the first chapter of this Thesis, we evaluated the role of 6-Phosphogluconate dehydrogenase (6PGD), the third enzyme of the ox-PPP which catalyzes the conversion of 6-phosphogluconate (6-PG) to ribulose-5-phosphate, over MCF7 and T47D breast cancer cells. We chose those cell models because of the high reliance of breast cancer cells on PPP and their dependence on ROS detoxification to manage their oxidative stress and maintain their survival [76, 298], and because we wanted to investigate the possible link between 6PGD and p53 (T47D carrying a mutant copy of p53 gene, contrary to MCF7 cells [9])

In order to explore the potential of 6PGD as a therapeutic drug target in breast cancer, we evaluated the effect of the inhibition of 6PGD enzyme by RNA interferase (RNAi) mediated silencing in those cell lines. Inhibition of 6PGD gene expression resulted in a significantly decreased proliferation rate, cell cycle arrest, and induction of apoptosis in both cell lines, with stronger effects in MCF7 cells. Inhibition of 6PGD was also shown to provoke an increase in the activaton of p53, which provides a link between the enzyme

and the tumor suppressor factor, and explains the higher effects of 6PGD inhibition over MCF7 cells in comparison with MCF7 cells. Strikingly, 6PGD knockdown also altered stem cell characteristics of both breast cancer cell lines by decreasing mammosphere formation capabilities, and altered central carbon metabolism by increasing glutamine consumption and increasing the activities of malic enzyme and isocitrate dehydrogenase. These metabolic alterations probably constitute an adaptive mechanism that breast cancer cells undergo in order to produce NADPH even after the oxidative phase of PPP has been blocked, and therefore the simultaneous inhibition of 6PGD together with ME or IDH may represent a promising strategy to deprive tumor cells of their ability to compensate oxidative stress through NADPH production. All in all, the experimental evidences presented in this work highlight the potential of 6PGD as a putative therapeutic drug target in breast cancer treatment, to be exploited alone or in combination with other simultaneous treatments.

In the light of the results of chapter one, which revealed that breast cancer cells might depend on glutamine consumption to increase cell survival in harsh conditions, in chapter two we decided to characterize the metabolic adaptations induced in breast cancer cells under glutamine deprivation. Since breast tumors also contain intra-tumor hypoxic regions where oxygen availability is considerably reduced [335] and mitochondrial functionality is therefore impaired, we also decided to characterize the metabolic adaptations induced in breast cancer cells under hypoxia-mimicking mitochondrial impairment conditions. The study of the metabolic adaptations undergone by cancer cells under those conditions might reveal new dependancies that could be exploited in therapy, in order to reduce the metabolic flexibility of breast cancer cells thus reducing their survivability. In this regard, we observed an increase in the activity of pyruvate cycle with glutamine deprivation, thus indicating that targeting the enzymes of this pathway such as malic enzyme could be a promising approach combined with inhibition of glutaminase (GLS) enzyme. On the other hand, we observed that mimicking hypoxia through oligomycin treatment redirected breast cancer cells to increase reductive carboxylation. Considering that hypoxia is a common condition in the tumor environment, targeting reductive carboxylation mechanism could be a novel strategy to fight against cancer.

Furthermore, in order to perform a systemic study of the regulation of breast cancer metabolism in the frame of a multinational European project, the trasncriptomics, metabolomics and fluxomics data generated in chapter 2 will be combined with the proteomics and phosphoproteomics data generated by a partner group in the project, in order to produce a multi-layer Genome-Scale Metabolic Model (GSMM) which will allow us to study the regulation of breast cancer metabolism from an holistic point of view. This systems biology approach will allow us to study the metabolic adaptations in response to glutamine deprivation providing information that the inhibition of individual genes on its own is not possible to reveal [364].

In the first two chapters we unveiled the important role of PPP and glutamine in the proliferation, survival and adaptation of breast cancer cells. Considering the promising results, which could pave the way for the development of new combined treatments against breast cancer, we decided to apply the same strategy on a different cell model. In the third chapter of this Thesis, we studied to study the effects of PPP inhibition and glutamine deprivation in HT29 colon cancer cells. After inhibiting Glucose-6-phosphate Dehydrogenase (one of the most important enxymes of the pentose phosphate pathway) by using RNAi mediated silencing, we observed that G6PD inhibition not only caused a significant decrease in the proliferation rates of colon cancer cells, but also resulted in an arrest in cell cycle and a subsequent induction of apoptosis-mediated cell death. The effectos of G6PD inhibition over HT29 colon cancer cells were similar to the ones observed previously in our research group when using MCF7 breast cancer cell lines as a model (data not published), despite the fact that the achieved inhibition of G6PD gene expression in colon cancer cells was much higher than the one previously obtained with breast cancer cells (92 % and 60 % respectively). Considering that i) p53 inhibits G6PD by binding to it to impede its dimer formation [87], and ii) MCF7 cells carry mutated p53 while HT29 has wild type p53 [9, 365], we can conclude that HT29 cells have much higher G6PD activity and therefore a much stronger G6PD inhibition is needed to get the same phenotypic results than with MCF7 cells.

Regarding glutamine dependency in HT29 colon cancer cells, we showed that while both glucose and glutamine deprivation led to a decrease in HT29 cells proliferation, glutamine deprivation had a much higher effect in the increase of G6PD expression

levels. We investigated the mechanism relating glutamine deprivation and G6PD overexpression, and we showed that G6PD is overexpressed in HT29 cells upon glutamine withdrawal in a process involving ROS augmentation and the induction of NRF2 transcription factor. This role of glutamine in PPP regulation suggests that combining glutamine metabolism inhibition with the PPP inhibition might be a promising approach in the development of new therapies against cancer, an hypothesis that is strengthened by the fact that chemotherapy carried out during fasting has been proven to be more effective than chemotherapy alone [366].

Throughout the different chapters of this dissertation, the analysis of tumor metabolic reprogramming in different cancer cells has highlighted new potential targets for cancer treatment. In this regard, we have studied and proposed pentose phosphate pathway (PPP) enzymes as putative therapeutic targets against both breast and colon cancers, and we have demonstrated the relationship between glutamine availability and the regulation of the oxidative branch of PPP, highlighting the potential of novel combined therapies. We have also explored the glutamine metabolism in breast cancer cells and the metabolic network adaptations that they undergo in order to circumvent glutamine deprivation and general mitochondrial impairment, highlighting novel putative therapeutic targets to reduce cancer cells survivability in hypoxic conditions, which are common in many different tumors. Moreover, we have generated a large amount of data to be used for the construction of a genome scale metabolic model (GSMM), in order to obtain a global view of the regulation of metabolic alterations in breast cancer cells using a Systems Biology approach.

Taken together, all the results provided in this thesis demonstrate the importance of metabolic reprogramming in cancer cell proliferation and survival, and the potential of studying it to unveil novel therapeutic targets and design more effective combined treatments. This work also highlights the importance of Systems Biology approaches to comprehend the molecular mechanisms underlying complex multifactorial diseases.

7. CONCLUSIONS

7. CONCLUSIONS

I) 6PGD knockdown decreases both cell proliferation through cell cycle arrest and apoptosis induction mediated by activation of p53 tumor suppressor gene and the stem cell like characteristics in MCF7 and T47D breast cancer cells. G6PD inhibition also alters central carbon metabolism by increasing glutamine consumption and the activities of malic enzyme and isocitrate dehydrogenase, in which probably constitutes an adaptive mechanism that breast cancer cells undergo in order to produce NADPH even after the oxidative phase of PPP has been blocked. This highlights the potential of 6PGD as a putative therapeutic drug target in breast cancer treatment, on its own or as part of combined treatments, and the importance of glutamine consumption in cancer cells' adaptation to stress conditions.

II) Glutamine deprivation causes an increase in the activity of pyruvate cycle in MCF7 cells, suggesting that targeting enzymes such as malic enzyme in combination with glutaminase could be a promising therapeutic approach. Mimicking hypoxia through oligomycin treatment redirected breast cancer cells to increase reductive carboxylation, suggesting that targeting reductive carboxylation mechanism could be a novel strategy to reduce cancer cells survivability in hypoxic conditions, which are common in many tumors.

III) Both G6PD enzyme and glutamine have important roles in the proliferation and survival of HT29 colon cancer cells, highlighting the importance of PPP and glutamine dependence in different types of cancer. Glutamine deprivation leads to overexpression of G6PD through a mechanism involving increased ROS levels and NRF2 transcription factor induction, which

constitutes a previously undescribed connection between PPP and glutamine metabolism.

8. REFERENCES

8. REFERENCES

1. WHO. *Cancer; Fact sheet N°297*. 2015 February 2015 [cited June 2016; World Health Organization].
2. Anand, P., et al., *Cancer is a preventable disease that requires major lifestyle changes.* Pharm Res, 2008. **25**(9): p. 2097-116.
3. WHO, *Global status report on noncommunicable diseases 2014*. 2014, World Health Organization: Geneva.
4. Ferlay, J., et al., *Cancer incidence and mortality worldwide: sources, methods and major patterns in GLOBOCAN 2012.* Int J Cancer, 2015. **136**(5): p. E359-86.
5. World Health Organization. *Global health observatory data repository*. 2012 [cited 2016 14 Jan]; Available from: http://apps.who.int/gho/data/node.main.CODWORLD?lang=en.
6. Jemal, A., et al., *Global patterns of cancer incidence and mortality rates and trends.* Cancer Epidemiol Biomarkers Prev, 2010. **19**(8): p. 1893-907.
7. Wang, Y., et al., *Prediction of poor prognosis in breast cancer patients based on microRNA-21 expression: a meta-analysis.* PLoS One, 2015. **10**(2): p. e0118647.
8. Yersal, O. and S. Barutca, *Biological subtypes of breast cancer: Prognostic and therapeutic implications.* World J Clin Oncol, 2014. **5**(3): p. 412-24.
9. Holliday, D.L. and V. Speirs, *Choosing the right cell line for breast cancer research.* Breast Cancer Res, 2011. **13**(4): p. 215.
10. AmericanCancerSociety, *Colorectal Cancer Facts & Figures 2014-2016.* 2014, American Cancer Society: Atlanta, Ga.
11. Zhang, J., Y.H. Chen, and Q. Lu, *Pro-oncogenic and anti-oncogenic pathways: opportunities and challenges of cancer therapy.* Future Oncol, 2010. **6**(4): p. 587-603.
12. Javier, B.M., et al., *Recurrent, truncating Sox9 mutations are associated with sox9 overexpression, KRAS mutation, and TP53 wild type status in colorectal carcinoma.* Oncotarget, 2016.
13. Bejar, R., *Splicing Factor Mutations in Cancer.* Adv Exp Med Biol, 2016. **907**: p. 215-28.
14. Hanahan, D. and R.A. Weinberg, *The hallmarks of cancer.* Cell, 2000. **100**(1): p. 57-70.
15. Hanahan, D. and R.A. Weinberg, *Hallmarks of cancer: the next generation.* Cell, 2011. **144**(5): p. 646-74.
16. Xiao, D., et al., *Melanoma cell-derived exosomes promote epithelial-mesenchymal transition in primary melanocytes through paracrine/autocrine signaling in the tumor microenvironment.* Cancer Lett, 2016. **376**(2): p. 318-27.
17. Vogelstein, B. and K.W. Kinzler, *Cancer genes and the pathways they control.* Nat Med, 2004. **10**(8): p. 789-99.
18. Ward, P.S. and C.B. Thompson, *Metabolic reprogramming: a cancer hallmark even warburg did not anticipate.* Cancer Cell, 2012. **21**(3): p. 297-308.
19. Liu, J., et al., *Tumor suppressor p53 and its mutants in cancer metabolism.* Cancer Lett, 2015. **356**(2 Pt A): p. 197-203.
20. Mullen, A.R. and R.J. DeBerardinis, *Genetically-defined metabolic reprogramming in cancer.* Trends Endocrinol Metab, 2012. **23**(11): p. 552-9.

21. Levine, A.J. and A.M. Puzio-Kuter, *The control of the metabolic switch in cancers by oncogenes and tumor suppressor genes.* Science, 2010. **330**(6009): p. 1340-4.
22. Hennessy, B.T., et al., *Exploiting the PI3K/AKT pathway for cancer drug discovery.* Nat Rev Drug Discov, 2005. **4**(12): p. 988-1004.
23. Wei, W. and J.M. Sedivy, *Differentiation between senescence (M1) and crisis (M2) in human fibroblast cultures.* Exp Cell Res, 1999. **253**(2): p. 519-22.
24. Blasco, M.A., *Telomeres and human disease: ageing, cancer and beyond.* Nat Rev Genet, 2005. **6**(8): p. 611-22.
25. Lewis, K.A. and T.O. Tollefsbol, *Regulation of the Telomerase Reverse Transcriptase Subunit through Epigenetic Mechanisms.* Front Genet, 2016. **7**: p. 83.
26. Ekedahl, H., et al., *High TERT promoter mutation frequency in non-acral cutaneous metastatic melanoma.* Pigment Cell Melanoma Res, 2016.
27. Hanahan, D. and J. Folkman, *Patterns and emerging mechanisms of the angiogenic switch during tumorigenesis.* Cell, 1996. **86**(3): p. 353-64.
28. Ferrara, N., *Vascular endothelial growth factor.* Arterioscler Thromb Vasc Biol, 2009. **29**(6): p. 789-91.
29. Talmadge, J.E. and I.J. Fidler, *AACR centennial series: the biology of cancer metastasis: historical perspective.* Cancer Res, 2010. **70**(14): p. 5649-69.
30. Manuel Iglesias, J., et al., *Mammosphere formation in breast carcinoma cell lines depends upon expression of E-cadherin.* PLoS One, 2013. **8**(10): p. e77281.
31. Roger, L., et al., *Gain of oncogenic function of p53 mutants regulates E-cadherin expression uncoupled from cell invasion in colon cancer cells.* J Cell Sci, 2010. **123**(Pt 8): p. 1295-305.
32. Lim, W., et al., *Association between cancer stem cell-like properties and epithelial-to-mesenchymal transition in primary and secondary cancer cells.* Int J Oncol, 2016.
33. Berdasco, M. and M. Esteller, *Aberrant epigenetic landscape in cancer: how cellular identity goes awry.* Dev Cell, 2010. **19**(5): p. 698-711.
34. Song, Y., F. Wu, and J. Wu, *Targeting histone methylation for cancer therapy: enzymes, inhibitors, biological activity and perspectives.* J Hematol Oncol, 2016. **9**(1): p. 49.
35. Hendrayani, S.F., et al., *The inflammatory/cancer-related IL-6/STAT3/NF-kappaB positive feedback loop includes AUF1 and maintains the active state of breast myofibroblasts.* Oncotarget, 2016.
36. Grivennikov, S.I., F.R. Greten, and M. Karin, *Immunity, inflammation, and cancer.* Cell, 2010. **140**(6): p. 883-99.
37. Vinay, D.S., et al., *Immune evasion in cancer: Mechanistic basis and therapeutic strategies.* Semin Cancer Biol, 2015. **35 Suppl**: p. S185-98.
38. Pavlova, Natalya N. and Craig B. Thompson, *The Emerging Hallmarks of Cancer Metabolism.* Cell Metabolism, 2015. **23**(1): p. 27-47.
39. Yoshida, G.J., *Metabolic reprogramming: the emerging concept and associated therapeutic strategies.* J Exp Clin Cancer Res, 2015. **34**: p. 111.
40. Warburg, O., *On the origin of cancer cells.* Science, 1956. **123**(3191): p. 309-14.
41. Cairns, R.A., I.S. Harris, and T.W. Mak, *Regulation of cancer cell metabolism.* Nat Rev Cancer, 2011. **11**(2): p. 85-95.
42. Dang, C.V., *Links between metabolism and cancer.* Genes Dev, 2012. **26**(9): p. 877-90.
43. Coller, H.A., *Is cancer a metabolic disease?* Am J Pathol, 2014. **184**(1): p. 4-17.
44. Menendez, J.A., et al., *The Warburg effect version 2.0: metabolic reprogramming of cancer stem cells.* Cell Cycle, 2013. **12**(8): p. 1166-79.
45. Cantor, J.R. and D.M. Sabatini, *Cancer cell metabolism: one hallmark, many faces.* Cancer Discov, 2012. **2**(10): p. 881-98.

46. Gross, S., et al., *Cancer-associated metabolite 2-hydroxyglutarate accumulates in acute myelogenous leukemia with isocitrate dehydrogenase 1 and 2 mutations.* J Exp Med, 2010. **207**(2): p. 339-44.
47. Kroemer, G. and J. Pouyssegur, *Tumor cell metabolism: cancer's Achilles' heel.* Cancer Cell, 2008. **13**(6): p. 472-82.
48. Phan, L.M., S.C. Yeung, and M.H. Lee, *Cancer metabolic reprogramming: importance, main features, and potentials for precise targeted anti-cancer therapies.* Cancer Biol Med, 2014. **11**(1): p. 1-19.
49. Kan, Z., et al., *Diverse somatic mutation patterns and pathway alterations in human cancers.* Nature, 2010. **466**(7308): p. 869-73.
50. Marin de Mas, I., et al., *Cancer cell metabolism as new targets for novel designed therapies.* Future Med Chem, 2014. **6**(16): p. 1791-810.
51. Vizán, P., S. Mazurek, and M. Cascante, *Robust metabolic adaptation underlying tumor progression.* Metabolomics, 2008. **4**(1): p. 1-12.
52. Rathmell, J.C., et al., *Akt-directed glucose metabolism can prevent Bax conformation change and promote growth factor-independent survival.* Mol Cell Biol, 2003. **23**(20): p. 7315-28.
53. Conrad, M. and H. Sato, *The oxidative stress-inducible cystine/glutamate antiporter, system x (c) (-) : cystine supplier and beyond.* Amino Acids, 2012. **42**(1): p. 231-46.
54. Commisso, C., et al., *Macropinocytosis of protein is an amino acid supply route in Ras-transformed cells.* Nature, 2013. **497**(7451): p. 633-637.
55. Krajcovic, M., et al., *mTOR regulates phagosome and entotic vacuole fission.* Mol Biol Cell, 2013. **24**(23): p. 3736-45.
56. Meng, M., et al., *Nitrogen anabolism underlies the importance of glutaminolysis in proliferating cells.* Cell Cycle, 2010. **9**(19): p. 3921-32.
57. Lee, J.V., et al., *Akt-dependent metabolic reprogramming regulates tumor cell histone acetylation.* Cell Metab, 2014. **20**(2): p. 306-19.
58. Roy, D.M., L.A. Walsh, and T.A. Chan, *Driver mutations of cancer epigenomes.* Protein Cell, 2014. **5**(4): p. 265-96.
59. Vander Heiden, M.G., L.C. Cantley, and C.B. Thompson, *Understanding the Warburg effect: the metabolic requirements of cell proliferation.* Science, 2009. **324**(5930): p. 1029-33.
60. Koppenol, W.H., P.L. Bounds, and C.V. Dang, *Otto Warburg's contributions to current concepts of cancer metabolism.* Nat Rev Cancer, 2011. **11**(5): p. 325-37.
61. Vander Heiden, M.G., L.C. Cantley, and C.B. Thompson, *Understanding the Warburg effect: the metabolic requirements of cell proliferation.* Science, 2009. **324**.
62. Savic, L.J., et al., *Targeting glucose metabolism in cancer: new class of agents for loco-regional and systemic therapy of liver cancer and beyond?* Hepat Oncol, 2016. **3**(1): p. 19-28.
63. Estevez-Garcia, I.O., et al., *Glucose and glutamine metabolism control by APC and SCF during the G1-to-S phase transition of the cell cycle.* J Physiol Biochem, 2014. **70**(2): p. 569-81.
64. Scholnick, P., D. Lang, and E. Racker, *Regulatory mechanisms in carbohydrate metabolism. IX. Stimulation of aerobic glycolysis by energy-linked ion transport and inhibition by dextran sulfate.* J Biol Chem, 1973. **248**(14): p. 5175.
65. Warburg, O., F. Wind, and E. Negelein, *THE METABOLISM OF TUMORS IN THE BODY.* J Gen Physiol, 1927. **8**(6): p. 519-30.
66. Tan, A.S., et al., *Mitochondrial genome acquisition restores respiratory function and tumorigenic potential of cancer cells without mitochondrial DNA.* Cell Metab, 2015. **21**(1): p. 81-94.

67. Bonnet, S., et al., *A mitochondria-K+ channel axis is suppressed in cancer and its normalization promotes apoptosis and inhibits cancer growth.* Cancer Cell, 2007. **11**(1): p. 37-51.
68. Ying, H., et al., *Oncogenic Kras maintains pancreatic tumors through regulation of anabolic glucose metabolism.* Cell, 2012. **149**(3): p. 656-70.
69. Itkonen, H.M., et al., *O-GlcNAc transferase integrates metabolic pathways to regulate the stability of c-MYC in human prostate cancer cells.* Cancer Res, 2013. **73**(16): p. 5277-87.
70. Possemato, R., et al., *Functional genomics reveal that the serine synthesis pathway is essential in breast cancer.* Nature, 2011. **476**(7360): p. 346-50.
71. Fan, J., et al., *Quantitative flux analysis reveals folate-dependent NADPH production.* Nature, 2014. **510**(7504): p. 298-302.
72. Swietach, P., R.D. Vaughan-Jones, and A.L. Harris, *Regulation of tumor pH and the role of carbonic anhydrase 9.* Cancer Metastasis Rev, 2007. **26**(2): p. 299-310.
73. Almuhaideb, A., N. Papathanasiou, and J. Bomanji, *18F-FDG PET/CT imaging in oncology.* Ann Saudi Med, 2011. **31**(1): p. 3-13.
74. Riganti, C., et al., *The pentose phosphate pathway: an antioxidant defense and a crossroad in tumor cell fate.* Free Radic Biol Med, 2012. **53**(3): p. 421-36.
75. Lunt, S.Y. and M.G. Vander Heiden, *Aerobic glycolysis: meeting the metabolic requirements of cell proliferation.* Annu Rev Cell Dev Biol, 2011. **27**: p. 441-64.
76. Patra, K.C. and N. Hay, *The pentose phosphate pathway and cancer.* Trends Biochem Sci, 2014. **39**(8): p. 347-54.
77. Vizan, P., et al., *Modulation of pentose phosphate pathway during cell cycle progression in human colon adenocarcinoma cell line HT29.* Int J Cancer, 2009. **124**(12): p. 2789-96.
78. Stincone, A., et al., *The return of metabolism: biochemistry and physiology of the pentose phosphate pathway.* Biol Rev Camb Philos Soc, 2014.
79. Wamelink, M.M., E.A. Struys, and C. Jakobs, *The biochemistry, metabolism and inherited defects of the pentose phosphate pathway: a review.* J Inherit Metab Dis, 2008. **31**(6): p. 703-17.
80. Li, D., et al., *A new G6PD knockdown tumor-cell line with reduced proliferation and increased susceptibility to oxidative stress.* Cancer Biother Radiopharm, 2009. **24**(1): p. 81-90.
81. Au, S.W., et al., *Human glucose-6-phosphate dehydrogenase: the crystal structure reveals a structural NADP(+) molecule and provides insights into enzyme deficiency.* Structure, 2000. **8**(3): p. 293-303.
82. Ham, M., et al., *Glucose-6-phosphate dehydrogenase deficiency improves insulin resistance with reduced adipose tissue inflammation in obesity.* Diabetes, 2016.
83. Hilf, R., et al., *Multiple molecular forms of glucose-6-phosphate dehydrogenase in normal, preneoplastic, and neoplastic mammary tissues of mice.* Cancer Res, 1975. **35**(8): p. 2109-16.
84. Jonas, S.K., et al., *Increased activity of 6-phosphogluconate dehydrogenase and glucose-6-phosphate dehydrogenase in purified cell suspensions and single cells from the uterine cervix in cervical intraepithelial neoplasia.* Br J Cancer, 1992. **66**(1): p. 185-91.
85. Jerby, L., et al., *Metabolic associations of reduced proliferation and oxidative stress in advanced breast cancer.* Cancer Res, 2012. **72**(22): p. 5712-20.
86. Asensio, C., et al., *Irreversible inhibition of glucose-6-phosphate dehydrogenase by the coenzyme A conjugate of ketoprofen: a key to oxidative stress induced by non-steroidal anti-inflammatory drugs?* Biochem Pharmacol, 2007. **73**(3): p. 405-16.
87. Benito, A., et al., *Role of the Pentose Phosphate Pathway in Tumour Metabolism*, in *Tumor Cell Metabolism: Pathways, Regulation and Biology*, S. Mazurek and M. Shoshan, Editors. 2015, Springer Vienna: Vienna. p. 143-163.

88. Rawat, D.K., et al., *Glucose-6-phosphate dehydrogenase and NADPH redox regulates cardiac myocyte L-type calcium channel activity and myocardial contractile function.* PLoS One, 2012. **7**(10): p. e45365.
89. Vizan, P., et al., *K-ras codon-specific mutations produce distinctive metabolic phenotypes in NIH3T3 mice [corrected] fibroblasts.* Cancer Res, 2005. **65**(13): p. 5512-5.
90. Jiang, P., et al., *p53 regulates biosynthesis through direct inactivation of glucose-6-phosphate dehydrogenase.* Nat Cell Biol, 2011. **13**(3): p. 310-6.
91. Mitsuishi, Y., et al., *Nrf2 redirects glucose and glutamine into anabolic pathways in metabolic reprogramming.* Cancer Cell, 2012. **22**(1): p. 66-79.
92. DeNicola, G.M., et al., *Oncogene-induced Nrf2 transcription promotes ROS detoxification and tumorigenesis.* Nature, 2011. **475**(7354): p. 106-9.
93. Adem, S. and M. Ciftci, *Purification and biochemical characterization of glucose 6-phosphate dehydrogenase, 6-phosphogluconate dehydrogenase and glutathione reductase from rat lung and inhibition effects of some antibiotics.* J Enzyme Inhib Med Chem, 2016: p. 1-7.
94. Hartmannsberger, D., et al., *Transketolase-like protein 1 confers resistance to serum withdrawal in vitro.* Cancer Lett, 2011. **300**(1): p. 20-9.
95. Lin, C.J., et al., *Impaired dephosphorylation renders G6PD-knockdown HepG2 cells more susceptible to H(2)O(2)-induced apoptosis.* Free Radic Biol Med, 2010. **49**(3): p. 361-73.
96. Sukhatme, V.P. and B. Chan, *Glycolytic cancer cells lacking 6-phosphogluconate dehydrogenase metabolize glucose to induce senescence.* FEBS Lett, 2012. **586**(16): p. 2389-95.
97. Chan, B., P.A. VanderLaan, and V.P. Sukhatme, *6-Phosphogluconate dehydrogenase regulates tumor cell migration in vitro by regulating receptor tyrosine kinase c-Met.* Biochem Biophys Res Commun, 2013. **439**(2): p. 247-51.
98. De Preter, G., et al., *Inhibition of the pentose phosphate pathway by dichloroacetate unravels a missing link between aerobic glycolysis and cancer cell proliferation.* Oncotarget, 2015.
99. Coy, J.F., et al., *Mutations in the transketolase-like gene TKTL1: clinical implications for neurodegenerative diseases, diabetes and cancer.* Clin Lab, 2005. **51**(5-6): p. 257-73.
100. Bentz, S., et al., *Hypoxia induces the expression of transketolase-like 1 in human colorectal cancer.* Digestion, 2013. **88**(3): p. 182-92.
101. Trachootham, D., J. Alexandre, and P. Huang, *Targeting cancer cells by ROS-mediated mechanisms: a radical therapeutic approach?* Nat Rev Drug Discov, 2009. **8**(7): p. 579-91.
102. Ramos-Montoya, A., et al., *Pentose phosphate cycle oxidative and nonoxidative balance: A new vulnerable target for overcoming drug resistance in cancer.* Int J Cancer, 2006. **119**(12): p. 2733-41.
103. Frezza, C. and E. Gottlieb, *Mitochondria in cancer: not just innocent bystanders.* Semin Cancer Biol, 2009. **19**(1): p. 4-11.
104. Wallace, D.C., *Mitochondria and cancer.* Nat Rev Cancer, 2012. **12**(10): p. 685-98.
105. Weinberg, F., et al., *Mitochondrial metabolism and ROS generation are essential for Kras-mediated tumorigenicity.* Proc Natl Acad Sci U S A, 2010. **107**(19): p. 8788-93.
106. Yan, B., L. Dong, and J. Neuzil, *Mitochondria: An intriguing target for killing tumour-initiating cells.* Mitochondrion, 2016. **26**: p. 86-93.
107. Gaude, E. and C. Frezza, *Defects in mitochondrial metabolism and cancer.* Cancer Metab, 2014. **2**: p. 10.
108. Salway, J.G., *Metabolism at a Glance*. 2nd ed. 2000: Oxford: Blackwell Science.
109. Acin-Perez, R. and J.A. Enriquez, *The function of the respiratory supercomplexes: the plasticity model.* Biochim Biophys Acta, 2014. **1837**(4): p. 444-50.
110. Hatzivassiliou, G., et al., *ATP citrate lyase inhibition can suppress tumor cell growth.* Cancer Cell, 2005. **8**(4): p. 311-21.

111. Cardaci, S. and M.R. Ciriolo, *TCA Cycle Defects and Cancer: When Metabolism Tunes Redox State.* Int J Cell Biol, 2012. **2012**: p. 161837.
112. Desideri, E., R. Vegliante, and M.R. Ciriolo, *Mitochondrial dysfunctions in cancer: genetic defects and oncogenic signaling impinging on TCA cycle activity.* Cancer Lett, 2015. **356**(2 Pt A): p. 217-23.
113. Chen, J.Q. and J. Russo, *Dysregulation of glucose transport, glycolysis, TCA cycle and glutaminolysis by oncogenes and tumor suppressors in cancer cells.* Biochim Biophys Acta, 2012. **1826**(2): p. 370-84.
114. Gottlieb, E. and I.P. Tomlinson, *Mitochondrial tumour suppressors: a genetic and biochemical update.* Nat Rev Cancer, 2005. **5**(11): p. 857-66.
115. Mullen, A.R., et al., *Reductive carboxylation supports growth in tumour cells with defective mitochondria.* Nature, 2012. **481**(7381): p. 385-8.
116. Hao, W., et al., *Oligomycin-induced bioenergetic adaptation in cancer cells with heterogeneous bioenergetic organization.* J Biol Chem, 2010. **285**(17): p. 12647-54.
117. Daye, D. and K.E. Wellen, *Metabolic reprogramming in cancer: unraveling the role of glutamine in tumorigenesis.* Semin Cell Dev Biol, 2012. **23**(4): p. 362-9.
118. DeBerardinis, R.J. and T. Cheng, *Q's next: the diverse functions of glutamine in metabolism, cell biology and cancer.* Oncogene, 2010. **29**(3): p. 313-24.
119. Obre, E. and R. Rossignol, *Emerging concepts in bioenergetics and cancer research: metabolic flexibility, coupling, symbiosis, switch, oxidative tumors, metabolic remodeling, signaling and bioenergetic therapy.* Int J Biochem Cell Biol, 2015. **59**: p. 167-81.
120. Yuneva, M.O., et al., *The metabolic profile of tumors depends on both the responsible genetic lesion and tissue type.* Cell Metab, 2012. **15**(2): p. 157-70.
121. Wise, D.R. and C.B. Thompson, *Glutamine addiction: a new therapeutic target in cancer.* Trends Biochem Sci, 2010. **35**(8): p. 427-33.
122. Eagle, H., *The growth requirements of two mammalian cell lines in tissue culture.* Trans Assoc Am Physicians, 1955. **68**: p. 78-81.
123. Kovacevic, Z., *The pathway of glutamine and glutamate oxidation in isolated mitochondria from mammalian cells.* Biochem J, 1971. **125**(3): p. 757-63.
124. Korangath, P., et al., *Targeting Glutamine Metabolism in Breast Cancer with Aminooxyacetate.* Clin Cancer Res, 2015. **21**(14): p. 3263-73.
125. DeBerardinis, R.J., et al., *Beyond aerobic glycolysis: transformed cells can engage in glutamine metabolism that exceeds the requirement for protein and nucleotide synthesis.* Proc Natl Acad Sci U S A, 2007. **104**(49): p. 19345-50.
126. Yuneva, M., et al., *Deficiency in glutamine but not glucose induces MYC-dependent apoptosis in human cells.* J Cell Biol, 2007. **178**(1): p. 93-105.
127. Gross, M.I., et al., *Antitumor activity of the glutaminase inhibitor CB-839 in triple-negative breast cancer.* Mol Cancer Ther, 2014. **13**(4): p. 890-901.
128. Metallo, C.M., et al., *Reductive glutamine metabolism by IDH1 mediates lipogenesis under hypoxia.* Nature, 2012. **481**(7381): p. 380-4.
129. Fendt, S.M., et al., *Reductive glutamine metabolism is a function of the alpha-ketoglutarate to citrate ratio in cells.* Nat Commun, 2013. **4**: p. 2236.
130. Gameiro, P.A., et al., *In vivo HIF-mediated reductive carboxylation is regulated by citrate levels and sensitizes VHL-deficient cells to glutamine deprivation.* Cell Metab, 2013. **17**(3): p. 372-85.
131. Smolkova, K., et al., *Waves of gene regulation suppress and then restore oxidative phosphorylation in cancer cells.* Int J Biochem Cell Biol, 2011. **43**(7): p. 950-68.
132. Smolkova, K., et al., *Reductive carboxylation and 2-hydroxyglutarate formation by wild-type IDH2 in breast carcinoma cells.* Int J Biochem Cell Biol, 2015. **65**: p. 125-33.

133. Tsun, Z.Y. and R. Possemato, *Amino acid management in cancer.* Semin Cell Dev Biol, 2015. **43**: p. 22-32.
134. Jain, M., et al., *Metabolite profiling identifies a key role for glycine in rapid cancer cell proliferation.* Science, 2012. **336**(6084): p. 1040-4.
135. Liu, W., et al., *Reprogramming of proline and glutamine metabolism contributes to the proliferative and metabolic responses regulated by oncogenic transcription factor c-MYC.* Proc Natl Acad Sci U S A, 2012. **109**(23): p. 8983-8.
136. Bhutia, Y.D., et al., *Amino Acid transporters in cancer and their relevance to "glutamine addiction": novel targets for the design of a new class of anticancer drugs.* Cancer Res, 2015. **75**(9): p. 1782-8.
137. Locasale, J.W., *Serine, glycine and one-carbon units: cancer metabolism in full circle.* Nat Rev Cancer, 2013. **13**(8): p. 572-83.
138. Tedeschi, P.M., et al., *Contribution of serine, folate and glycine metabolism to the ATP, NADPH and purine requirements of cancer cells.* Cell Death Dis, 2013. **4**: p. e877.
139. Tibbetts, A.S. and D.R. Appling, *Compartmentalization of Mammalian folate-mediated one-carbon metabolism.* Annu Rev Nutr, 2010. **30**: p. 57-81.
140. Nicklin, P., et al., *Bidirectional transport of amino acids regulates mTOR and autophagy.* Cell, 2009. **136**(3): p. 521-34.
141. Yuan, H.X., Y. Xiong, and K.L. Guan, *Nutrient sensing, metabolism, and cell growth control.* Mol Cell, 2013. **49**(3): p. 379-87.
142. Lamb, R.F., *Amino acid sensing mechanisms: an Achilles heel in cancer?* FEBS J, 2012. **279**(15): p. 2624-31.
143. Prasad, S.K., *Biochemistry of Lipids*. 2010: Discovery Publishing House: New Delhi, DEL, India.
144. Besnard, P., P. Passilly-Degrace, and N.A. Khan, *Taste of Fat: A Sixth Taste Modality?* Physiol Rev, 2016. **96**(1): p. 151-76.
145. Krycer, J.R., et al., *The Akt-SREBP nexus: cell signaling meets lipid metabolism.* Trends Endocrinol Metab, 2010. **21**(5): p. 268-76.
146. Santos, C.R. and A. Schulze, *Lipid metabolism in cancer.* FEBS J, 2012. **279**(15): p. 2610-23.
147. Menendez, J.A. and R. Lupu, *Fatty acid synthase and the lipogenic phenotype in cancer pathogenesis.* Nat Rev Cancer, 2007. **7**(10): p. 763-77.
148. Swinnen, J.V., K. Brusselmans, and G. Verhoeven, *Increased lipogenesis in cancer cells: new players, novel targets.* Curr Opin Clin Nutr Metab Care, 2006. **9**(4): p. 358-65.
149. Icard, P., L. Poulain, and H. Lincet, *Understanding the central role of citrate in the metabolism of cancer cells.* Biochim Biophys Acta, 2012. **1825**(1): p. 111-6.
150. Huang, C. and C. Freter, *Lipid metabolism, apoptosis and cancer therapy.* Int J Mol Sci, 2015. **16**(1): p. 924-49.
151. Lee, M.W., et al., *The involvement of reactive oxygen species (ROS) and p38 mitogen-activated protein (MAP) kinase in TRAIL/Apo2L-induced apoptosis.* FEBS Lett, 2002. **512**(1-3): p. 313-8.
152. Giannoni, E., et al., *Intracellular reactive oxygen species activate Src tyrosine kinase during cell adhesion and anchorage-dependent cell growth.* Mol Cell Biol, 2005. **25**(15): p. 6391-403.
153. Gao, P., et al., *HIF-dependent antitumorigenic effect of antioxidants in vivo.* Cancer Cell, 2007. **12**(3): p. 230-8.
154. Takahashi, A., et al., *Mitogenic signalling and the p16INK4a-Rb pathway cooperate to enforce irreversible cellular senescence.* Nat Cell Biol, 2006. **8**(11): p. 1291-7.
155. Garrido, C., et al., *Mechanisms of cytochrome c release from mitochondria.* Cell Death Differ, 2006. **13**(9): p. 1423-33.

156. Sullivan, L.B. and N.S. Chandel, *Mitochondrial reactive oxygen species and cancer.* Cancer Metab, 2014. **2**: p. 17.
157. Chen, Y., et al., *Mitochondrial Redox Signaling and Tumor Progression.* Cancers (Basel), 2016. **8**(4).
158. Schafer, Z.T., et al., *Antioxidant and oncogene rescue of metabolic defects caused by loss of matrix attachment.* Nature, 2009. **461**(7260): p. 109-13.
159. Martindale, J.L. and N.J. Holbrook, *Cellular response to oxidative stress: signaling for suicide and survival.* J Cell Physiol, 2002. **192**(1): p. 1-15.
160. Ranjan, P., et al., *Redox-dependent expression of cyclin D1 and cell proliferation by Nox1 in mouse lung epithelial cells.* Antioxid Redox Signal, 2006. **8**(9-10): p. 1447-59.
161. Gupta, R.K., et al., *Oxidative stress and antioxidants in disease and cancer: a review.* Asian Pac J Cancer Prev, 2014. **15**(11): p. 4405-9.
162. Leslie, N.R., et al., *Redox regulation of PI 3-kinase signalling via inactivation of PTEN.* EMBO J, 2003. **22**(20): p. 5501-10.
163. Gorrini, C., I.S. Harris, and T.W. Mak, *Modulation of oxidative stress as an anticancer strategy.* Nat Rev Drug Discov, 2013. **12**(12): p. 931-47.
164. Diaz-Moralli, S., et al., *Targeting cell cycle regulation in cancer therapy.* Pharmacol Ther, 2013. **138**(2): p. 255-71.
165. Bartek, J., J. Lukas, and J. Bartkova, *Perspective: defects in cell cycle control and cancer.* J Pathol, 1999. **187**(1): p. 95-9.
166. Shapiro, G.I., *Cyclin-dependent kinase pathways as targets for cancer treatment.* J Clin Oncol, 2006. **24**(11): p. 1770-83.
167. Buchakjian, M.R. and S. Kornbluth, *The engine driving the ship: metabolic steering of cell proliferation and death.* Nat Rev Mol Cell Biol, 2010. **11**(10): p. 715-27.
168. Pardee, A.B., *A restriction point for control of normal animal cell proliferation.* Proc Natl Acad Sci U S A, 1974. **71**(4): p. 1286-90.
169. Lee, I.H. and T. Finkel, *Metabolic regulation of the cell cycle.* Curr Opin Cell Biol, 2013. **25**(6): p. 724-9.
170. Bean, G.R., et al., *PUMA and BIM are required for oncogene inactivation-induced apoptosis.* Sci Signal, 2013. **6**(268): p. ra20.
171. Elmore, S., *Apoptosis: a review of programmed cell death.* Toxicol Pathol, 2007. **35**(4): p. 495-516.
172. Pommier, Y., et al., *Apoptosis defects and chemotherapy resistance: molecular interaction maps and networks.* Oncogene, 2004. **23**(16): p. 2934-49.
173. Scatena, R., *Mitochondria and cancer: a growing role in apoptosis, cancer cell metabolism and dedifferentiation.* Adv Exp Med Biol, 2012. **942**: p. 287-308.
174. Jones, N.P. and A. Schulze, *Targeting cancer metabolism--aiming at a tumour's sweet-spot.* Drug Discov Today, 2012. **17**(5-6): p. 232-41.
175. Stratton, M.R., *Exploring the genomes of cancer cells: progress and promise.* Science, 2011. **331**(6024): p. 1553-8.
176. Obacz, J., et al., *Cross-talk between HIF and p53 as mediators of molecular responses to physiological and genotoxic stresses.* Mol Cancer, 2013. **12**(1): p. 93.
177. Ajdukovic, J., *HIF-1 - a big chapter in the cancer tale.* Exp Oncol, 2016. **38**(1): p. 9-12.
178. Wise, D.R., et al., *Myc regulates a transcriptional program that stimulates mitochondrial glutaminolysis and leads to glutamine addiction.* Proc Natl Acad Sci USA, 2008. **105**.
179. Chen, B.J., et al., *Small molecules targeting c-Myc oncogene: promising anti-cancer therapeutics.* Int J Biol Sci, 2014. **10**(10): p. 1084-96.
180. Shaw, R.J. and L.C. Cantley, *Ras, PI(3)K and mTOR signalling controls tumour cell growth.* Nature, 2006. **441**(7092): p. 424-30.

181. Dan, H.C., et al., *Akt-dependent activation of mTORC1 complex involves phosphorylation of mTOR (mammalian target of rapamycin) by IkappaB kinase alpha (IKKalpha).* J Biol Chem, 2014. **289**(36): p. 25227-40.
182. Porstmann, T., et al., *SREBP activity is regulated by mTORC1 and contributes to Akt-dependent cell growth.* Cell Metab, 2008. **8**(3): p. 224-36.
183. Alvarez, M.S., et al., *Stable SREBP-1a knockdown decreases the cell proliferation rate in human preadipocyte cells without inducing senescence.* Biochem Biophys Res Commun, 2014. **447**(1): p. 51-6.
184. Wang, S.J. and W. Gu, *To be, or not to be: functional dilemma of p53 metabolic regulation.* Curr Opin Oncol, 2014. **26**(1): p. 78-85.
185. Puzio-Kuter, A.M., *The Role of p53 in Metabolic Regulation.* Genes Cancer, 2011. **2**(4): p. 385-91.
186. Sinthupibulyakit, C., et al., *p53 Protects lung cancer cells against metabolic stress.* Int J Oncol, 2010. **37**(6): p. 1575-81.
187. Hu, W., et al., *Glutaminase 2, a novel p53 target gene regulating energy metabolism and antioxidant function.* Proc Natl Acad Sci USA, 2010. **107**.
188. Zhang, X.D., Z.H. Qin, and J. Wang, *The role of p53 in cell metabolism.* Acta Pharmacol Sin, 2010. **31**(9): p. 1208-12.
189. Massari, F., et al., *Metabolic phenotype of bladder cancer.* Cancer Treat Rev, 2016. **45**: p. 46-57.
190. Xiao, M., et al., *Inhibition of alpha-KG-dependent histone and DNA demethylases by fumarate and succinate that are accumulated in mutations of FH and SDH tumor suppressors.* Genes Dev, 2012. **26**(12): p. 1326-38.
191. Frezza, C., et al., *Haem oxygenase is synthetically lethal with the tumour suppressor fumarate hydratase.* Nature, 2011. **477**(7363): p. 225-8.
192. Hsu, C.C., L.M. Tseng, and H.C. Lee, *Role of mitochondrial dysfunction in cancer progression.* Exp Biol Med (Maywood), 2016.
193. Zong, W.-X., Joshua D. Rabinowitz, and E. White, *Mitochondria and Cancer.* Molecular Cell, 2016. **61**(5): p. 667-676.
194. Butler, E.B., et al., *Stalling the engine of resistance: targeting cancer metabolism to overcome therapeutic resistance.* Cancer Res, 2013. **73**(9): p. 2709-17.
195. Chan, A.K., J. Bruce, and A.K. Siriwardena, *Glucose metabolic phenotype of pancreatic cancer.* World J Gastroenterol, 2016. **22**(12): p. 3471-85.
196. Heidelberger, C., et al., *Fluorinated pyrimidines, a new class of tumour-inhibitory compounds.* Nature, 1957. **179**(4561): p. 663-6.
197. Crane, R.K. and A. Sols, *The non-competitive inhibition of brain hexokinase by glucose-6-phosphate and related compounds.* J Biol Chem, 1954. **210**(2): p. 597-606.
198. Dwarakanath, B.S., et al., *Clinical studies for improving radiotherapy with 2-deoxy-D-glucose: present status and future prospects.* J Cancer Res Ther, 2009. **5 Suppl 1**: p. S21-6.
199. Kankotia, S. and P.W. Stacpoole, *Dichloroacetate and cancer: new home for an orphan drug?* Biochim Biophys Acta, 2014. **1846**(2): p. 617-29.
200. Ganapathy-Kanniappan, S., et al., *Glyceraldehyde-3-phosphate dehydrogenase (GAPDH) is pyruvylated during 3-bromopyruvate mediated cancer cell death.* Anticancer Res, 2009. **29**(12): p. 4909-18.
201. Zhao, Y., E.B. Butler, and M. Tan, *Targeting cellular metabolism to improve cancer therapeutics.* Cell Death Dis, 2013. **4**: p. e532.
202. Pereira da Silva, A.P., et al., *Inhibition of energy-producing pathways of HepG2 cells by 3-bromopyruvate.* Biochem J, 2009. **417**(3): p. 717-26.
203. Telang, S., et al., *Ras transformation requires metabolic control by 6-phosphofructo-2-kinase.* Oncogene, 2006. **25**(55): p. 7225-34.

204. Yalcin, A., et al., *Regulation of glucose metabolism by 6-phosphofructo-2-kinase/fructose-2,6-bisphosphatases in cancer.* Exp Mol Pathol, 2009. **86**(3): p. 174-9.
205. Clem, B., et al., *Small-molecule inhibition of 6-phosphofructo-2-kinase activity suppresses glycolytic flux and tumor growth.* Mol Cancer Ther, 2008. **7**(1): p. 110-20.
206. Hitosugi, T., et al., *Tyrosine phosphorylation inhibits PKM2 to promote the Warburg effect and tumor growth.* Sci Signal, 2009. **2**(97): p. ra73.
207. Stefano, G.D., et al., *Lactate dehydrogenase inhibition: exploring possible applications beyond cancer treatment.* Future Med Chem, 2016.
208. Vander Heiden, M.G., *Targeting cancer metabolism: a therapeutic window opens.* Nat Rev Drug Discov, 2011. **10**(9): p. 671-84.
209. Frank, J.E., *Diagnosis and management of G6PD deficiency.* Am Fam Physician, 2005. **72**(7): p. 1277-82.
210. Fico, A., et al., *Glucose-6-phosphate dehydrogenase plays a crucial role in protection from redox-stress-induced apoptosis.* Cell Death Differ, 2004. **11**(8): p. 823-31.
211. Ho, H.Y., et al., *Enhanced oxidative stress and accelerated cellular senescence in glucose-6-phosphate dehydrogenase (G6PD)-deficient human fibroblasts.* Free Radic Biol Med, 2000. **29**(2): p. 156-69.
212. Lin, R., et al., *6-Phosphogluconate dehydrogenase links oxidative PPP, lipogenesis and tumour growth by inhibiting LKB1-AMPK signalling.* Nat Cell Biol, 2015. **17**(11): p. 1484-96.
213. Boros, L.G., et al., *Oxythiamine and dehydroepiandrosterone inhibit the nonoxidative synthesis of ribose and tumor cell proliferation.* Cancer Res, 1997. **57**(19): p. 4242-8.
214. Rais, B., et al., *Oxythiamine and dehydroepiandrosterone induce a G1 phase cycle arrest in Ehrlich's tumor cells through inhibition of the pentose cycle.* FEBS Lett, 1999. **456**(1): p. 113-8.
215. Wang, J.B., et al., *Targeting mitochondrial glutaminase activity inhibits oncogenic transformation.* Cancer Cell, 2010. **18**(3): p. 207-19.
216. Xiang, Y., et al., *Targeted inhibition of tumor-specific glutaminase diminishes cell-autonomous tumorigenesis.* J Clin Invest, 2015. **125**(6): p. 2293-306.
217. Jacque, N., et al., *Targeting glutaminolysis has antileukemic activity in acute myeloid leukemia and synergizes with BCL-2 inhibition.* Blood, 2015. **126**(11): p. 1346-56.
218. Deepa, P.R., et al., *Therapeutic and toxicologic evaluation of anti-lipogenic agents in cancer cells compared with non-neoplastic cells.* Basic Clin Pharmacol Toxicol, 2012. **110**(6): p. 494-503.
219. Zaidi, N., J.V. Swinnen, and K. Smans, *ATP-citrate lyase: a key player in cancer metabolism.* Cancer Res, 2012. **72**(15): p. 3709-14.
220. Van Den Neste, E., G. Van den Berghe, and F. Bontemps, *AICA-riboside (acadesine), an activator of AMP-activated protein kinase with potential for application in hematologic malignancies.* Expert Opin Investig Drugs, 2010. **19**(4): p. 571-8.
221. Xiang, X., et al., *AMP-activated protein kinase activators can inhibit the growth of prostate cancer cells by multiple mechanisms.* Biochemical and Biophysical Research Communications, 2004. **321**(1): p. 161-167.
222. Longo, P.G., et al., *The Akt/Mcl-1 pathway plays a prominent role in mediating antiapoptotic signals downstream of the B-cell receptor in chronic lymphocytic leukemia B cells.* Blood, 2008. **111**(2): p. 846-55.
223. Hoellenriegel, J., et al., *The phosphoinositide 3'-kinase delta inhibitor, CAL-101, inhibits B-cell receptor signaling and chemokine networks in chronic lymphocytic leukemia.* Blood, 2011. **118**(13): p. 3603-12.
224. Samatar, A.A. and P.I. Poulikakos, *Targeting RAS-ERK signalling in cancer: promises and challenges.* Nat Rev Drug Discov, 2014. **13**(12): p. 928-42.

225. Badimon, L., G. Vilahur, and T. Padro, *Systems biology approaches to understand the effects of nutrition and promote health.* Br J Clin Pharmacol, 2016.
226. Pavlou, M.P., A. Dimitromanolakis, and E.P. Diamandis, *Coupling proteomics and transcriptomics in the quest of subtype-specific proteins in breast cancer.* Proteomics, 2013. **13**(7): p. 1083-95.
227. Habermann, J.K., et al., *Genomic instability influences the transcriptome and proteome in endometrial cancer subtypes.* Mol Cancer, 2011. **10**: p. 132.
228. Claudino, W.M., et al., *Metabolomics: available results, current research projects in breast cancer, and future applications.* J Clin Oncol, 2007. **25**(19): p. 2840-6.
229. Turan, N., et al., *A systems biology approach identifies molecular networks defining skeletal muscle abnormalities in chronic obstructive pulmonary disease.* PLoS Comput Biol, 2011. **7**(9): p. e1002129.
230. Cascante, M. and S. Marin, *Metabolomics and fluxomics approaches.* Essays Biochem, 2008. **45**: p. 67-81.
231. Griffin, J.L. and J.P. Shockcor, *Metabolic profiles of cancer cells.* Nat Rev Cancer, 2004. **4**(7): p. 551-61.
232. Urbanczyk-Wochniak, E., et al., *Parallel analysis of transcript and metabolic profiles: a new approach in systems biology.* EMBO Rep, 2003. **4**(10): p. 989-93.
233. Kell, D.B., et al., *Metabolic footprinting and systems biology: the medium is the message.* Nat Rev Microbiol, 2005. **3**(7): p. 557-65.
234. Booth, S.C., A.M. Weljie, and R.J. Turner, *Computational tools for the secondary analysis of metabolomics experiments.* Comput Struct Biotechnol J, 2013. **4**: p. e201301003.
235. Nagrath, D., et al., *Metabolomics for mitochondrial and cancer studies.* Biochim Biophys Acta, 2011. **1807**(6): p. 650-63.
236. Gao, D., et al., *Metabolomics study on the antitumor effect of marine natural compound flexibilide in HCT-116 colon cancer cell line.* J Chromatogr B Analyt Technol Biomed Life Sci, 2016. **1014**: p. 17-23.
237. Zhang, T., et al., *Current Trends and Innovations in Bio-Analytical Techniques of Metabolomics.* Crit Rev Anal Chem, 2015: p. 0.
238. Vernocchi, P., et al., *Integration of datasets from different analytical techniques to assess the impact of nutrition on human metabolome.* Front Cell Infect Microbiol, 2012. **2**: p. 156.
239. Wishart, D.S., et al., *HMDB: the human metabolome database.* Nucleic Acids Res, 2007. **35**.
240. Wishart, D.S., et al., *HMDB 3.0--The Human Metabolome Database in 2013.* Nucleic Acids Res, 2013. **41**(Database issue): p. D801-7.
241. Cortassa, S., et al., *From metabolomics to fluxomics: a computational procedure to translate metabolite profiles into metabolic fluxes.* Biophys J, 2015. **108**(1): p. 163-72.
242. Winter, G. and J.O. Kromer, *Fluxomics - connecting 'omics analysis and phenotypes.* Environ Microbiol, 2013. **15**(7): p. 1901-16.
243. Antoniewicz, M.R., *Methods and advances in metabolic flux analysis: a mini-review.* J Ind Microbiol Biotechnol, 2015. **42**(3): p. 317-25.
244. Sauer, U., *Metabolic networks in motion: 13C-based flux analysis.* Molecular systems biology, 2006. **2**(1).
245. Hasenour, C.M., et al., *Mass spectrometry-based microassay of 2H and 13C plasma glucose labeling to quantify liver metabolic fluxes in vivo.* American Journal of Physiology-Endocrinology and Metabolism, 2015. **309**(2): p. E191-E203.
246. António, C., et al., *Regulation of primary metabolism in response to low oxygen availability as revealed by carbon and nitrogen isotope redistribution.* Plant physiology, 2015: p. pp. 00266.2015.

247. Niedenfuhr, S., W. Wiechert, and K. Noh, *How to measure metabolic fluxes: a taxonomic guide for C fluxomics.* Curr Opin Biotechnol, 2015. **34C**: p. 82-90.
248. Paul Lee, W.N., et al., *Tracer-based metabolomics: concepts and practices.* Clin Biochem, 2010. **43**(16-17): p. 1269-77.
249. Jung, J.Y. and M.K. Oh, *Isotope labeling pattern study of central carbon metabolites using GC/MS.* J Chromatogr B Analyt Technol Biomed Life Sci, 2015. **974**: p. 101-8.
250. Fan, T.W. and A.N. Lane, *Applications of NMR spectroscopy to systems biochemistry.* Prog Nucl Magn Reson Spectrosc, 2016. **92-93**: p. 18-53.
251. Walther, J.L., et al., *Optimization of 13C isotopic tracers for metabolic flux analysis in mammalian cells.* Metab Eng, 2012. **14**(2): p. 162-71.
252. Metallo, C.M., J.L. Walther, and G. Stephanopoulos, *Evaluation of 13C isotopic tracers for metabolic flux analysis in mammalian cells.* J Biotechnol, 2009. **144**(3): p. 167-74.
253. Antoniewicz, M.R., *13C metabolic flux analysis: optimal design of isotopic labeling experiments.* Curr Opin Biotechnol, 2013. **24**(6): p. 1116-21.
254. Crown, S.B., W.S. Ahn, and M.R. Antoniewicz, *Rational design of (1)(3)C-labeling experiments for metabolic flux analysis in mammalian cells.* BMC Syst Biol, 2012. **6**: p. 43.
255. Marin, S., et al., *Metabolic strategy of boar spermatozoa revealed by a metabolomic characterization.* FEBS Lett, 2003. **554**(3): p. 342-6.
256. Munger, J., et al., *Systems-level metabolic flux profiling identifies fatty acid synthesis as a target for antiviral therapy.* Nat Biotechnol, 2008. **26**(10): p. 1179-86.
257. Mullen, A.R., et al., *Oxidation of alpha-ketoglutarate is required for reductive carboxylation in cancer cells with mitochondrial defects.* Cell Rep, 2014. **7**(5): p. 1679-90.
258. Nargund, S. and G. Sriram, *Designer labels for plant metabolism: statistical design of isotope labeling experiments for improved quantification of flux in complex plant metabolic networks.* Mol Biosyst, 2013. **9**(1): p. 99-112.
259. Au, J., et al., *Parallel labeling experiments validate Clostridium acetobutylicum metabolic network model for C metabolic flux analysis.* Metab Eng, 2014. **26C**: p. 23-33.
260. Leighty, R.W. and M.R. Antoniewicz, *Parallel labeling experiments with [U-13C]glucose validate E. coli metabolic network model for 13C metabolic flux analysis.* Metab Eng, 2012. **14**(5): p. 533-41.
261. Ahn, W.S. and M.R. Antoniewicz, *Parallel labeling experiments with [1,2-(13)C]glucose and [U-(13)C]glutamine provide new insights into CHO cell metabolism.* Metab Eng, 2013. **15**: p. 34-47.
262. Crown, S.B. and M.R. Antoniewicz, *Parallel labeling experiments and metabolic flux analysis: Past, present and future methodologies.* Metab Eng, 2013. **16**: p. 21-32.
263. Zamboni, N., *13C metabolic flux analysis in complex systems.* Curr Opin Biotechnol, 2011. **22**(1): p. 103-8.
264. Buescher, J.M., et al., *A roadmap for interpreting (13)C metabolite labeling patterns from cells.* Curr Opin Biotechnol, 2015. **34**: p. 189-201.
265. Alcarraz-Vizan, G., et al., *Validation of NCM460 cell model as control in antitumor strategies targeting colon adenocarcinoma metabolic reprogramming: trichostatin A as a case study.* Biochim Biophys Acta, 2014. **1840**(6): p. 1634-9.
266. Marin, S., et al., *Dynamic profiling of the glucose metabolic network in fasted rat hepatocytes using [1,2-13C2]glucose.* Biochem J, 2004. **381**(Pt 1): p. 287-94.
267. Masoudi-Nejad, A., et al., *Cancer systems biology and modeling: microscopic scale and multiscale approaches.* Semin Cancer Biol, 2015. **30**: p. 60-9.
268. Borodina, I. and J. Nielsen, *From genomes to in silico cells via metabolic networks.* Curr Opin Biotechnol, 2005. **16**(3): p. 350-5.
269. Selivanov, V.A., et al., *Software for dynamic analysis of tracer-based metabolomic data: estimation of metabolic fluxes and their statistical analysis.* Bioinformatics, 2006. **22**(22): p. 2806-12.

270. Selivanov, V.A., et al., *An optimized algorithm for flux estimation from isotopomer distribution in glucose metabolites.* Bioinformatics, 2004. **20**(18): p. 3387-97.
271. Selivanov, V.A., et al., *Rapid simulation and analysis of isotopomer distributions using constraints based on enzyme mechanisms: an example from HT29 cancer cells.* Bioinformatics, 2005. **21**(17): p. 3558-64.
272. de Mas, I.M., et al., *Compartmentation of glycogen metabolism revealed from 13C isotopologue distributions.* BMC Syst Biol, 2011. **5**: p. 175.
273. Mosmann, T., *Rapid colorimetric assay for cellular growth and survival: application to proliferation and cytotoxicity assays.* J Immunol Methods, 1983. **65**(1-2): p. 55-63.
274. Hammill, A.K., J.W. Uhr, and R.H. Scheuermann, *Annexin V staining due to loss of membrane asymmetry can be reversible and precede commitment to apoptotic death.* Exp Cell Res, 1999. **251**(1): p. 16-21.
275. Kunst, A., B. Draeger, and J. Ziegenhorn, *UV methods with hexokinase and glucose-6-phosphate dehydrogenase.*, in *Methods of enzymatic analysis*, H.U. Bergmeyer., Editor. 1984, Verlag Chemie: Weinheim, Germany. p. 163-172.
276. J.V. Passonneau, O.H.L., *Enzymatic Analysis: A Practical Guide*. 1993, Totowa, New Jersey, USA: The Humana Press Inc.
277. Lund., P., *L-glutamine and L-glutamate; UV-method with glutaminase and glutamate dehydrogenase.*, in *methods of enzymatic analysis.* 1985, Verlag Chemie.: Weinheim, Germany.
278. Irizarry, R.A., et al., *Summaries of Affymetrix GeneChip probe level data.* Nucleic Acids Res, 2003. **31**(4): p. e15.
279. Wilson, C.L. and C.J. Miller, *Simpleaffy: a BioConductor package for Affymetrix Quality Control and data analysis.* Bioinformatics, 2005. **21**(18): p. 3683-5.
280. Smyth, G.K., *Linear models and empirical bayes methods for assessing differential expression in microarray experiments.* Stat Appl Genet Mol Biol, 2004. **3**: p. Article3.
281. Benjamini, Y., et al., *Controlling the false discovery rate in behavior genetics research.* Behav Brain Res, 2001. **125**(1-2): p. 279-84.
282. Vizan, P., et al., *Characterization of the metabolic changes underlying growth factor angiogenic activation: identification of new potential therapeutic targets.* Carcinogenesis, 2009. **30**(6): p. 946-52.
283. Lee, W.N., et al., *Mass isotopomer study of the nonoxidative pathways of the pentose cycle with [1,2-13C2]glucose.* Am J Physiol, 1998. **274**(5 Pt 1): p. E843-51.
284. Lee, W.N., et al., *Mass isotopomer analysis: theoretical and practical considerations.* Biol Mass Spectrom, 1991. **20**(8): p. 451-8.
285. Selivanov, V.A., et al., *Edelfosine-induced metabolic changes in cancer cells that precede the overproduction of reactive oxygen species and apoptosis.* BMC Syst Biol, 2010. **4**: p. 135.
286. Sanchez-Tena, S., et al., *Epicatechin gallate impairs colon cancer cell metabolic productivity.* J Agric Food Chem, 2013. **61**(18): p. 4310-7.
287. Boren, J., et al., *The stable isotope-based dynamic metabolic profile of butyrate-induced HT29 cell differentiation.* J Biol Chem, 2003. **278**(31): p. 28395-402.
288. Lee, W.N., et al., *Isotopomer study of lipogenesis in human hepatoma cells in culture: contribution of carbon and hydrogen atoms from glucose.* Anal Biochem, 1995. **226**(1): p. 100-12.
289. Jiang, L., et al., *Reductive carboxylation supports redox homeostasis during anchorage-independent growth.* Nature, 2016. **532**(7598): p. 255-8.
290. Jang, M., S.S. Kim, and J. Lee, *Cancer cell metabolism: implications for therapeutic targets.* Exp Mol Med, 2013. **45**: p. e45.
291. Lamonte, G., et al., *Acidosis induces reprogramming of cellular metabolism to mitigate oxidative stress.* Cancer Metab, 2013. **1**(1): p. 23.

292. Stanton, R.C., *Glucose-6-phosphate dehydrogenase, NADPH, and cell survival.* IUBMB Life, 2012. **64**(5): p. 362-9.
293. Amir-Ahmady, B. and L.M. Salati, *Regulation of the processing of glucose-6-phosphate dehydrogenase mRNA by nutritional status.* J Biol Chem, 2001. **276**(13): p. 10514-23.
294. Shan, C., et al., *Lysine acetylation activates 6-phosphogluconate dehydrogenase to promote tumor growth.* Mol Cell, 2014. **55**(4): p. 552-65.
295. Sommercorn, J. and R.A. Freedland, *Regulation of hepatic phosphofructokinase by 6-phosphogluconate.* J Biol Chem, 1982. **257**(16): p. 9424-8.
296. Smith, S.B. and R.A. Freedland, *Activation of pyruvate kinase by 6-phosphogluconate.* J Biol Chem, 1979. **254**(21): p. 10644-8.
297. Popova, T.N., L.V. Matasova, and A.A. Lapot'ko, *Purification and some catalytic properties of phosphoglucomutase from maize leaves.* Biochemistry (Mosc), 1998. **63**(6): p. 697-701.
298. Meadows, A.L., et al., *Metabolic and morphological differences between rapidly proliferating cancerous and normal breast epithelial cells.* Biotechnol Prog, 2008. **24**(2): p. 334-41.
299. Pucci, B., M. Kasten, and A. Giordano, *Cell cycle and apoptosis.* Neoplasia, 2000. **2**(4): p. 291-9.
300. Bratton, D.L., et al., *The mechanism of internalization of platelet-activating factor in activated human neutrophils. Enhanced transbilayer movement across the plasma membrane.* J Immunol, 1992. **148**(2): p. 514-23.
301. Vojtesek, B. and D.P. Lane, *Regulation of p53 protein expression in human breast cancer cell lines.* J Cell Sci, 1993. **105 (Pt 3)**: p. 607-12.
302. Schafer, J.M., et al., *Rapid development of tamoxifen-stimulated mutant p53 breast tumors (T47D) in athymic mice.* Clin Cancer Res, 2000. **6**(11): p. 4373-80.
303. Zancan., P., et al., *Differential expression of phosphofructokinase-1 isoforms correlates with the glycolytic efficiency of breast cancer cells.* Molecular Genetics and Metabolism, 2010. **100 (2010)** p. 372-378.
304. Hensley, C.T., A.T. Wasti, and R.J. DeBerardinis, *Glutamine and cancer: cell biology, physiology, and clinical opportunities.* J Clin Invest, 2013. **123**(9): p. 3678-84.
305. Kung, H.N., J.R. Marks, and J.T. Chi, *Glutamine synthetase is a genetic determinant of cell type-specific glutamine independence in breast epithelia.* PLoS Genet, 2011. **7**(8): p. e1002229.
306. Kondo, T., *Stem cell-like cancer cells in cancer cell lines.* Cancer Biomark, 2007. **3**(4-5): p. 245-50.
307. Hong, S.M., et al., *NAMPT suppresses glucose deprivation-induced oxidative stress by increasing NADPH levels in breast cancer.* Oncogene, 2015.
308. Blanquer-Rossello Mdel, M., et al., *Leptin regulates energy metabolism in MCF-7 breast cancer cells.* Int J Biochem Cell Biol, 2016. **72**: p. 18-26.
309. Aka, J.A. and S.X. Lin, *Comparison of functional proteomic analyses of human breast cancer cell lines T47D and MCF7.* PLoS One, 2012. **7**(2): p. e31532.
310. Mooney, L.M., et al., *Apoptotic mechanisms in T47D and MCF-7 human breast cancer cells.* Br J Cancer, 2002. **87**(8): p. 909-17.
311. Filosa, S., et al., *Failure to increase glucose consumption through the pentose-phosphate pathway results in the death of glucose-6-phosphate dehydrogenase gene-deleted mouse embryonic stem cells subjected to oxidative stress.* Biochem J, 2003. **370**(Pt 3): p. 935-43.
312. Pandolfi, P.P., et al., *Targeted disruption of the housekeeping gene encoding glucose 6-phosphate dehydrogenase (G6PD): G6PD is dispensable for pentose synthesis but essential for defense against oxidative stress.* EMBO J, 1995. **14**(21): p. 5209-15.

313. Muller, F.L., E.A. Aquilanti, and R.A. DePinho, *Collateral Lethality: A new therapeutic strategy in oncology.* Trends Cancer, 2015. **1**(3): p. 161-173.
314. Galluzzi, L., et al., *Metabolic targets for cancer therapy.* Nat Rev Drug Discov, 2013. **12**(11): p. 829-46.
315. Vikas P. Sukhatme, C.B.C., *Patent: Methods and compositions for 6-phosphogluconate dehydrogenase (6-pgd) as a target for lung cancer therapy.*, W. A8, Editor. 2014.
316. Chen, R. and M. Snyder, *Systems biology: personalized medicine for the future?* Curr Opin Pharmacol, 2012. **12**(5): p. 623-8.
317. Cascante, M., et al., *Metabolic network adaptations in cancer as targets for novel therapies.* Biochem Soc Trans, 2010. **38**(5): p. 1302-6.
318. Wolkenhauer, O., et al., *Systems biologists seek fuller integration of systems biology approaches in new cancer research programs.* Cancer Res, 2010. **70**(1): p. 12-3.
319. Yizhak, K., et al., *Model-based identification of drug targets that revert disrupted metabolism and its application to ageing.* Nat Commun, 2013. **4**: p. 2632.
320. Pelicano, H., et al., *Mitochondrial dysfunction in some triple-negative breast cancer cell lines: role of mTOR pathway and therapeutic potential.* Breast Cancer Res, 2014. **16**(5): p. 434.
321. Sotgia, F., et al., *Mitochondria "fuel" breast cancer metabolism: fifteen markers of mitochondrial biogenesis label epithelial cancer cells, but are excluded from adjacent stromal cells.* Cell Cycle, 2012. **11**(23): p. 4390-401.
322. Jones, J.G., *Hepatic glucose and lipid metabolism.* Diabetologia, 2016. **59**(6): p. 1098-103.
323. De Vitto, H., J. Perez-Valencia, and J.A. Radosevich, *Glutamine at focus: versatile roles in cancer.* Tumour Biol, 2016. **37**(2): p. 1541-58.
324. Deberardinis, R.J., et al., *The biology of cancer: metabolic reprogramming fuels cell growth and proliferation.* Cell Metab, 2008. **7**.
325. Zhang, W., F. Li, and L. Nie, *Integrating multiple 'omics' analysis for microbial biology: application and methodologies.* Microbiology, 2010. **156**(Pt 2): p. 287-301.
326. Durot, M., P.Y. Bourguignon, and V. Schachter, *Genome-scale models of bacterial metabolism: reconstruction and applications.* FEMS Microbiol Rev, 2009. **33**(1): p. 164-90.
327. Vinay-Lara, E., et al., *Genome-scale reconstruction of metabolic networks of Lactobacillus casei ATCC 334 and 12A.* PLoS One, 2014. **9**(11): p. e110785.
328. Fondi, M., et al., *Genome-scale metabolic reconstruction and constraint-based modelling of the Antarctic bacterium Pseudoalteromonas haloplanktis TAC125.* Environ Microbiol, 2015. **17**(3): p. 751-66.
329. Wu, X., X. Wang, and W. Lu, *Genome-scale reconstruction of a metabolic network for Gluconobacter oxydans 621H.* Biosystems, 2014. **117**: p. 10-4.
330. Smith, H., et al., *The Effects of Severe Hypoxia on Glycolytic Flux and Enzyme Activity in a Model of Solid Tumors.* J Cell Biochem, 2016. **117**(8): p. 1890-901.
331. Angelova, P.R. and A.Y. Abramov, *Functional Role of Mitochondrial Reactive Oxygen Species in Physiology.* Free Radic Biol Med, 2016.
332. Cheng, C.P., et al., *The mechanisms of malic enzyme 2 in the tumorigenesis of human gliomas.* Oncotarget, 2016.
333. Ogawara, Y., et al., *IDH2 and NPM1 Mutations Cooperate to Activate Hoxa9/Meis1 and Hypoxia Pathways in Acute Myeloid Leukemia.* Cancer Res, 2015. **75**(10): p. 2005-16.
334. van Winden, W., P. Verheijen, and S. Heijnen, *Possible pitfalls of flux calculations based on (13)C-labeling.* Metab Eng, 2001. **3**(2): p. 151-62.
335. Semenza, G.L., *Molecular mechanisms mediating metastasis of hypoxic breast cancer cells.* Trends Mol Med, 2012. **18**(9): p. 534-43.
336. Jiang, P., W. Du, and M. Wu, *Regulation of the pentose phosphate pathway in cancer.* Protein Cell, 2014. **5**(8): p. 592-602.

337. Di Monaco, M., et al., *Role of glucose-6-phosphate dehydrogenase inhibition in the antiproliferative effects of dehydroepiandrosterone on human breast cancer cells.* Br J Cancer, 1997. **75**(4): p. 589-92.
338. Tian, W.N., et al., *Importance of glucose-6-phosphate dehydrogenase activity for cell growth.* J Biol Chem, 1998. **273**(17): p. 10609-17.
339. Joshi, S., et al., *Hypoxia-induced oxidative stress promotes MUC4 degradation via autophagy to enhance pancreatic cancer cells survival.* Oncogene, 2016.
340. Chettimada, S., et al., *Hypoxia-induced glucose-6-phosphate dehydrogenase overexpression and -activation in pulmonary artery smooth muscle cells: implication in pulmonary hypertension.* Am J Physiol Lung Cell Mol Physiol, 2015. **308**(3): p. L287-300.
341. Huang, F., et al., *Expression of glutaminase is upregulated in colorectal cancer and of clinical significance.* Int J Clin Exp Pathol, 2014. **7**(3): p. 1093-100.
342. Chen, L. and H. Cui, *Targeting Glutamine Induces Apoptosis: A Cancer Therapy Approach.* Int J Mol Sci, 2015. **16**(9): p. 22830-55.
343. Cai, T., et al., *Glucose-6-phosphate dehydrogenase and NADPH oxidase 4 control STAT3 activity in melanoma cells through a pathway involving reactive oxygen species, c-SRC and SHP2.* Am J Cancer Res, 2015. **5**(5): p. 1610-20.
344. Nicolay, B.N., et al., *Loss of RBF1 changes glutamine catabolism.* Genes Dev, 2013. **27**(2): p. 182-96.
345. Gold, R., et al., *Placebo-controlled phase 3 study of oral BG-12 for relapsing multiple sclerosis.* N Engl J Med, 2012. **367**(12): p. 1098-107.
346. Ikediobi, O.N., et al., *Mutation analysis of 24 known cancer genes in the NCI-60 cell line set.* Mol Cancer Ther, 2006. **5**(11): p. 2606-12.
347. Mitsuishi, Y., H. Motohashi, and M. Yamamoto, *The Keap1-Nrf2 system in cancers: stress response and anabolic metabolism.* Front Oncol, 2012. **2**: p. 200.
348. Zhang, C., et al., *Glucose-6-phosphate dehydrogenase: a biomarker and potential therapeutic target for cancer.* Anticancer Agents Med Chem, 2014. **14**(2): p. 280-9.
349. Fang, Z., et al., *A comprehensive analysis of membrane and morphology of erythrocytes from patients with glucose-6-phosphate dehydrogenase deficiency.* J Struct Biol, 2016. **194**(3): p. 235-43.
350. Nobrega-Pereira, S., et al., *G6PD protects from oxidative damage and improves healthspan in mice.* Nat Commun, 2016. **7**: p. 10894.
351. Fang, Z., et al., *Effects of G6PD activity inhibition on the viability, ROS generation and mechanical properties of cervical cancer cells.* Biochim Biophys Acta, 2016. **1863**(9): p. 2245-2254.
352. Sauer, L.A., J.W. Stayman, 3rd, and R.T. Dauchy, *Amino acid, glucose, and lactic acid utilization in vivo by rat tumors.* Cancer Res, 1982. **42**(10): p. 4090-7.
353. Eggleston, L.V. and H.A. Krebs, *Regulation of the pentose phosphate cycle.* Biochem J, 1974. **138**(3): p. 425-35.
354. Preuss, J., et al., *Identification and characterization of novel human glucose-6-phosphate dehydrogenase inhibitors.* J Biomol Screen, 2013. **18**(3): p. 286-97.
355. Sahin, A., et al., *Investigation of inhibition of human glucose 6-phosphate dehydrogenase by some 99mTc chelators by in silico and in vitro methods.* J Enzyme Inhib Med Chem, 2016: p. 1-7.
356. Chettimada, S., et al., *Glucose-6-phosphate dehydrogenase plays a critical role in hypoxia-induced CD133+ progenitor cells self-renewal and stimulates their accumulation in the lungs of pulmonary hypertensive rats.* Am J Physiol Lung Cell Mol Physiol, 2014. **307**(7): p. L545-56.
357. Zhang, Z., et al., *High glucose inhibits glucose-6-phosphate dehydrogenase via cAMP in aortic endothelial cells.* J Biol Chem, 2000. **275**(51): p. 40042-7.

358. Li, Z., et al., *GRP78 enhances the glutamine metabolism to support cell survival from glucose deficiency by modulating the beta-catenin signaling.* Oncotarget, 2014. **5**(14): p. 5369-80.
359. Saqcena, M., et al., *Amino acids and mTOR mediate distinct metabolic checkpoints in mammalian G1 cell cycle.* PLoS One, 2013. **8**(8): p. e74157.
360. Zhang, J., et al., *Asparagine plays a critical role in regulating cellular adaptation to glutamine depletion.* Mol Cell, 2014. **56**(2): p. 205-18.
361. Kovac, S., et al., *Nrf2 regulates ROS production by mitochondria and NADPH oxidase.* Biochim Biophys Acta, 2015. **1850**(4): p. 794-801.
362. Son, J., et al., *Glutamine supports pancreatic cancer growth through a KRAS-regulated metabolic pathway.* Nature, 2013. **496**(7443): p. 101-5.
363. Qiu, B. and M.C. Simon, *Oncogenes strike a balance between cellular growth and homeostasis.* Semin Cell Dev Biol, 2015. **43**: p. 3-10.
364. Jerby, L. and E. Ruppin, *Predicting drug targets and biomarkers of cancer via genome-scale metabolic modeling.* Clin Cancer Res, 2012. **18**(20): p. 5572-84.
365. He, X., et al., *Functional repair of p53 mutation in colorectal cancer cells using trans-splicing.* Oncotarget, 2015. **6**(4): p. 2034-45.
366. Dorff, T.B., et al., *Safety and feasibility of fasting in combination with platinum-based chemotherapy.* BMC Cancer, 2016. **16**: p. 360.

APPENDIX I

Appendix I-A: Gene Expression Profile of MCF7 Cells with Oligomycin Supplementation

Transcript Cluster ID	Fold Change	Gene Symbol	Description
16725041	-4.45	FAM111B	family with sequence similarity 111, member B
16841575	-4.19		
16877451	-3.82		
16651801	-3.75		
16651535	-3.69		
16771534	-3.62		
16999070	-3.52		
16716507	-3.5	PPP1R3C	protein phosphatase 1, regulatory subunit 3C
16841561	-3.16	PMP22	peripheral myelin protein 22
16988902	-3.1	KIAA1024L	KIAA1024-like
17078981	-3.07		
16650469	-3.02		
17121916	-2.95		
17078870	-2.93	MMP16	matrix metallopeptidase 16 (membrane-inserted)
16983456	-2.9		
17043152	-2.89		
16955822	-2.87	ADAMTS9	ADAM metallopeptidase with thrombospondin type 1 motif, 9
17064848	-2.86		
16721675	-2.85		
17119208	-2.78		
16841530	-2.77	MIR548H3	microRNA 548h-3
16975458	-2.77		
16678343	-2.73		
17104519	-2.7	RNY4P23	RNA, Ro-associated Y4 pseudogene 23
16881863	-2.69		
16653299	-2.67		
16653401	-2.67		

16998661	-2.66		
17079293	-2.66	CCNE2	cyclin E2
17085558	-2.64		
16656889	-2.62		
16701398	-2.6	SMYD3-IT1	SMYD3 intronic transcript 1 (non-protein coding)
16828886	-2.59	GINS2	GINS complex subunit 2 (Psf2 homolog)
16857921	-2.59		
17042860	-2.58	GPER	G protein-coupled estrogen receptor 1
16994703	-2.57	CDH18	cadherin 18, type 2
16939509	-2.57		
16970465	-2.56	FAT4	FAT tumor suppressor homolog 4 (Drosophila)
16906636	-2.55		
17005884	-2.55	OR2B6	olfactory receptor, family 2, subfamily B, member 6
16771478	-2.54		
16781386	-2.53		
16707695	-2.51	HELLS	helicase, lymphoid-specific
16920006	-2.5		
16650927	-2.49		
16702571	-2.48	MCM10	minichromosome maintenance complex component 10
16907902	-2.48	MIR548F2	microRNA 548f-2
17013809	-2.46	ESR1	estrogen receptor 1
16677201	-2.45	DTL	denticleless E3 ubiquitin protein ligase homolog (Drosophila)
17055501	-2.43	AGR2	anterior gradient 2 homolog (Xenopus laevis)
17094656	-2.43		
16652191	-2.42		
16800355	-2.41	WDR76	WD repeat domain 76
16988874	-2.39	ADAMTS19	ADAM metallopeptidase with thrombospondin type 1 motif, 19
17100691	-2.38		
17120346	-2.37		
16916958	-2.36	PCNA	proliferating cell nuclear antigen
16900225	-2.35	ANKRD20A8P	ankyrin repeat domain 20 family, member A8, pseudogene
17085217	-2.35		
17085489	-2.35		
17085543	-2.35	ANKRD20A4	ankyrin repeat domain 20 family, member A4

17094284	-2.35		
16650843	-2.34		
17078976	-2.33		
16651115	-2.32		
16681891	-2.32	PRAMEF3	PRAME family member 3
17105401	-2.32	CENPI	centromere protein I
16674578	-2.3		
16850477	-2.3	TYMS	thymidylate synthetase
17020237	-2.3		
16774130	-2.29	FREM2	FRAS1 related extracellular matrix protein 2
16802677	-2.29		
16805151	-2.28		
16998648	-2.28		
16656857	-2.27		
16708728	-2.27	SFXN2	sideroflexin 2
16970762	-2.27	PCDH10	protocadherin 10
16654917	-2.25		
16767851	-2.25	E2F7	E2F transcription factor 7
16823199	-2.25		
16869588	-2.24	ASF1B	ASF1 anti-silencing function 1 homolog B (S. cerevisiae)
16704154	-2.23	RET	ret proto-oncogene
16752132	-2.23	MUCL1	mucin-like 1
17120344	-2.23		
16988801	-2.22	SLC12A2	solute carrier family 12 (sodium/potassium/chloride transporters), member 2
16653671	-2.21		
16655129	-2.21		
16658192	-2.21	TP73	tumor protein p73
16837348	-2.21	MAP2K6	mitogen-activated protein kinase kinase 6
16857258	-2.19	UHRF1	ubiquitin-like with PHD and ring finger domains 1
17016110	-2.19	DCDC2	doublecortin domain containing 2
17122168	-2.19		
16726790	-2.18	POLA2	polymerase (DNA directed), alpha 2, accessory subunit
16784135	-2.18	RN5S385	RNA, 5S ribosomal 385
17010760	-2.18	NT5E	5'-nucleotidase, ecto (CD73)

16702982	-2.17	C10orf112	chromosome 10 open reading frame 112
16968521	-2.17	MIR4451	microRNA 4451
17023465	-2.17		
16655599	-2.16		
16754177	-2.16	TMEM19	transmembrane protein 19
16832852	-2.16	ATAD5	ATPase family, AAA domain containing 5
16904780	-2.16	SPC25	SPC25, NDC80 kinetochore complex component, homolog (S. cerevisiae)
17096205	-2.16	ZNF367	zinc finger protein 367
16857932	-2.16		
16907863	-2.15	ERBB4	v-erb-a erythroblastic leukemia viral oncogene homolog 4 (avian)
17017174	-2.15		
16803616	-2.14		
16942038	-2.14		
16998549	-2.14	RN5S188	RNA, 5S ribosomal 188
17015637	-2.14	ELOVL2	ELOVL fatty acid elongase 2
16657055	-2.13		
16743405	-2.13		
16977350	-2.13		
16650841	-2.12		
16785509	-2.12		
16897144	-2.12		
16953279	-2.12	CDC25A	cell division cycle 25 homolog A (S. pombe)
17021792	-2.12	EPHA7	EPH receptor A7
17078969	-2.12		
17112623	-2.12	SYTL4	synaptotagmin-like 4
16889743	-2.12		
16679411	-2.11	EXO1	exonuclease 1
16921724	-2.1	NCAM2	neural cell adhesion molecule 2
16714504	-2.08	ZWINT	ZW10 interactor
16755900	-2.08		
16770780	-2.08		
16804631	-2.08	C15orf42	chromosome 15 open reading frame 42
16911823	-2.08		
16918976	-2.08	DSN1	DSN1, MIND kinetochore complex component, homolog (S. cerevisiae)

16970118	-2.07	SYNPO2	synaptopodin 2
17094313	-2.07		
16992347	-2.06	FGF18	fibroblast growth factor 18
17045103	-2.06		
16771532	-2.06		
16857917	-2.06		
16824583	-2.05	GPR139	G protein-coupled receptor 139
16914952	-2.05		
16941871	-2.05	IL17RB	interleukin 17 receptor B
16954154	-2.05	AMIGO3, GMPPB	adhesion molecule with Ig-like domain 3, GDP-mannose pyrophosphorylase B
16957170	-2.05	KIAA1524	KIAA1524
16849379	-2.04	TK1	thymidine kinase 1, soluble
16924190	-2.04		
16790256	-2.04		
16655959	-2.03		
16669944	-2.03	PDZK1	PDZ domain containing 1
16742636	-2.03		
16950987	-2.03		
16987298	-2.03	ANKRD32	ankyrin repeat domain 32
17104408	-2.03		
16653717	-2.02		
16826160	-2.02	SHCBP1	SHC SH2-domain binding protein 1
16911330	-2.02	LOC100128668	uncharacterized LOC100128668
17022610	-2.02		
17070705	-2.02		
17100679	-2.02		
17100729	-2.02		
16771551	-2.02		
16655549	-2.01		
16794437	-2.01		
16998639	-2.01		
17121990	-2.01		
16984032	-2	SKP2	S-phase kinase-associated protein 2, E3 ubiquitin protein ligase
17020019	-2	MCM3	minichromosome maintenance complex component 3

17062359	-2	RNF148	ring finger protein 148
17065047	-2		
16855168	-2		
16652773	2		
16654525	2		
16715738	2	DUSP13	dual specificity phosphatase 13
16796414	2	SYNE3	spectrin repeat containing, nuclear envelope family member 3
17028037	2	C6orf48	chromosome 6 open reading frame 48
16654129	2.01		
16655121	2.01		
16786607	2.01	JDP2	Jun dimerization protein 2
16957285	2.01		
16962661	2.01	CLDN1	claudin 1
16740572	2.01		
16654595	2.02		
16693996	2.02	THBS3	thrombospondin 3
16794313	2.02		
16907979	2.02	ABCA12	ATP-binding cassette, sub-family A (ABC1), member 12
17080630	2.02	SNTB1	syntrophin, beta 1 (dystrophin-associated protein A1, 59kDa, basic component 1)
16651571	2.03		
17006313	2.03		
16903491	2.04	RND3	Rho family GTPase 3
17050381	2.04	IFRD1	interferon-related developmental regulator 1
17052935	2.04	OR2A20P, OR2A9P	olfactory receptor, family 2, subfamily A, member 20 and 9 pseudogenes
16678327	2.04		
17079427	2.04		
16650273	2.05		
16778067	2.05	DCLK1	doublecortin-like kinase 1
16871000	2.05		
16911108	2.05	SMOX	spermine oxidase
17067963	2.05	EIF4EBP1	eukaryotic translation initiation factor 4E binding protein 1
16934609	2.05		
16651469	2.06		
16879721	2.06	EPAS1, LOC100652809	endothelial PAS domain protein 1, uncharacterized LOC100652809

17028041	2.06	C6orf48	chromosome 6 open reading frame 48
16759346	2.07		
16866849	2.07	MKNK2	MAP kinase interacting serine/threonine kinase 2
17089525	2.07	LCN2	lipocalin 2
17090296	2.07	ASS1	argininosuccinate synthase 1
17120402	2.07		
16654535	2.08		
16716918	2.08	BLNK	B-cell linker
16832350	2.08	KSR1	kinase suppressor of ras 1
16959441	2.08	AMOTL2	angiomotin like 2
17079210	2.08	GEM	GTP binding protein overexpressed in skeletal muscle
16993405	2.08		
16755526	2.08		
16652973	2.09		
16845336	2.09	VAT1	vesicle amine transport protein 1 homolog (T. californica)
17123894	2.09		
16821479	2.1	ATP2C2	ATPase, Ca++ transporting, type 2C, member 2
16654413	2.11		
17083614	2.11	LURAP1L	leucine rich adaptor protein 1-like
17107118	2.11	ZNF449	zinc finger protein 449
16747661	2.12	MIR200C	microRNA 200c
16876517	2.12		
16663809	2.12		
16651371	2.13		
17097560	2.14	AKNA	AT-hook transcription factor
16653127	2.15		
17079417	2.15		
17127647	2.16		
16652863	2.17		
16910618	2.17	RBCK1	RanBP-type and C3HC4-type zinc finger containing 1
17101126	2.17	LOC100293744	uncharacterized LOC100293744
17115881	2.17	LOC100293744	uncharacterized LOC100293744
17126254	2.17		
16992467	2.18	CREBRF	CREB3 regulatory factor

17075392	2.18		
16709128	2.19	DUSP5	dual specificity phosphatase 5
16974968	2.19	SEL1L3	sel-1 suppressor of lin-12-like 3 (C. elegans)
16656491	2.2		
16818610	2.2	GPT2	glutamic pyruvate transaminase (alanine aminotransferase) 2
16961551	2.2	PLD1	phospholipase D1, phosphatidylcholine-specific
17104049	2.2	SNORA11, MAGED2	small nucleolar RNA, H/ACA box 11, melanoma antigen family D, 2
16650269	2.21		
16655099	2.21		
16656629	2.21		
16872966	2.22	PSG9	pregnancy specific beta-1-glycoprotein 9
16796412	2.23	LINC00341	long intergenic non-protein coding RNA 341
16934238	2.23		
16700673	2.25	IRF2BP2	interferon regulatory factor 2 binding protein 2
16948540	2.25	B3GNT5	UDP-GlcNAc:betaGal beta-1,3-N-acetylglucosaminyltransferase 5
17096457	2.25	CORO2A	coronin, actin binding protein, 2A
16654463	2.26		
16681827	2.27	DHRS3	dehydrogenase/reductase (SDR family) member 3
16827764	2.28	AARS	alanyl-tRNA synthetase
16661544	2.3	SESN2	sestrin 2
16873060	2.3	PLAUR	plasminogen activator, urokinase receptor
16652769	2.31		
16705810	2.31	UNC5B	unc-5 homolog B (C. elegans)
16858137	2.33	ICAM1	intercellular adhesion molecule 1
16970068	2.33	SNHG8	small nucleolar RNA host gene 8 (non-protein coding)
16914812	2.34	CEBPB	CCAAT/enhancer binding protein (C/EBP), beta
16917004	2.34	GPCPD1	glycerophosphocholine phosphodiesterase GDE1 homolog (S. cerevisiae)
16859819	2.36		
16687875	2.39	JUN	jun proto-oncogene
16694361	2.39	ARHGEF2	Rho/Rac guanine nucleotide exchange factor (GEF) 2
16718241	2.41		
16752877	2.42	INHBE	inhibin, beta E
16796694	2.44	WARS	tryptophanyl-tRNA synthetase
16962022	2.45	LAMP3	lysosomal-associated membrane protein 3

16999575	2.45		
16735141	2.45		
17021596	2.46	RRAGD	Ras-related GTP binding D
17085901	2.46	ANXA1	annexin A1
16999580	2.46		
16863877	2.47	PPP1R15A	protein phosphatase 1, regulatory subunit 15A
17123236	2.47		
17125360	2.47		
16755528	2.48		
16865681	2.48		
16751518	2.49	KRT86	keratin 86
16681304	2.5	ERRFI1	ERBB receptor feedback inhibitor 1
17013195	2.51	RN5S221	RNA, 5S ribosomal 221
17119472	2.51		
16652771	2.52		
16670479	2.53	C1orf51	chromosome 1 open reading frame 51
16948572	2.53	KLHL24	kelch-like 24 (Drosophila)
16914117	2.54	PABPC1L	poly(A) binding protein, cytoplasmic 1-like
17106526	2.54	LONRF3	LON peptidase N-terminal domain and ring finger 3
16919158	2.55	TGM2	transglutaminase 2
16846291	2.58	HOXB9	homeobox B9
17044253	2.58	GPNMB	glycoprotein (transmembrane) nmb
16657013	2.59		
16651383	2.63		
16669389	2.65	PHGDH	phosphoglycerate dehydrogenase
16841907	2.66	RASD1	RAS, dexamethasone-induced 1
16919547	2.66	SLPI	secretory leukocyte peptidase inhibitor
16738512	2.68	SLC43A1	solute carrier family 43, member 1
16665932	2.69	GADD45A	growth arrest and DNA-damage-inducible, alpha
16782548	2.69	PCK2	phosphoenolpyruvate carboxykinase 2 (mitochondrial)
16840723	2.69	SAT2	spermidine/spermine N1-acetyltransferase family member 2
16931763	2.69		
16722445	2.71		
16656649	2.72		

16678348	2.73		
16844509	2.75	KRT23	keratin 23 (histone deacetylase inducible)
17095703	2.75	NFIL3	nuclear factor, interleukin 3 regulated
17080788	2.78	FBXO32	F-box protein 32
16705961	2.81	DDIT4	DNA-damage-inducible transcript 4
16852683	2.81	PMAIP1	phorbol-12-myristate-13-acetate-induced protein 1
16860644	2.85	CEBPG	CCAAT/enhancer binding protein (C/EBP), gamma
16711343	2.88	AKR1C2	aldo-keto reductase family 1, member C2
16791219	2.94	TGM1	transglutaminase 1 (protein-glutamine-gamma-glutamyltransferase)
16890207	2.94	MAP2	microtubule-associated protein 2
16725783	2.95	BEST1	bestrophin 1
16686201	3	SLC6A9	solute carrier family 6 (neurotransmitter transporter, glycine), member 9
16918074	3		
16910609	3.07	TRIB3	tribbles homolog 3 (Drosophila)
16971420	3.11		
16739208	3.14	FTH1	ferritin, heavy polypeptide 1
16821737	3.14	LOC100506670	uncharacterized LOC100506670
16847771	3.2	ERN1	endoplasmic reticulum to nucleus signaling 1
17090320	3.25		
17120106	3.26		
16934608	3.27		
16874097	3.28	HSD17B14	hydroxysteroid (17-beta) dehydrogenase 14
16697196	3.35	FAM129A	family with sequence similarity 129, member A
16830577	3.35	CD68	CD68 molecule
17086193	3.41	PSAT1	phosphoserine aminotransferase 1
17019484	3.46	GTPBP2	GTP binding protein 2
17126054	3.47		
17126164	3.47		
16985950	3.55	MAP1B	microtubule-associated protein 1B
17009093	3.64	VEGFA	vascular endothelial growth factor A
17022736	3.64	TUBE1	tubulin, epsilon 1
17125034	3.7		
16975302	3.86		
17060061	4.04	ASNS	asparagine synthetase (glutamine-hydrolyzing)

16859800	4.2	MIR3189	microRNA 3189
16799739	4.25	CHAC1	ChaC, cation transport regulator homolog 1 (E. coli)
16825371	4.31	NUPR1	nuclear protein, transcriptional regulator, 1
17125036	4.41		
17125030	4.49		
16811684	5.13	CYP1A1	cytochrome P450, family 1, subfamily A, polypeptide 1
17125028	5.26		
16769481	5.44	ALDH1L2	aldehyde dehydrogenase 1 family, member L2
16931766	5.46	KLHDC7B	kelch domain containing 7B
17125032	5.61		
16850663	5.84	MGC11082	uncharacterized LOC84777
16766578	6.4	DDIT3	DNA-damage-inducible transcript 3
16929562	6.74	HMOX1	heme oxygenase (decycling) 1
16979917	6.83	SLC7A11	solute carrier family 7 (anionic amino acid transporter light chain, xc- system
16980051	7.82	CLGN	calmegin
16873686	7.97		
17013657	12.39	ULBP1	UL16 binding protein 1

Appendix I-B: Gene Expression Profile of MCF7 Cells with Glutamine Deprivation

Transcript Cluster ID	Fold Change	Gene Symbol	Description
16655785	-3.95		
16678343	-3.36		
16769753	-3.05		
16650765	-2.97		
16939509	-2.92		
16652995	-2.81		
17043152	-2.8		
16835635	-2.77		
16771470	-2.7		
16678323	-2.69		
16771532	-2.66		
16650285	-2.58		
16722387	-2.55		
16651697	-2.53		
16835617	-2.47		
16764106	-2.43		
16934243	-2.42		
16656835	-2.4		
16651031	-2.35		
16771468	-2.23		
16657077	-2.14		
16722401	-2.14		
16769742	-2.11		
17104408	-2.1		
16769734	-2.1		
16924190	-2.09		
17121916	-2.08		

16674578	-2.07		
16770461	-2.07		
16650733	-2.05		
16651207	-2.03		
16735804	-2.02		
16990143	2		
17127661	2.02		
16771538	2.02		
16654231	2.04		
16654477	2.08		
16939508	2.08		
16655365	2.13		
16654229	2.15		
17090320	2.15		
16880240	2.15		
16898486	2.16		
16678348	2.16		
17092738	2.18		
16771448	2.19		
16669389	2.22	PHGDH	phosphoglycerate dehydrogenase
17125030	2.25		
16889717	2.29		
17006313	2.3		
17073244	2.35		
17104049	2.38	SNORA11, MAGED2	small nucleolar RNA, H/ACA box 11, melanoma antigen family D, 2
17125036	2.46		
16769481	2.49	ALDH1L2	aldehyde dehydrogenase 1 family, member L2
16855164	2.5		
16934238	2.53		
17120106	2.54		
16735141	2.55		
17013195	2.61	RN5S221	RNA, 5S ribosomal 221
17119472	2.61		
17086193	2.67	PSAT1	phosphoserine aminotransferase 1

16799739	2.68	CHAC1	ChaC, cation transport regulator homolog 1 (E. coli)
16807312	2.68		
17125028	2.7		
16650925	2.71		
16811684	2.74	CYP1A1	cytochrome P450, family 1, subfamily A, polypeptide 1
17125034	2.78		
17060061	2.96	ASNS	asparagine synthetase (glutamine-hydrolyzing)
17017207	3.18		
16934608	3.33		
16975302	3.35		
16979917	3.4	SLC7A11	solute carrier family 7 (anionic amino acid transporter light chain, xc- system), member 11
17125032	3.67		
16873686	4.07		
17013657	4.74	ULBP1	UL16 binding protein 1

APPENDIX II

APPENDIX II: Complete spectrophotometer measurements results presented in chapter 5.2

Spectrophotometric measurements (µmol·millioncell^{-1}·h^{-1})						
			Glucose Consumption	Lactate Production	Glutamine Consumption (x5)	Glutamate Production (x20)
8 hrs data	Control	Mean	0.9950	1.2066	2.2358	0.2805
		SD	0.1256	0.0376	0.1971	0.0682
	-Q	Mean	0.9145	0.6868		
		SD	0.0254	0.0131		
	Oligomycin	Mean	1.8198	2.6139	2.9514	0.9066
		SD	0.0262	0.0413	0.4890	0.0094
24 hrs data	Control	Mean	0.9248	1.2680	1.9800	0.7226
		SD	0.0310	0.0348	0.0350	0.0735
	-Q	Mean	0.6852	0.8533		
		SD	0.0491	0.0275		
	Oligomycin	Mean	1.8775	3.2092	1.5350	0.7378
		SD	0.0370	0.0102	0.0500	0.0183

APPENDIX III

APPENDIX III: Suplementary data for mass isotopomer distribution of metabolites presented in chapter 5.2

Lactate												
			8 Hrs Data					24 Hrs Data				
Tracer	Condition		M0	M1	M2	M3	ΣM	M0	M1	M2	M3	ΣM
[1,2-$^{13}C_2$]-glucose	Control	Mean	0.575	0.025	0.394	0.006	0.425	0.589	0.043	0.321	0.017	0.411
		SD	0.007	0.002	0.010	0.002	0.007	0.032	0.020	0.014	0.003	0.032
	-Q	Mean	0.589	0.025	0.380	0.006	0.411	0.602	0.031	0.308	0.004	0.398
		SD	0.003	0.005	0.005	0.002	0.003	0.036	0.012	0.019	0.001	0.036
	Oligomycin	Mean	0.554	0.009	0.434	0.002	0.446	0.548	0.011	0.440	0.001	0.452
		SD	0.002	0.001	0.004	0.001	0.002	0.020	0.001	0.022	0.001	0.020
[U-$^{13}C_5$]-glutamine	Control	Mean	0.984	0.006	0.004	0.006	0.016	0.981	0.009	0.002	0.007	0.019
		SD	0.002	0.001	0.000	0.002	0.002	0.008	0.007	0.001	0.001	0.008
	Oligomycin	Mean	0.995	0.001	0.002	0.003	0.005	1.000	0.000	-0.001	0.001	0.000
		SD	0.001	0.001	0.000	0.001	0.001	0.003	0.001	0.000	0.001	0.003

Glutamate (C2-C4)												
			8 Hrs Data					24 Hrs Data				
Tracer	Condition		M0	M1	M2	M3	ΣM	M0	M1	M2	M3	ΣM
$[1,2\text{-}^{13}C_2]$-glucose	Control	Mean	1.012	0.000	0.000	0.000	0.000	0.993	0.005	0.002	0.001	0.007
		SD	0.006	0.005	0.001	0.001	0.006	0.001	0.001	0.000	0.000	0.001
	-Q	Mean	0.845	0.117	0.019	0.020	0.155	0.809	0.121	0.052	0.018	0.191
		SD	0.061	0.046	0.006	0.009	0.061	0.004	0.003	0.001	0.002	0.004
	Oligomycin	Mean	1.007	0.000	-0.001	0.000	0.000	0.994	0.004	0.001	0.001	0.006
		SD	0.006	0.005	0.001	0.001	0.006	0.001	0.000	0.000	0.000	0.001
$[U\text{-}^{13}C_5]$-glutamine	Control	Mean	0.076	0.015	0.021	0.888	0.924	0.059	0.009	0.033	0.898	0.941
		SD	0.004	0.004	0.000	0.008	0.004	0.000	0.000	0.000	0.000	0.000
	Oligomycin	Mean	0.081	0.014	0.021	0.884	0.919	0.067	0.008	0.035	0.891	0.933
		SD	0.003	0.003	0.000	0.006	0.003	0.004	0.000	0.000	0.004	0.004

Glutamate (C2-C5)														
			8 Hrs Data						24 Hrs Data					
Tracer	Condition		M0	M1	M2	M3	M4	ΣM	M0	M1	M2	M3	M4	ΣM
[1,2-$^{13}C_2$]-glucose	Control	Mean	0.996	0.000	0.001	0.000	0.002	0.004	0.996	0.000	0.004	0.001	0.000	0.004
		SD	0.004	0.000	0.000	0.000	0.004	0.004	0.000	0.000	0.000	0.000	0.000	0.000
	-Q	Mean	0.971	0.008	0.016	0.002	0.002	0.029	0.825	0.053	0.080	0.027	0.015	0.175
		SD	0.003	0.000	0.000	0.002	0.002	0.003	0.000	0.001	0.000	0.000	0.002	0.000
	Oligomycin	Mean	1.000	0.000	0.001	0.000	0.000	0.000	0.997	0.000	0.004	0.000	0.000	0.003
		SD	0.000	0.000	0.000	0.000	0.000	0.000	0.000	0.000	0.000	0.000	0.000	0.000
[U-$^{13}C_5$]-glutamine	Control	Mean	0.050	0.002	0.010	0.027	0.911	0.950	0.057	0.004	0.015	0.036	0.887	0.943
		SD	0.002	0.000	0.000	0.000	0.002	0.002	0.000	0.000	0.000	0.000	0.000	0.001
	Oligomycin	Mean	0.055	0.002	0.010	0.027	0.906	0.945	0.064	0.003	0.016	0.036	0.880	0.936
		SD	0.002	0.000	0.000	0.000	0.001	0.002	0.003	0.000	0.000	0.000	0.003	0.003

Ribose																
			8 Hrs Data							24 Hrs Data						
Tracer	Condition		M0	M1	M2	M3	M4	M5	ΣM	M0	M1	M2	M3	M4	M5	ΣM
[1,2-$^{13}C_2$]-glucose	Control	Mean	0.876	0.074	0.014	0.025	0.009	0.001	0.124	0.762	0.108	0.034	0.074	0.022	0.002	0.238
		SD	0.005	0.004	0.000	0.001	0.001	0.000	0.005	0.005	0.003	0.001	0.001	0.001	0.000	0.005
	-Q	Mean	0.930	0.041	0.009	0.015	0.005	0.000	0.070	0.923	0.003	0.022	0.037	0.013	0.001	0.077
		SD	0.007	0.003	0.001	0.002	0.001	0.001	0.007	0.005	0.003	0.001	0.001	0.000	0.000	0.005
	Oligomycin	Mean	0.958	0.022	0.004	0.011	0.005	0.000	0.042	0.974	0.000	0.011	0.034	0.013	0.001	0.026
		SD	0.001	0.001	0.000	0.000	0.001	0.001	0.001	0.001	0.000	0.000	0.001	0.000	0.000	0.001
[U-$^{13}C_5$]-glutamine	Control	Mean	0.992	0.003	0.000	0.004	0.000	0.000	0.008	1.104	0.000	-0.002	0.000	-0.001	0.000	-0.104
		SD	0.009	0.006	0.005	0.008	0.002	0.002	0.009	0.001	0.001	0.000	0.000	0.000	0.000	0.001
	Oligomycin	Mean	1.000	0.000	0.001	-0.001	0.001	0.000	0.000	1.104	0.000	-0.003	-0.001	-0.001	0.000	-0.104
		SD	0.001	0.001	0.000	0.000	0.001	0.000	0.001	0.005	0.002	0.000	0.000	0.001	0.001	0.005

Citrate																	
			8 Hrs Data								24 Hrs Data							
Tracer	Condition		M0	M1	M2	M3	M4	M5	M6	ΣM	M0	M1	M2	M3	M4	M5	M6	ΣM
[1,2-$^{13}C_2$]-glucose	Control	Mean	0.664	0.054	0.286	0.014	0.000	0.000	0.000	0.336	0.433	0.082	0.335	0.065	0.072	0.012	0.002	0.567
		SD	0.004	0.001	0.003	0.002	0.001	0.000	0.000	0.004	0.005	0.001	0.004	0.002	0.001	0.000	0.000	0.005
	-Q	Mean	0.593	0.075	0.308	0.027	0.013	0.000	0.000	0.407	0.383	0.099	0.334	0.076	0.092	0.013	0.003	0.617
		SD	0.014	0.006	0.002	0.003	0.003	0.000	0.000	0.014	0.003	0.003	0.000	0.000	0.001	0.001	0.000	0.003
	Oligomycin	Mean	0.900	0.002	0.151	0.000	0.000	0.003	0.000	0.100	0.656	0.047	0.251	0.003	0.038	0.006	0.000	0.344
		SD	0.025	0.025	0.049	0.018	0.002	0.002	0.001	0.025	0.001	0.003	0.005	0.005	0.002	0.001	0.001	0.001
[U-$^{13}C_5$]-glutamine	Control	Mean	0.579	0.099	0.063	0.074	0.178	0.026	0.000	0.421	0.457	0.117	0.142	0.079	0.167	0.036	0.002	0.543
		SD	0.006	0.002	0.002	0.002	0.001	0.004	0.000	0.006	0.004	0.002	0.011	0.002	0.006	0.003	0.000	0.004
	Oligomycin	Mean	0.630	0.033	0.027	0.102	0.167	0.058	0.000	0.370	0.481	0.058	0.100	0.100	0.145	0.114	0.003	0.519
		SD	0.022	0.015	0.003	0.011	0.005	0.019	0.000	0.022	0.019	0.005	0.005	0.005	0.004	0.008	0.001	0.019

α-Ketoglutarate																
			8 Hrs Data							24 Hrs Data						
Tracer	Condition		M0	M1	M2	M3	M4	M5	ΣM	M0	M1	M2	M3	M4	M5	ΣM
[1,2-$^{13}C_2$]-glucose	Control	Mean	0.832	0.043	0.115	0.015	0.000	0.000	0.171	0.635	0.073	0.209	0.046	0.032	0.004	0.365
		SD	0.014	0.004	0.010	0.000	0.001	0.000	0.014	0.003	0.000	0.002	0.001	0.001	0.000	0.003
	-Q	Mean	0.734	0.072	0.152	0.031	0.014	-0.002	0.269	0.516	0.107	0.243	0.074	0.053	0.009	0.484
		SD	0.016	0.002	0.011	0.002	0.001	0.001	0.016	0.018	0.008	0.007	0.001	0.004	0.001	0.018
	Oligomycin	Mean	0.940	-0.002	0.072	0.001	-0.008	-0.002	0.062	0.848	0.018	0.108	0.014	0.010	0.002	0.152
		SD	0.026	0.005	0.020	0.002	0.001	0.000	0.026	0.004	0.002	0.003	0.001	0.001	0.001	0.004
[U-$^{13}C_5$]-glutamine	Control	Mean	0.419	0.075	0.043	0.129	0.009	0.326	0.255	0.314	0.096	0.076	0.147	0.021	0.346	0.686
		SD	0.032	0.004	0.007	0.006	0.001	0.016	0.017	0.004	0.002	0.002	0.001	0.000	0.003	0.004
	Oligomycin	Mean	0.204	0.041	0.063	0.142	0.023	0.527	0.269	0.207	0.035	0.064	0.123	0.031	0.540	0.793
		SD	0.009	0.002	0.001	0.006	0.000	0.004	0.005	0.020	0.005	0.004	0.006	0.002	0.014	0.020

Fumarate														
			8 Hrs Data						24 Hrs Data					
Tracer	Condition		M0	M1	M2	M3	M4	ΣM	M0	M1	M2	M3	M4	ΣM
[1,2-$^{13}C_2$]-glucose	Control	Mean	0.805	0.053	0.118	0.022	0.002	0.195	0.744	0.073	0.165	0.012	0.006	0.256
		SD	0.013	0.001	0.003	0.007	0.002	0.013	0.001	0.001	0.001	0.001	0.000	0.001
	-Q	Mean	0.713	0.070	0.191	0.021	0.004	0.287	0.719	0.100	0.222	0.000	0.002	0.281
		SD	0.007	0.007	0.014	0.001	0.000	0.007	0.012	0.004	0.002	0.000	0.018	0.012
	Oligomycin	Mean	0.875	0.027	0.080	0.017	0.002	0.125	0.873	0.029	0.097	0.000	0.002	0.127
		SD	0.005	0.002	0.003	0.007	0.001	0.005	0.007	0.002	0.000	0.005	0.000	0.007
[U-$^{13}C_5$]-glutamine	Control	Mean	0.457	0.089	0.135	0.105	0.213	0.543	0.418	0.103	0.157	0.100	0.222	0.582
		SD	0.009	0.002	0.002	0.005	0.002	0.009	0.013	0.002	0.003	0.004	0.004	0.013
	Oligomycin	Mean	0.448	0.038	0.111	0.201	0.201	0.552	0.389	0.040	0.127	0.218	0.226	0.611
		SD	0.018	0.005	0.004	0.004	0.005	0.018	0.006	0.003	0.003	0.007	0.001	0.006

Malate														
			8 Hrs Data						24 Hrs Data					
Tracer	Condition		M0	M1	M2	M3	M4	ΣM	M0	M1	M2	M3	M4	ΣM
[1,2-$^{13}C_2$]-glucose	Control	Mean	0.812	0.051	0.123	0.014	0.000	0.188	0.741	0.070	0.159	0.025	0.005	0.259
		SD	0.001	0.000	0.001	0.000	0.000	0.001	0.004	0.001	0.003	0.000	0.000	0.004
	-Q	Mean	0.755	0.056	0.172	0.015	0.002	0.245	0.712	0.068	0.188	0.024	0.008	0.288
		SD	0.015	0.006	0.008	0.002	0.000	0.015	0.009	0.003	0.005	0.001	0.001	0.009
	Oligomycin	Mean	0.884	0.026	0.082	0.007	0.000	0.116	0.876	0.025	0.090	0.008	0.002	0.124
		SD	0.007	0.002	0.005	0.000	0.000	0.007	0.003	0.001	0.002	0.000	0.000	0.003
[U-$^{13}C_5$]-glutamine	Control	Mean	0.486	0.096	0.141	0.099	0.178	0.514	0.478	0.105	0.149	0.094	0.175	0.522
		SD	0.002	0.001	0.001	0.001	0.001	0.002	0.040	0.006	0.011	0.011	0.012	0.040
	Oligomycin	Mean	0.462	0.047	0.122	0.197	0.172	0.538	0.408	0.046	0.125	0.234	0.188	0.592
		SD	0.012	0.003	0.003	0.009	0.004	0.012	0.000	0.000	0.000	0.004	0.003	0.000

Aspartate														
			8 Hrs Data						24 Hrs Data					
Tracer	Condition		M0	M1	M2	M3	M4	ΣM	M0	M1	M2	M3	M4	ΣM
[1,2-$^{13}C_2$]-glucose	Control	Mean	0.867	0.038	0.084	0.011	0.001	0.133	0.784	0.062	0.129	0.022	0.004	0.216
		SD	0.006	0.002	0.004	0.002	0.000	0.006	0.005	0.001	0.003	0.001	0.000	0.005
	-Q	Mean	0.963	0.011	0.030	-0.004	0.000	0.037	0.940	0.018	0.041	0.000	0.001	0.060
		SD	0.004	0.002	0.006	0.008	0.000	0.004	0.003	0.000	0.001	0.002	0.000	0.003
	Oligomycin	Mean	0.915	0.019	0.059	0.006	0.001	0.085	0.936	0.014	0.046	0.002	0.001	0.064
		SD	0.010	0.002	0.007	0.001	0.000	0.010	0.000	0.000	0.000	0.000	0.000	0.000
[U-$^{13}C_5$]-glutamine	Control	Mean	0.660	0.068	0.097	0.061	0.115	0.340	0.586	0.089	0.120	0.067	0.137	0.414
		SD	0.007	0.002	0.003	0.002	0.002	0.007	0.008	0.002	0.002	0.001	0.003	0.008
	Oligomycin	Mean	0.698	0.031	0.074	0.096	0.101	0.302	0.748	0.023	0.056	0.094	0.080	0.252
		SD	0.026	0.001	0.005	0.012	0.007	0.026	0.009	0.001	0.002	0.006	0.001	0.009

Palmitate													
Time	**Tracer**	**Condition**		**M0**	**M1**	**M2**	**M3**	**M4**	**M5**	**M6**	**M7**	**M8**	**ΣM**
8 Hrs Data	**[1,2-$^{13}C_2$]-glucose**	**Control**	**Mean**	0.907	0.001	0.018	0.007	0.022	0.009	0.020	0.006	0.011	0.093
			SD	0.000	0.001	0.000	0.000	0.000	0.000	0.000	0.000	0.000	0.000
		-Q	**Mean**	0.934	0.000	0.013	0.005	0.016	0.006	0.014	0.004	0.008	0.066
			SD	0.002	0.000	0.000	0.000	0.000	0.000	0.001	0.000	0.000	0.002
		Oligomycin	**Mean**	0.954	0.000	0.013	0.002	0.013	0.002	0.010	0.001	0.005	0.046
			SD	0.009	0.000	0.002	0.000	0.002	0.000	0.002	0.000	0.002	0.009
	[U-$^{13}C_5$]-glutamine	**Control**	**Mean**	0.932	0.002	0.036	0.005	0.015	0.002	0.005	0.001	0.001	0.068
			SD	0.001	0.000	0.001	0.000	0.000	0.000	0.000	0.000	0.000	0.001
		Oligomycin	**Mean**	0.947	0.001	0.018	0.002	0.015	0.002	0.010	0.001	0.004	0.053
			SD	0.001	0.001	0.000	0.000	0.000	0.000	0.000	0.000	0.000	0.001
24 Hrs Data	**[1,2-$^{13}C_2$]-glucose**	**Control**	**Mean**	0.794	0.004	0.030	0.014	0.046	0.021	0.046	0.017	0.028	0.206
			SD	0.011	0.001	0.002	0.001	0.002	0.001	0.002	0.001	0.001	0.011
		-Q	**Mean**	0.858	0.003	0.022	0.010	0.032	0.015	0.030	0.011	0.018	0.142
			SD	0.012	0.001	0.002	0.001	0.003	0.001	0.002	0.001	0.001	0.012
		Oligomycin	**Mean**	0.892	0.002	0.029	0.005	0.031	0.006	0.021	0.003	0.010	0.108
			SD	0.001	0.000	0.000	0.000	0.000	0.000	0.000	0.000	0.000	0.001
	[U-$^{13}C_5$]-glutamine	**Control**	**Mean**	0.877	0.006	0.065	0.010	0.027	0.004	0.008	0.001	0.002	0.123
			SD	0.007	0.000	0.005	0.001	0.002	0.000	0.001	0.000	0.000	0.007
		Oligomycin	**Mean**	0.901	0.001	0.028	0.003	0.028	0.004	0.021	0.002	0.012	0.099
			SD	0.013	0.001	0.003	0.000	0.003	0.000	0.003	0.000	0.002	0.013

APPENDIX IV

APPENDIX IV: Suplementary data for the measured fluxes presented in chapter 5.2

Reaction	By means of	Absolute Fluxes (µmol·L^{-1}·min^{-1})		
		Control	(-Q)	Oligo
Glycolysis-Glyconeogenesis				
Glc → G6P	HK	0.92500	0.68500	1.87800
F6P → F16BP	PFK	0.90018	1.01668	1.88337
F16BP → F6P	FBPase	0.04782	0.37451	0.11875
F16BP → T3P	Aldolase (f)	1.60939	1.48197	2.35636
T3P → F16BP	Aldolase (r)	0.75704	0.85010	0.62602
F16BP → T3P	Aldolase (net flux)	0.85236	0.63187	1.73035
T3P → → PEP	Low glycolysis (f)	1.72229	1.27374	3.50095
PEP →→ T3P	Low glycolysis (r)	0.00033	0.00031	0.00022
T3P →→ PEP	Low glycolysis (net flux)	1.72196	1.27343	3.50073
PEP → Pyr(cyt)	PK	1.71688	1.26065	3.50009
Pyr(cyt)) → Pyr(mit)	Pyruvate Transport (f)	0.32178	0.06800	0.07220
Pyr(mit) →Pyr(cyt)	Pyruvate Transport (r)	0.00250	0.01226	0.00651
Pyr(cyt)) → Pyr(mit)	Pyruvate Transport (net flux)	0.31928	0.05574	0.06570
Pyr(cyt) →Lac	LDH (f)	1.58931	1.53494	3.67047
Lac → Pyr(cyt)	LDH (r.)	0.00184	0.00100	0.04143
Pyr(cyt) →Lac	LDH (net flux)	1.58747	1.53394	3.62903
Krebs Cycle Intermediates				
Pyr(mit) → Ac-CoA	PDH	0.42714	0.10320	0.14094
(Oaa+Ac-CoA) → Cit (mit)	CS (citrate Synthase)	0.33669	0.13356	0.21734
Cit (mit) → Cit (cyt)	Citrate Transport (f)	0.53485	0.34518	0.76519
Cit (cyt) → Cit (mit)	Citrate Transport (r)	0.34149	0.23369	0.60515
Cit (mit) → Cit (cyt)	Citrate Transport (net flux)	0.19336	0.11150	0.16005
Cit (mit) →→ αKG (mit)	Multiple Enzymes	0.07129	0.01907	0.03631
αKG(mit) → αKG(cyt)/Glu(cyt)	αKG Transport (f)	0.47719	0.74918	0.91378
αKG(cyt)/Glu(cyt) → αKG (mit)	αKG Transport (r)	0.72995	0.78238	1.25771
αKG(mit) → αKG(cyt)/Glu(cyt)	αKG Transport (net flux)	-0.25276	-0.03320	-0.34394
αKG (mit) →→ Fum(mit)	Multiple Enzymes	0.31494	0.05190	0.31338
Fum(mit) → Mal(mit)	Fumarase (f)	0.31445	0.06011	0.41322
Mal(mit) → Fum(mit)	Fumarase (r)	0.02914	0.00830	0.15071
Fum(mit) → Mal(mit)	Fumarase (net flux)	0.28530	0.05181	0.26251
Mal(mit) → Oaa(mit)	MDH (f)	0.61049	0.42115	9.74136
Oaa(mit) → Mal(mit)	MDH (r)	0.41855	1.70690	9.76261
Mal(mit) → Oaa(mit)	MDH (net flux)	0.19194	-1.28575	-0.02126
Pyr(mit) → Oaa(mit)	PC	0.14491	1.42278	0.27596
Mal(mit) → Pyr(mit)	ME (Malic Enzyme)	0.16828	1.38581	0.28468
Mal(mit) → Mal(cyt)	Malate Transport (f)	0.01483	0.01098	0.09019
Oaa(cyt) → Mal(mit)	Malate Transport (r)	0.10512	0.07178	0.14730
Mal(cyt) → Pyr(cyt)	ME (Malic Enzyme)	0.00116	0.00070	0.00804

Reaction	By means of	Absolute Fluxes (µmol·L^{-1}·min^{-1})		
		Control	(-Q)	Oligo
Glutaminolysis - Lipid Synthesis -β Oxidation				
Gln → Glu(cyt)	Glutaminase	0.04822	0.00000	0.05669
Glu(cyt) → Gln	GS (Glutamine Synthetase)	0.00000	0.00000	0.00000
Gln → Protein	Protein synthesis	0.21699	0.00000	0.09070
Glu(ext) → Glu(cyt)	Glutamate Transport (f)	0.34411	0.00000	0.48269
Glu(cyt) → Glu(ext)	Glutamate Transport (r)	0.11959	0.00000	0.19454
Glu(ext) → Glu(cyt)	Glutamate Transport (net flux)	0.22453	0.00000	0.28815
αKG(cyt)/Glu(cyt) →→ cyt (cyt)	Multiple Enzymes (f)	0.00979	0.00018	0.02086
cyt (cyt) →→ αKG(cyt)/Glu(cyt)	Multiple Enzymes (r)	0.03244	0.03746	0.03574
αKG(cyt)/Glu(cyt) →→ cyt (cyt)	Multiple Enzymes (net flux)	-0.02265	-0.03728	-0.01488
Ac-CoA(cyt) →→ Lipids	Multiple Enzymes	0.10388	0.06609	0.10584
Lipids →→ AcCoA(mit)	Multiple Enzymes	0.04110	0.03043	0.07718
Amino Acids				
Pro(ext) → Pro(cyt)	Proline Transport (f)	0.04255	0.02980	0.00000
Pro(cyt) → Pro(ext)	Proline Transport (r)	0.01338	0.00801	0.00292
Pro(ext) → Pro(cyt)	Proline Transport (net flux)	0.02917	0.02178	-0.00292
Pro(cyt) → Protein	Protein synthesis	0.00080	0.00056	0.00000
Pro(cyt) → Glu(cyt)	Proline Oxidase	0.00000	0.00000	0.00000
Ala(cyt) → Ala(ext)	Alanine Transport (f)	0.06735	0.04168	0.11381
Ala(ext) → Ala(cyt)	Alanine Transport (r)	0.27792	0.36520	0.30566
Ala(ext) → Ala(cyt)	AlanineTransport (net flux)	0.21057	0.32353	0.19184
Ala(cyt) → Protein	Protein synthesis	0.00208	0.00097	0.00504
Trp (cyt) →→ Ala(cyt)	Multiple Enzymes	0.00500	0.00019	0.00939
Cys(ext) → Cys(cyt)	Cystein Transport	0.01188	0.00794	0.02230
Ser(ext) → Ser(cyt)	Serine Transport	0.00000	0.00000	0.00000
T3P →→ Ser(cyt)	Multiple Enzymes	0.00812	0.00355	0.00399
Ser(cyt) → Protein	Protein synthesis	0.00776	0.00829	0.00000
Ser(cyt) → `Pyr(cyt)	Serine Dehyratase	0.12311	0.08764	0.04476
Asp(cyt) → Asp(ext)	Aspartate Transport (f)	0.00363	0.00185	0.00677
Asp(ext) → Asp(cyt)	Aspartate Transport (r)	0.00000	0.00000	0.00000
Asp(ext) → Asp(cyt)	Aspartate Transport (net flux)	-0.00363	-0.00185	-0.00677
Asp(ext) → Protein	Protein synthesis	0.01852	0.01367	0.00214

Reaction	By means of	Absolute Fluxes (µmol·L^{-1}·min^{-1})		
		Control	(-Q)	Oligo
Pentose Phosphate Pathway				
G6P → R5P(cyt)	Multiple Enzymes	0.07250857	0.042479349	0.113079502
R5P(cyt) → R5P(metabolized)	Metabolism	0.01246857	0.008767824	0.005619906
R5P(Metabolized) →→ R5P(cyt)	Metabolism			
Transaldolase:				
S7P → F6P	TALD	0.0000710	0.0000035	0.0001571
F6P → S7P	TALD	0.0000190	0.0000111	0.0000342
F6P → G3P	TALD	0.0000248	0.0032662	0.0000452
S7P → E4P	TALD	0.0000191	0.0000111	0.0000343
		0.0000000	0.0000000	0.0000000
Transketolase:		0.0000000	0.0000000	0.0000000
XU5P →S7P	TKT	0.0343197	0.0258169	0.0663955
S7P → XU5P	TKT	0.0039965	0.0059109	0.0095775
F6P → XU5P	TKT	0.0000000	0.0000002	0.0000000
XU5P →F6P	TKT	0.0000249	0.0001229	0.0000517
F6P → S7P	TKT	0.0000000	0.0000020	0.0000000
S7P → F6P	TKT	0.0000642	0.0002645	0.0001257
XU5P → G3P	TKT	0.0378317	0.0313862	0.0752556
F6P → E4P	TKT	0.0000000	0.0000024	0.0000000
R5P → S7P	TKT	0.0974107	0.0675354	0.1830376

APPENDIX V

Review
Mini-Focus Issue: Systems biology

Future Medicinal Chemistry

Cancer cell metabolism as new targets for novel designed therapies

Metabolic processes are altered in cancer cells, which obtain advantages from this metabolic reprogramming in terms of energy production and synthesis of biomolecules that sustain their uncontrolled proliferation. Due to the conceptual progresses in the last decade, metabolic reprogramming was recently included as one of the new hallmarks of cancer. The advent of high-throughput technologies to amass an abundance of omic data, together with the development of new computational methods that allow the integration and analysis of omic data by using genome-scale reconstructions of human metabolism, have increased and accelerated the discovery and development of anticancer drugs and tumor-specific metabolic biomarkers. Here we review and discuss the latest advances in the context of metabolic reprogramming and the future in cancer research.

Igor Marín de Mas[‡,1,2], Esther Aguilar[‡,1], Anusha Jayaraman[‡,1], Ibrahim H Polat[1], Alfonso Martín-Bernabé[1], Rohit Bharat[1], Carles Foguet[1], Enric Milà[1], Balázs Papp[2], Josep J Centelles[1] & Marta Cascante*[,1]

[1]Department of Biochemistry & Molecular Biology, Faculty of Biology, IBUB, Universitat de Barcelona & Institut d'Investigacions Biomèdiques August Pi i Sunyer (IDIBAPS), Unit Associated with CSIC, Diagonal 643, E-08028-Barcelona, Spain

[2]Institute of Biochemistry, Biological Research Center of the Hungarian Academy of Sciences, Temesvári krt. 62, H-6726 Szeged, Hungary

*Author for correspondence:
Tel.: +34 934021593
Fax: +34 934021559
martacascante@ub.edu

[‡]Authors contributed equally

Cancer is still one of the major causes of death worldwide and the statistics are devastating. According to the WHO the global burden of cancer has risen to 14.1 million new cases and 8.2 million cancer deaths in 2012 and the estimates predict that it could increase in its global incidence [1].

It was proposed 15 years ago by Hanahan and Weinberg that cancer development relies on the following basic biological capabilities, known as the 'hallmarks of cancer' that are acquired during the multistep process of tumor development: the capability to sustain proliferative signaling, resistance to cell death, evasion of growth suppression, ability of replicative immortality, tumor-promoting inflammation, genome instability and mutation, induction of angiogenesis and activation of invasion and metastasis. Owing to conceptual progress in the last decade, two new hallmarks, metabolic reprogramming and evasion of immune destruction, have been identified (Figure 1) [2].

Nowadays, it is widely recognized that metabolic reprogramming is essential to sustain tumor progression. Several metabolic adaptations described in cancer cells, such as the metabolization of glucose to lactate in the presence of oxygen (Warburg effect), are quite common among different cancer types. These changes are promoted by genetic and epigenetic alterations producing mutations or alterations in the expression of key metabolic enzymes that modify flux distributions in metabolic networks, providing advantages to cancer cells in terms of energy production and synthesis of biomolecules [3,4].

Understanding the mechanisms that trigger metabolic reprogramming in cancer cells and its role in tumoral progression is crucial, not only from a biological but also from a clinical stance, since this can be the basis towards improving existing cancer therapies or developing new ones.

In this review, we discuss the role of: the crosstalk between oncogenic signaling pathways and metabolism; the influence of non-genetic factors, such as tumor microenvironment, on metabolic reprogramming of cancer and stromal cells; the changes in isoenzymes patterns as potential therapeutic targets; and the new computational tools used by a systems biology approach in drug-target and biomarker discovery based on genome-scale metabolic models (GSMMs). Finally, we also discuss the future challenges in

FUTURE SCIENCE part of fsg

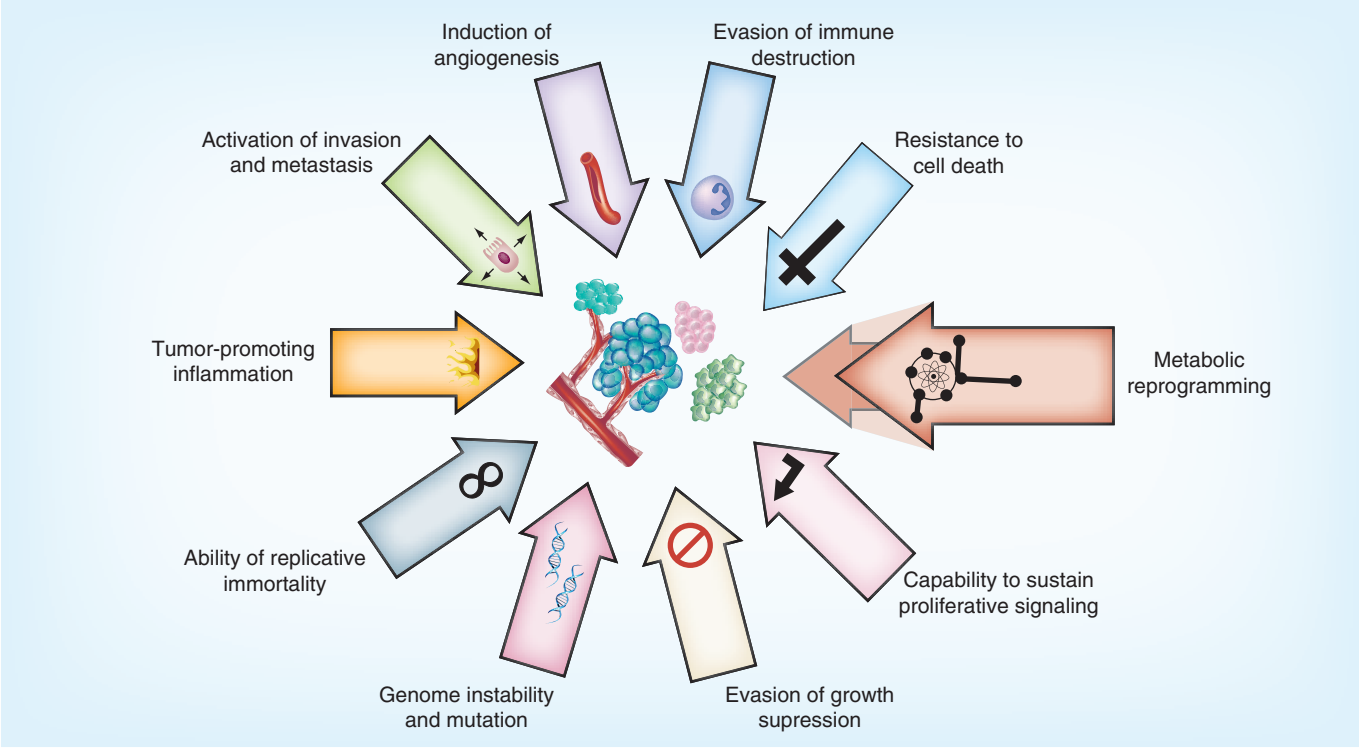

Figure 1. Hallmarks of cancer. The hallmarks of cancer comprise ten capabilities required during a multistep tumor pathogenesis to enable cancer cells to become tumorigenic and ultimately malignant. Metabolic reprogramming has been identified as an emerging hallmark and as a promising target for the treatment of cancer as there is a deregulation of bioenergetic controls and an abnormal use of metabolic pathways to sustain their biosynthetic and energetic needs.
Reproduced with permission from [2] © Elsevier.

developing new strategies and methods to drug and biomarker discovery, exploiting the reprogramming of metabolism that sustains cancer progression.

Crosstalk between oncogenic signaling events & cancer cell metabolism

Through a better understanding of the complex networks of oncogenic signaling pathways, altered cellular metabolism emerges as one of the major routes through which oncogenes promote tumor formation and progression. Many key oncogenic signaling pathways converge to adapt tumor cell metabolism in order to support their growth and survival. The identification of new metabolic coordination mechanisms between altered metabolism and regulators of cell signaling networks, controlling both proliferation and survival, triggers the interest for new metabolism-based anticancer therapies. Several oncogenes, tumor suppressor genes and cell cycle regulators controlling cell proliferation and survival are intimately involved in modulating glycolysis, mitochondrial oxidative phosphorylation (OXPHOS), lipid metabolism, glutaminolysis and many other metabolic pathways (Figure 2). The accumulation of genetic abnormalities required for oncogenesis leads to changes in energetic and biosynthetic requirements that in turn affects the metabolic signature of cancer cells through interactions between enzymes, metabolites, transporters and regulators. High-throughput sequencing data reveals that the mutational events causing tumorigenesis are much more complex than previously thought and that the mutational range can vary even among tumors with identical histopathological features [5]. Some of the metabolic adaptations driven by oncogenic signaling events have been described as common to different tumors, but metabolic profiles can be significantly tissue/cell specific [6]. Here, we will highlight some of the most prevalent examples of crosstalks between oncogenic signaling events and pivotal metabolic pathways. *HIF-1* is a key regulator that initiates

Key terms

Metabolic reprogramming: Process in which the cellular metabolism evolves in order to adapt to new environmental conditions and perturbations. In the case of tumor, the energy metabolism is reprogrammed in order to sustain the high proliferative rate of cancer cells.

Genome-scale metabolic models: Those models that summarize and codify the information known about the metabolism of an organism based on the literature and databases. These models represent the metabolic reaction encoded by an organism's genome and can be transformed into a mathematical formulation in order to study the metabolic cell behavior.

a coordinated transcriptional program activated by hypoxic stress (in response to low-oxygen conditions), to promote the metabolic shift from mitochondrial OXPHOS to glycolysis (Figure 2) through the induction of several genes, including glucose transporters and glycolytic enzymes, leading to an increased flux of glucose to lactate [7]. Additionally, *HIF-1* actively downregulates the OXPHOS flux by activation of PDK1, which inhibits the conversion of pyruvate to acetyl-CoA catalyzed by the tricarboxylic acid (TCA) cycle enzyme PDH.

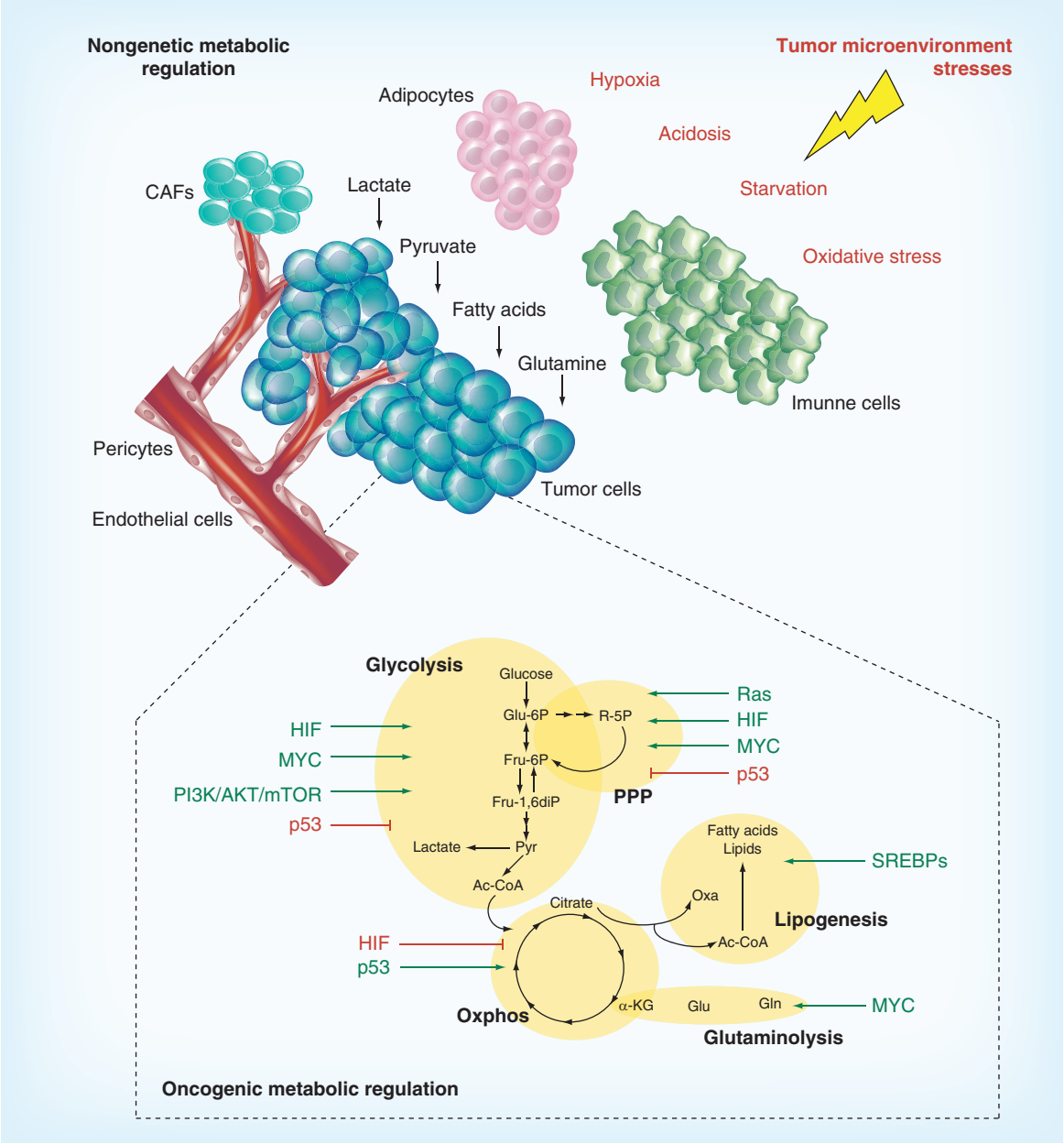

Figure 2. Nongenetic and oncogenic influences on tumor metabolic reprogramming. The nongenetic component (the tumor microenvironment) influences metabolic changes in tumor cells as a result of gradients of oxygenation and pH, nutrient availability, oxidative stress and the intercellular communication with stromal cells by means of metabolites such as lactate, pyruvate, fatty acids and glutamine. Combined with tumor microenvironment, the genetic component (oncogenes and tumor suppressors) plays a key role in metabolic reprogramming to ensure metabolites are shunted into pathways that support the energetic requirements and the biosynthesis of structural components, achieved by maintaining high rates of glycolysis and/or glutaminolysis, promoting the pentose phosphate pathway, slowing mitochondrial metabolism (oxidative phosphorylation) and utilizing tricarboxylic acid intermediates for biosynthetic precursors (e.g., fatty acids and lipids).
CAF: Cancer-associated fibroblastic cell; PPP: Pentose phosphate pathway; SREBP: Sterol regulatory element binding protein.

Similar to *HIF-1*, oncogenic activation of *Myc* also triggers a transcriptional program that enhances glycolysis by directly inducing glucose transporters and glycolytic enzymes. Indeed, there is a crosstalk between *HIF-1* and *Myc*, whereby they cooperate to confer metabolic advantages to tumor cells by oxygen-dependent mechanisms, with a difference that, contrary to *HIF-1*, *Myc* upregulation has more significant consequences for many cells as it alters not only glycolysis but also glutaminolysis (Figure 2) and many other biosynthetic pathways [8]. The *Myc* oncogene stimulates glutamine uptake and glutaminolysis by inducing glutamine transporters directly and GLS, the enzyme that converts glutamine to glutamate, indirectly [9]. Besides glycolysis, glutaminolysis is another important metabolic pathway in cancer cells, which contributes not only as a source to replenish the TCA cycle, but also to control the redox potentials through generation of reductive equivalents, such as NADPH. In addition to glucose, a vast amount of glutamine is consumed by cancer cells. Glutamine is converted to glutamate and then to α-ketoglutarate (α-KG), which feeds the TCA cycle. Some tumors that show an upregulation of glutamine metabolism have been reported to exhibit 'glutamine addiction', that is, glutamine becomes essential during rapid growth. However, glutamine consumption and addiction are dependent on the metabolic profile of the cancer cells and in particular on the oncogene/tumor suppressor involved in tumor progression [10].

Activated PI3K/AKT/mTOR pathway is one of the most common signaling cascades altered in tumor cells and this pathway is one of the most heavily targeted to develop anticancer therapies. Many cancers are driven by aberrations in the PI3K/AKT/mTOR pathway promoting metabolic transformation through multiple metabolic pathways, including an increase in glucose and amino acid uptake (Figure 2), upregulation of glycolysis and lipogenesis and enhanced protein translation through Akt-dependent mTOR activation [11].

In cancer cells, the increased rate of *de novo* lipid biosynthesis is an important aspect of the metabolic reprogramming during oncogenesis. Lipid metabolism is regulated via activation of the sterol regulatory element binding proteins (SREBPs) (Figure 2), which are important regulators of the Akt/mTOR signaling pathway [12]. Indeed, various genes coding for enzymes involved in fatty acid and cholesterol biogenesis are targets of SREBPs, including ATP-citrate lyase, acetyl-CoA carboxylase and fatty acid synthase [13]. Lipogenesis is also controlled by the *RAS* oncogene through the action of *HIF-1*, which has been reported to induce the expression of fatty acid synthase in human breast cancer cell lines [14]. However, the *RAS* oncogene also modulates mitochondrial metabolism roughly increasing the activity of *Myc* and *HIF-1* [4], glycolysis and the pentose phosphate pathway (PPP) [15]. Proliferating cells, such as tumors, require high amounts of pentose phosphates for biosynthesis of macromolecules and NADPH for redox homeostasis maintenance [16]. Therefore, PPP plays a fundamental role in defining the metabolic phenotype of tumor cells. Hence, there are also examples of coordinated crosstalk between the main enzymes that control the PPP during oncogenesis and oncogenic signaling pathways. K-RAS and PI3K signaling have been shown to positively regulate G6PD, whereas p53, which is a transcription factor and regulator of the cell cycle and apoptosis, physically interacts with G6PD to negatively modulate its activity [17], and thereby downregulates PPP. On the other hand, active *HIF-1* signaling has been linked to both TKT and TKTL1, the enzymes catalyzing the rate-limiting step of the non-oxidative branch of the PPP [18].

In addition, alterations in *p53* are frequent events in tumorigenesis. The loss or inactivation of *p53* downregulates OXPHOS by inducing aerobic glycolysis through inhibiting glucose transporters and the glycolytic enzyme PGM and inducing TP53-induced glycolysis and apoptosis regulator, a negative regulator of glycolysis [19]. On the other hand PHF20 stabilizes and upregulates p53 resulting in a gain of functionality that drives the reprogramming of the metabolism of certain cancers cell lines, such as U87 (glioblastoma) or MCF7 (breast cancer) [20].

Other examples of oncogene-mediated metabolic reprogramming include mutations in genes encoding FH and succinate dehydrogenase, which are loss-of-function mutations and behave as tumor suppressor genes [21]. On the other hand, mutations in IDH-1 and IDH-2, do not result in inactivation of normal IDH enzymatic function but generation of novel gain-of-function mutation that enables the conversion of α-KG to D2-HG, which may act as an 'oncometabolite' by inhibiting multiple α-KG–dependent dioxygenases involved in epigenetic regulation [22].

Tumorigenesis occurs as a consequence, not only of the dysregulation of numerous oncogenic pathways, but also due to many nongenetic factors, including tumor microenvironment stresses, such as hypoxia, lactic acidosis and nutrient deprivation. The integration of these nongenetic factors within the genetic framework of cancer is the next logical step in understanding

Key term

Tumor heterogeneity: Variability among different tumors in the same organ (intertumoral heterogeneity) or the variability among cells in a tumor (intratumoral heterogeneity).

tumor heterogeneity. Research over the years has elucidated the cellular and molecular interactions (including metabolic reprogramming) occurring in the tumor microenvironment and are closely linked to the processes of angiogenesis and metastasis.

Tumor microenvironment

Since the discovery of immune cells in tumor samples by Rudolf Virchow in 1863, various studies have shown the linkage of cancer to inflammation, vascularization and other conditions, which suggest that tumors do not act alone. Without its 'neighborhood' the survival of tumor cells could be a big question mark. The cellular heterogeneity in this microenvironment is complex and comprises of extracellular matrix, tumor cells and non-transformed normal cell types that co-evolve with the tumor cells (e.g., cancer-associated fibroblastic cells [CAFs], infiltrating immune cells and endothelial cells that constitute the tumor-associated vasculature) that are embedded within this matrix and nourished by the vascular network. In addition, there are many signaling molecules and chemicals, such as oxygen and protons, all of which can influence tumor cell proliferation, survival, invasion, metastasis and energy metabolism reprogramming. CAFs, one of the most abundant stromal cell types in different carcinomas, are activated fibroblasts that share similarities with fibroblasts, stimulated by inflammatory conditions or activated during wound healing. But, instead of suppressing tumor formation, CAFs can significantly promote tumorigenesis, invasion and *de novo* cancer initiation by some unique growth factors and cytokines secretion (e.g., EFG, FGF, IL6, IL8, VEGF etc), extensive tissue remodeling mediated by augmented expression of proteolytic enzymes (e.g., matrix metalloproteinases), deposition of extracellular matrix and pathogenic angiogenesis by liberating pro-angiogenic factors within the matrix [23]. Significant cell plasticity exists within this cell population, as both mesenchymal-to-epithelial and epithelial-to-mesenchymal transitions are known to occur, further enhancing stromal heterogeneity. Moreover, CAFs can enhance proliferation and invasion by inducing the epithelial-to-mesenchymal transitions on tumor cells [24,25]. Immune cell recruitment and localization in the tumor milieu vary widely in the lesions. Heterogeneity of tumor immune contexture is influenced by various factors, including those secreted by CAFs, the extension and permeability of the vasculature, and the tumor cells themselves. Importantly, macrophages comprise the most abundant immune population in the tumor microenvironment and are responsible for the production of cytokines, chemokines, growth factors, proteases and toxic intermediates, such as nitric oxide and reactive oxygen species [26]. Their contribution to tumor initiation, progression and metastasis can be attenuated by antioxidant treatments, such as butylated hydroxyanisole, as reactive oxygen species levels have been reported to regulate the differentiation and polarization state of macrophages. Endothelial cells that are 'hijacked' by the tumors play an important part in forming a transport system, although ineffective, but essential for its survival and growth. In addition, blood vessel formation needs a protein matrix for the endothelial cells to be attached to and also it needs pericytic cells to strengthen these vessels. But, since the pericytes are not known to function very well in tumor vessel formation, the vessels are always malformed and leaky [27].

In the last few years the concept of cancer stem cells (CSC), a small minority of cells in the tumor, has evolved to be a possible cause and source of tumor heterogeneity. Currently there are two models that describe tumor cell heterogeneity: the hierarchical CSC model, where self-renewing CSCs sustain the stem cell population while giving rise to progenitor cells that are not capable of self-renewal and can give rise to differentiating clones that contribute to overall tumor heterogeneity, and the stochastic (tumor microenvironment-driven). model in which cancer cells are clonally evolved, and virtually every single cell can self-renew and propagate tumors. In this model, the self-renewal capability of each cell is determined by distinct signals from the tumor microenvironment. Recent studies have suggested that tumor heterogeneity may exist in a model coordinating with both the CSC and the stochastic concepts [28].

Metabolic reprogramming associated with cancer & stromal cell interaction

Recently, the relationship between tumor microenvironment and metabolic reprogramming has been highlighted and there has been extensive research about metabolic symbiosis between cancer and stromal cells. Among these interactions, it was shown that epithelial tumor cells induce oxidative stress in the normal stroma, inducing aerobic glycolysis in CAFs, as well as changes in inflammation, autophagy and mitophagy (Figure 2). As a consequence of this rewiring in CAFs metabolism, energy-rich metabolites (such as lactate, pyruvate and ketones) are secreted, feeding adjacent cancer cells. This tumor–stroma metabolic relationship is referred to as the 'reverse Warburg effect'. CSCs that are present within the tumor also rely more heavily on glycolysis, even in the presence of oxygen (Warburg effect), and decrease their mitochondrial activity in order to limit reactive oxygen species production. As these glycolytic and mitochondrial signatures help to maintain the CSC phenotype, recent studies have

focused their attention to these metabolic weaknesses to be combined with traditional chemotherapy that, alone, usually fails to target CSCs [29,30]. In addition, other stromal cells, such as adipocytes, are able to act as energy sources, transferring fatty acids that come from lipolysis to ovarian tumor cells for β-oxidation [31]. Deregulated lipogenesis has been shown to play an important role in the interactions between cancer cells and the surrounding stromal cells. Studies suggest that it affects the epithelial cell polarity during the early stages of cancer development [32], inducing cancer cell migration [33] and activation of angiogenesis involving signaling lipids (e.g., diacyl glycerides, lysophosphatidic acid and prostaglandins), fatty acid synthesis enzymes and overof the monoglyceride-lipase [34–36].

Loss of stromal caveolin-1 in CAFs has been associated with tumor progression and metastasis [37] and causes oxidative stress and induction of autophagy, which results in increased levels of glutamine and ammonia in the stromal microenvironment. This glutamine could be consumed by cancer cells for energy and anaplerotic reactions and ammonia acts as a potent inducer of autophagy, creating a vicious cycle [37]. The migration stimulating factor, a truncated isoform of fibronectin identified to be overexpressed by CAFs and other 'activated' fibroblasts, has been shown to increase lactate production in the stromal environment and decrease mitochondrial activity, suggesting a shift towards glycolysis during hypoxia in addition to promoting tumor growth without affecting tumor angiogenesis [38].

Angiogenesis has been long known to play a major role in supporting cancer cell growth in the tumor microenvironment. But since the newly formed blood vessels are mostly defective there is always a nutrition deficiency and acidosis in these areas (Figure 2). A biomarker study in the gastric cancer environment where a quantitative analysis of the organic acids that are the end products of metabolism, using GC–MS, showed an increase in glycolytic end-products, such as pyruvic and lactic acids, with respect to normal tissues [39]. The pattern of high acidification in the tumor microenvironment due to the accumulation of glycolytic end-products results in a nutrient-deficient environment. In addition, metabolic reprogramming of tumor-associated endothelial cells has been showing up wide interests. Upon tumor angiogenic activation, endothelial cells are pushed to a state of metabolic stress for increasing their proliferation rate to form new blood vessels, although the resulting network is abnormal and inefficient. These normal cells show higher glycolytic enzyme activities and lactate production, even in the presence of oxygen [40], and they continue proliferating even in the presence of hostile conditions and high nutrient deficiency [41]. Also it has been shown that endothelial cells, similar to tumor cells, have a high expression of monocarboxylate transporter 1 required for the lactate influx, revealing that these cells seek alternative metabolites in a nutrition-deficient environment [42]. Moreover, the inhibition of glycogenolysis in human umbilical vein endothelial cells has been shown to decrease cell viability and migration, elucidating the importance of glycogen for the survival of these cells [43]. The role of the PPP in cell viability has also been demonstrated, in that, the direct inhibition of G6PDH has been shown to decrease endothelial cell survival [43]. When tumor cells choose the less energy-efficient metabolic pathways, such as glycolysis and glutaminolysis, both leading to the production of lactic acid, the pH of the tumor microenvironment decreases. It has been shown that endothelial cells behave in a similar fashion while forming new tumor blood vessels. While this phenomenon is known, it has also been found that the decrease in pH in the surrounding microenvironment actually increases cancer survival by immune suppression. Loss of T-cell function has been reported under low pH environment, while restoring the pH to normal conditions has been found to restore T-cell function [44]. Similarly, the lactic acid generated has shown to increase the proliferation of endothelial cells by increased interleukin8/CXCL8 production [41,45]. From a therapeutic point of view, targeting the altered metabolic pathways leading to lactic acid accumulation in tumor microenvironment could inhibit tumor growth as this mechanism would restore the impaired immune response and also a combinatorial therapy with antiangiogenesis drugs could reduce the proliferation of endothelial cells and formation of new blood vessels [46].

An important event that occurs during the changes in tumor microenvironment, as the cancer progresses, is the metastasis of some selected cancer cells to distant sites. A receptive microenvironment is required for tumor cells to engraft distant tissues and metastasize. Although several studies have indicated the formation of a premetastatic niche in the secondary sites before the primary tumor metastasizes [47], we have to consider how metastatic cells are able to adapt to their new metabolic environment, which can differ to a greater or lesser extent with respect to its nutrient and oxygen availability. Metastatic cells should exhibit a remarkable and dynamic flexibility that enables them to rapidly switch between metabolic states [48]. In addition, the homeostasis of the sites for metastasis can be disrupted as consequence of the metabolic activity of metastatic cells. This has been observed in bone, where metastatic prostate cancer cells secrete glutamate into their extracellular environment as a side effect of cel-

lular oxidative stress protection, promoting the development of pathological changes in bone turnover [49]. Further studies are required to analyze these metabolic interplays between metastatic cells and tumor microenvironment in order to obtain more specific treatments and therapies.

Isoenzymes: therapeutic targets in cancer

The technological advances that have occurred over the past decade and the increasing number of evidences that have emerged from previous studies show a wide array of metabolic rewiring in cancer cells. Many metabolic enzymes that are specific to important metabolic pathways and those altered in cancer cells have been identified. These enzymes have a key role in mediating the aberrant metabolism of cancer cells and could serve as a promising source of novel drug targets. Isoforms of many of these metabolic enzymes are found to be specifically expressed in tumor cells affecting important pathways of the energetic metabolism. The current research is being refocused on specifically targeting these isoforms that has shown to be a promising strategy to develop new anticancer treatments. In this part, we will highlight some of the most important, altered pathways and the specific isoenzymes, that could be used for drug targeting, in cancer disease.

Glycolytic isoenzymes

Glycolytic pathway serves as the principal energetic source for a cell. The higher dependency of cancer cells upon glycolytic metabolism for the production of ATP provides a greater motive to target glycolytic enzymes (Figure 2). Many isoforms of these enzymes have been found to be specifically expressed in tumor cells and are being exploited as potential candidates to be used as drug targets. The transport of glucose across the plasma membrane is regulated by various isoforms of glucose transporters (GLUT1–14 or SLC2A1–14). GLUT1, -3 and -4 are found to be expressed at higher levels in cancer [50]. GLUT3 and other transporters could be targeted by the use of specific antibodies or drugs, such as phloretin or ritonavir, causing the cells to starve by blocking their nutrient uptake through these transporters.

Another important metabolic enzyme of the glycolytic pathway is HK, which regulates the first rate-limiting step of glucose metabolism. Cancer cells are heavily dependent on HK isoforms, such as HK2 [51]. The specific expression of HK2 in adipose tissue and skeletal muscles provides an opportunity to target this enzyme without having the risk of affecting other tissues. Compounds such as methyl jasmonate isolated from plants have been shown to disrupt the association between mitochondria and HKs (HK1 and -2). involved in regulating apoptosis [52] and have shown to be lethal to cancer cells *in vitro* [53].

Recent publications suggest a key role of PK isoenzyme – PKM2 – in mediating the Warburg effect in cancer cells [54], proving its prospective as an enzymatic anticancer drug target. The enzyme activity of PKM2 is inhibited downstream of cellular growth signals [55]. Cell proliferation and aerobic glycolysis in tumors are greatly dependent on this ability to inhibit the activity of the PKM2 enzyme. Many approaches using small-molecule inhibitors and small-hairpin RNA-based inhibition of *PKM2* have been shown to cause cell death and slow down cell proliferation *in vitro* [54,56]. The PFKFB3 isoform is shown to be important in RAS-mediated tumors and inhibition of PFKFB3 by small-molecule inhibitors has been shown to have cytostatic effect on the growth of cancer [57]. Inhibition of LDHA using FX11 or oxamate has been shown to induce oxidative stress and cause cell death in cancer cells [58,59]. Targeting LDHA combined with NAMPT inhibitors has been shown to slow down tumor regression and thus making it a potential candidate for drug targets [59].

TCA isoenzymes/mitochondrial complex

PDK phosphorylates PDH and inhibits the conversion of pyruvate to acetyl-CoA, a key metabolite in the TCA cycle (Figure 2). Isoenzyme PDK3 is induced by upregulation of HIF-1α under hypoxic conditions and results in cells undergoing glycolysis instead of TCA for energy production. Inhibition of PDK3 increases the susceptibility of tumor cells towards anticancer drugs and causes inhibition of hypoxia-induced glycolysis [60]. Thus PDK3 could be used as a drug target to overcome drug resistance and improve chemotherapy.

Isoforms of IDH1 and -2 are found to be mutated in glioma and acute myeloid leukemia [61,62]. Mutations in IDH1 and -2 result in the overexpression of both of these enzymes and the production of 2-HG, which inhibits α-KG-dependent dioxygenase enzymes. Association between high levels of 2-HG and tumorigenicity is yet to be established, but interestingly the levels of several TCA metabolites remain unaltered, suggesting an alternate pathway that could be acting in normalizing the metabolite levels in cells with IDH1 mutations.

Isoenzymes of the PPP

Cancer cells are in a constant demand for greater amounts of purines and pyrimidines to maintain their high proliferative nature (Figure 2). The key enzyme for the oxidative PPP, the G6PDH enzyme, is overexpressed in certain types of cancers and it has been shown to transform fibroblasts and help in tumor cell

proliferation [63]. On the other hand, the overexpression of TKTL1 in many forms of cancer could increase the concentration of glyceraldehyde-3-phosphate and help in mediating the Warburg effect in cancer cells [64]. Combinatorial approach of targeting G6PDH and TKTL1 can help overcome drug resistance and may cause cell death [65].

Targeting isoenzymes of glutamine metabolism

Recent findings that point to the use of glutamine as a carbon source for the TCA cycle [66] in cancer cells encouraged researchers to consider enzymes of glutamine metabolism as potential therapeutic targets. 6-diazo-5-oxo-L-norleucine- or bis-2-(5-phenylacetamido-1,2,4-thiadiazol-2-yl)ethyl sulphide-mediated inhibition of GLS or siRNA-induced silencing of GLS and GDH have been shown to inhibit the activation of mTORC1 [67]. Thus, combinatorial targeting of GLS and GDH along with chemotherapy may prove to be more effective in cancer treatment. The differential expression of these cancer-associated isoenzymes can be used as potential biomarkers for early cancer prognosis or as enzymatic drug targets. However, the role and importance of these mutations in the reprogramming of the energetic metabolism observed in cancer cells is not always obvious. This makes it extremely difficult to evaluate the effects of these mutations in the cancer metabolism qualitatively or quantitatively. Additionally, the effects of these isoenzymes on metabolism can be attenuated or enhanced by compensatory and regulatory mechanisms. Taking into account these rationales, the need for a tool that permits a holistic analysis of the metabolic system is essential, in order to qualitatively evaluate the effects of a single or combination of different mutations within the whole metabolic network system. In the last few years, genome-scale metabolic network models have demonstrated their suitability for the integrated analysis of large and complex metabolic networks providing new clues for identifying drug targets.

GSMMs as new tools emerging from systems biology approach to drug discovery

In the previous sections, we have presented evidences that support cancer onset and that the progression relies on metabolic abnormalities to balance energy demand and biomolecular synthesis (metabolic reprogramming) [68]. GSMMs are emerging as a potential solution to decipher the molecular mechanisms underlying cancer in the context of systems biology [69]. GSMMs represent the metabolic reaction complement encoded by an organism's genome. These models are built based on the literature and databases and enable one to summarize and codify information known about the metabolism of an organism.

Over 100 GSMMs have been built for different species, ranging from archea to mammals [70–84]. Reconstructions of human metabolism, such as Recon1 [81], Edinburgh Human Metabolic Network [82] or the most recent reconstructions of human metabolism, Recon2 [83], are widely used to study the mechanism of diseases with a strong metabolic component, such as cancer or diabetes [85–88].

This systems biology tool enables the mathematical representation of biotransformations and metabolic processes occurring within the organism and offers an appropriate framework to integrate the increasing amount of 'omic' data generated by the different high-throughput technologies.

The transformation into a mathematical formulation is mostly driven by constraint-based modeling (CBM) [89] and allows the systematic simulation of different phenotypes, environmental conditions, gene deletion and so on. This approach allows for modeling the complexity of cancer metabolism and tackling more problematic biological questions, such as the role of metabolism in cancer disease [90].

Genome-scale constraint-based metabolic models have been used for a variety of applications, involving studies on evolution [91], metabolic engineering [92–94], genome annotation [95] or drug discovery [96], with a high relevance in cancer research.

Indeed, GSMMs can efficiently capture the complexity of cancer metabolism in a holistic manner and permit to improve existing therapies or develop new ones [97].

In this chapter we discuss methods for building GSMMs and computational approaches to analyze and integrate 'omic' data into these large-scale metabolic network models. Finally, we introduce some of the most relevant softwares and algorithms developed for drug-target discovery that can be used in cancer research.

GSMM reconstruction

Genome-scale metabolic reconstructions are created in a bottom-up manner based on genomic and bibliomic data and, thus, represent a biochemical, genetic and genomic knowledge base for the target organism [81–83]. However, to date we are still not able to completely and automatically reconstruct high-quality metabolic networks (Figure 3A) [98]. Genome-scale reconstruction starts with the generation of a draft,

Key term

Enzymatic drug target: A component in a metabolic pathway to which some other entity, such as a drug, is directed and/or binds.

automated reconstruction based on the genome annotation and biochemical databases of the target organism. This task can be achieved by using software tools, such as Pathways tool [99]. The genomic sequence of the targeted organism is coupled with the most recent annotations available from databases [100], such as GOLD or NCBI Entrez Gene databases [101,102].

Metabolic reactions can be associated with the annotated metabolic genes by using enzyme commission (E.C.), ID and biochemical reaction databases (e.g., KEGG [103] and BRENDA [104]). This process permits both linking metabolic genes with their corresponding encoded enzymes and determining the stoichiometric relationship of metabolic reactions with the metabolites and cofactors that they consume and/or produce.

The gene–protein-reaction association (GPR). is represented as Boolean relationships in which isoenzymes that catalyze the same reaction have an "OR" relation (only one of the genes that encode the different isoenzymes is required to have the reaction active) and the complexes that catalyze a reaction have an "AND" relation (all the genes that encode the different complex subunits are necessary to have the reaction active) [81]. GPR associations enable the mapping of transcriptomics or proteomics to the level of reactions.

Reactions can be located into different subcellular compartments based on protein location [81]. Reaction directionality can be determined from thermodynamic data. Additionally, artificial reactions, such as biomass reaction that define the ratio at which biomass constituents are produced (nucleic acids, lipid, proteins, etc) or exchange reactions that define the overall rate of nutrients consumption or production, are also defined in the reconstruction. These artificial reactions are necessary to predict or impose certain phenotypic conditions on the mathematical model.

Next, it is necessary to manually curate and refine the draft, automated reconstruction. The main objective of curation is to identify and correct incomplete or erroneous annotation, add reactions that occur spontaneously and remove gaps and metabolites that cannot be produced or consumed [81] through search on the literature and other databases.

Once the model is curated, it is evaluated and validated in an iterative fashion by using mathematical tools [105]. The aim of the validation process is to evaluate if the model is stoichiometrically balanced, find gaps in the network and search for candidate reactions for gap filling, quantitative evaluation of biomass precursor production and growth rate, compare predicted physiological properties with known properties and determine the metabolic capabilities of the model.

It is worth noting that once a GSMM has been constructed, it can be used in future reconstructions in order to expand and refine the model [81,83].

Constraint-based methods as tools for tumor metabolism characterization

As was previously mentioned, GSMMs include stoichiometric details for the set of known reactions in a given organism. These large scale metabolic models require computational methods to be qualitatively analyzed. Traditionally, approaches based on ordinary differential equation have been used for characterization of dynamic cell states. However, this full-scale dynamic modeling is frequently infeasible for large-scale networks because of a paucity of necessary parameter values.

Constraint-based methods (CBMs) permit the analysis of large-scale biochemical systems under conditions where kinetic parameters need not be defined (steady state). Genome-scale constraint-based metabolic models can be used to predict or describe cellular behaviors, such as growth rates, uptake/secretion rate or intracellular fluxes [89]. Flux balance analysis (FBA) is one of the most widely used CBMs for the study of biochemical networks. The variables used in FBA include the fluxes through transport and metabolic reactions and model parameters include reaction stoichiometry, biomass composition, ATP requirements and the upper and lower bounds for individual fluxes, which define the maximum and minimum allowable fluxes of the reactions.

The first step in FBA is the mathematical representation of the metabolic reactions in the form of a numerical matrix, with stoichiometric coefficients of each reaction (stoichiometric matrix), where the metabolites are represented in rows and reactions in columns. FBA employs mass actions formalism for the mathematical representation of the metabolic networks: $dC/Dt = S.v.$, where v and C are vectors of reaction fluxes and metabolite concentration respectively, t is time and S is the stoichiometric matrix (Figure 3A).

The next step is to impose constraints to the metabolic network. Constraints are fundamentally represented in two ways:

- Steady-state mass-balance imposes constraints on stoichiometry and network topology on the metabolic fluxes through the network. Additionally, steady state assumption also imposes constraints that narrow the space of solutions. By definition, the change in the concentration of a certain metabolite over time at steady state is 0: $dC/Dt = 0$, thus: $S.v = 0$. These constraints ensure that for each metabolite in the network the net production rate equals the net consumption rate;

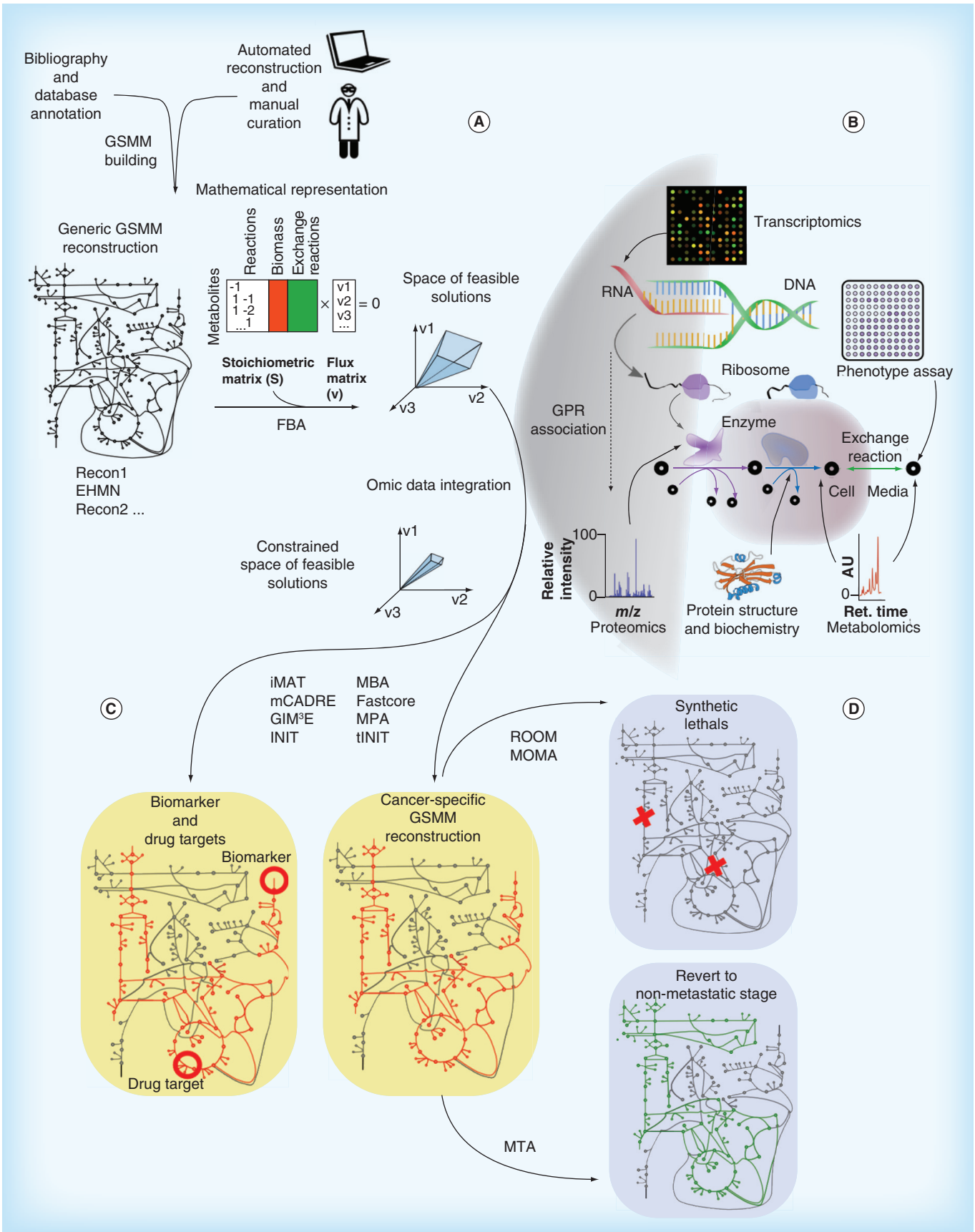
Bibliography and database annotation
Automated reconstruction and manual curation
GSMM building
Mathematical representation
Generic GSMM reconstruction
Reactions
Biomass
Exchange reactions
Metabolites
Stoichiometric matrix (S)
Flux matrix (v)
FBA
Space of feasible solutions
Recon1
EHMN
Recon2 ...
Omic data integration
Constrained space of feasible solutions
A
B
Transcriptomics
RNA
DNA
Ribosome
Phenotype assay
GPR association
Enzyme
Exchange reaction
Cell
Media
Relative intensity
m/z
Proteomics
Protein structure and biochemistry
AU
Ret. time
Metabolomics
C
iMAT
mCADRE
GIM³E
INIT
MBA
Fastcore
MPA
tINIT
ROOM
MOMA
D
Synthetic lethals
Biomarker and drug targets
Biomarker
Drug target
Cancer-specific GSMM reconstruction
Revert to non-metastatic stage
MTA

Figure 3. Genome-scale metabolic model building and analysis (facing page). (A) GSMM reconstruction starts with a draft automated version based on literature and databases, finally this version is manually curated in order to refine the model. Typically, these models are analyzed by using flux balance analysis, assuming steady state. **(B)** GSMMs can be used as a platform to integrate and combine omic data from multiple layers. In these models, metabolomics data can be associated with metabolites, while genomics, transcriptomics and proteomics can be associated with metabolic reactions, these associations are established through gene–protein-reaction associations. The phenotypic assays can constrain properties of the network, such as growth rate under certain experimental conditions. **(C)** By integrating omic data into a GSMM we can determine either tumor-specific biomarkers or anticancer drug-targets and reconstruct cancer-specific GSMM. **(D)** Cancer-specific reconstructions can be used to determine synthetic lethals specific for each cancer type for which the non-tumor cells are insensitive (ROOM and MOMA methods), Additionally if we reconstruct an initial GSMM describing metastatic phenotype and a target GSMM describing non-metastatic phenotype we can determine the actors that would permit to revert the metastatic phenotype into a non-metastatic one (MTA method).
FBA: Flux balance analysis; GSMM: Genome-scale metabolic model; Ret.: Retention.

- Inequalities that impose bounds on the system: every reaction can also be given upper and lower bounds. These restrictions are based on measured rates (e.g., metabolite uptake/secretion rates) or reaction reversibility (e.g., irreversible fluxes have a zero lower bound) and are used to define the environmental conditions in a given simulation, such as nutrient or O_2 availability, which can be related with a specific tumor microenvironment or stages in tumor progression.

Finally it is necessary to define a phenotype in the form of a biological objective that is relevant to the problem being studied (objective function). Typically, objective functions are related to growth rate prediction. GSMMs define this phenotype by an artificial biomass production reaction, that is, the rate at which metabolic compounds are converted into biomass constituents (nucleic acids, lipid, proteins, etc). The biomass reaction is based on experimental measurements of biomass composition and is unique for each organism or cell type. Thus, an objective function could be the maximization of growth rate that can be accomplished by calculating the set of metabolic fluxes that result in the maximum flux through biomass production reaction. Since uncontrolled cell growth is the basis of tumor progression, this approach is widely used in the simulation of cancer cell metabolism. The objective function can be adapted to the specific cell type or organism; however, the objective that better defines our case of study is not always obvious, especially in multicellular organisms [106].

Taken together, the mathematical representation of the metabolic reactions and of the objective function, is defined as a system of linear equations that are solved by a number of algorithms and software developed for this purpose [105]. Predictions of values for these fluxes are obtained by optimizing for an objective function, while simultaneously satisfying constraint specifications.

Omic data integration

The advent of high-throughput technologies have transformed molecular biology into a data-rich discipline by providing quantitative data for thousands of cellular components across a wide variety of scales. However, extraction of 'knowledge' from this ocean of omic data has been challenging [107]. GSMMs have emerged as an advantageous platform for the integration of omic data (e.g., [108]; Figure 3B). In this framework cellular and molecular phenotypes are simulated allowing the development of biological hypotheses and discoveries [109]. Metabolic reconstruction of the human metabolism has been successfully used for a variety of analyses of omic data, including applications in data visualization [110], deducing regulatory rules [111], network medicine [112], constructing tissue-specific models [113] or multicellular modeling [114]. Thus, omic data can be used to further constrain the non-uniqueness of constraint-based solutions space and thereby enhance the precision and accuracy of model prediction (Figure 3A–C) [109]. To achieve this aim a number of FBA-driven algorithms that integrate omic data into GSMMs have been developed. Table 1 highlights some of the most relevant approaches recently developed to incorporate experimental omic data into GSMMs [86,87,113,115–117]

Drug-target & biomarker discovery

Cancer cells maintain their high proliferation rate by adapting their metabolism based on the environmental conditions, such as pH, O_2 availability, vascularization or nutrient availability [118]. The elucidation of diverse metabolic alterations for the identification of biomarkers and novel drug targets has, therefore, been increased in recent years. An increasing number of methods and algorithms have been recently developed to integrate tumor-specific omic data into GSMMs. It has enabled the gain of further biological and mechanistic understanding of how cancer benefits from metabolic modifications [90]. This model-driven approach allows the discovery

Key term

Omic data integration: Computational process in which multi-omic data obtained from different high-throughput technologies, considering different aspects of the molecular biology, are integrated into genome-scale metabolic models in order to unveil emergent properties of the biological systems.

Table 1. Computation method for integrating omic data into global-scale metabolic models.

Name	Input	Description	Ref.
iMAT	Gene expression data	Seeks to maximize the similarity between the gene expression and the metabolic profiles	[115]
mCADRE	Gene expression and metabolomic data	Uses tissue-specific data to identify a set of core reactions. Seeks to build a consistent network using all the core reactions and the minimum number of non-core reactions	[86]
GIM^{3}E	Gene expression and metabolomic data	Builds a network that satisfies an objective function while penalizing the inclusion of reactions catalyzed by genes with expression below a certain threshold. It can be further constrained to produce certain metabolites based on experimental evidences	[116]
INIT	Gene expression and metabolomic data	Seeks to build a model prioritizing the addition of reactions with strong evidence of their presence based on gene expression data. Can be forced to produce metabolites that have been detected experimentally	[87]
MBA	Transcriptomic, proteomic, metabolomic, bibliomic data	Uses tissue-specific data to identify high and moderate probability core reactions. Seeks to build a network with all the high-probability core reactions, the maximum moderate probability core reactions and the non-core reaction required to prevent gaps	[113]
Fastcore	Transcriptomic, proteomic, metabolomic, bibliomic data	Identify a set of core reactions based on tissue-specific data. Seeks to build a network that contains all reactions from the core set with the minimum set of additional reactions necessary	[117]

of potential biomarkers and drug targets [87,97,119]. The identification of new biomarkers is of major importance to biomedical research for early diagnosis and monitoring treatments efficiently. The identification of cancer biomarkers is possible due to aberrant metabolism of tumors that alters the profile of absorption and nutrients secretion.

Omic data of clinical samples (mainly transcriptomics data) can be used to infer the exchange rates of different metabolites for each individual sample via GSMM analysis (alterations in exchange reactions in the model). Thus, those metabolites that significantly differ between two clinical groups in their exchange rates are then considered as potential biomarkers. However, this task is especially challenging in the case of cancer owing to metabolic abnormalities resulting from complex and elaborate genetic and epigenetic alterations that modify the expression of a variety of cancer-associated isoenzymes. In order to determine potential biomarkers in cancer, several computational approaches has been developed. For example, the metabolic phenotypic analysis (MPA) method uses GPR association to integrate transcriptomic and proteomic data within a GSMM to infer metabolic phenotypes [88]. MPA was used to study breast cancer metabolism and predict potential biomarkers. These predictions, wich include amino acid and choline-containing metabolites, are supported by a number of experimental evidences [120]. Another recently developed algorithm is mCADRE, which has been used to systematically simulate the metabolic function of 26 cancer cell types (among other cell types) [86]. This algorithm has been able to identify several pathways, such as folate metabolism, eicosanoid metabolism, fatty acid activation and nucleotide metabolism, that are enriched in tumor tissue compared with their corresponding normal tissue. Many enzymes involved in these pathways are already used as chemotherapy targets. Other approaches, such as flux variability analysis [121] or sampling analysis [122], are also suitable to predict metabolic biomarker candidates by integrating omic data into a GSMM. The novel drug discovery is based on the abnormalities existing in various reactions/pathways of cancer metabolism. These differences can be used as drug targets to attack specific weaknesses of the tumor and hence compromising its viability, but not that of non-cancerous cells [123]. For example, the INIT method [87] was used to identify characteristic metabolic features of cancer cells by inferring the active metabolic network of 16 different cancer types and compare them with the healthy cell types where they come from. These metabolic differences may play an important role in proliferation of cancer cells and could be potential drug targets. This method found

significant differences in polyamine metabolism, the isoprenoid biosynthesis and the prostaglandins and leukotrienes pathways in cancer cells compared with healthy cells. Some of the reactions that were found that have different activity in cancer cells, are already used in the clinical practice as therapeutic targets [124,125]. Based on the rationale that the differences between normal and tumoral cells can be potential therapeutic targets, several approaches have been developed that consider different aspects of cancer metabolism for the discovery of new drug targets:

Antimetabolite

One of the most common anticancer drugs are antimetabolites. An antimetabolite is structurally similar to a certain metabolite but it cannot be used to produce any physiologically important molecule. Antimetabolite-based drugs act on key enzymes preventing the use of endogenous metabolites, resulting in the disruption of the robustness of cancer cells and reduction or suppression of cell growth. For example, antimetabolites, such as antifolates or antipurines, mimic folic acid and purines [126]. The GSMM approach can be used to systematically simulate the effect of potential antimetabolites in cancer research. To achieve this, methods such as the tINIT (Task-driven Integrative Network Inference for Tissues) algorithm have been developed [97]. This method has been used to reconstruct personalized GSMMs for six hepatocellular carcinoma patients based on proteomics data and the Human Metabolic Reaction database [87] and identify anticancer drugs that are structural analogs to targeted metabolites (antimetabolites). The tINIT algorithm was able to identify 101 antimetabolites, 22 of which are already used in cancer therapies and the remaining can be considered as new potential anticancer drugs.

Synthetic lethal

The genetic lesions occurring in cancer not only promote the oncogenic state but are also associated with dependencies that are specific to these lesions and absent in non-cancer cells. Two genes are considered 'synthetic lethal' if the isolated mutation on either of them is compatible with cell viability but the simultaneous mutation is lethal [127]. Analogously, two genes are considered to interact in a 'synthetic sick' fashion, if simultaneous mutation reduces cell fitness below a certain threshold without being lethal [127].

Enzymes encoded by genes that are in synthetic lethal or sick interactions with known, non-druggable cancer-driving mutations can be potential anticancer drug targets. This approach has two main advantages: first, we can indirectly target non-druggable cancer-promoting lesions by inhibiting druggable synthetic lethal interactors and secondly we can achieve a high selectivity by exploiting true synthetic lethal interactions for anticancer therapy. This is especially remarkable in the case of cancer-specific isoenzymes, which are emerging as one of the most promising anticancer drug targets. GSMMs provide an excellent tool for the systematic simulation of specific pairs of gene knock-out (KO) to unveil those combinations that compromise the viability of cancer cells (synthetic lethal). By definition, gene KO is simulated by giving value zero to gene expression and the effect of gene deletion is transferred to the metabolic reaction level by GPR association. Thus, for instance, the flux through a reaction that is associated only to one knocked-out gene would be zero. If the reaction is catalyzed by isoenzymes or complexes, the effect of a gene deletion is more complex.

However, predicting the metabolic state of a cell after a gene KO is a challenging task, because after the gene KO the system evolves into a new steady-state that tends to be as close as possible to the original steady-state [128]. To overcome these difficulties several algorithms have been developed. For example, the MOMA algorithm minimizes the euclidean norm of flux differences between metabolic states of the KO compared with the wild type [129]. The ROOM method minimizes the total number of significant flux changes from the wild type flux distribution [129].

In other words, MOMA minimizes the changes in the overall flux distribution while ROOM minimizes the number of fluxes to be modified after the gene KO (Figure 3D). As an example of employing the concept of synthetic lethality in cancer, a GSMM approach has been used to develop a genome scale network model of cancer metabolism [119]. The model predicted 52 cytostatic drug targets (40% of which were known) and further predicted combinations of synthetic lethal drug targets, which were validated using NCI-60 cancer cell collection. In a remarkable example, synthetic lethality between heme oxygenase and fumarate hydratase was predicted by the GSMM approach and was also experimentally validated [130]. The number and the quality of these predictions prove the capabilities of this approach to identify synthetic lethal pairs of genes as potential novel drug target in cancer.

Future perspective

Metabolism represents the essence of how cells interact with their environment to provide themselves with energy and the essential building blocks for life. In this review, we highlighted the role of a wide range of factors that trigger the malignant transformation of cancer metabolism as well as experimental and computational approaches to develop new therapies. Despite the encouraging achievements and improvements in cancer

research, there still exist limitations that need to be overcome in order to enhance the effectiveness of drug therapies in cancer disease.

One of the major challenges in targeting key metabolic pathways is the lack of clear understanding of how the cancer cell metabolic profile varies from a non-tumor proliferating cell and the potential toxicity risk associated with targeting metabolism. A better understanding of how the metabolism differs in a specific type of cancer or within the same type may help us predict and identify targets without affecting non-tumor cells. In this context, combination of metabolic and signaling pathway inhibitors has been proposed as one of the rational approaches [131]. Using computational approaches permits the systematic simulation of gene perturbations, either metabolic and/or non-metabolic, that could contribute to unveil novel key signaling nodes resulting in potential anticancer drug targets. Recently developed algorithms, such as PROM [111], allow the integration of transcriptomic data into GSMMs while considering the gene regulatory network structure of a given organism. This approach has been developed for predicting metabolic changes that result from genetic or environmental perturbation in *Escherichia coli*. However, it is obvious that algorithms accounting for both gene regulatory and metabolic networks could be used to analyze more precisely the effect of perturbations on oncogenes in cancer metabolism.

Tumor heterogeneity represents a hurdle that must be overcome in order to develop new and more efficient anticancer therapies. One of the factors triggering intratumoral heterogeneity is the tumor microenvironment, which interferes with the ability of drugs to penetrate tumor tissue and reach the entire tumor cells in a potentially lethal concentration. In addition, heterogeneity within the tumor microenvironment leads to marked gradients in the rate of cell proliferation and to regions of hypoxia and acidity, all of which can influence the sensitivity of the tumor cells to drug treatment. Better understanding of how tumor microenvironment protects cancer cells, during and immediately after chemo- or radiotherapy is imperative to design new therapies aimed at targeting this tumor-protective niche [132,133]. The use of drug delivery systems can improve the pharmacological properties of traditional chemotherapeutics by altering pharmacokinetics and biodistribution to overcome the harsh conditions of the tumor microenvironment. Moreover, the co-administration of chemotherapeutics and tumor-associated stromal-depleting drugs helps to target the fibrous structure of the modified extracellular matrix, which can result in a less penetrable tumor microenvironment [134].

Another interesting approach considers therapies that interfere in the metabolic co-operation between cancer cells and stromal cells in their microenvironment [135] or between intratumoral subpopulations. The study of the metabolic coupling between different cellular populations as potential drug targets can be achieved by reconstructing an artificial tumor microenvironment by using GSMMs approach. To date several algorithms have been developed that integrate omic data into a GSMM reconstruction that permit to compute the secretion and uptake rates of nutrients (Table 1) and hence study the complementary secretomes within a heterogeneous cellular community. However, test and validation of a metabolic model becomes more complex if it considers a heterogeneous cellular population. Nevertheless, recent studies on artificial microbial ecosystems have demonstrated the potential of this type of approach to study synergies in heterogeneous cellular communities [136] that could be extrapolated to the study of cancer to unveil the mechanisms underlying the cooperation between tumoral and stromal cells, as well as between intratumoral subpopulations.

The intratumoral microenvironment also confers an extreme flexibility and adaptation capability to cancer cells that enhances tumor progression and represents a challenge for target-directed therapies [137]. The intratumoral heterogeneity is driven by two main processes: epithelial-to-mesenchymal transitions, by which epithelial cells gain invasive properties and lose at least part of their epithelial phenotypes [138]; and mesenchymal-to-epithelial transitions, by which mesenchymal cells can revert to an epithelial gene program displaying strong self-renewal and survival properties [138–140]. Drug targets that repress these processes have been proposed to significantly reduce tumoral progression.

Anti-angiogenic therapy has been proposed for a long time as an interesting approach to reduce tumor growth. Tumor blood vessels are surrounded by a very hostile environment, with a high amount of acidosis, low oxygen regions, weak pericyte–endothelial cell interaction, leading to its tortuous and leaky vessels with gaps that allow easy escape of invading tumor cells [141,142]. Additionally, restoring the blood vessels to a 'normal' state would get the tumor vessels back on track to its proper functional form, reducing hypoxia-induced metastasis and improving the effects of chemotherapy [143,144]. Also it is expected to reduce the spreading of cancer cells, because pericytes that are required to strengthen blood vessels would be acting more efficiently and hence prevent the intravasation of the cancer cells through the gaps found in the normally leaky tumor vessels.

Therapies based on both metastatic targets arresting cancer cells in a non-metastatic stage and angiogenic targets normalizing tumor vessels are promising strategies to design new anticancer therapies. Coupling

this strategy with associated key metabolic pathways is a good approach in cancer treatment and requires computational tools to identify the putative targets. Recently developed methods, such as the 'metabolic transformation algorithm' allows the identification of the actors involved in metabolic transformations [145]. This methodology identifies targets that alter the metabolism retrieving the cells back from a given metabolic state to another metabolic state (Figure 3D). This method has been successfully used to find drug targets that revert disrupted metabolism focused on aging. However, this approach could be suitable to determine drug targets arresting tumor in a non-metastatic stage, normalize tumor vessels or prevent tumor intravasation, resulting in a reduction of tumor progression. Additionally, GSMM predictions could be refined by integrating information from dynamic ^{13}C FBA [146].

Moreover, combinatorial therapies, targeting angiogenesis and metastatic targets, have been proposed as a way to enhance anticancer therapies [27]. Traditionally, these approaches has been focused on targeting signaling pathways, such as the VEGF inhibition or VEGF receptors (R1/R2) blockade [147,148] and CXCR4 protein, which is involved in tumor colonization, or the cytokine PIGF, which prepares the metastatic niche in bone marrow for the cells invading from breast cancer [149]. However, studies on the metabolic reprogramming in endothelial cells have opened new avenues to explore the combinatorial therapies of targeting both tumors and their angiogenesis, in the context of metabolism.

The approaches reviewed here provide a guideline to improve the anticancer drug-target therapies focused on metabolic reprogramming. However, the lack of a proper model depicting the complete map of metabolic reactions, regulatory processes as well as tumor heterogeneity and synergistic cooperation between cellular

Key term

Combinatorial therapies: Strategy that takes profit of the synergistic effects of two therapeutic treatments targeting different processes of the cellular biology.

Executive summary

Background

- Nowadays, it is widely recognized that metabolic reprogramming is essential to sustain tumor progression. These changes are promoted by genetic and epigenetic alterations producing mutations in key metabolic enzymes that modify flux distributions in metabolic networks, providing advantages to cancer cells in terms of energy production and synthesis of biomolecules.

Crosstalk between oncogenic signaling events & cancer cell metabolism

- Many key oncogenic signaling pathways, such as *HIF*, *Myc*, PI3K/AKT/mTOR or SREBPs, converge to adapt tumor cell metabolism in order to support their growth and survival. They are intimately involved in modulating glycolysis, mitochondrial oxidative phosphorylation, lipid metabolism and glutaminolysis.

Tumor microenvironment

- The tumor microenvironment is complex and comprises the extracellular matrix, tumor and stromal cells (e.g., epithelial cells, fibroblasts and inflammatory cells) that are embedded within this matrix and nourished by vascular network. The tumor heterogeneity, signaling molecules and chemicals, such as oxygen and protons, can influence tumor cell proliferation, survival, invasion, metastasis and energy metabolism reprogramming.

Isoenzymes: therapeutic targets in cancer

- Isoforms of many of the enzymes specific to important metabolic pathways are found to be overexpressed in tumor cells affecting important pathways of the energetic metabolism. These isoforms have a key role in mediating the aberrant metabolism of cancer cells and could serve as a promising source of novel drug targets.
- These tumor-specific isoforms can be involved in important pathways, such as glycolysis, tricarboxylic acid cycle, pentose phosphate pathway and glutamine metabolism, among other important energetic pathways

Genome-scale metabolic models as new tools emerging from systems biology approach to drug discovery

- Genome-scale metabolic models are emerging as a potential solution to decipher the molecular mechanisms underlying cancer in the context of systems biology. These models represent the metabolic reactions encoded by an organism's genome and summarize and codify information known about the metabolism of that organism.
- These models use constraint-based methods for the mathematical representation of biotransformations and metabolic processes occurring within the organism and offer an appropriate framework to integrate the increasing amount of 'omic' data generated by the different high-throughput technologies.
- Genome-scale metabolic models approaches have allowed to identify a number of tumor-specific biomarkers, anticancer drug-target and synthetic lethal genes opening a promising avenue in the development of new anticancer therapies.

communities, makes selecting the best possible target combinations difficult. Thus, in order to develop more efficient anticancer therapies, more efforts need to be made in developing new methods to study tumor metabolism and obtain a better understanding of the molecular processes underlying tumor progression and invasion.

Financial & competing interests disclosure

This work was supported by funds of European Commission METAFLUX (Marie Curie FP7-PEOPLE-2010 ITN-264780); Spanish Government and European Union FEDER Funds (SAF2011–25726); and Generalitat de Catalunya (2014SGR-1017 and Icrea Academia award 2010 granted to M Cascante). The authors have no other relevant affiliations orfinancial involvement with any organization or entity with a financial interest in or financial conflict with the subject matter or materials discussed in the manuscript. This includes employment, consultancies, honoraria, stock ownership or options, expert testimony, grants or patents received or pending, or royalties.

No writing assistance was utilized in the production of this manuscript.

References

1 Siegel R, Naishadham D, Jemal A. Cancer statistics, 2012. *CA Cancer J. Clin.* 62(1), 10–29 (2012).

2 Hanahan D, Weinberg RA. Hallmarks of cancer: the next generation. *Cell* 144(5), 646–674 (2011).

3 Ward PS, Thompson CB. Metabolic reprogramming: a cancer hallmark even warburg did not anticipate. *Cancer Cell* 21(3), 297–308 (2012).

4 Vander Heiden MG, Cantley LC, Thompson CB. Understanding the Warburg effect: the metabolic requirements of cell proliferation. *Science* 324(5930), 1029–1033 (2009).

5 Stratton MR. Exploring the genomes of cancer cells: progress and promise. *Science* 331(6024), 1553–1558 (2011).

6 Yuneva MO, Fan TW, Allen TD *et al.* The metabolic profile of tumors depends on both the responsible genetic lesion and tissue type. *Cell Metab.* 15(2), 157–170 (2012).

7 Obacz J, Pastorekova S, Vojtesek B, Hrstka R. Cross-talk between HIF and p53 as mediators of molecular responses to physiological and genotoxic stresses. *Mol. Cancer* 12(1), 93 (2013).

8 Dang CV. Links between metabolism and cancer. *Genes Dev.* 26(9), 877–890 (2012).

9 Wise DR, Deberardinis RJ, Mancuso A *et al.* Myc regulates a transcriptional program that stimulates mitochondrial glutaminolysis and leads to glutamine addiction. *Proc. Natl Acad. Sci. USA* 105(48), 18782–18787 (2008).

10 Pecqueur C, Oliver L, Oizel K, Lalier L, Vallette FM. Targeting metabolism to induce cell death in cancer cells and cancer stem cells. *Int. J. Cell Biol.* 2013, 805975 (2013).

11 Dan HC, Ebbs A, Pasparakis M, Van Dyke T, Basseres DS, Baldwin AS. Akt-dependent activation of mTORC1 Involves phosphorylation of mTOR by IKKalpha. *J. Biol. Chem.* 289(36), 25227–25240 (2014).

12 Porstmann T, Santos CR, Griffiths B *et al.* SREBP activity is regulated by mTORC1 and contributes to Akt-dependent cell growth. *Cell Metab.* 8(3), 224–236 (2008).

13 Alvarez MS, Fernandez-Alvarez A, Cucarella C, Casado M. Stable SREBP-1a knockdown decreases the cell proliferation rate in human preadipocyte cells without inducing senescence. *Biochem. Biophys. Res. Commun.* 447(1), 51–56 (2014).

14 Furuta E, Pai SK, Zhan R *et al.* Fatty acid synthase gene is up-regulated by hypoxia via activation of Akt and sterol regulatory element binding protein-1. *Cancer Res.* 68(4), 1003–1011 (2008).

15 Cascante M, Benito A, Zanuy M, Vizan P, Marin S, De Atauri P. Metabolic network adaptations in cancer as targets for novel therapies. *Biochem. Soc. Trans.* 38(5), 1302–1306 (2010).

16 Doherty JR, Yang C, Scott KEN *et al.* Blocking lactate export by inhibiting the MYC target MCT1 disables glycolysis and glutathione synthesis. *Cancer Res.* 74(3), 908–920 (2014).

17 Jiang P, Du W, Wang X *et al.* p53 regulates biosynthesis through direct inactivation of glucose-6-phosphate dehydrogenase. *Nat. Cell Biol.* 13(3), 310–316 (2011).

18 Bentz S, Cee A, Endlicher E *et al.* Hypoxia induces the expression of transketolase-like 1 in human colorectal cancer. *Digestion* 88(3), 182–192 (2013).

19 Sinthupibulyakit C, Ittarat W, St Clair WH, St Clair DK. p53 protects lung cancer cells against metabolic stress. *Int. J. Oncol.* 37(6), 1575–1581 (2010).

20 Cui G, Park S, Badeaux AI *et al.* PHF20 is an effector protein of p53 double lysine methylation that stabilizes and activates p53. *Nat. Struct. Mol. Biol.* 19(9), 916–924 (2012).

21 Xiao M, Yang H, Xu W *et al.* Inhibition of α-KG-dependent histone and DNA demethylases by fumarate and succinate that are accumulated in mutations of FH and SDH tumor suppressors. *Genes Dev.* 26(12), 1326–1338 (2012).

22 Xu W, Yang H, Liu Y *et al.* Oncometabolite 2-hydroxyglutarate is a competitive inhibitor of alpha-ketoglutarate-dependent dioxygenases. *Cancer Cell* 19(1), 17–30 (2011).

23 Commandeur S, Ho SH, De Gruijl FR, Willemze R, Tensen CP, El Ghalbzouri A. Functional characterization of cancer-associated fibroblasts of human cutaneous squamous cell carcinoma. *Exp. Dermatol.* 20(9), 737–742 (2011).

24 Zhou B, Chen WL, Wang YY *et al.* A role for cancer-associated fibroblasts in inducing the epithelial-to-mesenchymal transition in human tongue squamous cell carcinoma. *J. Oral Pathol. Med.* 43(8), 585–592 (2014).

25 Yu Y, Xiao CH, Tan LD, Wang QS, Li XQ, Feng YM. Cancer-associated fibroblasts induce epithelial-mesenchymal transition of breast cancer cells through paracrine TGF-[beta] signalling. *Br. J. Cancer* 110(3), 724–732 (2014).

26 Zhang Y, Choksi S, Chen K, Pobezinskaya Y, Linnoila I, Liu ZG. ROS play a critical role in the differentiation of alternatively activated macrophages and the occurrence of tumor-associated macrophages. *Cell Res.* 23(7), 898–914 (2013).

27 De Bock K, Mazzone M, Carmeliet P. Antiangiogenic therapy, hypoxia, and metastasis: risky liaisons, or not? *Nat. Rev. Clin. Oncol.* 8(7), 393–404 (2011).

28 Wang W, Quan Y, Fu Q *et al.* Dynamics between cancer cell subpopulations reveals a model coordinating with both hierarchical and stochastic concepts. *PLoS ONE* 9(1), e84654 (2014).

29 Feng W, Gentles A, Nair RV *et al.* Targeting unique metabolic properties of breast tumor initiating cells. *Stem Cells* 32(7), 1734–1745 (2014).

30 Ciavardelli D, Rossi C, Barcaroli D *et al.* Breast cancer stem cells rely on fermentative glycolysis and are sensitive to 2-deoxyglucose treatment. *Cell Death Dis.* 5, e1336 (2014).

31 Nieman KM, Kenny HA, Penicka CV *et al.* Adipocytes promote ovarian cancer metastasis and provide energy for rapid tumor growth. *Nat. Med.* 17(11), 1498–1503 (2011).

32 Willemarck N, Rysman E, Brusselmans K *et al.* Aberrant activation of fatty acid synthesis suppresses primary cilium formation and distorts tissue development. *Cancer Res.* 70(22), 9453–9462 (2010).

33 Park JB, Lee CS, Jang JH *et al.* Phospholipase signalling networks in cancer. *Nat. Rev. Cancer* 12(11), 782–792 (2012).

34 Nomura DK, Long JZ, Niessen S, Hoover HS, Ng SW, Cravatt BF. Monoacylglycerol lipase regulates a fatty acid network that promotes cancer pathogenesis. *Cell* 140(1), 49–61 (2010).

35 Karnezis T, Shayan R, Caesar C *et al.* VEGF-D promotes tumor metastasis by regulating prostaglandins produced by the collecting lymphatic endothelium. *Cancer Cell* 21(2), 181–195 (2012).

36 Seguin F, Carvalho MA, Bastos DC *et al.* The fatty acid synthase inhibitor orlistat reduces experimental metastases and angiogenesis in B16-F10 melanomas. *Br. J. Cancer* 107(6), 977–987 (2012).

37 Pavlides S, Tsirigos A, Migneco G *et al.* The autophagic tumor stroma model of cancer. Role of oxidative stress and ketone production in fueling tumor cell metabolism. *Cell Cycle* 9(17), 3485–3505 (2010).

38 Carito V, Bonuccelli G, Martinez-Outschoorn UE *et al.* Metabolic remodeling of the tumor microenvironment: migration stimulating factor (MSF) reprograms myofibroblasts toward lactate production, fueling anabolic tumor growth. *Cell Cycle* 11(18), 3403–3414 (2012).

39 Hur H, Paik MJ, Xuan Y *et al.* Quantitative measurement of organic acids in tissues from gastric cancer patients indicates increased glucose metabolism in gastric cancer. *PLoS ONE* 9(6), e98581 (2014).

40 Peters K, Kamp G, Berz A *et al.* Changes in human endothelial cell energy metabolic capacities during *in vitro* cultivation. The role of "aerobic glycolysis" and proliferation. *Cell Physiol. Biochem.* 24(5–6), 483–492 (2009).

41 Harjes U, Bensaad K, Harris AL. Endothelial cell metabolism and implications for cancer therapy. *Br. J. Cancer* 107(8), 1207–1212 (2012).

42 Vegran F, Boidot R, Michiels C, Sonveaux P, Feron O. Lactate influx through the endothelial cell monocarboxylate transporter MCT1 supports an NF-kappaB/IL-8 pathway that drives tumor angiogenesis. *Cancer Res.* 71(7), 2550–2560 (2011).

43 Vizan P, Sanchez-Tena S, Alcarraz-Vizan G *et al.* Characterization of the metabolic changes underlying growth factor angiogenic activation: identification of new potential therapeutic targets. *Carcinogenesis* 30(6), 946–952 (2009).

44 Calcinotto A, Filipazzi P, Grioni M *et al.* Modulation of microenvironment acidity reverses anergy in human and murine tumor-infiltrating T lymphocytes. *Cancer Res.* 72(11), 2746–2756 (2012).

45 Polet F, Feron O. Endothelial cell metabolism and tumour angiogenesis: glucose and glutamine as essential fuels and lactate as the driving force. *J. Intern. Med.* 273(2), 156–165 (2013).

46 Choi SY, Collins CC, Gout PW, Wang Y. Cancer-generated lactic acid: a regulatory, immunosuppressive metabolite? *J. Pathol.* 230(4), 350–355 (2013).

47 Wels J, Kaplan RN, Rafii S, Lyden D. Migratory neighbors and distant invaders: tumor-associated niche cells. *Genes Dev.* 22(5), 559–574 (2008).

48 Cardenas-Navia LI, Mace D, Richardson RA, Wilson DF, Shan S, Dewhirst MW. The pervasive presence of fluctuating oxygenation in tumors. *Cancer Res.* 68(14), 5812–5819 (2008).

49 Sharma MK, Seidlitz EP, Singh G. Cancer cells release glutamate via the cystine/glutamate antiporter. *Biochem. Biophys. Res. Commun.* 391(1), 91–95 (2010).

50 Meneses AM, Medina RA, Kato S *et al.* Regulation of GLUT3 and glucose uptake by the cAMP signalling pathway in the breast cancer cell line ZR-75. *J. Cell. Physiol.* 214(1), 110–116 (2008).

51 Chen J, Zhang S, Li Y, Tang Z, Kong W. Hexokinase 2 overexpression promotes the proliferation and survival of laryngeal squamous cell carcinoma. *Tumor Biol.* 35(4), 3743–3753 (2014).

52 Robey RB, Hay N. Mitochondrial hexokinases, novel mediators of the antiapoptotic effects of growth factors and Akt. *Oncogene* 25(34), 4683–4696 (2006).

53 Galluzzi L, Kepp O, Tajeddine N, Kroemer G. Disruption of the hexokinase-VDAC complex for tumor therapy. *Oncogene* 27(34), 4633–4635 (2008).

54 Christofk HR, Vander Heiden MG, Harris MH *et al.* The M2 splice isoform of pyruvate kinase is important for cancer metabolism and tumour growth. *Nature* 452(7184), 230–233 (2008).

55 Christofk HR, Vander Heiden MG, Wu N, Asara JM, Cantley LC. Pyruvate kinase M2 is a phosphotyrosine-binding protein. *Nature* 452(7184), 181–186 (2008).

56 Vander Heiden MG, Christofk HR, Schuman E *et al.* Identification of small molecule inhibitors of pyruvate kinase M2. *Biochem. Pharmacol.* 79(8), 1118–1124 (2010).

57 Clem B, Telang S, Clem A *et al.* Small-molecule inhibition of 6-phosphofructo-2-kinase activity suppresses glycolytic flux and tumor growth. *Mol. Cancer Ther.* 7(1), 110–120 (2008).

58 Zhou M, Zhao Y, Ding Y *et al.* Warburg effect in chemosensitivity: targeting lactate dehydrogenase-A re-sensitizes Taxol-resistant cancer cells to Taxol. *Mol. Cancer* 9(1), 33 (2010).

59 Le A, Cooper CR, Gouw AM *et al.* Inhibition of lactate dehydrogenase A induces oxidative stress and inhibits tumor progression. *Proc. Nat. Acad. Sci. USA* 107(5), 2037–2042 (2010).

60 Lu CW, Lin SC, Chen KF, Lai YY, Tsai SJ. Induction of pyruvate dehydrogenase kinase-3 by hypoxia-inducible factor-1 promotes metabolic switch and drug resistance. *J. Biol. Chem.* 283(42), 28106–28114 (2008).

61 Yan H, Parsons DW, Jin G *et al.* IDH1 and IDH2 mutations in gliomas. *N. Engl. J. Med.* 360(8), 765–773 (2009).

62 Dang L, Jin S, Su SM. IDH mutations in glioma and acute myeloid leukemia. *Trends Mol. Med.* 16(9), 387–397 (2010).

63 El-Ashmawy N, El-Bahrawy H, Shamloula M, El-Feky O. Biochemical/metabolic changes associated with hepatocellular carcinoma development in mice. *Tumor Biol.* 35(6), 5459–5466 (2014).

64 Xu X, Zur Hausen A, Coy JF, Löchelt M. Transketolase-like protein 1 (TKTL1) is required for rapid cell growth and full viability of human tumor cells. *Int. J. Cancer* 124(6), 1330–1337 (2009).

65 Vizán P, Alcarraz-Vizán G, Díaz-Moralli S, Solovjeva ON, Frederiks WM, Cascante M. Modulation of pentose phosphate pathway during cell cycle progression in human colon adenocarcinoma cell line HT29. *Int. J. Cancer* 124(12), 2789–2796 (2009).

66 Dang CV. Glutaminolysis: supplying carbon or nitrogen or both for cancer cells? *Cell Cycle* 9(19), 3914–3916 (2010).

67 Durán RV, Oppliger W, Robitaille AM *et al.* Glutaminolysis activates Rag-mTORC1 signaling. *Mol. Cell* 47(3), 349–358 (2012).

68 Deberardinis RJ, Thompson CB. Cellular metabolism and disease: what do metabolic outliers teach us? *Cell* 148(6), 1132–1144 (2012).

69 Mardinoglu A, Nielsen J. Systems medicine and metabolic modelling. *J. Intern. Med.* 271(2), 142–154 (2012).

70 Gonnerman MC, Benedict MN, Feist AM, Metcalf WW, Price ND. Genomically and biochemically accurate metabolic reconstruction of *Methanosarcina barkeri fusaro*, iMG746. *Biotechnol. J.* 8(9), 1070–1079 (2013).

71 Benedict MN, Gonnerman MC, Metcalf WW, Price ND. Genome-scale metabolic reconstruction and hypothesis testing in the methanogenic archaeon *Methanosarcina acetivorans* C2A. *J. Bacteriol.* 194(4), 855–865 (2012).

72 Lee NR, Lakshmanan M, Aggarwal S *et al.* Genome-scale metabolic network reconstruction and *in silico* flux analysis of the thermophilic bacterium *Thermus thermophilus* HB27. *Microb. Cell Fact.* 13(1), 61 (2014).

73 Orth JD, Conrad TM, Na J *et al.* A comprehensive genome-scale reconstruction of *Escherichia coli* metabolism – 2011. *Mol. Syst. Biol.* 7(1), 535 (2011).

74 Nagarajan H, Sahin M, Nogales J *et al.* Characterizing acetogenic metabolism using a genome-scale metabolic reconstruction of *Clostridium ljungdahlii*. *Microb. Cell Fact.* 12(1), 118 (2013).

75 Song C, Chiasson MA, Nursimulu N *et al.* Metabolic reconstruction identifies strain-specific regulation of virulence in *Toxoplasma gondii*. *Mol. Syst. Biol.* 9(1), 708 (2013).

76 Heavner B, Smallbone K, Barker B, Mendes P, Walker L. Yeast 5 – an expanded reconstruction of the *Saccharomyces cerevisiae* metabolic network. *BMC Syst. Biol.* 6(1), 55 (2012).

77 Caspeta L, Shoaie S, Agren R, Nookaew I, Nielsen J. Genome-scale metabolic reconstructions of *Pichia stipitis* and *Pichia pastoris* and *in silico* evaluation of their potentials. *BMC Syst. Biol.* 6(1), 24 (2012).

78 Liu J, Gao Q, Xu N, Liu L. Genome-scale reconstruction and *in silico* analysis of *Aspergillus terreus* metabolism. *Mol. Biosyst.* 9(7), 1939–1948 (2013).

79 Arnold A, Nikoloski Z. Bottom-up metabolic reconstruction of arabidopsis and its application to determining the metabolic costs of enzyme production. *Plant Physiol.* 165(3), 1380–1391 (2014).

80 Dal'molin CG, Quek LE, Palfreyman RW, Brumbley SM, Nielsen LK. C4GEM, a genome-scale metabolic model to study C4 plant metabolism. *Plant Physiol.* 154(4), 1871–1885 (2010).

81 Duarte NC, Becker SA, Jamshidi N *et al.* Global reconstruction of the human metabolic network based on genomic and bibliomic data. *Proc. Natl Acad. Sci. USA* 104(6), 1777–1782 (2007).

82 Hao T, Ma HW, Zhao XM, Goryanin I. The reconstruction and analysis of tissue specific human metabolic networks. *Mol. Biosyst.* 8(2), 663–670 (2012).

83 Thiele I, Swainston N, Fleming RM *et al.* A community-driven global reconstruction of human metabolism. *Nat. Biotech.* 31(5), 419–425 (2013).

84 Sigurdsson MI, Jamshidi N, Steingrimsson E, Thiele I, Palsson BØ. A detailed genome-wide reconstruction of mouse metabolism based on human Recon 1. *BMC Syst. Biol.* 4(1), 140 (2010).

85 Bordbar A, Feist AM, Usaite-Black R, Woodcock J, Palsson BØ, Famili I. A multi-tissue type genome-scale metabolic network for analysis of whole-body systems physiology. *BMC Syst. Biol.* 5(1), 180 (2011).

86 Wang Y, Eddy JA, Price ND. Reconstruction of genome-scale metabolic models for 126 human tissues using mCADRE. *BMC Syst. Biol.* 6(1), 153 (2012).

87 Agren R, Bordel S, Mardinoglu A, Pornputtapong N, Nookaew I, Nielsen J. Reconstruction of genome-scale active metabolic networks for 69 human cell types and 16 cancer types using INIT. *PLoS Comput. Biol.* 8(5), e1002518 (2012).

88 Jerby L, Wolf L, Denkert C *et al.* Metabolic associations of reduced proliferation and oxidative stress in advanced breast cancer. *Cancer Res.* 72(22), 5712–5720 (2012).

89 Orth JD, Thiele I, Palsson BØ. What is flux balance analysis? *Nat. Biotech.* 28(3), 245–248 (2010).

90 Rajcevic U, Knol J, Piersma S *et al.* Colorectal cancer derived organotypic spheroids maintain essential tissue characteristics but adapt their metabolism in culture. *Proteome Sci.* 12(1), 39 (2014).

91 Papp B, Notebaart RA, Pál C. Systems-biology approaches for predicting genomic evolution. *Nat. Rev. Genet.* 12(9), 591–602 (2011).

92 Matsuda F, Furusawa C, Kondo T, Ishii J, Shimizu H, Kondo A. Engineering strategy of yeast metabolism for higher alcohol production. *Microb. Cell Fact.* 10(1), 70 (2011).

93 Park JM, Song H, Lee HJ, Seung D. Genome-scale reconstruction and *in silico* analysis of *Klebsiella oxytoca* for 2,3-butanediol production. *Microb. Cell Fact.* 12(1), 20 (2013).

94 Lütke-Eversloh T, Bahl H. Metabolic engineering of *Clostridium acetobutylicum*: recent advances to improve butanol production. *Curr. Opin. Biotechnol.* 22(5), 634–647 (2011).

95 Kumar VS, Maranas CD. GrowMatch: an automated method for reconciling *in silico*/*in vivo* growth predictions. *PLoS Comput. Biol.* 5(3), e1000308 (2009).

96 Kim HU, Kim SY, Jeong H *et al.* Integrative genome-scale metabolic analysis of *Vibrio vulnificus* for drug targeting and discovery. *Mol. Syst. Biol.* 7(1), 460 (2011).

97 Agren R, Mardinoglu A, Asplund A, Kampf C, Uhlen M, Nielsen J. Identification of anticancer drugs for hepatocellular carcinoma through personalized genome-scale metabolic modeling. *Mol. Syst. Biol.* 10(3), 721 (2014).

98 Feist AM, Herrgård MJ, Thiele I, Reed JL, Palsson BØ. Reconstruction of biochemical networks in microorganisms. *Nat. Rev. Microbiol.* 7(2), 129–143 (2009).

99 Caspi R, Altman T, Dale JM *et al.* The MetaCyc database of metabolic pathways and enzymes and the BioCyc collection of pathway/genome databases. *Nucleic Acids Res.* 38(Suppl. 1), D473–D479 (2010).

100 Henry CS, Dejongh M, Best AA, Frybarger PM, Linsay B, Stevens RL. High-throughput generation, optimization and analysis of genome-scale metabolic models. *Nat. Biotech.* 28(9), 977–982 (2010).

101 Coordinators NR. Database resources of the National Center for Biotechnology Information. *Nucleic Acids Res.* 41(D1), D8–D20 (2013).

102 Pagani I, Liolios K, Jansson J *et al.* The Genomes OnLine Database (GOLD) v.4: status of genomic and metagenomic projects and their associated metadata. *Nucleic Acids Res.* 40(D1), D571–D579 (2012).

103 Kanehisa M, Goto S, Sato Y, Furumichi M, Tanabe M. KEGG for integration and interpretation of large-scale molecular data sets. *Nucleic Acids Res.* 40(D1), D109–D114 (2012).

104 Chang A, Scheer M, Grote A, Schomburg I, Schomburg D. BRENDA, AMENDA and FRENDA the enzyme information system: new content and tools in 2009. *Nucleic Acids Res.* 37(Suppl. 1), D588–D592 (2009).

105 Schellenberger J, Que R, Fleming RM *et al.* Quantitative prediction of cellular metabolism with constraint-based models: the COBRA Toolbox v2. 0. *Nat. Protoc.* 6(9), 1290–1307 (2011).

106 Wintermute E, Lieberman T, Silver P. An objective function exploiting suboptimal solutions in metabolic networks. *BMC Syst. Biol.* 7(1), 98 (2013).

107 Palsson B, Zengler K. The challenges of integrating multi-omic data sets. *Nat. Chem. Biol.* 6(11), 787–789 (2010).

108 Bordbar A, Mo ML, Nakayasu ES *et al.* Model-driven multi-omic data analysis elucidates metabolic immunomodulators of macrophage activation. *Mol. Syst. Biol.* 8(1), 558 (2012).

109 Lewis NE, Nagarajan H, Palsson BØ. Constraining the metabolic genotype–phenotype relationship using a phylogeny of *in silico* methods. *Nat. Rev. Microbiol.* 10(4), 291–305 (2012).

110 Jensen PA, Papin JA. MetDraw: automated visualization of genome-scale metabolic network reconstructions and high-throughput data. *Bioinformatics* 30(9), 1327–1328 (2014).

111 Chandrasekaran S, Price ND. Probabilistic integrative modeling of genome-scale metabolic and regulatory networks in *Escherichia coli* and *Mycobacterium tuberculosis*. *Proc. Natl Acad. Sci. USA* 107(41), 17845–17850 (2010).

112 Barabási AL, Gulbahce N, Loscalzo J. Network medicine: a network-based approach to human disease. *Nat. Rev. Genet.* 12(1), 56–68 (2011).

113 Jerby L, Shlomi T, Ruppin E. Computational reconstruction of tissue-specific metabolic models: application to human liver metabolism. *Mol. Syst. Biol.* 6(1), 401 (2010).

114 Lewis NE, Schramm G, Bordbar A *et al.* Large-scale *in silico* modeling of metabolic interactions between cell types in the human brain. *Nat. Biotech.* 28(12), 1279–1285 (2010).

115 Zur H, Ruppin E, Shlomi T. iMAT: an integrative metabolic analysis tool. *Bioinformatics* 26(24), 3140–3142 (2010).

116 Schmidt BJ, Ebrahim A, Metz TO, Adkins JN, Palsson BØ, Hyduke DR. GIM3E: condition-specific models of cellular metabolism developed from metabolomics and expression data. *Bioinformatics* 29(22), 2900–2908 (2013).

117 Galhardo M, Sinkkonen L, Berninger P, Lin J, Sauter T, Heinäniemi M. Integrated analysis of transcript-level regulation of metabolism reveals disease-relevant nodes of the human metabolic network. *Nucleic Acids Res.* 42(3), 1474–1496 (2013).

118 Lazar MA, Birnbaum MJ. De-meaning of metabolism. *Science* 336(6089), 1651–1652 (2012).

119 Folger O, Jerby L, Frezza C, Gottlieb E, Ruppin E, Shlomi T. Predicting selective drug targets in cancer through metabolic networks. *Mol. Syst. Biol.* 7(1), 501 (2011).

120 Davis VW, Bathe OF, Schiller DE, Slupsky CM, Sawyer MB. Metabolomics and surgical oncology: potential role for small molecule biomarkers. *J. Surg. Oncol.* 103(5), 451–459 (2011).

121 Murabito E, Simeonidis E, Smallbone K, Swinton J. Capturing the essence of a metabolic network: a flux balance analysis approach. *J. Theor. Biol.* 260(3), 445–452 (2009).

122 Schellenberger J, Palsson BØ. Use of randomized sampling for analysis of metabolic networks. *J. Biol. Chem.* 284(9), 5457–5461 (2009).

123 Duggal R, Minev B, Geissinger U *et al.* Biotherapeutic approaches to target cancer stem cells. *J. Stem Cells* 8(3–4), 135–149 (2013).

124 Philips MR, Cox AD. Geranylgeranyltransferase I as a target for anti-cancer drugs. *J. Clin. Invest.* 117(5), 1223–1225 (2007).

125 Dudakovic A, Tong H, Hohl R. Geranylgeranyl diphosphate depletion inhibits breast cancer cell migration. *Invest. New Drugs* 29(5), 912–920 (2011).

126 Hebar A, Valent P, Selzer E. The impact of molecular targets in cancer drug development: major hurdles and future strategies. *Expert Rev. Clin. Pharmacol.* 6(1), 23–34 (2013).

127 Conde-Pueyo N, Munteanu A, Solé RV, Rodríguez-Caso C. Human synthetic lethal inference as potential anti-cancer target gene detection. *BMC Syst. Biol.* 3(1), 116 (2009).

128 Barbash DA, Lorigan JG. Lethality in *Drosophilamelanogaster*/*Drosophilasimulans* species hybrids is not associated with substantial transcriptional misregulation. *J. Exp. Zool. Part B Mol. Dev. Evol.* 308(1), 74–84 (2007).

129 Ren S, Zeng B, Qian X. Adaptive bi-level programming for optimal gene knockouts for targeted overproduction under phenotypic constraints. *BMC Bioinformatics* 14(Suppl. 2), S17 (2013).

130 Frezza C, Zheng L, Folger O *et al.* Haem oxygenase is synthetically lethal with the tumour suppressor fumarate hydratase. *Nature* 477(7363), 225–228 (2011).

131 Zhao Y, Butler EB, Tan M. Targeting cellular metabolism to improve cancer therapeutics. *Cell Death Dis.* 4, e532 (2013).

132 Vaupel P. Tumor microenvironmental physiology and its implications for radiation oncology. *Sem. Radiat. Oncol.* 14(3), 198–206 (2004).

133 Tannock IF, Lee CM, Tunggal JK, Cowan DS, Egorin MJ. Limited penetration of anticancer drugs through tumor tissue a potential cause of resistance of solid tumors to chemotherapy. *Clin. Cancer Res.* 8(3), 878–884 (2002).

134 Olive KP, Jacobetz MA, Davidson CJ *et al.* Inhibition of Hedgehog signaling enhances delivery of chemotherapy in a mouse model of pancreatic cancer. *Science* 324(5933), 1457–1461 (2009).

135 Hulit J, Howell A, Gandara R, Sartini M, Arafat H, Bevilacqua G. Creating a tumor-resistant microenvironment. *Cell Cycle* 12(3), 480–490 (2013).

136 Ye C, Zou W, Xu N, Liu L. Metabolic model reconstruction and analysis of an artificial microbial ecosystem for vitamin C production. *J. Biotech.* 182, 61–67 (2014).

137 Peinado H, Olmeda D, Cano A. Snail, Zeb and bHLH factors in tumour progression: an alliance against the epithelial phenotype? *Nat. Rev. Cancer* 7(6), 415–428 (2007).

138 Celià-Terrassa T, Meca-Cortés Ó, Mateo F *et al.* Epithelial-mesenchymal transition can suppress major attributes of human epithelial tumor-initiating cells. *J. Clin. Invest.* 122(5), 1849 (2012).

139 Korpal M, Ell BJ, Buffa FM *et al.* Direct targeting of Sec23a by miR-200s influences cancer cell secretome and promotes metastatic colonization. *Nat. Med.* 17(9), 1101–1108 (2011).

140 Ocaña OH, Córcoles R, Fabra Á *et al.* Metastatic colonization requires the repression of the epithelial-mesenchymal transition inducer Prrx1. *Cancer Cell* 22(6), 709–724 (2012).

141 Rundqvist H, Johnson RS. Hypoxia and metastasis in breast cancer. In: *Diverse Effects of Hypoxia on Tumor Progression.* Simon MC (Ed.) Springer, Berlin/Heidelberg, Germany, 121–139 (2010).

142 Nagy JA, Chang S-H, Shih S-C, Dvorak AM, Dvorak HF. Heterogeneity of the tumor vasculature. *Semin. Thromb. Hemost.* 36(3), 321–331 (2010).

143 Mazzone M, Dettori D, Leite De Oliveira R *et al.* Heterozygous deficiency of PHD2 restores tumor oxygenation and inhibits metastasis via endothelial normalization. *Cell* 136(5), 839–851 (2009).

144 Rolny C, Mazzone M, Tugues S *et al.* HRG inhibits tumor growth and metastasis by inducing macrophage polarization and vessel normalization through downregulation of PlGF. *Cancer Cell* 19(1), 31–44 (2011).

145 Yizhak K, Gabay O, Cohen H, Ruppin E. Model-based identification of drug targets that revert disrupted metabolism and its application to ageing. *Nat. Commun.* 4, 2632 (2013).

146 De Mas IM, Selivanov VA, Marin S *et al.* Compartmentation of glycogen metabolism revealed from 13C isotopologue distributions. *BMC Syst. Biol.* 5(1), 175 (2011).

147 Hassan S, Buchanan M, Jahan K *et al.* CXCR4 peptide antagonist inhibits primary breast tumor growth, metastasis and enhances the efficacy of anti-VEGF treatment or docetaxel in a transgenic mouse model. *Int. J. Cancer* 129(1), 225–232 (2011).

148 Coenegrachts L, Maes C, Torrekens S *et al.* Anti-placental growth factor reduces bone metastasis by blocking tumor cell engraftment and osteoclast differentiation. *Cancer Res.* 70(16), 6537–6547 (2010).

149 Hiratsuka S, Duda DG, Huang Y *et al.* CXC receptor type 4 promotes metastasis by activating p38 mitogen-activated protein kinase in myeloid differentiation antigen (Gr-1)-positive cells. *Proc. Natl Acad. Sci. USA* 108(1), 302–307 (2011).

APPENDIX VI

Pharmacological Research 102 (2015) 218–234

Contents lists available at ScienceDirect

Pharmacological Research

journal homepage: www.elsevier.com/locate/yphrs

Methylseleninic acid promotes antitumour effects via nuclear FOXO3a translocation through Akt inhibition

Míriam Tarrado-Castellarnau[a,b], Roldán Cortés[a,b], Miriam Zanuy[a,b,1], Josep Tarragó-Celada[a,b], Ibrahim H. Polat[a,b], Richard Hill[c,d,e], Teresa W.M. Fan[f], Wolfgang Link[c,d], Marta Cascante[a,b,*]

[a] Department of Biochemistry and Molecular Biology, Faculty of Biology, Universitat de Barcelona, Av Diagonal 643, Barcelona 08028, Spain
[b] Institute of Biomedicine of Universitat de Barcelona (IBUB) and CSIC-Associated Unit, Barcelona, Spain
[c] Centre for Biomedical Research (CBMR), University of Algarve, Campus of Gambelas, Building 8, Room 2.22, 8005-139 Faro, Portugal
[d] Regenerative Medicine Program, Department of Biomedical Sciences and Medicine University of Algarve, Campus de Gambelas, 8005-139 Faro, Portugal
[e] Brain Tumour Research Centre, School of Pharmacy and Biomedical Sciences, University of Portsmouth, PO1 2DT, United Kingdom
[f] Department of Toxicology, Markey Cancer Center and Center for Environmental and Systems Biochemistry (CESB), University of Kentucky, Lexington, KY 40536, USA

ARTICLE INFO

Article history:
Received 30 March 2015
Received in revised form 28 August 2015
Accepted 10 September 2015
Available online 4 November 2015

Chemical compounds studied in this article:
Methylseleninic acid (PubChem CID: 161597)
Sodium selenite (PubChem CID: 24934)
Cisplatin (PubChem CID: 441203)
LY294002 (PubChem CID: 3973)

Keywords:
Methylseleninic acid
Selenium
FOXO
Akt
PI3K
Cisplatin

ABSTRACT

Selenium supplement has been shown in clinical trials to reduce the risk of different cancers including lung carcinoma. Previous studies reported that the antiproliferative and pro-apoptotic activities of methylseleninic acid (MSA) in cancer cells could be mediated by inhibition of the PI3K pathway. A better understanding of the downstream cellular targets of MSA will provide information on its mechanism of action and will help to optimize its use in combination therapies with PI3K inhibitors. For this study, the effects of MSA on viability, cell cycle, metabolism, apoptosis, protein and mRNA expression, and reactive oxygen species production were analysed in A549 cells. FOXO3a subcellular localization was examined in A549 cells and in stably transfected human osteosarcoma U2foxRELOC cells. Our results demonstrate that MSA induces FOXO3a nuclear translocation in A549 cells and in U2OS cells that stably express GFP-FOXO3a. Interestingly, sodium selenite, another selenium compound, did not induce any significant effects on FOXO3a translocation despite inducing apoptosis. Single strand break of DNA, disruption of tumour cell metabolic adaptations, decrease in ROS production, and cell cycle arrest in G1 accompanied by induction of apoptosis are late events occurring after 24 h of MSA treatment in A549 cells. Our findings suggest that FOXO3a is a relevant mediator of the antiproliferative effects of MSA. This new evidence on the mechanistic action of MSA can open new avenues in exploiting its antitumour properties and in the optimal design of novel combination therapies. We present MSA as a promising chemotherapeutic agent with synergistic antiproliferative effects with cisplatin.

1. Introduction

Lung cancer is a leading cause of cancer-related mortality and has one of the lowest cure rate worldwide [1]. In early stages of the disease, surgery is the common choice while chemotherapy is the main treatment in advanced lung cancer. The search for new synthetic or natural drugs with low systemic toxicity and high efficiency holds great promise to decrease the morbidity and mortality of cancer. The trace element selenium (Se) in various chemical

Abbreviations: MSA, methylseleninic acid; Se, selenium; PPP, pentose phosphate pathway; TCA, tricarboxylic acid; ROS, reactive oxygen species; 1D HSQC, one dimension heteronuclear single quantum coherence; ^{1}H-NMR, proton nuclear magnetic resonance; $^{72h}IC_{50}$, concentration that caused 50% of inhibition of cell growth at 72 h of treatment; FOXO, forkhead box O; FOXM1, forkhead box protein M1; Akt, protein kinase B; PI3K, phosphoinositide-3-kinase; mTOR, mammalian target of rapamycin; CDK, cyclin-dependent kinase; JNK, Jun N-terminal kinase; Bax, B-cell lymphoma-2-associated X protein; PARP, poly(ADP-ribose) polymerase; PRAS40, proline-rich Akt substrate 40 kDa; ERK2, extracellular signal-regulated kinase 2.

* Corresponding author at: Department of Biochemistry and Molecular Biology, Faculty of Biology, Universitat de Barcelona, Av Diagonal 643, Barcelona 08028, Spain. Tel.: +34 93 402 15 93; fax: +34 93 402 15 23.
E-mail addresses: mtarrado@ub.edu (M. Tarrado-Castellarnau), roldancortes@ub.edu (R. Cortés), mzanuy@hotmail.com (M. Zanuy), joseptarrago11@gmail.com (J. Tarragó-Celada), ihapolat@gmail.com (I.H. Polat), drrjhill@gmail.com (R. Hill), twmfan@gmail.com (T.W.M. Fan), walink@ualg.pt (W. Link), martacascante@ub.edu (M. Cascante).
[1] Present address: Almirall R&D Centre, Laureano Miró, 408-410, 08980 Sant Feliu de Llobregat, Barcelona, Spain.

http://dx.doi.org/10.1016/j.phrs.2015.09.009
1043-6618/

forms is nutritionally essential for humans but has toxic activity at higher levels [2,3]. To date, the antioxidant and chemopreventive role of different Se agents as a dietary supplement has not been completely elucidated [4]. Se compounds such as sodium selenite (Na_2SeO_3) [5,6] and methylseleninic acid (CH_3SeO_2H, abbreviated as MSA) have also been studied as potential anticancer agents. MSA is a synthetic precursor of methylselenol (CH_3SeH) which induces several cellular, transcriptional and biochemical responses that differ from those induced by selenium forms that are transformed via hydrogen selenide, such as sodium selenite [7,8].

As a constituent of the selenocysteine-containing selenoproteins, selenium has a key role in redox regulation and defence against oxidative stress by greatly enhancing the activity of some antioxidant enzyme systems [9]. Several selenoenzymes, including thioredoxin reductase, iodothyronine deiodinase and glutathione peroxidase, may be associated with cancer development and progression by modulating cell proliferation, transformation, migration and protection against oxidative damage [2]. Selenium deficiency has also been linked to cancer development since it was observed that populations with low selenium intake had greater cancer incidence. Numerous studies and clinical trials have shown that supranutritional doses of individual and mixed selenium compounds inhibit proliferation of cancer cells, induce tumour cell apoptosis, suppress tumour formation and metastasis in animal models and reduce the risk of prostate, lung, breast, and colorectal cancers in humans [9–11]. However, not all selenium compounds have efficacy in chemoprevention, as in a recent large clinical trial (SELECT), selenomethionine was concluded to be ineffective in reducing the risk for prostate cancer development [12].

Using a stable isotope-resolved metabolomic (SIRM) approach, Fan et al. [13] reported that several metabolites, including lactate, glutathione and glutamate are depleted in A549 lung cancer cells by selenite but not by selenomethionine, suggesting multiple perturbations of the central metabolic networks. Interestingly, the reduction in glycolysis, tricarboxylic acid cycle (TCA) and pentose phosphate pathway (PPP) fluxes observed is opposite to those observed when phosphoinositide-3-kinase (PI3K) pathway is activated [14], pointing to the hypothesis that Se agents target this signalling pathway. Among the selenium compounds with anticancer properties, it has been reported that MSA is a potent inhibitor of the growth and survival of human umbilical vein endothelial cells (HUVECs) and that this antiproliferative effect could be enacted through the PI3K pathway [15,16]. Studies with prostate cancer LNCaP, PC-3 (high basal Akt activity) and DU145 cells (low basal Akt activity) have also shown that Akt plays an important role in regulating apoptosis sensitivity to MSA [17]. However, the molecular mechanism of action of MSA is still not fully elucidated.

PI3K/Akt pathway has been shown to be activated in numerous tumours, including lung cancer [18], as it is essential for cell proliferation and survival. Akt is a serine-threonine kinase that is regulated via activation of PI3K. Forkhead box O (FOXO) transcription factors are direct targets of Akt that modulate cellular differentiation, cell cycle, growth, survival, apoptosis, metabolism, DNA repair, resistance to oxidative stress and tumour suppressor pathways [19]. In mammals, FOXO1, FOXO3a and FOXO4 are ubiquitously expressed while FOXO6 is expressed predominantly in neural cells. As transcription factors, FOXO proteins activate or repress the transcription of their target genes through nuclear translocation regulated by post-translational modifications such as phosphorylation, acetylation and ubiquitination [20]. FOXO phosphorylation by Akt impairs its DNA binding activity and promotes its interaction with the chaperone protein 14-3-3, resulting in nuclear exclusion, cytoplasmic accumulation and ubiquitin-proteasome pathway-dependent degradation, thus promoting cell survival. In contrast, FOXO proteins are activated and released from 14-3-3 in the presence of oxidative stress through Jun N-terminal kinase (JNK) signalling [19,21,22]. A hallmark of most cancers where the PI3K pathway is hyperactivated (caused by RAS, PTEN or PI3K mutations) is inactivation of FOXO proteins [23]. In contrast, PI3K depletion results in a significant activation of FOXO transcription factors, induction of apoptosis, decrease of cell viability and G1 cell cycle arrest with inhibition of CDK4/6, cyclin D and accumulation of p27 [24]. Therefore, the search for compounds that promote activation and relocalization of FOXO from the cytoplasm to the nucleus is a promising therapeutic approach for cancer treatment and prevention [25].

In this study, using A549 and U2foxRELOC cells expressing a GFP–FOXO3a fusion protein, we have demonstrated that MSA induces FOXO3a dephosphorylation and nuclear translocation. These findings provide a molecular mechanism to the cytotoxicity, apoptosis, ROS detoxification, cell cycle arrest and metabolic changes observed in A549 cells and implicate FOXO3a as a relevant mediator of MSA antitumour effects.

Moreover, since it has been reported that the antitumour effects of cisplatin are enhanced when it is combined with FOXO nuclear export inhibitors [26–29] and that MSA synergistically sensitized cancer cells in combination with certain chemotherapeutic drugs [30,31], we hypothesized that combined treatment of MSA with cisplatin could be a promising new strategy in cancer therapy.

2. Methods

All products were purchased from Sigma–Aldrich Co. (St Louis, MO, USA), unless otherwise specified.

2.1. Chemicals

MSA was supplied by Dr. Fan (University of Kentucky, KY, USA). Sodium selenite was purchased from Sigma–Aldrich. Stock solutions of 10 mM were prepared with Dulbecco's phosphate buffered saline (PBS). The PI3K inhibitor LY294002 was purchased from Calbiochem (San Diego, CA, USA), antibiotic (10,000 U mL^{-1} penicillin, 10 mg mL^{-1} streptomycin), PBS, Trypsin EDTA solution C (0.05% trypsin −0.02% EDTA) from Biological Industries (Kibbutz Beit Haemet, Israel) and Fetal Bovine Serum (FBS) from Invitrogen (Carlsbad, CA, USA).

2.2. Cell culture

Human lung carcinoma A549 cells (ATCC, Manassas, VA, USA) were grown in RPMI-1640 medium with L-glutamine and 10 mM D-glucose prepared following the manufacturer's instructions. Human osteosarcoma stably transfected U2foxRELOC cells (a gift from Dr. Wolfgang Link), human osteosarcoma U2OS cells, human large cell lung cancer NCI-H460 cells, human ovary adenocarcinoma OVCAR3 cells, human embryonic kidney 293 (HEK293) cells and adipocyte-like differentiated 3T3-L1 cells (ATCC) were grown in DMEM with L-glutamine and 25 mM D-glucose. Human colorectal carcinoma HCT116 cells (ATCC) were cultured in DMEM:HAM F12 (1:1) with L-glutamine and 12.5 mM D-glucose. Human breast adenocarcinoma MCF7 cells (ATCC) were cultured in MEM medium without phenol red (Gibco, Thermo Fisher Scientific Inc., Waltham, MA, USA) containing 10 mM D-glucose, 2 mM L-glutamine, 1 mM pyruvate (Biological Industries), 0.01 mg mL^{-1} insulin and 1% non-essential aminoacids (Biological Industries). Media were supplemented with 10% heat-inactivated FBS, penicillin (50 U mL^{-1}) and streptomycin (50 μg mL^{-1}). U2foxRELOC cells, which express a resistance to Geneticin, were incubated with G418 (Gibco) at 100 μg mL^{-1}. 3T3-L1 pre-adipocyte cells were grown in DMEM

with 0% FBS, 10% NCS and 0.5% streptomycin/penicillin. Cells were incubated at 37 °C in a humidified atmosphere with 5% CO_2.

2.3. 3T3-L1 differentiation

Pre-adipocyte 3T3-L1 cells were seeded in 96-well-flat-bottomed microtitre plates. Medium was changed two days after confluence with DMEM containing 0% NCS, 10% FBS and induction cocktail (250 μM isobutylmethylxanthine, 1 μM dexamethasone and 0.98 μM insulin). After 72 h, medium was replaced with 10% FBS DMEM containing 0.98 μM insulin and cells were incubated for 72 h. Then, medium was replaced with 10% FBS DMEM. Cells were fully differentiated into adipocytes within 48 h and cell viability assay was performed on them.

2.4. Cell growth inhibition

The assay was performed using a modified method described by Mosmann [32]. Increasing concentrations of the inhibitor were added in sextuplicate in 96-well-flat-bottomed microtitre plates where 2×10^3 A549 cells/well had been seeded 24 h before. MSA was added to 3T3-L1 cells once the differentiation process was completed. MSA was depleted after >24 h of treatment, so media was refreshed every day. After 24, 48 or 72 h, 1 mg mL^{-1} 3-(4,5-dimethylthiazol-2-yl)-2,5-diphenyltetrazolium bromide (MTT) in PBS was added at a final concentration of 0.5 mg mL^{-1}. After 1 h, supernatant was removed and the formazan product was dissolved in 100 μL of dimethyl sulfoxide (DMSO). The absorbance was measured on an ELISA plate reader (Tecan Sunrise MR20-301, TECAN, Salzburg, Austria) at 550 nm. Concentrations that caused 50% of inhibition of cell growth (IC_{50}) were calculated using Graphpad Prism 6 software (La Jolla, CA, USA).

2.5. Cell cycle analysis

A 5×10^4 A549 cells/well were seeded in 6-well plates and treated 24 h later with MSA for 24, 48 and 72 h. Both adherent and detached cells were collected by centrifugation after trypsinization, resuspended in 0.5 mL PBS and added dropwise to 4.5 mL 70% (v/v) cold ethanol. Cells were stained in PBS containing 50 mg mL^{-1} propidium iodide (PI), 0.2 mg mL^{-1} DNAse free RNAse (Roche, Basel, Switzerland) and 0.1% Triton X-100. Fluorescence-activated cell sorter (FACS) analysis was carried out at 488 nm in an Epics XL flow cytometer (Coulter Corporation, Hialeah, FL, USA). Data of 1×10^4 cells were collected and analysed using multicycle program (Phoenix Flow Systems, San Diego, CA, USA). All experiments were performed three times with three replicates per experiment.

2.6. Apoptosis assay

Cells were seeded and treated as described in the cell cycle analysis assay. After centrifugation, cells were washed and resuspended in binding buffer (10 mM Hepes pH 7.4, 140 mM sodium chloride, 2.5 mM calcium chloride). Annexin V coupled with fluorescein isothiocyanate (FITC) was added according to the Annexin V-FITC kit (Bender System MedSystem, Viena, Austria). Following 30 min of incubation at room temperature in darkness, PI was added at 20 μg mL^{-1} 1 min before FACS analysis. Experiments were performed in triplicate and repeated three independent times. Data from 2×10^4 cells were collected and analysed in each experiment.

Apoptosis was also assessed using the membrane-permeable fluorescent dye bisbenzimide Hoechst. After 24 h in the absence or presence of $^{72h}IC_{50}$ MSA, cells were harvested by mild trypsinization, collected by centrifugation and fixed with 3.7% paraformaldehyde for 10 min at −20 °C. Cells were washed with PBS, 0.5% Triton X-100 was added for 5 min at 4 °C and cells were stained with 50 ng mL^{-1} Hoechst 33342 dye for 15 min before placing them onto slides and mounting the coverslips with Mowiol 4-88. Chromatin condensation was visualized by fluorescence microscopy.

2.7. Single cell gel electrophoresis (SCGE)

A 3×10^4 A549 cells/well were seeded in 6-well plates and treated the next day with $^{72h}IC_{50}$ MSA, hydrogen peroxide 100 μM (positive control) and vehicle (negative control). After 24, the comet assay was carried out according to Tice et al. [33]. Briefly, 6×10^5 cells mL^{-1} were mixed with 140 μL of 1% low-melting-point agarose and 70 μL were spread onto pre-coated microscope slides (1% of normal-melting-point agarose). Glass cover slips (Menzel-Glaser, Braunschweig, Germany) were placed on the gels, which were allowed to set at 4 °C. Then, cover slips were removed and cells embedded in agarose were lysed for 1 h by immersion in 2.5 M NaCl, 100 mM Na_2-EDTA, 10 mM Trizma–HCl (pH 10) and 1% Triton X-100 at 4 °C. The slides were placed on a horizontal gel electrophoresis tank and the DNA was allowed to unwind for 40 min in freshly prepared alkaline electrophoresis buffer (300 mM NaOH and 1 mM Na_2-EDTA, pH > 13). Electrophoresis was carried out in the same buffer for 30 min at 25 V in an ice bath condition. The slides were rinsed 3×5 min with 400 mM Trizma (pH 7.5) to neutralize the excess alkali, washed in water (10 min), stained with 25 μL of 4,6-diamidino-2-phenylindole (DAPI) (invitrogen) and covered with a cover. DAPI stained nuclei were evaluated with a Nikon Eclipse TE 300 fluorescence microscope (Nikon, Tokyo, Japan). A total of 100 comets on each gel were visually scored and classified as belonging to one of five classes according to the tail intensity. Each comet class was given a value between 0 (undamaged) and 4 (maximum damage). Total score was calculated by the following equation: (percentage of cells in class 0×0) + (percentage of cells in class 1×1) + (percentage of cells in class 2×2) + (percentage of cells in class 3×3) + (percentage of cells in class 4×4). Consequently, the total score was in the range from 0 to 400. Experiments were performed in triplicate.

2.8. [U-^{13}C]-glucose tracer experiments

A549 cells were seeded in 10 cm plates and grown in the RPMI medium as described above for 24–36 h before the medium was changed to the RPMI medium with dialyzed FBS and [U-^{13}C]-glucose, and in the absence (control) or presence of 5 μM MSA. Cells in the tracer medium were grown for another 24 h before harvest by trypsinization, followed by 2 washes in excess cold PBS to remove medium components. The final cell pellet obtained from spin at 1700 g, 4 °C for 5 min was flash-frozen in liquid N_2 before extraction with ice-cold 10% trichloroacetic acid, as described previously [34]. The polar extracts were aliquoted and lyophilized for analysis by GC–MS and 1D ^{13}C-edited HSQC NMR at 14.1 *T*: 20 °C using a 5 mm HCN triple resonance cold probe (Agilent Technologies, Santa Clara, CA). For GC–MS analysis, the extracts were derivatized in MTBSTFA before analysis, and for NMR analysis, the extracts were dissolved in 100% D_2O, as described previously [35].

2.9. A549 transient transfection with FOXO3a-GFP reporter plasmid

A549 cells were grown on the surface of cover slips (Menzel-Glaser, Braunschweig, Germany) placed in 6-well plates. When confluence reached 80%, cells were transiently transfected with a previously incubated (30 min) mix containing 2 μg of the GFP-FOXO3a reporter plasmid and 2 μL of X-tremeGENE HP reagent (Roche) in 200 μL medium.

2.10. FOXO translocation assay

Twenty four hours after seeding U2foxRELOC cells in 6-well plates containing cover slips or 21 h after transfection in the case of A549 cells, media were replaced with media containing MSA, sodium selenite, LY294002 20 μM (positive control) or vehicle (negative control). After 6 h of incubation, media were replaced with fresh media containing 1 μM CellTracker Red (invitrogen) and incubated for 10 min. Then, media were removed and the cover slips containing the cells were washed 3 × 5 min with PBS, fixed with paraformaldehyde for 15 min and washed again 3 × 5 min with PBS containing 20 mM glycine. The cover slips were then mounted on slides using 20 μL ProLong Gold (invitrogen). After 16 h, the slides were visualized in a TCS SPE Leica confocal microscope (Leica Microsystems, Wetzlar, Germany) and the intensity of the GFP fluorescence in nuclei and cytoplasm was measured from a minimum of 50 random cells per condition using ImageJ software (public domain National Institutes of Health, USA, http://rsbweb.nih.gov/ij/).

2.11. Time course relocalization assay and data analysis

The U2foxRELOC-based assay was performed as described previously [36]. All liquid handling for compound treatment, washing, fixing and staining steps was performed by a robotic workstation [37]. Briefly, 1×10^5 cells mL^{-1} were seeded in black-walled clear-bottomed 96-well microplates (BD Biosciences, San Jose, CA, USA) in a final volume of 200 μL/well using a multidrop automatic dispenser. After 12 h, cells were treated with 5 μM MSA for 1.5, 3, 6, 11 or 24 h and 10 μM LY294002 (positive control) and vehicle (negative control) for 1.5 h. Cells were washed with PBS, fixed in paraformaldehyde, washed again and stained with DAPI for 20 min at room temperature to define the nucleus. Assay plates were read on the BD Pathway 855 Bioimager (BD Biosciences) equipped with a 488/10 nm EGFP excitation filter, a 380/10 nm DAPI excitation filter, a 515 LP nm EGFP emission filter and a 435 LP nm DAPI emission filter. Images were acquired in the DAPI and GFP channels of each well by using 20Q dry objective. Data was exported from the BD Pathway Bioimager as text files and imported into the data analysis software BD Image Data Explorer (BD Biosciences) for processing. Cells presenting nuclear accumulation of the fluorescent reporter above 60% of the signal obtained from wells treated with 10 μM LY294002 were considered as hits.

2.12. Total protein extraction

A 3×10^5 A549 cells per well were seeded in 6-well plates and treated the next day with MSA, sodium selenite, LY294002 or vehicle at the specified concentrations for 6 and 24 h. At the end of the treatment, cells were washed twice with ice-cold PBS, incubated for 30 min on ice in lysis buffer containing 20 mM Trizma Base (pH 7.5), 1 mM dithriothreitol, 1 mM EDTA, 0.0002% Triton X-100, 0.5 mM sodium deoxycholate, 0.4 mM PMSF, 1% protease inhibitor cocktail and 1% phosphatase inhibitor cocktail (Thermo Scientific, Thermo Fisher Scientific Inc., Waltham, MA, USA). Cells were scraped, sonicated and centrifuged at 16,000 *g* for 20 min at 4 °C. Supernatants were recovered and the protein content was quantified by the bicinchoninic acid (BCA) kit (Pierce Biotechnology, Rockford, IL, USA).

2.13. Cytosolic and nuclear protein extracts

A549 cells were cultured and treated as described in total protein extraction section. In this case, cells were incubated for 10 min on ice with hypotonic buffer containing 20 mM HEPES (pH 7.6), 10 mM NaCl, 1.5 mM $MgCl_2$, 0.2 mM EDTA, 20% (v/v) glycerol, 0.1% (v/v) Triton X-100, 1% protease inhibitor cocktail and 1% phosphatase inhibitor cocktail. Cells were scraped and pipetted into cooled eppendorf tubes and then centrifuged at 1000 rpm in a swinging-bucket centrifuge at 4 °C. Supernatant was the cytoplasmic extract and the pellet contained the nuclei. To extract

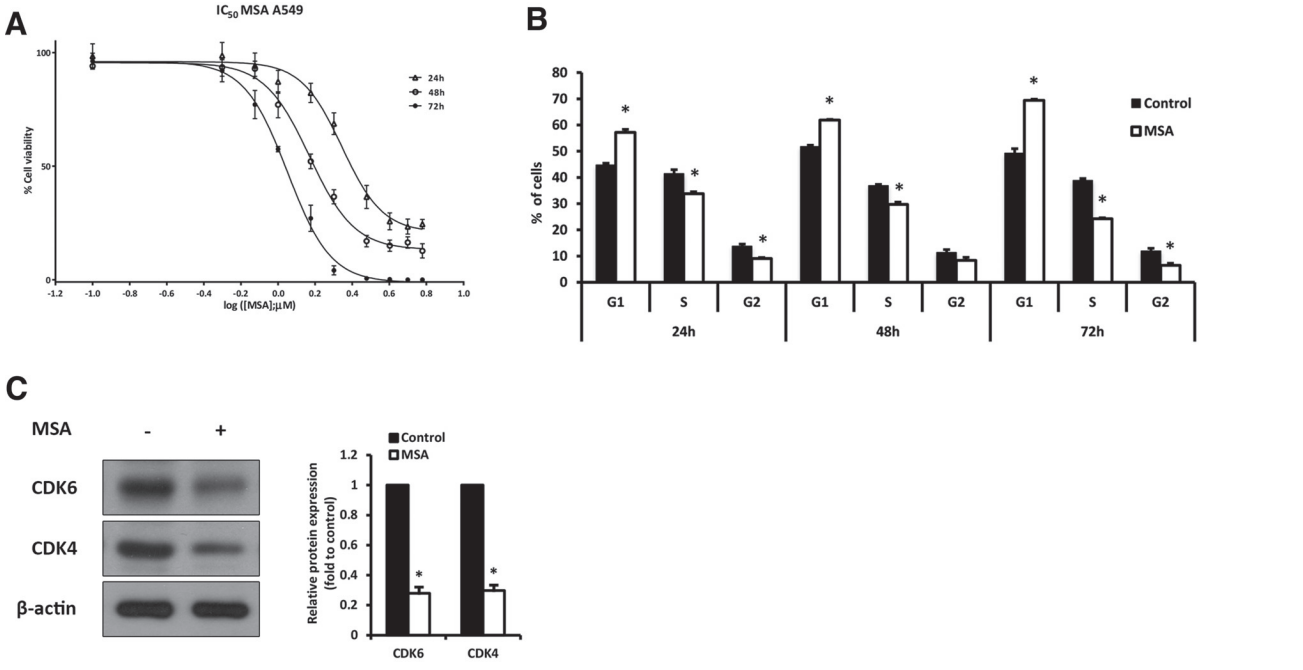

Fig. 1. MSA effects on cell viability and cell cycle in A549 cells. (A) Growth inhibition of MSA on A549 lung cancer cells after 24, 48 and 72 h measured by MTT assay. Exponentially growing cells were treated with the indicated concentration of MSA for 24, 48 and 72 h. The assay was carried out using six replicates and repeated three times. Data are represented as mean ± SD. (B) Cell cycle analysis of MSA-treated cells. A549 cells treated for 24, 48, 72 h with 1.3 μM MSA presented a G1 arrest. Cell cycle analysis was conducted after propidium iodide staining. Values represent mean ± SD and statistically significant differences between treated and control cells at $p < 0.05$ are indicated with an asterisk (*). (C) Western blot analysis showed a significant CDK4 and CDK6 inhibition at 6 h treatment with 5 μM MSA. Protein expression levels were quantified using ImageJ software and are expressed as mean band intensity normalized to β-actin and relative to control condition (* $p < 0.05$).

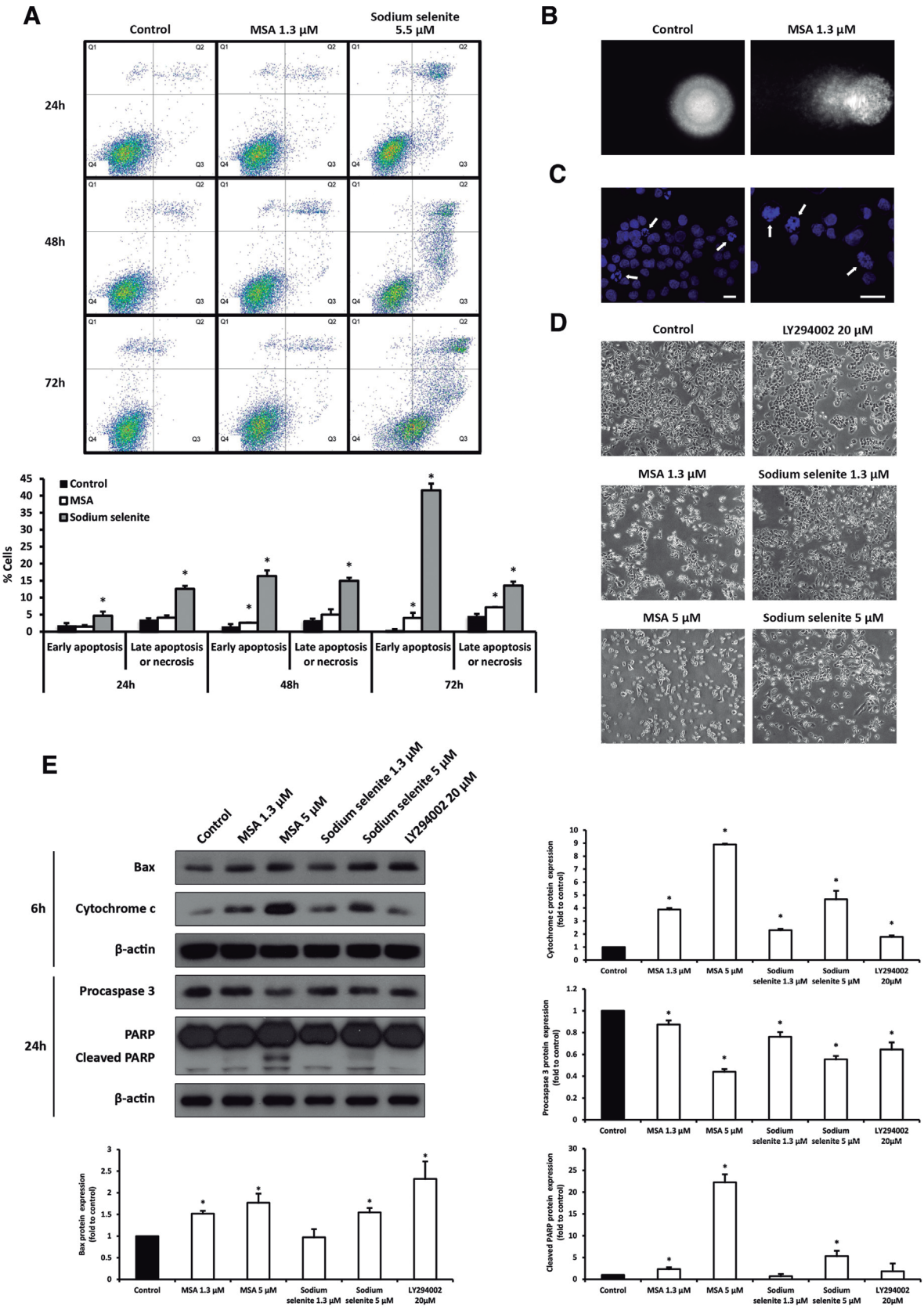

Fig. 2. Apoptosis assays in A549 cells. (A) Flow cytometry analysis of Annexin V-FITC staining and propidium iodide accumulation after exposure of A549 cells to MSA and sodium selenite at their respective $^{72h}IC_{50}$ concentrations for 24, 48 and 72 h. PI staining at 488 nm is represented on the *y*-axis and annexin V-FITC staining at 488 nm on the *x*-axis. Quadrant 4 ($PI^-/FITC^-$) represents non-apoptotic cells, early apoptosis is shown in right bottom quadrant ($PI^-/FITC^+$) and quadrants 1 and 2 (PI^+) depict late apoptotic/necrotic cells. Plots illustrate the percentage of cells in early apoptosis and late apoptosis/necrosis. Values are expressed as mean ± SD of three experiments in triplicate. Differences between treated and control groups were considered statistically significant at $p < 0.05$ (*). (B) DAPI staining of A549 cells DNA after electrophoresis in agarose gel (single-cell gel electrophoresis, comet assay). Control condition treatment with vehicle showed no induction of single strand breaks while 24 h MSA exposure at $^{72h}IC_{50}$ concentration caused DNA fragmentation in A549 cells. (C) Morphological changes in nuclei were examined after 72 h MSA treatment at $^{72h}IC_{50}$ concentration.

the nuclear proteins, the pellet was resuspended in five times its volume with hypertonic buffer (hypotonic buffer adding 500 mM NaCl), rocked for one hour at 4 °C and spinned at maximum speed at 4 °C for 5 min. The nuclear extract was the supernatant. Both cytosolic and nuclear extracts were assayed for protein concentration using the BCA kit.

2.14. Western blot analysis

An equal volume of protein was size-separated by electrophoresis on SDS-polyacrylamide gels and electroblotted onto polyvinylidene fluoride transfer membranes (PVDF) (Bio-Rad Laboratories, Hercules, CA, USA). After 1 h of blocking at room temperature with 5% skim milk in PBS 0.1% Tween, blots were incubated with the specific primary antibodies overnight at 4 °C. Then, membranes were treated with the appropriate secondary antibody for 1 h at room temperature. All blots were treated with Immobilon ECL Western Blotting Detection Kit Reagent (EMD Millipore, Billerica, MA, USA) and developed after exposure to an autoradiography film (VWR International, Radnor, PA, USA). The primary antibodies used were Phospho-Akt (#9271), Akt (#9272), Phospho-mTOR (#5536) and procaspase 3 (#9662) from Cell Signaling (Beverly, MA, USA); FOXO3a (#06-951) from Upstate (EMD Millipore); Phospho-FOXO3a (sc-101683), Phospho-JNK (sc-6254), FOXM1 (sc-500), Bax (sc-493), CDK4 (sc-260), CDK6 (sc-177), ERK 2 (sc-154) and Lamin B (sc-6217) from Santa Cruz Biotechnology (Santa Cruz, CA, USA); Phospho-PRAS40 (#44-1100) from BioSource International (Camarillo, CA, USA); PARP (#556493) and cytochrome c (#556433) from BD Pharmingen (BD Biosciences); p27 (#610242) from BD Transduction Laboratories (BD Biosciences) and β-actin (#69100) form MP Biomedicals (Santa Ana, CA, USA).

2.15. FOXO1 gene expression. RNA extraction, quantification, retrotranscription and quantitative reverse transcription-polymerase chain reaction (qRT-PCR)

RNA was isolated from frozen plates using trizol reagent (invitrogen) following the manufacturer's instructions. Briefly, Trizol cell homogenates were mixed with chloroform and centrifuged, obtaining an aqueous phase and an organic phase. In order to precipitate RNA, cold isopropanol was added in the aqueous phase and centrifuged at 12,000 *g* for 15 min at 4 °C. RNA was purified by several cold 75% ethanol washes and finally resuspended in RNAse free water. RNA was quantified using a Nanodrop (ND 1000 V3.1.0, Thermo Fisher Scientific Inc.). Reverse transcription was carried out with 1 μg RNA at 37 °C for 1 h with the following reagents: Buffer 5× (invitrogen), DTT 0.1 M (invitrogen), Random Hexamers (Roche), RNAsin 40 U μL^{-1} (Promega, Fitchburg, WI, USA), dNTPs 40 mM (Bioline, London, UK), M-MLV-RT 200 U μL^{-1} (invitrogen). Gene expression analysis was performed on an Applied Biosystems 7500 Real-Time PCR System according to the manufacturer's protocol, using Taqman gene specific sequences (*FOXO1*: Hs01054576_m1, Applied Biosystems, Thermo Fisher Scientific Inc.). Reactions were performed in 20 μL volume, using 9 μL of the cDNA mixture and 11 μL of the specific Taqman in Master Mix (Applied Biosystems). Real-time PCR was conducted according to the following parameters: an initial incubation at 50 °C for 2 min, a denaturalization at 95 °C for 10 min, followed by 40 cycles at 95 °C and 60 °C for 15 s and 1 min, respectively. Expression was quantified by ΔDCt method using Cyclophilin A (*PPIA*: Hs99999904_m1, Applied Biosystems) as reference gene.

2.16. Determination of intracellular reactive oxygen species (ROS) levels

A549 cells were grown on 6-well plates to 70% confluence, washed once with warm PBS, and incubated with 5 μM 2′-7′-dichlorodihydrofluorescein diacetate (H_2DCFDA, Invitrogen) in PBS supplemented with 5.5 mM glucose. After 30 min at 37 °C, PBS was replaced with complete culture medium and incubated for another 50 min at 37 °C. Finally, cells were trypsinized and resuspended thoroughly with 0.4 mL of PBS, H_2DCFDA (50 μM) and PI (20 μg mL^{-1}). Intracellular internalized probe reacts with ROS and emits fluorescence when excited at 492 nm. Emitted fluorescence was recorded by flow cytometry at 520 nm using an Epics XL flow cytometer (Coulter Corporation, Hialeah, FL, USA). Data of DCF fluorescence concentrations from 1×10^4 PI negative cells were collected and analysed using multicycle program (Phoenix Flow Systems, San Diego, CA, USA).

2.17. Stable shRNA cell line generation

U2OS and HEK293 stable FOXO3a knockdown cell lines were generated by Effectene (Qiagen, Hilden, Germany) reagent-mediated transfection with three different FOXO3a shRNA constructs originated from The Netherlands Cancer Institute (NKI) shRNA library [38]. FOXO3a shRNA sequences FOXO3a KD#1 (GCAGGCCTCATCTCAGAGCTCTCTTGAAGCTCTGAGATGAGGCCTGC), FOXO3a KD#2 (CTGCGACGGCTGACTGAAATCTCTTGAATTTCAGTCAGCAGTCGCAG) and FOXO3a KD#3 (CCTGATGGGGGAAANANCTCTCTTGAANCTCTGANATGANGCCTGC) were cloned into pRetroSuper vector (NKI, Amsterdam, The Netherlands). Empty pRetroSuper vector was used for control cells (Ctrl). Cells were selected in complete medium containing 1 μg mL^{-1} puromycin.

2.18. Data analysis and statistical methods

Experiments were carried out at least in triplicate and repeated three times. To evaluate the effects of combined drug treatments the multiple drug-effect analysis of Chou and Talalay [39] was used with the CompuSyn software (ComboSyn, Inc., Paramus, NJ, USA). MSA interactions with cisplatin and carboplatin were quantified by determining the Combination Index (CI), where CI < 1, CI = 1, and CI > 1 indicate synergism, additivity, and antagonism, respectively. All data are expressed as mean ± standard deviation (SD). Statistical analyses were performed using statgraphics statistical package (Statgraphics Centurion XVI, StatPoint technologies Inc., Warrenton, VA, USA). Control and treatment measurements were compared using Kruskal–Wallis, ANOVA and two-tailed independent sample Student's *t*-tests. Differences were considered to be significant at $p < 0.05$.

Hoechst stained nuclei were evaluated with a fluorescence microscope (200 and 400×, scale bar 3 μm) to detect increased condensation and margination of chromatin to the nuclear envelope and the formation of apoptotic bodies (white arrows). Apoptotic bodies were not observed in control condition. (D) Cells were incubated with MSA, sodium selenite and LY294002 at the indicated concentrations for 24 h and observed using an inverted phase contrast microscope. (E) Western blot analysis of total protein fractions of A549 cells. Protein expression was determined by densitometry analysis using ImageJ software and is represented as mean band intensity normalized to β-actin and related to untreated controls. MSA apoptosis activation is represented by enhancement of Bax and cytosolic cytochrome c expression, decrease of procaspase 3 levels and PARP cleavage (* $p < 0.05$). Sodium selenite induced changes in the same direction but to a significantly lower extent.

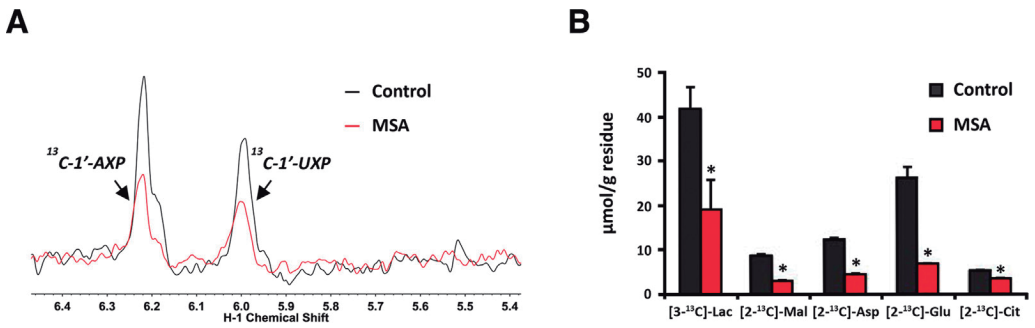

Fig. 3. MSA perturbs glycolysis, TCA cycle and nucleotide biosynthesis. A549 cells were grown in 0.2% [U-^{13}C]-glucose in the presence or absence of 5 μM MSA for 24 h. The polar metabolites were extracted in ice-cold 10% trichloroacetic acid and analysed by 1D HSQC NMR ((A): acquired at 14.1 T, 20 °C) and GC–MS (B). (A) Representative 1D HSQC NMR spectrum. The abundance of the ribosyl unit of adenine (^{13}C-1′-AXP) and uracil (^{13}C-1′-UXP) nucleotides was significantly attenuated 24 h after MSA treatment, relative to the control treatment. (B) The GC–MS analysis revealed reduced synthesis of TCA cycle metabolites, [2-^{13}C]-malate (Mal), [2-^{13}C]-aspartate (Asp), [2-^{13}C]-glutamate (Glu) and [2-^{13}C]-citrate (Cit), in addition to the glycolytic product, [3-^{13}C]-lactate (Lac). *p*-values <0.05 (*) were considered statistically significant.

3. Results

3.1. MSA inhibits cell proliferation and causes G1 arrest in human lung carcinoma A549 cells

The effect of MSA on human lung carcinoma A549 cell proliferation was examined using the MTT (3-[4,5-dimethylthiazol-2-yl]-2,5-diphenyltetrazolium bromide) colorimetric viability assay. Significant dose-dependent growth inhibition was observed in this cell line after treatment with 10 different concentrations of MSA for 24, 48 and 72 h (Fig. 1A).

The MSA concentrations required for achieving a 50% growth inhibition on A549 cells after 24, 48 and 72 h of treatment ($^{24h}IC_{50}$, $^{48h}IC_{50}$ and $^{72h}IC_{50}$) were 2.2 ± 0.3 μM, 1.6 ± 0.2 and 1.3 ± 0.1 μM, respectively.

Flow cytometric analyses of cell cycle distribution of A549 cells that had been exposed to $^{72h}IC_{50}$ MSA showed an increase of the G1 population at 24, 48 and 72 h of treatment as compared to control cells (increasing by 41% at 72 h). With the same treatment, a concomitant decrease was also observed in the percentage of cells in the S phase after 24, 48 and 72 h of treatment with respect to the untreated cells (38% decrease at 72 h), suggesting a G0/G1 arrest (Fig. 1B). A reduction in the percentage of cells in the G2 phase was also observed at all times.

The interphase cyclin-dependent kinases CDK4 and CDK6 control cell cycle re-entry and progression through G1 phase. In response to mitogenic stimuli, CDK4/6-cyclin D complexes phosphorylate the retinoblastoma (RB) protein family leading to their partial inactivation and relieving the transcriptional repression mediated by the RB-E2F complex [40]. Accordingly, MSA-induced cell cycle arrest could result from negative regulation of CDK4/6-cyclin D complexes. To test this idea, CDK4 and CDK6 protein expression was analysed after incubating A549 cells with 5 μM MSA for 6 h. A significant decrease in the protein levels of CDK4/6 was observed in MSA-treated cells (Fig. 1C).

To determine whether the concentrations of MSA used in the present study can acidify the media, we measured the pH values before and after the addition of MSA at 1.3 and 5 μM final concentrations. We also assessed the pH values after the addition of acetic acid, which is a weak acid with an acid dissociation constant (K_a) of 1.8×10^{-5} and a similar molecular structure as MSA. While the addition of acetic acid at 5 μM decreased the pH of the medium by 0.5 units, the same concentration of MSA did not cause any significant effects. Therefore, we conclude that the media were not acidified by the doses of MSA used in this study.

3.2. MSA induces apoptosis in A549 cells

Apoptosis was assessed in A549 cells after 24, 48 and 72 h of treatment with 1.3 μM MSA ($^{72h}IC_{50}$ for growth inhibition). FACS analysis using annexin V-FITC staining and PI accumulation was performed to differentiate non-apoptotic cells (annexin V^- and PI^-), early apoptotic cells (annexin V^+ and PI^-) and late apoptotic/necrotic cells (PI^+).

To determine if MSA effects were specific or general to other selenium compounds, sodium selenite was included in our analysis (Fig. 2A). MSA treatment for 24 h caused no significant effect on A549 cell apoptosis, while at 48 and 72 h, MSA exposure generated an increase in early apoptotic cells. In contrast, the apoptotic effect of sodium selenite was visible at 24 h and greatly enhanced at 48 and 72 h (reaching around 40% for early apoptotic cells) whereas the percentage of late apoptotic and necrotic cells remained constant at the three time points. Therefore, the extent of apoptosis caused by MSA was much reduced compared to that induced by sodium selenite, which can be due to different mechanisms of apoptosis activation.

Apoptotic cells undergo a series of characteristic morphological changes, such as shrinkage of the cell, chromatin condensation, apoptotic body formation and internucleosomal fragmentation of genomic DNA [41]. In order to evaluate DNA integrity, a single-cell gel electrophoresis was performed (Comet assay). Single strand break of DNA was observed after 24 h treatment with 1.3 μM MSA (Fig. 2B). Total Comet score of treated and untreated cells were 199 and 74, respectively. The presence of apoptotic bodies following 72 h MSA treatment at $^{72h}IC_{50}$ concentration was detected by Hoechst 33342 staining (Fig. 2C). Other typical apoptotic features such as rounding, shrinkage, detachment and loss of contact with adjacent cells were observed in MSA-treated cells (Fig. 2D) using an inverted phase contrast microscope.

Activation of the caspase pathway plays an important role in apoptosis. Caspases are constitutive cysteine proteases that are normally present as inactive proenzymes. Their enzymatic activity is induced during apoptosis in a self-amplifying cascade. Cleaved upstream caspases (caspases 2, 8, 9 and 10) activate effector caspases (caspases 3, 6 and 7) by proteolysis initiating the apoptotic cascade of events [41]. The intrinsic apoptosis pathway involves the release of cytochrome c into cytosol and the formation of the apoptosome complex by association with APAF-1. This complex activates caspase 9 which in turn cleaves procaspase 3, implicated in the proteolysis of poly (ADP-ribose) polymerase (PARP).

To elucidate the mechanisms involved in MSA or sodium selenite-mediated induction of apoptosis in A549 cells, whole-cell lysates were extracted and Western blot analyses were performed.

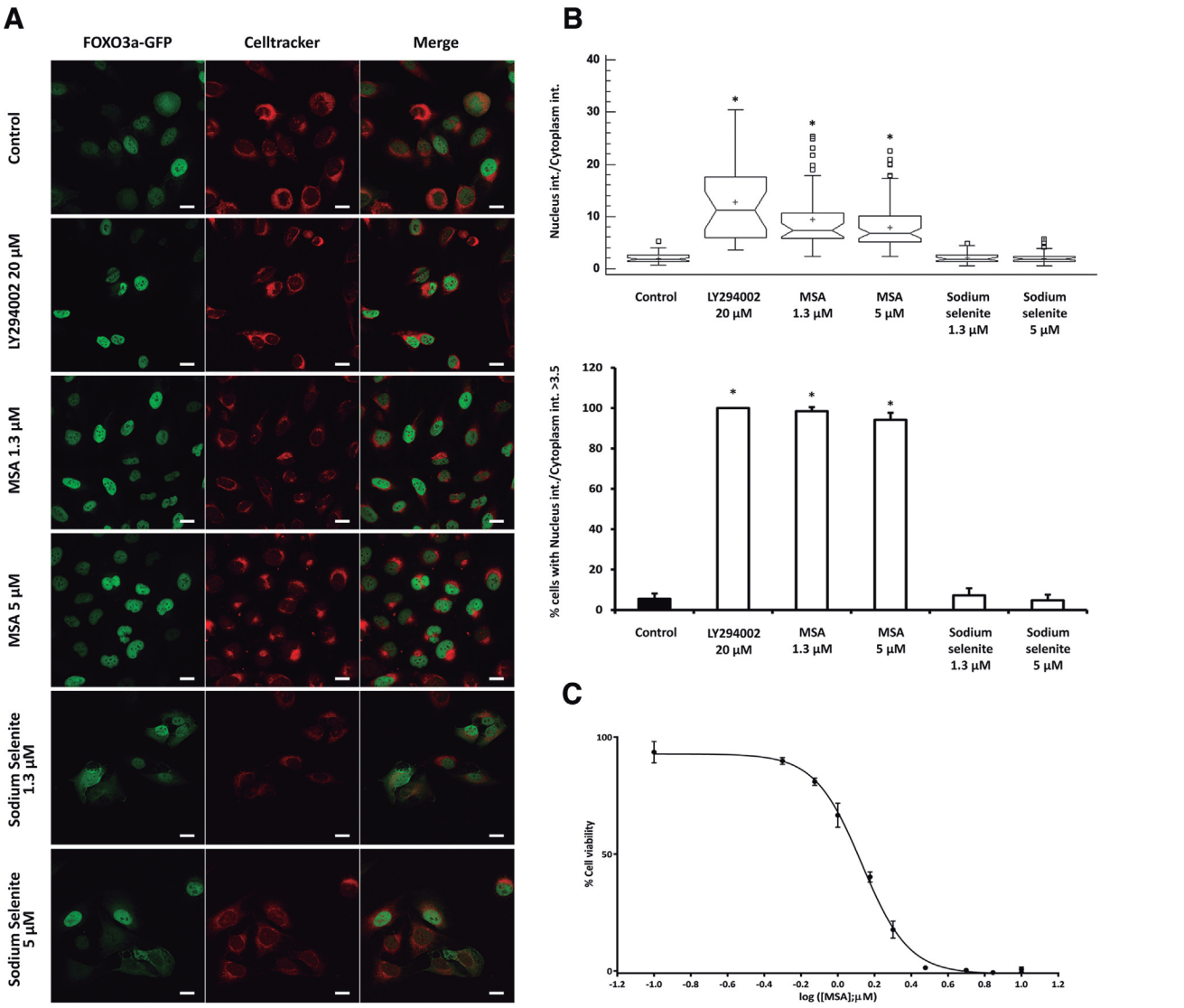

Fig. 4. Nuclear translocation of GFP–FOXO following MSA treatment in U2foxRELOC cells. U2foxRELOC cells stably expressing GFP–FOXO fusion protein were treated with vehicle, LY294002 (PI3K pathway inhibitor), MSA or sodium selenite for 6 h. (A) Representative confocal microscopy images for U2foxRELOC cells. Left row (green) indicates the subcellular location of FOXO3a-GFP. Celltracker location (red) identifies the cytoplasm. Scale bar, 5 μm. (B) Box and whiskers plot for the correlation between the nuclear and cytoplasmic green fluorescence intensity. Higher values represent a higher FOXO3a-GFP presence in the nucleus compared to the cytoplasm. Bar graph shows the percentage of the cells in each condition exhibiting nuclear/cytoplasmic ratios of fluorescence intensity greater than 3.5. MSA and LY294002 treatments display statistically significant differences (*) with the control condition using a multiple rang test (Kruskal–Wallis test) with 99% confidence. (C) Viability assay with MSA in U2foxRELOC cells at 72 h. Exponentially growing cells were treated with the indicated concentration of MSA for 72 h. The assay was carried out using six replicates and repeated three times. Data are represented as mean ± SD. (For interpretation of the references to color in this figure legend, the reader is referred to the web version of this article.)

The effects of LY294002, a known PI3K inhibitor [42], were also assessed. As shown in Fig. 2E, incubation with 5 μM MSA enhanced the expression of pro-apoptotic Bax and cytosolic cytochrome c, decreased the level of procaspase 3 and caused PARP cleavage. Sodium selenite 5 μM treatment induced changes in the same direction but to a significantly lower extent (sodium selenite $^{72h}IC_{50}$ in A549 cells is 5.5 ± 0.4 μM, data not shown).

3.3. MSA blocks glycolysis, TCA cycle and nucleotide biosynthesis

The effect of MSA on A549 cell metabolism was examined using the stable isotope-resolved metabolomics (SIRM) approach [43–45]. A549 cells were treated with uniformly ^{13}C-labeled glucose ([U-^{13}C]-glucose) in the absence (control) or presence of 5 μM MSA for 24 h. The glucose transformation products were analyzed by 1D HSQC NMR and GC–MS, as shown in Fig. 3. MSA-treated A549 cells had reduced synthesis of ^{13}C labelled lactate (glycolytic product), malate, aspartate, glutamate, citrate (TCA cycle metabolites), as well as adenine and uracil nucleotides (with the ribose unit derived from the PPP), relative to untreated A549 cells. These results suggest that MSA attenuates the activity of glycolysis, TCA cycle, PPP and/or nucleotide biosynthesis.

3.4. MSA causes nuclear translocation of FOXO3a in U2foxRELOC cells

Taking into account the arrest of cell cycle (G1), apoptosis induction, the metabolic effects of MSA on A549 cells and their correlation with those described for the PI3K inhibition [14], and the observed effects of MSA on PI3K signalling, we evaluated the effect of MSA on FOXO factors known to be the major transcriptional downstream effecter proteins of the PI3K/Akt signal transduction pathway [46]. As the activity of FOXO factors is mainly regulated by their subcellular localization [47], we first investi-

gated if MSA induced FOXO nuclear translocation. To this end, we used U2foxRELOC cells, a previously established cell system based on U2OS osteosarcoma cells that stably express a GFP–FOXO3a reporter [36,48,49].

In order to select the optimal MSA concentration for analyzing its effects on FOXO translocation, the MSA $^{72h}IC_{50}$ in U2foxRELOC cells was determined by incubating the cells with 10 different concentrations of MSA for 72 h and performing colorimetric viability assay. The values for dose-dependent growth inhibition were similar to the results obtained for A549 cells (Fig. 4C). We next analyzed the spatio-temporal kinetics of FOXO nuclear translocation upon MSA treatment. We exposed U2foxRELOC cells to 5 μM MSA for 1.5, 3, 6, 11 and 24 h and determined subcellular localization of the fluorescent FOXO reporter protein. MSA treatment induced GFP-FOXO3a nuclear translocation from 1.5 to 24 h, reaching a maximum effect between 3 and 6 h (data not shown).

With the assay conditions optimised, U2foxRELOC cells were treated with 1.3 and 5 μM MSA for 6 h and the subcellular localization of GFP-FOXO3a was monitored by confocal microscopy. Vehicle was used as a negative control and LY294002 (20 μM) as a positive control. As shown in Fig. 4A, GFP-FOXO3a was present in the cytosol of untreated cells as well as in the nucleus, whereas in MSA- and LY294002-incubated cells GFP-FOXO3a was localized almost exclusively in the nuclei. The percentage of cells in which GFP-FOXO3a nuclear intensity was at least 3.5 times higher than GFP-FOXO3a cytoplasmic intensity was less than 6% for control cells, more than 95% for LY294002-treated cells and more than 94% for MSA-treated cells (at both concentrations) (Fig. 4B). To determine whether FOXO3a nuclear translocation was specifically driven by MSA or was a general characteristic of selenium compounds, U2foxRELOC cells were also incubated with sodium selenite at the same concentrations as MSA. The intracellular distribution of GFP-FOXO3a remained unaltered in the presence of sodium selenite (Fig. 4A). These results support our hypothesis that MSA specifically induces FOXO3a nuclear translocation.

3.5. MSA induces GFP-FOXO3a nuclear translocation and increases nuclear FOXO3a in A549 cells

To further confirm our hypothesis and test if the translocation effect of MSA is also relevant for lung cancer cells, the effect of MSA on FOXO3a in A549 cells was analyzed. To this end, we transiently transfected GFP-FOXO into A549 cells and exposed them to MSA. Fig. 5A and B illustrate the results obtained after 6 h incubation with 5 μM MSA, 20 μM LY294002 or vehicle. MSA induced nuclear accumulation of FOXO3a in A549 cells, resulting in over 90% of cells exhibiting nuclear fluorescence intensity at least 1.5 times greater than cytoplasmic fluorescence intensity, compared to less than 2.5% of cells for the control conditions. To confirm the nuclear translocation of endogenous FOXO3a in non-transfected A549 cells in response to MSA treatment, Western blot assays of cells incubated in the same conditions were performed. As shown in Fig. 5C, MSA causes an increase in nuclear FOXO3a concentration and a decrease in the levels of cytoplasmic phosphorylated FOXO3a at the Ser253 residue (a known Akt phosphorylation site), consistent with our aforementioned results.

Since it is been described that FOXO1 transcription is stimulated by FOXO3a in a positive feedback loop [50,51], the effect of MSA on FOXO1 mRNA levels was analyzed. Cells were incubated with 5 μM MSA for different time periods from 1 h up to 24 h. Induction of FOXO1 expression was detected from 2 h to 24 h and increased in a time-dependent manner (Fig. 5D).

To validate the results obtained with confocal microscopy of U2foxRELOC cells treated with MSA and sodium selenite, the levels of active FOXO3a in non-transfected A549 cells were analysed by Western blot. As shown in Fig. 6, MSA induced FOXO3a expression while sodium selenite caused its inhibition. To confirm this observation, FOXM1 protein expression was examined as previous studies have reported that FOXO3a is a negative regulator of FOXM1 at the transcriptional level [52,53]. In agreement with these observations and further supporting MSA's mode of action through FOXO3a activity, MSA treatment significantly decreased FOXM1 expression while sodium selenite enhanced the level of this transcription factor (Fig. 6).

In order to identify the mechanisms involved in FOXO subcellular redistribution, changes in FOXO-regulating signal transduction pathways in response to MSA treatment were studied. It was previously reported that cell cycle arrest induced by FOXO proteins is mediated by enhanced transcription and protein expression of the cyclin-dependent kinase inhibitor p27 [54,55] and reduced protein expression of cyclins D1 and D2 [56]. Both cases result in an impaired capacity of CDK4 and CDK6 to hyperphosphorylate the RB protein family, leading to G1 arrest [40]. Moreover, while FOXO3a has been reported to induce the transcription of p27, PI3K/Akt pathway is known to suppress its expression in order to proceed with cell cycle [57]. To investigate whether MSA-induced G1 cell cycle arrest is associated with Akt and FOXO signalling, p27 and phosphorylation of Akt on Ser 473 status were analysed by Western blot. Six-hour treatment with MSA (at both 1.3 and 5 μM) significantly suppressed Akt phosphorylation without affecting its total protein level (Fig. 6). These results suggest that FOXO3a dephosphorylation and nuclear accumulation in response to MSA are mediated by Akt inactivation. The PI3K inhibitor LY294002 showed the same behaviour as MSA while sodium selenite increased Akt phosphorylation in a dose-dependent manner. The overactivation of Akt mediated by sodium selenite could account for the depletion in FOXO3a levels observed (Fig. 6). PRAS-40, an Akt substrate, followed the same phosphorylation pattern, further supporting our hypothesis (Fig. 6). mTOR pathway was downregulated by MSA as phosphorylated mTOR levels were reduced significantly after MSA treatment while sodium selenite activated this signalling pathway by increasing P-mTOR level. Dephosphorylation of Akt and FOXO activation preceded the caspase-mediated apoptosis and the transcription of FOXO3a target genes such as p27 (Fig. 6). As expected, p27 levels were notably increased after exposure to 5 μM MSA and 20 μM LY294002 for 24 h, even though p27 level was only slightly enhanced by exposure to 1.3 μM MSA. These data corroborate with previous results that showed MSA and sodium selenite inducing distinct biochemical and cellular responses [7,58,59].

3.6. MSA elicits ROS detoxification

FOXO proteins have been reported to induce detoxification of reactive oxygen species (ROS) by up-regulating free radical scavenging enzymes, including manganese superoxide dismutase and catalase [25]. FOXO transcription factors regulate two aspects of cellular resistance to stress: repair of damages caused by ROS and detoxification of ROS [19]. Given that MSA causes FOXO3a translocation to the nucleus, we measured ROS levels in A549 cells. The results show that 1.3 μM MSA caused a significant decrease in the levels of ROS at 24 and 48 h (Fig. 7). This decrease is consistent with the increased cellular free thiol levels observed by Poerschke et al. [60] after 24 h MSA incubation. Cells incubated with MSA for 72 h had similar ROS level to control cells. In contrast, sodium selenite inhibited ROS production at 24 h but enhanced it at 48 and 72 h.

Previous studies described the role of JNK as a FOXO activator mediating the phosphorylation of 14-3-3 proteins, thus releasing FOXO factors and trigging their nuclear relocalization [61–63]. As shown in Fig. 6, MSA incubation resulted in an increase in P-JNK, which is consistent with FOXO activation by Akt dephosphorylation. Sodium selenite enhancement in P-JNK levels could be a

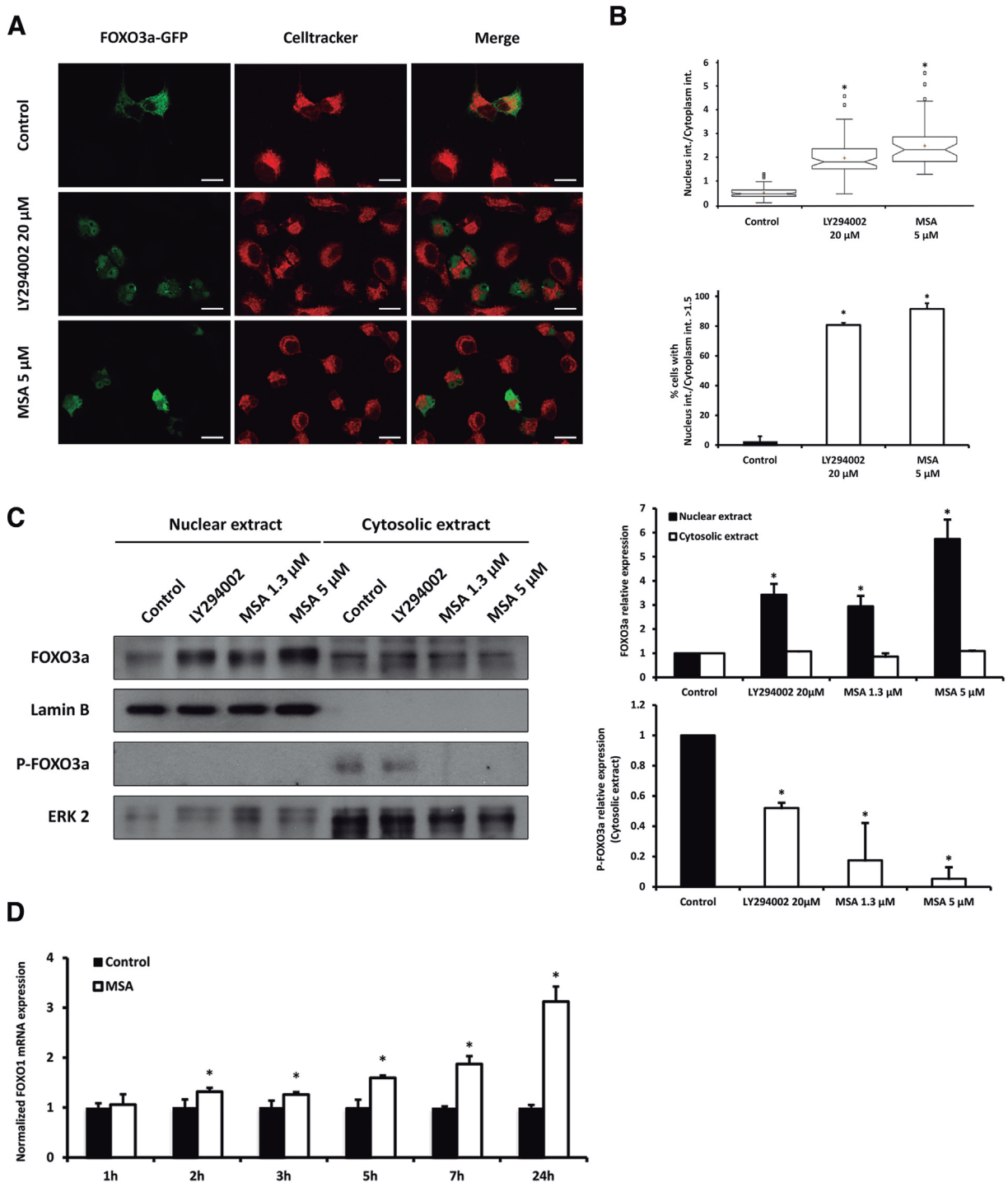

Fig. 5. MSA induces GFP-FOXO3a nuclear translocation and increases endogenous nuclear FOXO3a in A549 cells. (A) Representative confocal microscopy images for A549 cells transfected with a FOXO3a-GFP reporter plasmid and treated with vehicle, 20 μM LY294002 or 5 μM MSA for 6 h. Left row (green) indicates the intracellular location of FOXO3a-GFP. Celltracker location (red) identifies the cytoplasm. Scale bar, 5 μm. (B) Box and whiskers plot for the correlation between the nuclear and cytoplasmic green fluorescence intensity. Higher values indicate a higher FOXO3a-GFP presence in the nucleus compared to the cytoplasm. Bar graph represents the percentage of the cells in each condition displaying nuclear/cytoplasmic ratios of fluorescence intensity greater than 1.5. MSA and LY294002 treatments present statistically significant differences (*) with the control condition using a multiple rang test (Kruskal–Wallis test) with 99% confidence. (C) Western blots for the nuclear and cytoplasmic fractions of A549 cells. Protein expression levels were quantified using ImageJ software and are expressed as mean band intensity normalized to Lamin B (nuclear extract) or ERK 2 (cytosolic extract) and related to untreated controls. Endogenous nuclear FOXO3a levels increase with 6 h MSA and LY294002 treatments whereas phosphorylated FOXO3a cytoplasmic levels decrease (* $p < 0.05$). (D) mRNA levels of FOXO1 were analysed by qRT-PCR. Cells were incubated with 5 μM MSA from 1 h up to 24 h. The graph bar represents the expression of FOXO1 relative to control, which was assigned a value of 1. FOXO1 expression was significantly (* $p < 0.05$) and progressively induced from 2 h to 24 h. (For interpretation of the references to color in this figure legend, the reader is referred to the web version of this article.)

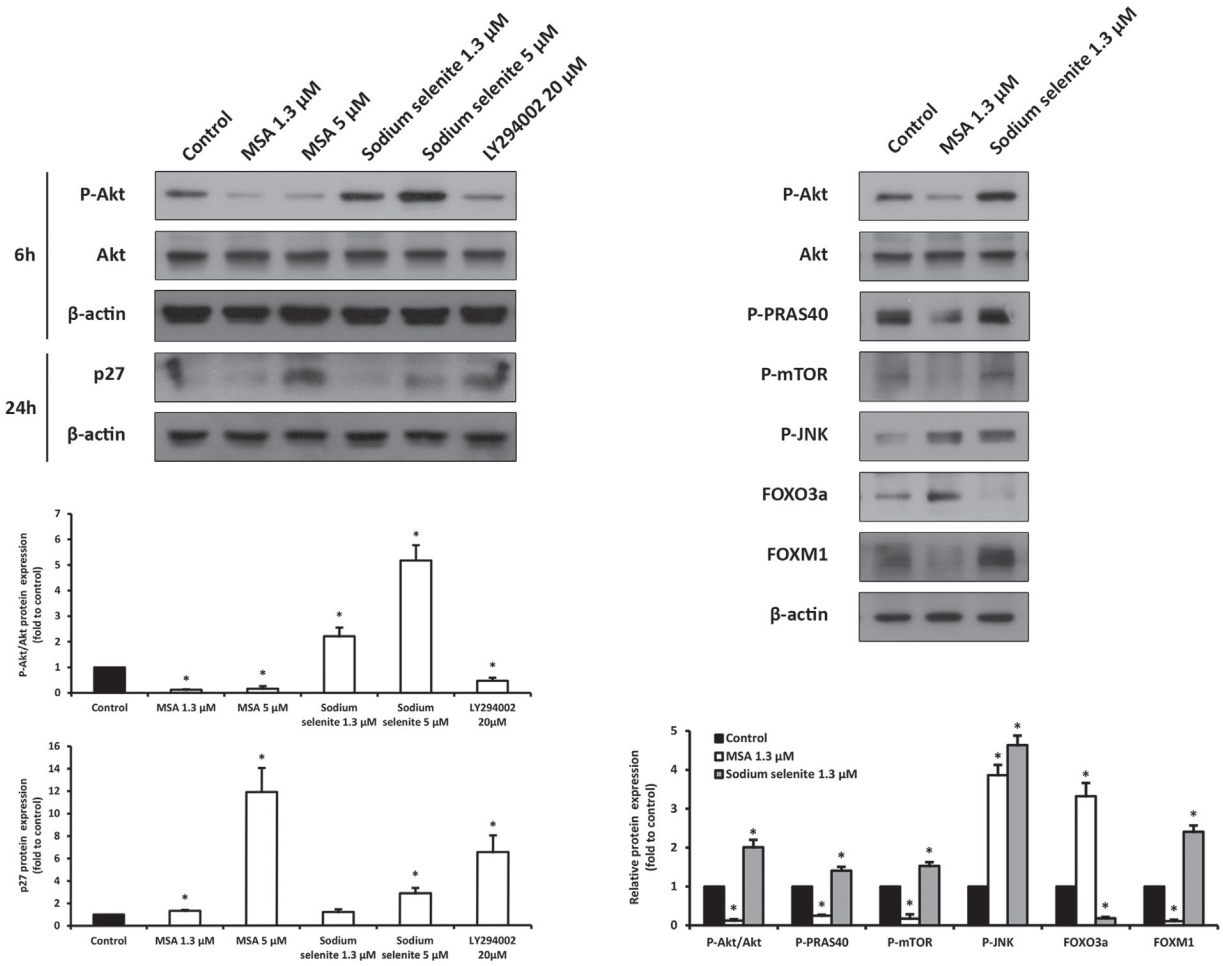

Fig. 6. MSA-induced G1 arrest and apoptosis are associated with Akt inhibition. Total protein fractions of A549 cells were analysed by Western blot. Protein expression was quantified by densitometric analysis using ImageJ software and is represented as mean band intensity normalized to β-actin and related to untreated controls. MSA induces the dephosphorylation of mTOR and Akt and its downstream target PRAS-40, the phosphorylation of JNK, an increase of FOXO3a levels, a reduction of FOXM1 protein expression and a G1 arrest represented by p27 accumulation. Differences between treated and control groups were considered statistically significant at $p < 0.05$ (*).

consequence of selenite-induced ROS production since JNK cascade can be independently activated by environmental stresses [64].

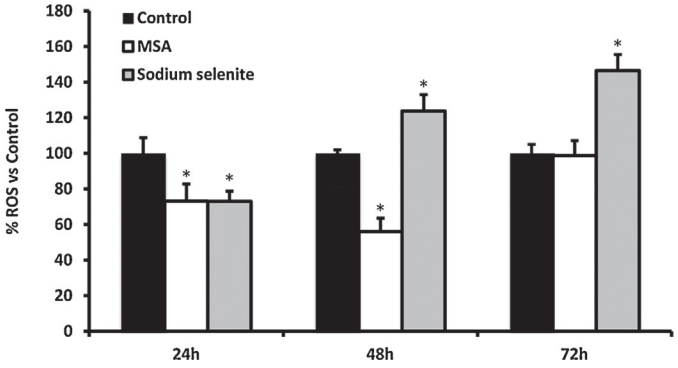

Fig. 7. ROS detoxification by MSA treatment. (A) decrease in ROS levels was observed in MSA-treated A549 cells. This reduction was only statistically significant after 24 and 48 h (* $p < 0.05$). Cells treated with sodium selenite for 24 h presented similar ROS level to MSA-treated cells but significantly enhanced the production of ROS in a time-dependent manner after 48 and 72 h incubations.

3.7. FOXO3a knockdown attenuates MSA effects

In order to confirm the role of FOXO3a as a mediator of MSA antitumour effects, we stably silenced FOXO3 in two different cell lines using shRNA vectors. We established U2OS and HEK293 cells that stably expressed three different hairpin sequences and validated the efficiency of FOXO3a knockdown by Western blot. The results revealed that FOXO3a KD#1 construct exhibited the strongest knockdown effect, followed by FOXO3a KD#2 (Fig. 8 A). Hence, the U2OS cell lines transfected with these two constructs and the FOXO3a KD#1HEK293 cell line were selected to perform the following experiments.

We incubated Ctrl (empty vector) and FOXO3a knockdown cells with 1 μM MSA or vehicle (PBS) and measured cell proliferation, cell cycle and apoptosis after 72 h (Fig. 8B–G), and ROS after 48 h treatment (Fig. 8H–I). The results showed that MSA effects were attenuated or even abolished by FOXO3a knockdown. In fact, the observed antiproliferative effect of MSA was significantly reduced after FOXO3a inhibition, while no differences in cell cycle, apoptosis and ROS levels were found between untreated and MSA-treated FOXO3a knockdown cells. These results further confirm that the antitumour response of MSA treatment is mediated by FOXO3a.

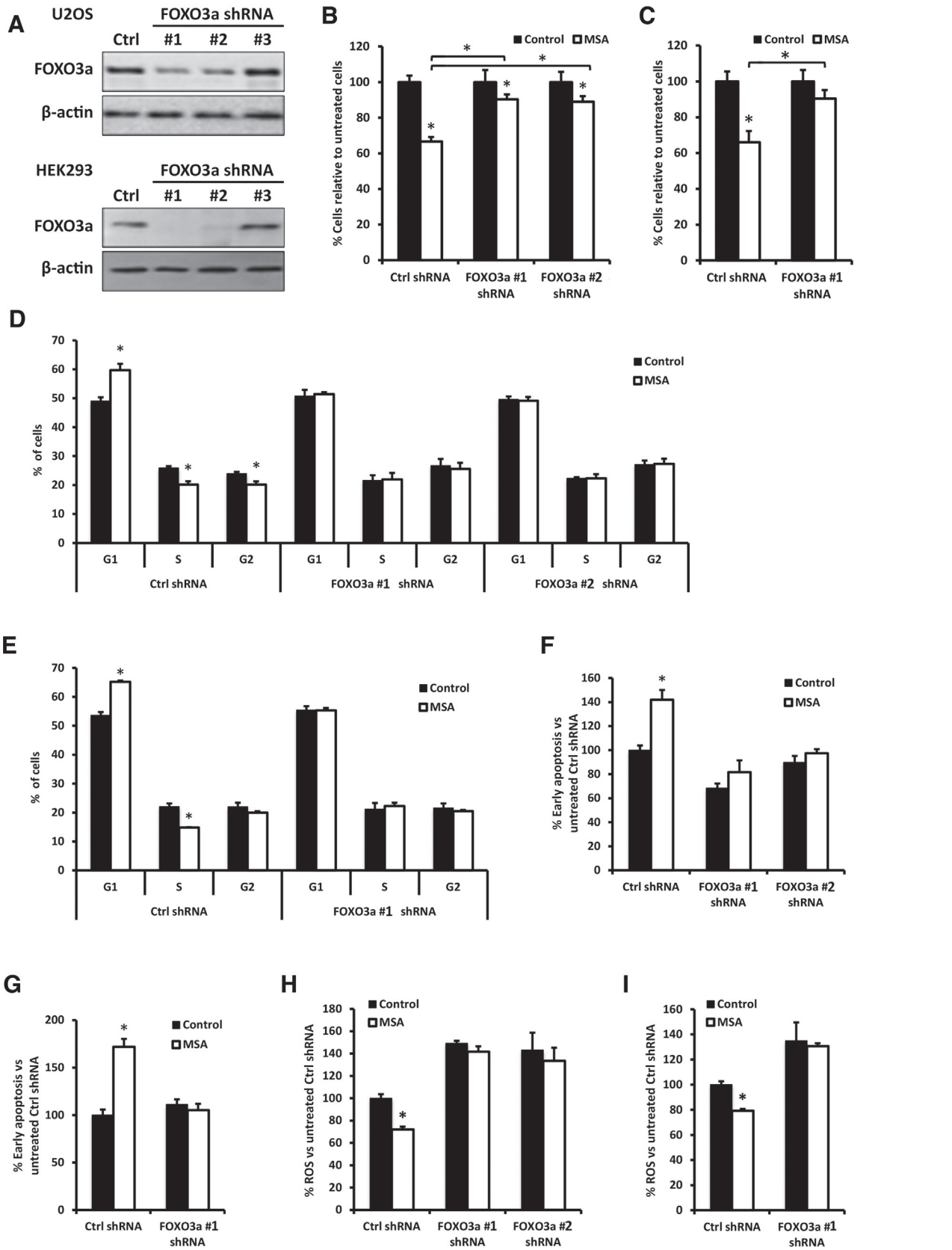

Fig. 8. Effects of FOXO3a knockdown on MSA activity. U2OS and HEK293 cells were stably transfected with control shRNA (Ctrl) or constructs expressing two different FOXO3a-specific shRNA sequences (FOXO3a #1 and FOXO3a #2). (A) Western blot analysis of total protein fractions of U2OS and HEK293 cells. β-actin was used as a protein loading control. Sequence #1 exhibited the highest knockdown efficiency. (B and C) Viability assays after treatment with 1 μM MSA for 72 h in (B) U2OS shRNA transfected cells and (C) HEK293 shRNA transfected cells. Data are expressed as percentage of viability relative to untreated cells. (D and E) Cell cycle analysis of 1 μM MSA-treated cells for 72 h in (D) U2OS shRNA transfected cells and (E) HEK293 shRNA transfected cells. Cell cycle analysis was conducted after propidium iodide staining. (F and G) Percentage of early apoptotic cells relative to untreated Ctrl shRNA cells obtained by flow cytometry analysis of Annexin V-FITC staining and propidium iodide accumulation after exposure of (F) U2OS shRNA transfected cells and (G) HEK293 shRNA transfected cells to 1 μM MSA for 72 h. (H and I) Intracellular ROS levels determined by flow cytometry

3.8. MSA as a promising chemotherapeutic agent

Cisplatin-based therapy is a conventional chemotherapeutic treatment for cancer. However, its clinical efficacy is compromised by acquired resistance and dose-limiting side effects [65]. Consequently, the search for combination therapies and chemosensitizing agents to cisplatin is essential for improving its treatment outcome. Given that previous studies reported the enhancement of cisplatin's antitumour effects in combination with FOXO nuclear export inhibitors [26–29], we hypothesized that combined treatment of MSA with cisplatin could be a promising new strategy in cancer therapy.

To quantify the synergy of dose-dependent effect on cell viability, we used the combination index (CI) equation of Chou and Talalay [39]. We examined the synergistic effects of MSA and cisplatin in A549, HCT116 (colorectal carcinoma), MCF7 (breast adenocarcinoma) and OVCAR3 (ovary adenocarcinoma) cells which are considered to present cisplatin-resistance, exhibiting IC_{50} values higher than 10 μM [66] (http://www.cancerrxgene.org/translation/Drug/1005). The combination of MSA and cisplatin treatment in a wide dose range showed a significant synergism in the antiproliferative effects with a CI < 1 in each tested cell line (Table 1).

In addition, we studied the synergism of MSA and carboplatin, a derivative of cisplatin commonly used in conventional chemotherapy with similar efficacy, in the same cell lines. Likewise, the combination of MSA and carboplatin treatment in a wide dose range exhibited a synergistic (CI < 1) antiproliferative effect in each tested cell line (Table 2).

Compared with cisplatin or carboplatin single treatments, dosage of these conventional chemotherapeutics could be remarkably reduced in combination therapy with MSA to gain the same inhibitory effect on cell proliferation. Therefore, the synergism observed in HCT116, MCF7, A549 and OVCAR3 cells suggests the combined MSA/cisplatin or carboplatin treatment as an efficient strategy to decrease the chemotherapeutic doses and consequently, mitigate the overall toxicity.

In order to determine if MSA treatment obtained similar growth inhibitory results in other cancer cell lines, the effect of MSA on cell viability in NCI-H460 (large cell lung cancer) and HCT116 (colorectal carcinoma) cell lines was measured. The $^{72h}IC_{50}$ values obtained were in the same range as for A549 cells, being 1.7 ± 0.2 μM and 1.9 ± 0.2 μM for NCI-H460 and HCT116 cells, respectively (Fig. 9A). To investigate if FOXO activation mediated by MSA is a general mechanism and not cell-dependent, HCT116 cell line was used to evaluate FOXO1 mRNA expression, which showed a significant increase in a time-dependent manner beginning at 2 h with 5 μM MSA treatment (data not shown).

To test the selective cytotoxicity of MSA for cancer cells, a MTT colorimetric viability assay using a non-tumour non-proliferating cell line was performed. Differentiated 3T3-L1 adipocytes were incubated for 72 h with 9 different MSA concentrations and the effect on cell proliferation and the $^{72h}IC_{50}$ value were determined (Fig. 9A). $^{72h}IC_{50}$ for MSA in 3T3-L1 cells was three to five times the value for all tumour cell lines that have been studied (Fig. 9B), supporting MSA as a promising chemotherapeutic agent with selective antiproliferative effects on cancer cells.

Table 1
Synergistic antiproliferative effect of MSA and cisplatin combination treatment.

(A) A549 cells, ratio 1:10

MSA (μM)	Cisplatin (μM)	Viability (%)	CI Value
0.05	0.5	91.1 ± 1.8	0.570
0.1	1	78.9 ± 1.1	0.447
0.3	3	56.5 ± 2.0	0.631
0.5	5	41.1 ± 3.4	0.707
0.75	7.5	27.9 ± 2.6	0.751
1	10	17.3 ± 0.5	0.729
1.3	13	8.5 ± 0.5	0.663
1.5	15	4.2 ± 0.5	0.578
2	20	1.8 ± 0.5	0.595

(B) HCT116 cells, ratio 1:5

MSA (μM)	Cisplatin (μM)	Viability (%)	CI Value
0.75	3.75	74.5 ± 4.9	0.717
1	5	62.8 ± 3.9	0.667
1.5	7.5	45.1 ± 3.0	0.669
2	10	34.9 ± 3.9	0.725
2.5	12.5	26.0 ± 2.4	0.750
3	15	16.8 ± 2.1	0.716
3.5	17.5	11.0 ± 1.3	0.695
4	20	3.6 ± 0.7	0.517
5	25	2.6 ± 0.6	0.579

(C) MCF7 cells, ratio 1:4

MSA (μM)	Cisplatin (μM)	Viability (%)	CI Value
0.5	2	78.0 ± 1.2	0.275
0.75	3	74.6 ± 2.3	0.363
1	4	74.1 ± 2.1	0.476
1.5	6	70.2 ± 0.5	0.629
2	8	66.6 ± 0.1	0.753
2.5	10	49.5 ± 2.3	0.608
3	12	39.5 ± 3.2	0.575
3.5	14	19.9 ± 2.1	0.392
4	16	13.5 ± 1.4	0.350

(D) OVCAR3 cells, ratio 1:5

MSA (μM)	Cisplatin (μM)	Viability (%)	CI Value
0.75	3.75	49.8 ± 2.9	0.431
1	5	36.7 ± 2.6	0.446
1.5	7.5	25.5 ± 2.3	0.523
2	10	18.4 ± 1.1	0.573
2.5	12.5	11.6 ± 0.7	0.555
3	15	7.4 ± 0.6	0.530
3.5	17.5	6.9 ± 0.4	0.597
4	20	4.6 ± 0.2	0.557
5	25	2.7 ± 0.6	0.538

Cells were treated for 72 h at the indicated concentrations of MSA and cisplatin in a constant ratio. (A) A549 cells, ratio 1:10. (B) HCT116 cells, ratio 1:5. (C) MCF7 cells, ratio 1:4. (D) OVCAR3 cells, ratio 1:5. The CI results obtained with CompuSyn software revealed a synergy (CI < 1) in the antiproliferative effects of MSA and cisplatin at each dose combination tested.

4. Discussion

Selenium is an essential trace element fundamental to human health with pivotal structural and enzymatic functions in selenoproteins. Selenium deficiency has been acknowledged as a contributing factor to a series of distinct pathophysiological conditions, including cancer. Several selenium compounds have shown cancer chemopreventive and chemotherapeutic activities in both animal models and humans [11,67,68]. It is important to note that both dose and chemical form of selenium are crucial for the antitumour activity. MSA and sodium selenite are among the forms with high anticarcinogenic activity while selenomethionine used

after 1 μM MSA incubation for 48 h of (H) U2OS shRNA transfected cells and (I) HEK293 shRNA transfected cells. Results are expressed as percentage of mean fluorescent intensity relative to untreated Ctrl shRNA cells. In all cases, values represent mean ± SD and statistically significant differences between treated and control cells at $p < 0.05$ are indicated with an asterisk (*).

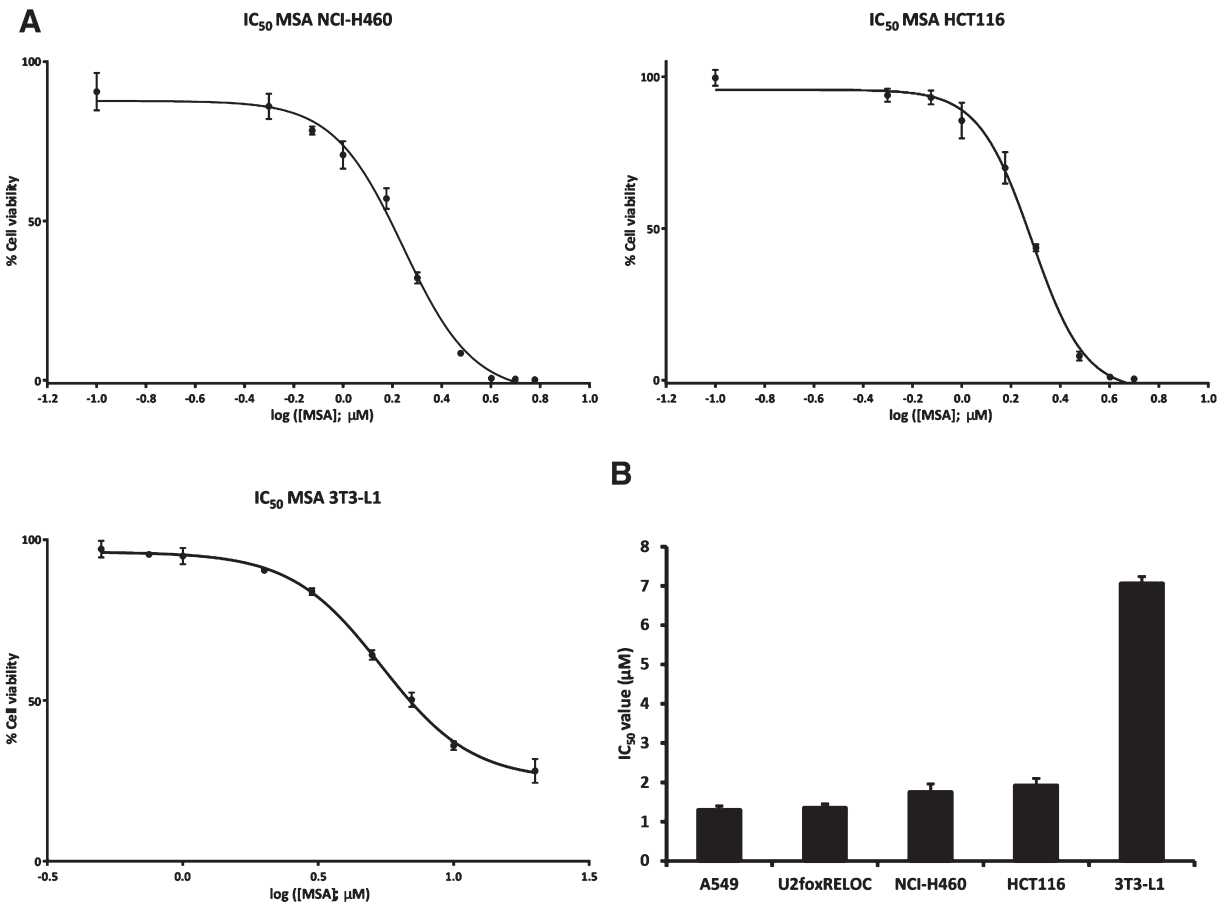

Fig. 9. Effect of MSA on cell viability. (A) Viability assays with MSA in NCI-H460, HCT116 and differentiated 3T3-L1 cells. (B) Comparison between the $^{72h}IC_{50}$ values for the tested cell lines. The MSA concentration that caused 50% inhibition of cell viability at 72 h of treatment for the 3T3-L1 non-tumour cell line was three to five times the value for all tumour cell lines analyzed.

in the SELECT trial was ineffective in cancer prevention in humans [11,69,70].

There are several in vivo studies involving dietary selenium supplementation for cancer therapy and prevention. The evaluation of the effects of different diets containing MSA, sodium selenite or selenomethionine in tumour xenografts in mice has led to the conclusion that MSA exhibits a superior in vivo inhibitory efficacy against human prostate and breast cancers over selenomethionine or sodium selenite [8,10,71]. Indeed, dietary supplementation with MSA significantly inhibits xenograft tumour growth and reduces angiogenesis and spontaneous metastasis [8,10,71–73]. Importantly, supplementation with MSA does not affect neither the animal body weight nor the food consumption when compared with control diet animals, and histological alterations in organs are not observed, altogether indicating a good tolerance to the used dosage of MSA without adverse side effects [8,71,72]. Moreover, MSA supplementation results in less accumulation of selenium both in liver and primary tumour when compared with selenomethionine, while causes no increment in kidney selenium levels relative to controls [8,10,71]. These results are consistent with the fact that MSA is efficiently transformed into methylselenol which in turn can be methylated and excreted [74]. Therefore, MSA treatment presents superior in vivo antitumour efficacy with good tolerance results over other selenium derivates [8,10,71,72].

The fact that the molecular mechanism underlying MSA's antitumour properties has not been fully elucidated is a bottle neck in designing combination therapies with MSA. In this study, we described that lung carcinoma A549 cells are very sensitive to MSA treatment, in terms of growth inhibition, cell cycle arrest in G1 phase, attenuated intracellular ROS levels and apoptosis. However, some studies have described selenium derivatives as pro-oxidant products at higher doses than those used in this study [13]. This property could be due to dose dependence: at low concentrations MSA could serve as an antioxidant product, while at higher concentrations it could act as a pro-oxidant compound [69]. The antioxidant function could be mediated via the synthesis of selenocysteine, which is an essential residue of important ROS-detoxifying selenoproteins, such as glutathione peroxidases, thioredoxin reductases and possibly selenoprotein P [75]. Our results suggest distinct redox modulations of the two selenocompounds tested and thus different mechanisms of action. Heightened levels of ROS generated by sodium selenite can cause damage to DNA and mitochondria, leading to apoptosis. Considering these and previous results [6], sodium selenite induces apoptosis through generation of ROS while MSA-mediated apoptosis is regulated by a different molecular pathway like FOXO activation.

We have also shown that MSA induces FOXO translocation to the nucleus after 1.5 h of a 5 μM treatment and this localization is maintained for at least 24 h. In addition, we have demonstrated that FOXO translocation after 1.5 h is the early event that occurs before the observed molecular and metabolic effects of MSA. Moreover, we have shown that the inhibition of the PI3K pathway through Akt and FOXO3a dephosphorylation could be the molecular mechanism underlying inhibition of cell proliferation, disruption of tumour cell metabolic adaptations, induction of apoptosis, ROS detoxification and cell cycle arrest in A549 cells. Indeed, FOXO3a knockdown attenuated or even abolished the antiproliferative effects of MSA. It is worth noting that although MSA activity is mediated through

Table 2
Synergistic antiproliferative effect of MSA and carboplatin combination treatment.

(A) A549 cells, ratio 1:6			
MSA (μM)	Cisplatin (μM)	Viability (%)	CI Value
0.5	3	81.2 ± 4.1	0.408
0.75	4.5	71.3 ± 5.2	0.642
1	6	61.2 ± 0.4	0.637
1.5	9	48.2 ± 1.4	0.775
2	12	30.7 ± 3.2	0.781
2.5	15	19.3 ± 0.9	0.626
3	18	12.8 ± 2.1	0.792
3.5	21	10.5 ± 1.3	0.816
4	24	8.1 ± 0.5	0.887
(B) HCT116 cells, ratio 1:10			
MSA (μM)	Cisplatin (μM)	Viability (%)	CI Value
0.25	2.5	89 ± 1.3	0.306
0.5	5	77 ± 1.9	0.398
1	10	72 ± 0.2	0.661
1.5	15	55 ± 0.6	0.731
2	20	38 ± 3.4	0.711
2.5	25	22 ± 2.0	0.674
3	30	14 ± 0.6	0.692
3.5	35	12 ± 1.5	0.752
4	40	4 ± 2.8	0.608
5	50	2 ± 0.6	0.567
(C) MCF7 cells, ratio 1:6			
MSA (μM)	Cisplatin (μM)	Viability (%)	CI Value
0.5	3	84.9 ± 5.4	0.295
0.75	4.5	70.3 ± 3.9	0.299
1	6	63.5 ± 5.0	0.347
1.5	9	55.2 ± 2.0	0.445
2	12	46.7 ± 4.3	0.510
2.5	15	36.1 ± 5.0	0.523
3	18	15.8 ± 4.2	0.381
3.5	21	13.4 ± 1.3	0.408
4	24	11.2 ± 0.7	0.424
5	30	8.7 ± 0.7	0.469
(D) OVCAR3 cells, ratio 1:6			
MSA (μM)	Cisplatin (μM)	Viability (%)	CI Value
0.75	4.5	85.1 ± 1.8	0.668
1	6	77.5 ± 5.1	0.697
1.5	9	66.9 ± 0.5	0.908
2	12	44.4 ± 0.0	0.862
2.5	15	37.1 ± 1.0	0.966
3	18	24.7 ± 0.6	0.937
3.5	21	14.9 ± 0.1	0.874
4	24	6.5 ± 2.0	0.719
5	30	3.2 ± 0.6	0.686

Cells were treated for 72 h at the indicated concentrations of MSA and carboplatin in a constant ratio. (A) A549 cells, ratio 1:6. (B) HCT116 cells, ratio 1:10. (C) MCF7 cells, ratio 1:6. (D) OVCAR3 cells, ratio 1:6. The CI results obtained with CompuSyn software revealed a synergistic (CI < 1) antiproliferative effect of MSA and carboplatin at each dose combination tested.

inhibition of Akt, it does not have an effect on other signalling pathways such as MAPK [7].

FOXO proteins are potentially key targets for new therapeutic strategies for blocking tumourigenesis due to their ability to control cell cycle and promote apoptosis [76]. The tumour suppressor properties of FOXO factors are inhibited mostly by overactivation of their inhibitory signalling, in contrast to other tumour suppressors, whose activities are abrogated by genetic or epigenetic changes. These characteristics call for strategies on rescuing FOXO activity by its reactivation and targeting of its inhibitors [25]. As such, MSA is well-suited to serve as an anticancer agent by inhibiting the PI3K/Akt/mTOR axis and activating JNK signalling pathway, leading to FOXO nuclear relocalization and restoration of its gene expression. Moreover, combination therapies that target PI3K/Akt pathway and promote nuclear FOXO retention are considered to be a promising approach to treat several tumour types. For example, in recent studies it has been proposed that cytotoxicity of cisplatin in sensitive cells can be enhanced and drug resistance in unresponsive cells reversed by using agents that target the PI3K/Akt/FOXO pathway in combination with cisplatin [26–29]. Our studies support such hypothesis as MSA both synergised with cisplatin and its derivative carboplatin in blocking A549, HCT116, MCF7 and OVCAR3 cell proliferation. Thus, the combination of MSA with either cisplatin or carboplatin could represent a promising new approach to lung cancer treatment in terms of reducing platinum derivatives doses or toxicity as well as drug resistance.

5. Conclusions

Our data support a strong antiproliferative action of MSA in the low micromolar range on A549 cells, which is mediated by blocking G1 progression and triggering apoptosis. These MSA effects are associated with the inhibition of the Akt pathway, leading to dephosphorylation of FOXO proteins and their nuclear translocation, which in turn activate the expression of FOXO target genes. The time course data suggest that FOXO dephosphorylation and relocalization to the nucleus are early events that activate the antiproliferative response of A549 cells to MSA. By targeting the PI3K/Akt/FOXO pathway, MSA could synergise with cisplatin in combination therapy to reduce the commonly observed toxicity and resistance development of cisplatin-based chemotherapy.

Conflict of interest

All the authors are aware of and agree to the content of the paper and their being listed as an author on the paper. The authors state no conflicts of interest.

Authors' contributions

M.T.C., R.C., M.Z., J.T.C., I.H.P., R.H. and T.W.M.F. carried out the experiments and performed the statistical analysis. M.T.C., R.C., M.Z., W.L. and M.C. conceived and designed the study. M.T.C., R.C., M.Z., T.W.M.F., W.L. and M.C. analyzed the data, interpreted the results and drafted the manuscript. All authors read and approved the final manuscript.

Acknowledgements

This study received financial support from the Ministerio de Ciencia e Innovación, Spain (SAF2011-25726), the Agència de Gestió d'Ajuts Universitaris i de Recerca (AGAUR)-Generalitat de Catalunya (2014SGR1017), the Ministerio de Economía y Competitividad, Spain (SAF2014-56059-R) the Fundação para a Ciência e a Tecnologia (FCT) Research Center (grant UID/BIM/04773/2013CBMR 1334) and the National Institute of Health, USA (grant numbers 1R01CA118434-01A2 and 1P01CA163223-01A1). We would also like to acknowledge the National Science Foundation, USA (grant number EPS-0447479) for support of the 18.8 Tesla NMR system at the University of Louisville. R.H. is the recipient of a FCT 2012 research grant (SFRH/BPD/84634/2012) FCT. M.C. acknowledges the support received through the prize ICREA Academia for excellence in research, funded by ICREA Foundation-Generalitat de Catalunya. The authors thank Ursula Valls and Erika Zodda for their technical support and Dr. Sengodagounder Arumugam for acquiring the NMR data.

Appendix A. Supplementary data

Supplementary data associated with this article can be found, in the online version, at http://dx.doi.org/10.1016/j.phrs.2015.09.009.

References

[1] J. Ferlay, I.I. Soerjomataram, R. Dikshit, S. Eser, C. Mathers, M. Rebelo, et al., Cancer incidence and mortality worldwide: sources, methods and major patterns in GLOBOCAN 2012, Int. J. Cancer (2014).
[2] H.E. Ganther, Selenium metabolism selenoproteins and mechanisms of cancer prevention: complexities with thioredoxin reductase, Carcinogenesis 20 (1999) 1657–1666.
[3] G.N. Schrauzer, Selenium and selenium-antagonistic elements in nutritional cancer prevention, Crit. Rev. Biotechnol. 29 (2009) 10–17.
[4] R. Muecke, L. Schomburg, J. Buentzel, K. Kisters, O. Micke, Selenium or no selenium—that is the question in tumor patients: a new controversy, Integr. Cancer Ther. 9 (2010) 136–141.
[5] J.J. An, K.J. Shi, W. Wei, F.Y. Hua, Y.L. Ci, Q. Jiang, et al., The ROS/JNK/ATF2 pathway mediates selenite-induced leukemia NB cell cycle arrest and apoptosis in vitro and in vivo, Cell Death Dis. 4 (2013) e973.
[6] S.H. Park, Induction of apoptosis and autophagy by sodium selenite in A549 human lung carcinoma cells through generation of reactive oxygen species, Toxicol. Lett. 212 (2012) 252–261.
[7] C. Jiang, Z. Wang, H. Ganther, J. Lü, Distinct effects of methylseleninic acid versus selenite on apoptosis, cell cycle, and protein kinase pathways in DU145 human prostate cancer cells, Mol. Cancer Ther. 1 (2002) 1059–1066.
[8] G.X. Li, H.J. Lee, Z. Wang, H. Hu, J.D. Liao, J.C. Watts, et al., Superior in vivo inhibitory efficacy of methylseleninic acid against human prostate cancer over selenomethionine or selenite, Carcinogenesis 29 (2008) 1005–1012.
[9] L. Patrick, Selenium biochemistry and cancer: a review of the literature, Altern. Med. Rev. 9 (2004) 239–258.
[10] Y.C. Chen, K.S. Prabhu, A. Das, A.M. Mastro, Dietary selenium supplementation modifies breast tumor growth and metastasis, Int. J. Cancer 133 (2013) 2054–2064.
[11] A.K. Sharma, S. Amin, Post SELECT selenium on trial, Future Med. Chem. 5 (2013) 163–174.
[12] S.M. Lippman, E.A. Klein, P.J. Goodman, M.S. Lucia, I.M. Thompson, L.G. Ford, et al., Effect of selenium and vitamin E on risk of prostate cancer and other cancers: the selenium and vitamin E cancer prevention trial (SELECT), JAMA 301 (2009) 39–51.
[13] T.W. Fan, R.M. Higashi, A.N. Lane, Integrating metabolomics and transcriptomics for probing SE anti mechanisms, Drug Metab. Rev. 38 (2006) 707–732.
[14] R.B. Robey, N. Hay, Is Akt the Warburg kinase?-Akt-energy metabolism interactions and oncogenesis, Semin. Cancer Biol. 19 (2009) 25–31.
[15] Z. Wang, C. Jiang, H. Ganther, J. Lu, Antimitogenic and proapoptotic activities of methylseleninic acid in vascular endothelial cells and associated effects on PI3K-AKT, ERK, JNK and p38 MAPK signaling, Cancer Res. 61 (2001) 7171–7178.
[16] Y. Wu, Delineating the mechanism by which selenium deactivates Akt in prostate cancer cells, Mol. Cancer Ther. 5 (2006) 246–252.
[17] H. Hu, C. Jiang, G. Li, J. Lu, PKB/AKT and ERK regulation of caspase-mediated apoptosis by methylseleninic acid in LNCaP prostate cancer cells, Carcinogenesis 26 (2005) 1374–1381.
[18] X. Lin, A.S. Bohle, P. Dohrmann, I. Leuschner, A. Schulz, B. Kremer, et al., Overexpression of phosphatidylinositol 3-kinase in human lung cancer, Langenbecks Arch. Surg. 386 (2001) 293–301.
[19] E.L. Greer, A. Brunet, FOXO transcription factors at the interface between longevity and tumor suppression, Oncogene 24 (2005) 7410–7425.
[20] E.W. Lam, J.J. Brosens, A.R. Gomes, C.Y. Koo, Forkhead box proteins: tuning forks for transcriptional harmony, Nat. Rev. Cancer 13 (2013) 482–495.
[21] A. Eijkelenboom, B.M.T. Burgering, FOXOs signalling integrators for homeostasis maintenance, Nat. Rev. Mol. Cell Biol. 14 (2013) 83–97.
[22] D.R. Calnan, A. Brunet, The FoxO code, Oncogene 27 (2008) 2276–2288.
[23] D.A. Altomare, J.R. Testa, Perturbations of the AKT signaling pathway in human cancer, Oncogene 24 (2005) 7455–7464.
[24] S. Reagan-Shaw, RNA interference-mediated depletion of phosphoinositide 3-kinase activates forkhead box class O transcription factors and induces cell cycle arrest and apoptosis in breast carcinoma cells, Cancer Res. 66 (2006) 1062–1069.
[25] X. Zhang, N. Tang, T.J. Hadden, A.K. Rishi, Akt, FoxO and regulation of apoptosis, Biochim. Biophys. Acta (BBA) Mol. Cell Res. 1813 (2011) 1978–1986.
[26] S. Fernandez de Mattos, P. Villalonga, J. Clardy, E.W. Lam, FOXO3a mediates the cytotoxic effects of cisplatin in colon cancer cells, Mol. Cancer Ther. 7 (2008) 3237–3246.
[27] R. Cortés, M. Tarrado-Castellarnau, D. Talancón, C. López, W. Link, D. Ruiz, et al., A novel cyclometallated Pt(ii)–ferrocene complex induces nuclear FOXO3a localization and apoptosis and synergizes with cisplatin to inhibit lung cancer cell proliferation, Metallomics 6 (2014) 622.
[28] H. Liu, J. Yin, C. Wang, Y. Gu, M. Deng, Z. He, FOXO3a mediates the cytotoxic effects of cisplatin in lung cancer cells, Anticancer Drugs 25 (2014) 898–907.
[29] L. Fang, H. Wang, L. Zhou, D. Yu, FOXO3a reactivation mediates the synergistic cytotoxic effects of rapamycin and cisplatin in oral squamous cell carcinoma cells, Toxicol. Appl. Pharm. 251 (2011) 8–15.
[30] S. Yin, Y. Dong, J. Li, L. Fan, L. Wang, J. Lu, et al., Methylseleninic acid potentiates multiple types of cancer cells to ABT-737-induced apoptosis by targeting Mcl-1 and bad, Apoptosis 17 (2011) 388–399.
[31] H. Hu, C. Jiang, C. Ip, Y.M. Rustum, J. Lu, Methylseleninic acid potentiates apoptosis induced by chemotherapeutic drugs in androgen-independent prostate cancer cells, Clin. Cancer Res. 11 (2005) 2379–2388.
[32] T. Mosmann, Rapid colorimetric assay for ular growth and survival: application to proliferation and cytotoxicity assays, J. Immunol. Methods 65 (1983) 55–63.
[33] R.R. Tice, E. Agurell, D. Anderson, B. Burlinson, A. Hartmann, H. Kobayashi, et al., Single gel/comet assay: guidelines for in vitro and in vivo genetic toxicology testing, Environ. Mol. Mutagen. 35 (2000) 206–221.
[34] T.W. Fan, Considerations of Sample Preparation for Metabolomics Investigation, Handbook of Metabolomics, New York, 2012, pp. 7–27.
[35] A.N. Lane, T.W. Fan, R.M. Higashi, Isotopomer-based metabolomic analysis by NMR and mass spectrometry, Methods Cell Biol. 84 (2008) 541–588.
[36] F. Zanella, A. Rosado, B. Garcia, A. Carnero, W. Link, Chemical genetic analysis of FOXO nuclear-cytoplasmic shuttling by using image-based cell screening, Chembiochemistry 9 (2008) 2229–2237.
[37] A. Rosado, F. Zanella, B. Garcia, A. Carnero, W. Link, A dual-color fluorescence-based platform to identify selective inhibitors of Akt signaling, PloS One 3 (2008) e1823.
[38] K. Berns, E.M. Hijmans, J. Mullenders, T.R. Brummelkamp, A. Velds, M. Heimerikx, et al., A large-scale RNAi screen in human cells identifies new components of the p53 pathway, Nature 428 (2004) 431–437.
[39] T.C. Chou, P. Talalay, Quantitative analysis of dose-effect relationships: the combined effects of multiple drugs or enzyme inhibitors, Adv. Enzyme Regul. 22 (1984) 27–55.
[40] S. Diaz-Moralli, M. Tarrado-Castellarnau, A. Miranda, M. Cascante, Targeting cell cycle regulation in cancer therapy, Pharmacol. Ther. 138 (2013) 255–271.
[41] A. Saraste, K. Pulkki, Morphologic and biochemical hallmarks of apoptosis, Cardiovasc. Res. 45 (2000) 528–537.
[42] C.J. Vlahos, W.F. Matter, K.Y. Hui, R.F. Brown, A specific inhibitor of phosphatidylinositol 3-kinase, 2-(4-morpholinyl)-8-phenyl-4H-1-benzopyran-4-one (LY294002), J. Biol. Chem. 269 (1994) 5241–5248.
[43] T.W. Fan, A.N. Lane, R.M. Higashi, M.A. Farag, H. Gao, M. Bousamra, et al., Altered regulation of metabolic pathways in human lung cancer discerned by (13)C stable isotope-resolved metabolomics (SIRM), Mol. Cancer 8 (2009) 41.
[44] T.W. Fan, A.N. Lane, R.M. Higashi, J. Yan, Stable isotope resolved metabolomics of lung cancer in a SCID mouse model, Metabolomics 7 (2011) 257–269.
[45] T.W. Fan, P. Yuan, A.N. Lane, R.M. Higashi, Y. Wang, A.B. Hamidi, et al., Stable isotope-resolved metabolomic analysis of lithium effects on glial-neuronal metabolism and interactions, Metabolomics 6 (2010) 165–179.
[46] F. Zanella, W. Link, A. Carnero, Understanding FOXO new views on old transcription factors, Curr. Cancer Drug Targets 10 (2010) 135–146.
[47] F. Zanella, N.R. dos Santos, W. Link, Moving to the core: spatiotemporal analysis of forkhead box O (FOXO) and nuclear factor-κB (NF-κB) nuclear translocation, Traffic 14 (2013) 247–258.
[48] W. Link, J. Oyarzabal, B.G. Serelde, M.I. Albarran, O. Rabal, A. Cebria, et al., Chemical interrogation of FOXO3a nuclear translocation identifies potent and selective inhibitors of phosphoinositide 3-kinases, J. Biol. Chem. 284 (2009) 28392–28400.
[49] F. Zanella, A. Rosado, B. Garcia, A. Carnero, W. Link, Using multiplexed regulation of luciferase activity and GFP translocation to screen for FOXO modulators, BMC Cell Biol. 10 (2009) 14.
[50] A. Essaghir, N. Dif, C.Y. Marbehant, P.J. Coffer, J.B. Demoulin, The transcription of FOXO genes is stimulated by FOXO3 and repressed by growth factors, J. Biol. Chem. 284 (2009) 10334–10342.
[51] L. Fang, H. Wang, L. Zhou, D. Yu, Akt-FOXO3a signaling axis dysregulation in human oral squamous cell carcinoma and potent efficacy of FOXO3a-targeted gene therapy, Oral Oncol. 47 (2011) 16–21.
[52] M.M. Yung, D.W. Chan, V.W. Liu, K.M. Yao, H.Y. Ngan, Activation of AMPK inhibits cervical cancer cell growth through AKT/FOXO3a/FOXM1 signaling cascade, BMC Cancer 13 (2013) 327.
[53] L. Jiang, X.C. Cao, J.G. Cao, F. Liu, M.F. Quan, X.F. Sheng, et al., Casticin induces ovarian cancer cell apoptosis by repressing FoxM1 through the activation of FOXO3a, Oncol. Lett. 5 (2013) 1605–1610.
[54] R.H. Medema, G.J.P.L. Kops, J.L. Bos, B.M.T. Burgering, AFX-like Forkhead transcription factors mediate cell-cycle regulation by Ras and PKB through p27kip1, Nature 404 (2000) 782–787.
[55] C.J. Li, J.K. Chang, C.H. Chou, G.J. Wang, M.L. Ho, The PI3K/Akt/FOXO3a/p27Kip1 signaling contributes to anti-inflammatory drug-suppressed proliferation of human osteoblasts, Biochem. Pharmacol. 79 (2010) 926–937.
[56] M. Schmidt, S. Fernandez de Mattos, A. van der Horst, R. Klompmaker, G.J.P.L. Kops, E.W.F. Lam, et al., Cell cycle inhibition by FoxO forkhead transcription factors involves downregulation of cyclin D, Mol. Cell. Biol. 22 (2002) 7842–7852.
[57] J. Liang, J.M. Slingerland, Multiple roles of the PI3K/PKB (Akt) pathway in cell cycle progression, Cell Cycle 2 (2003) 336–342.

[58] G.X. Li, H. Hu, C. Jiang, T. Schuster, J. Lü, Differential involvement of reactive oxygen species in apoptosis induced by two classes of selenium compounds in human prostate cancer cells, Int. J. Cancer 120 (2007) 2034–2043.
[59] J.X. de Miranda, F.D. Andrade, A.D. Conti, M.L. Dagli, F.S. Moreno, T.P. Ong, Effects of selenium compounds on proliferation and epigenetic marks of breast cancer cells, J. Trace Elem. Med. Biol. 28 (2014) 486–491.
[60] R.L. Poerschke, M.R. Franklin, P.J. Moos, Modulation of redox status in human lung cell lines by organoseleno compounds: selenazolidines, selenomethionine, and methylseleninic acid, Toxicol. In Vitro 22 (2008) 1761–1767.
[61] X. Wang, W.R. Chen, D. Xing, A pathway from JNK through decreased ERK and Akt activities for FOXO3a nuclear translocation in response to UV irradiation, J. Cell. Physiol. 227 (2012) 1168–1178.
[62] J. Sunayama, JNK antagonizes Akt-mediated survival signals by phosphorylating 14-3-3, J. Cell Biol. 170 (2005) 295–304.
[63] A. Sunters, Paclitaxel-induced nuclear translocation of FOXO3a in breast cancer cells is mediated by c-Jun NH2-terminal kinase and Akt, Cancer Res. 66 (2006) 212–220.
[64] Y. Zou, P. Niu, J. Yang, J. Yuan, T. Wu, X. Chen, The JNK signaling pathway is involved in sodium-selenite-induced apoptosis mediated by reactive oxygen in HepG2 cells, Cancer Biol. Ther. 7 (2008) 689–696.
[65] S. Dasari, P.B. Tchounwou, Cisplatin in cancer therapy: molecular mechanisms of action, Eur. J. Pharmacol. 740 (2014) 364–378.
[66] M.J. Garnett, E.J. Edelman, S.J. Heidorn, C.D. Greenman, A. Dastur, K.W. Lau, et al., Systematic identification of genomic markers of drug sensitivity in cancer cells, Nature 483 (2012) 570–575.
[67] O. Micke, L. Schomburg, J. Buentzel, K. Kisters, R. Muecke, Selenium in oncology: from chemistry to clinics, Molecules (Basel, Switzerland) 14 (2009) 3975–3988.
[68] M.P. Rayman, Selenium in cancer prevention: a review of the evidence and mechanism of action, Proc. Nutr. Soc. 64 (2005) 527–542.
[69] E.N. Drake, Cancer chemoprevention: selenium as a prooxidant, not an antioxidant, Med. Hypotheses 67 (2006) 318–322.
[70] M. Vinceti, G. Dennert, C.M. Crespi, M. Zwahlen, M. Brinkman, M.P. Zeegers, et al., Selenium for preventing cancer, Cochrane Database Syst. Rev. 3 (2014) CD005195.
[71] L. Yan, L.C. DeMars, Dietary supplementation with methylseleninic acid, but not selenomethionine, reduces spontaneous metastasis of Lewis lung carcinoma in mice, Int. J. Cancer 131 (2012) 1260–1266.
[72] H. Zeng, M. Wu, The inhibitory efficacy of methylseleninic acid against colon cancer xenografts in C57BL/6 mice, Nutr. Cancer (2015) 1–8.
[73] Z. Wang, H. Hu, G. Li, H.J. Lee, C. Jiang, S.H. Kim, et al., Methylseleninic acid inhibits microvascular endothelial G1 cell cycle progression and decreases tumor microvessel density, Int. J. Cancer 122 (2008) 15–24.
[74] H.E. Ganther, Pathways of selenium metabolism including respiratory excretory products, Int. J. Toxicol. 5 (1) (1986) 1–5.
[75] H. Steinbrenner, H. Sies, Protection against reactive oxygen species by selenoproteins, Biochim. Biophys. Acta 1790 (2009) 1478–1485.
[76] W. Link, FOXO proteins as potential targets for anticancer therapy, Curr. Drug Targets 12 (2011) 1232–1234.